Preparation and Characterization of Organomodified Co-Al and Ni-Al Layered Double Hydroxides (LDHs) Reinforced Polystyrene (PS) Nanocomposites

Thesis submitted in partial fulfillment of the requirements for the degree of

DOCTOR OF PHILOSOPHY

by

Kelothu Suresh

Department of Chemical Engineering

Indian Institute of Technology Guwahati

Guwahati - 781039, India

Preparation and Characterization of Organomodified Co-Al and Ni-Al Layered Double Hydroxides (LDHs) Reinforced Polystyrene (PS) Nanocomposites

Kelothu Suresh

Preparation and Characterization of Organomodified Co-Al and Ni-Al Layered Double Hydroxides (LDHs) Reinforced Polystyrene (PS) Nanocomposites

Thesis submitted in partial fulfillment of the requirements for the degree of

DOCTOR OF PHILOSOPHY

by

Kelothu Suresh
Roll No.: 126107001

Department of Chemical Engineering
Indian Institute of Technology Guwahati
Guwahati - 781039, India

July, 2017

Dedicated To

My Wife and Parents

Department of Chemical Engineering
Indian Institute of Technology Guwahati
Guwahati - 781039, India

CERTIFICATE

This is to certify that the thesis entitled **"Preparation and Characterization of Organomodified Co-Al and Ni-Al Layered Double Hydroxides (LDHs) Reinforced Polystyrene (PS) Nanocomposites"** being submitted by ***Kelothu Suresh (Roll No.: 126107001)*** for the award of degree of Doctor of philosophy is an authentic record of the results obtained from the research work carried out under my supervision in the Department of Chemical Engineering, Indian Institute of Technology Guwahati, India and this work has not been submitted elsewhere for a degree.

(Dr. G. Pugazhenthi)
Professor
Department of Chemical Engineering,
Indian Institute of Technology Guwahati
Guwahati - 781039, India.

Acknowledgements

I owe my deepest gratitude to all those who made my Ph.D. thesis possible. I would like to take the opportunity to express my sincere gratitude to my supervisor **Prof. G. Pugazhenthi.** Without the valuable suggestions, encouragement and continuous support of my thesis supervisor, the thesis would not have been possible to reach its maturity and highest standard of academic research. I would like to thank him for spending his precious time for discussion by which I have gained immense skills of knowledge in the tenure of my research. My most heartfelt thanks is also due to **Prof. Ramgopal V. S. Uppaluri** for his kind help, suggestions and constant encouragement in writing manuscripts as well as editing the thesis files of my research work within stipulated short period of time.

I would like to express my sincere gratitude to all my doctoral committee members **Dr. Chandan Das**, **Dr. Mahyua De** and **Prof. Parameswar Krishnan Iyer** for their advices that are full of insights and valuable suggestions to enhance standard and quality of conducted research.

My sincere acknowledgement goes to **Prof. V.S. Moholkar** and **Prof. B. P. Mandal**, who are respectively former and present Heads of Chemical Engineering Department. I thank them for their encouragement, guidance and support for my PhD work.

My sincere thanks is also to faculty and staff at the Department of Chemical Engineering for their constant support. The kind and constant help of the staff members of CIPET Lucknow and Department of Mechanical Engineering, IIT Guwahati is also duly acknowledged. I am also thankful to the Indian Institute of Technology Guwahati for providing me with the infrastructure and facilities for advanced research. I also acknowledge

Ministry of Human Resources Development, New Delhi for providing me fellowship to pursue Ph.D.

My sincere thanks go to **Prof. S. Senthilvelan** and **Prof. S. Kanagaraj**, Department of Mechanical Engineering for allowing me to work in Material Science Laboratory. I am also thankful to **S. Arun** and **Jiten Basumatary** for assisting in material compounding. It is my pleasure to work with **Sarita Bharti** in tribology laboratory. I must acknowledge **S. Narendren** from CoE-SUSPOL, IIT Guwahati for assisting in water vapor transmission rate test.

I would like to acknowledge Central instrument facility (CIF) HOC of IITG and staff **Prof. G. Krishnamoorthy**, **Dr. K. K. Senapati**, **Mr. Chandan Borgahain**, **Mr. Singh** and **Mr. Madhurjya Borah** for providing me facilities to carry out the necessary characterization studies. I am grateful to the Centre of Excellence for Sustainable Polymers (CoE-SUSPOL), IIT Guwahati for providing the characterization facility of WVTR instrument.

I am thankful to my friends at IIT Guwahati **Akhilesh Dubey**, **Ravi Kumar Biroju**, **Maharshi** and **Santhosh** for making my stay comfortable and cheerful in campus. I am also thankful to **Mood Mohan**, **Dr. Bandi Chandra Sekhar**, **Dr. V. Shyam Kumar Yadav**, **Dr. Murali pujari** for always being there for me whenever I needed their support. I am immensely thankful to my seniors **Manish Kumar**, **Vasanth**, research group member **Ashim Kumar Basumathary**, **Vinoth Kumar**, **Kanchapogu Suresh**, **Lalith**, **Arul**, **Mohan**, **Ms. Payel Sen**, **Ms. Prithi**, **Ms. Githanjali** and lobby mates **Binay Deogam**, **Kishant Kumar**, **Sathanarayana**, **Bisweswar Das**, **Abhik Bhattacharjee** and **Rupak Kishore**. It was a pleasure having their association during the entire Ph.D. tenure.

No words would suffice to express my gratitude to my wife **Prathyusha** whose constant love, support, suggestions and understanding throughout these years inspired me the dedication to work. This would not have been possible without her constant companionship and soothing words during tough and difficult times of the Ph.D. tenure.

My Ph.D endeavour would not have been successful without love, trust, support and blessings of my grandparents (**Smt Patni** and **Sri Lalu**), parents (**Smt Lakshmi** and **Sri Ramsingh**) and parent-in-laws (**Smt Malathi** and **Sri Raju Naik**) for all the sacrifices they made for my better future and giving me freedom to take my own decisions. I also thank my Uncles and Aunts for their constant support and blessings. I thank my brothers, **Naresh** and **Bharath,** brother-in-laws **Rajkumar** and **Vishal Babu** for their immense care, encouragement and moral support in achieving this level and always standing by me in all phases of my life.

I would express my deepest gratitude to all my wishers.

Last but not least, I express my thanks to **Almighty** for blessing me and giving the strength to complete this work.

July, 2017 Kelothu Suresh

Abstract

Due to enhanced mechanical and thermal stability, low gas permeability and improved fire retardancy, the past two decades witnessed extensive investigation in polymer nanocomposites. Among various polymers and nanofillers, polystyrene (PS) and layered double hydroxide (LDH) nanomaterials are highly desired combinations as matrix and nanomaterials, respectively during nanocomposite fabrication. With effective rigidity, transparency and less moisture absorption tendency, PS is ideal polymer matrix for optical, packaging and electrical appliances. The poor thermal stability of the PS matrix can be effectively addressed by incorporating LDHs nanofiller materials in the PS matrix. While alternate LDHs have numerous applications and promising features, Co-Al LDH and Ni-Al LDH nanofillers are highly promising for antibacterial, optical, packaging and wastewater treatment applications. Thereby, the central objective of the Ph.D. thesis is to fabricate Co-Al LDH and Ni-Al LDH based PS nanocomposites by adopting various competitive fabrication methods and carry out characterization studies in terms of thermal and mechanical properties.

The Ph.D. thesis has been sequentially categorized into five major themes that have been arranged in Chapters 2 – 6. These are:

a) Co-precipitation based synthesis of Co-Al LDH and Ni-Al LDH nanofillers followed with characterization studies. (Chapter 2)
b) Rheological studies of PS and PS/LDH blend solutions. (Chapter 3)
c) Solvent blending based fabrication and characterization of PS/Co-Al LDH and PS/Ni-Al LDH nanocomposites. (Chapter 4)
d) Melt intercalation based fabrication and characterization of PS/Co-Al LDH and PS/Ni-Al LDH nanocomposites. (Chapter 5)

e) Durability studies of most competitive PS/LDH nanocomposite and PS based spur gears. (Chapter 6)

Characterization studies involved X-ray diffraction (XRD), Fourier transform infrared spectroscopy (FTIR), Thermogravimetric analysis (TGA), Differential scanning colorimetry (DSC), activation energy evalution using Coats-Redfern method, integral procedural decomposition temperature (IPDT) evaluation, thermal degradation reaction mechanism evaluation, rheological measurements, storage and loss modulus and complex viscosity studies.

The XRD studies of modified LDH nanofiller materials conveys that for Co-Al LDH, a characteristic peak corresponding to (003) plane is observed at 2θ value of 3.14° and corresponding basal spacing (d-spacing) of 2.8 nm. However, for the Ni-Al LDH, the basal spacing (d_{003}) of (003) peak appeared at 2θ value of 6.54° is evaluated to be 1.35 nm. During TGA study, considering 10% mass loss as a reference, the degradation temperatures of modified Co-Al LDH and Ni-Al LDH have been found to be 266.4 and 430.1 °C, respectively. Corresponding residues obtained at 700 °C have been estimated to be 75.05 and 83.67 wt.%, respectively. Among these investigated modified LDHs, modified Co-Al LDH exhibited lower residue content due to more content of modifier present in the modified Co-Al LDH.

Rheological studies were conducted for solvent blending method based pristine PS and PS/Co-Al blend solutions (3, 5 and 7 wt.% nanofiller content) at 20, 30 and 40 °C and for shear rates of 0.1 – 100 s^{-1}. The solution rheology has been evaluated to be strongly influenced by shear rate, Co-Al LDH content and temperature. As expected, the blend solution viscosity increased with increasing concentration of polymer and nanofiller. In

comparison with pristine PS solutions, the incorporation of Co-Al LDH in PS polymer enhanced viscosity of PS/Co-Al LDH blend solutions. Among alternate theoretical rheological models, based on regression coefficient and bias factor analysis, for both pristine PS and PS/Co-Al LDH blend solutions, measured rheological parameters fit well with Hershel-Bulkley and Cross model at low temperature (20 °C) and high temperature (30 and 40 °C).

The solvent blending based fabrication involved utilization of xylene as a solvent to achieve PS/Co-Al LDH and PS/Ni-Al LDH nanocomposites with desired nanofiller loading content (1, 3, 5 and 7 wt.%). For the PS/LDH nanocomposites, XRD pattern suggested formation of exfoliated structure. However, transmission electron microscopy (TEM) images indicated intercalated morphology of PS nanocomposites obtained with higher LDH loading of 7 wt.%. FTIR spectra of the nanocomposites confirmed existence of LDH functional groups in the PS matrix. For all nanocomposite samples, improved thermal stability has been confirmed by glass transition temperature (T_g) and TGA data. For a maximum nanofiller loading of 7 wt.% LDH, the T_g value of Co-Al LDH and Ni-AL LDH nanocomposites increased to 74.8 and 75 °C, respectively T_g of pristine PS is 69.3 °C.

The TGA data indicated that for 15% weight loss reference point, PS/Co-Al LDH nanocomposites exhibit highest enhancement in thermal decomposition temperatures (10.5 – 28.5 °C) in comparison with corresponding value of pristine PS. Incidentally, these values are 12.3 – 29.1 °C for PS/Ni-Al LDH nanocomposites, thereby conveying that PS/Ni-Al LDH nanocomposites possessed better thermal properties than PS/Co-Al LDH nanocomposites.

The obtained IPDT and activation energy data (obtained from Coats-Redfern method) are in very good agreement with the inference drawn from TGA data that inferred enhanced thermal

stability of the nanocomposites. Criado method based thermal degradation reaction mechanism analysis conveyed that thermal degradation occurred as per F1 reaction mechanism (random nucleation with one nucleus on the individual particle) at lower temperature followed with A4 reaction mechanism (nucleation and growth) at higher temperature for the PS nanocomposites. Incidentally, pristine PS followed F1 reaction mechanism for the entire temperature range. Melt rheological analysis of PS/LDH nanocomposites conveyed that storage and loss modulus increases with increasing nanofiller loading. The complex viscosity of pristine PS and PS nanocomposites decreased with increasing angular frequency. Among alternate models, Guth model provided best fitness for obtained melt rheology data of the nanocomposites.

The melt intercalation based Co-Al LDH and Ni-Al LDH nanocomposites with desired nanofiller loading content (1, 3, 5 and 7 wt.%) indicated few similar and few dissimilar results in comparison with all results obtained for solvent blending based PS/LDH nanocomposites. Precisely, notable differences existed in the optimality of nanofiller loading for these nanocomposites. XRD analysis signifies exfoliated structure of LDHs in PS polymer. Therefore, nanocomposite fabrication method is opened to have a strong role in influencing nanocomposite properties. Compared to the pristine PS values, the 1 wt.% Co-Al LDH nanocomposite possessed maximum enhancements in mechanical properties such as tensile strength (32%), flexural strength (21.2%) and impact strength (19%). These values for 1 wt.% Ni-Al LDH are 34.5, 27.5 and 22 % respectively. The tensile strength enhancement for the nanocomposite is due to exfoliation of rigid LDH nanolayers in PS polymer and significant interfacial interactions between PS and LDH materials. The reduction in mechanical properties at higher loading has been due to formation of agglomerates. TEM analysis

conveyed that intercalated morphology existed at higher loading. On the other hand, investigated thermal characterization parameters conveyed that optimal nanofiller loading is 7 wt.% for both Co-Al LDH and Ni-Al LDH nanocomposites, which is quite different from the optimal nanofiller loading obtained from mechanical property optimization perspective. For 15% weight loss reference point, the 7 wt.% Co-Al LDH and Ni-Al LDH nanocomposites possessed enhanced degradation temperature of 384.1 and 385.4 °C, respectively, which are significantly higher than those obtained for pristine PS (358 °C). Similarly, DSC studies conveyed that, in comparison with pristine PS polymer values, T_g of 7 wt.% Co-Al LDH and Ni-Al LDH increased by 4.1 and 4.3 ^oC, respectively. Results obtained from Coats Redfern, Criado model, IDPT temperature, reaction mechanism analysis, storage modulus, loss modulus and complex viscosity studies have been similar to those obtained for solvent blending based PS/LDH nanocomposites.

Along with pristine PS, the 1 wt.% melt intercalated Co-Al LDH and Ni-Al LDH nanocomposites were utilized in injection moulding equipment to fabricate spur gears for durability studies. Apart from XRD, TEM and FTIR studies, power absorption gear tests (1.5 Nm torque, 800 rpm and 1 h conditions) have been carried out for the said materials. XRD and TEM analysis signify exfoliated structure of LDH in PS polymer for 1 wt.% LDH loading. The presence of various functional groups in the PS/Co-Al LDH and PS/Ni-Al LDH nanocomposites has been conveyed by FTIR analysis. For PS nanocomposite gears, measured net surface temperature has improved with respect to value obtained for pristine PS gears. The transmission efficiency of test-steel gear pair was evaluated using measured in-line torque values. In comparison with pristine PS values, for 1 wt.% Co-Al LDH and 1 wt.% Ni-Al LDH nanocomposites, the transmission efficiency enhanced by 1.4 and 2.6%, respectively. Tooth

surfaces of worn-out gears observed using digital and scanning electron microscope also conveyed better wear out durability of the PS nanocomposites.

In summary, the Ph.D. thesis has been instrumental to provide additional knowledge in the chosen field of research. Thereby, it is expected that the results reported in this work could serve as benchmark for the enhanced application of PS/Co-Al LDH and PS/Ni-Al LDH nanocomposites.

NOVELTY STATEMENT

- Rheological studies of PS/Co-Al LDH blend solutions
- Mechanical, permeability, thermal and melt rheology based characterization of PS/Ni-Al LDH and PS/Co-Al LDH nanocomposites fabricated with solvent blending and melt intercalation.
- Evaluation of thermal degradation kinetics and reaction mechanism for PS/Co-Al LDH and PS/Ni-Al LDH nanocomposites.
- Durability studies of PS/Co-Al LDH and PS/Ni-Al LDH nanocomposite spur gears.

RESEARCH HIGHLIGHTS

- Xylene based PS/Co-Al LDH blend solutions possessed highest viscosity and shear stress profiles at highest nanofiller loading (7 wt.%).
- Optimality of solvent blending based PS/LDH nanocomposites indicates highest nanofiller loading (7 wt.%) for thermal property enhancement. However, melt intercalation conveyed that mechanical property enhancement is maximum for low nanofiller loading (1 wt.%) and thermal property enhancement is maximum for highest nanofiller loading (7 wt.%).
- For both solvent blending and melt intercalation PS/LDH nanocomposite processes, all characterizations (mechanical, permeability, thermal and durability studies) inferred that PS/Ni-Al LDH nanocomposites are competitive than PS/Co-Al LDH nanocomposites and PS polymer.

Contents

List of Tables

List of Figures

Abbreviations

AFM	Atomic force microscopy
ASTM	American Society for Testing and Materials
BMI	Bismalemide
CF	Carbon fibre
DNA	Deoxyribonucleic acid
CNT	Carbon nanotubes
DMA	Dynamic mechanical analysis
DSC	Differential Scanning Calorimetry
EPDM	Ethylene propylene diene monomer
EVA	Ethyl vinyl acetate
FESEM	Field Emission Scanning Electron Microscopy
FEA	Finite element analysis
FTIR	Fourier transmission infrared spectroscopy
HDPE	High density polyethylene
HIPS	High impact polystyrene
IPDT	Integral procedural decomposition temperature
LDH	Layered Double Hydroxide
LDPE	Low density polyethylene
LG	N-lauroyl-glutamate
MAH	Maleic anhydride
MMA	Methyl methacrylate
MMT	Montmorillonite

MWCNT	Multi-walled carbon nanotubes
OMMT	Organo-modified-Montmorillonite
PA	Polyamide
PAN	Polyacrylonitrile
PBTDI	Poly(1,4-butandiol) tolylene 2,4-diisocyanate
PEE	Polyethylene elastomer
PET	Polyethylene terephthalate
PI	Polyimide
POM	Polyoxymethylene
PLA	Poly(lactic acid)
PLNs	Polymer/layered nanocomposites
PMA	Poly methyl acrylate
PMMA	Polymethyl methacrylate
PP	Polypropylene
PPC	Polypropylene carbonate
PPO	Polyphenylene oxide
PPS	polyphenylene sulphide
PS	Polystyrene
PSF	Polysulfone
SE	Standard error
SEC	Size exclusion chromatographic
SEM	Scanning Electron Microscopy
SFEP	Soap-free emulsion polymerization
SPN	Oligo-(oxypropylene)-, diethyl-, methyl-ammonium chloride

STN	Methyl-trioctil-ammonium chloride
TDI	Toluene diisocyanate
TEM	Transmission Electron Microscopy
TGA	Thermo gravimetric analysis
UP	Unsaturated polyester
VASE	Variable angle spectroscopic ellipsometry
XNBR	Carboxylated nitrile rubber
XRD	X-Ray Diffraction

Notations

nm	Nanometer
θ	Diffraction Angle
λ	Cu-Kα Radiation Wavelength
τ	Shear Stress
γ	Shear Rate
K	Consistency index
B_f	Bias factor
R^2	Regression coefficient
T_d	Decomposition temperature
T_{max}	Maximum degradation temperature
T_i	Initial experimental temperature
T_f	Final experimental temperature
T_g	Glass transition temperature
α	Fractional Conversion

β	Rate of Heating
k	Rate Constant
E_a	Activation Energy
A	Pre-Exponential Factor
n	Order of Reaction
R	Gas Constant
G′	Storage Modulus
G″	Loss modulus
tan δ	Loss Factor
η*	Complex Viscosity
ω	Angular Frequency
η	Viscosity

Chapter 1:

Introduction, Literature Review and Objective

Chapter 1

Introduction, Literature Review and Objectives

This chapter presents a brief summary of the basic fundamentals, classification and applications involved in polymer nanocomposites along with the basis of the problem chosen for the Ph.D. thesis. Specific advantages of polymer nanocomposites with respect to conventional composites have been highlighted. The state-of-the-art associated with the preparation and characterization of polymer nanocomposites and their applications have been elaborately summarized. Subsequently, the literature summary has been addressed along with possible scope for further research. Thereafter, the chapter presents objectives and organization of the thesis.

1.1 Introduction

Nanocomposite material is defined as a material made of at least two constituent phases, in which one is a matrix and another is reinforcing phase with significant variation in physical and chemical properties. Metal, ceramic or polymer materials could be the reinforcing materials and matrix. Usually, reinforcing materials possess lower density and matrix materials are ductile or tougher materials. In general, composites are designed and fabricated to synthesize additional aspects of the reinforced material along with the toughness of the matrix to achieve a material with properties that cannot be achievable with any single material.

Examples of natural composite materials are bone, teeth and wood which are made up of two or more constituents. Bone and teeth are made up of toughened collagen matrix. With

a combination of flesh and bones, the entire human body is a wonderful illustration as a natural biological composite. On other hand, wood is made up of cellulose fibres as reinforcing in lignin matrix. The fundamental conception behind nanocomposites is to improve characteristics of matrix materials through reinforcement principle. In polymer/layered double hydroxide (LDH) nanocomposites, LDH layers are dispersed in polymer matrix to enhance thermal, mechanical, barrier properties and reduce flammability (Ray et al., 2002; Ray and Okamoto, 2003).

1.2 History and background

Around 1500 BC, first use of manmade composite materials were reported in the form of mud (matrix) and straw (reinforced material) composites being used for building strong and durable housing by Egyptian and Mesopotamian citizens. Also, straw reinforcement was existent from such time frame in composite commodities such as pottery and material for applications in boats. The Mongol citizens, in 1200 AD, invented the first composite for weapon as bows, using a combination of wood, bone and animal glue. To enhance the strength of bows, they were pressed and wrapped up with bark of birch tree. This composite bow was the most powerful arm on earth until the invention of automatic weapons (Ashby, 1987; Johnson, 2013).

Late 1930s witnessed the development of polymer/clay nanocomposites. In 1932, a researcher at Owens-Illinois invented a process for mass production of glass fibre strands. Owens collaborated with the corning to produce its patented glass fibre. A suitable resin for combining the glass fibre with a polymer matrix was developed in 1936 by Du-Pont (Johnson, 2013).

In 1940s, latex system was developed and the technology for the production of highly dispersible organobentonite was developed by Jordan et al. (1940). Functional and silica modified kaolin was developed by J. M. Huber Corporation from 1960. Despite having high cost, these materials were applied commercially for the enhancement of mechanical properties of elastomers (Chaiko, 2006).

The real revolution came in 1985, when Nylon/Montmorillonite (MMT) nanocomposites were first developed in Toyota Central R & D lab (Okada et al., 2006). This new nanocomposite concept widened the scope of polymer science in the context of novel applications for automotive, food packaging and electric industries. In 1989, polymer nanocomposite equipped passenger cars were launched. Thereafter, extensive research was targeted towards polymer nanocomposite in both industrial and academic sectors.

1.3 Polymer selection

Polystyrene (PS) is an important amorphous thermoplastic material. PS is a promising polymer matrix owing to the advantages of effective rigidity, transparency and formability with less moisture absorption. PS is resistant to many inorganic reagents, nonpolar solvents, aliphatic hydrocarbons, alkaline and acidic solutions. PS is extensively applied for packaging and electrical appliances. However, its application at elevated temperature is limited. One feasible approach that can be adopted to overcome this limitation is to improve polymer performance through reinforcement of nanoparticles such as clays, silica or carbon nanotubes into the polymer matrix. Also, LDH reinforced polymer nanocomposites exhibit enhanced thermal and mechanical properties.

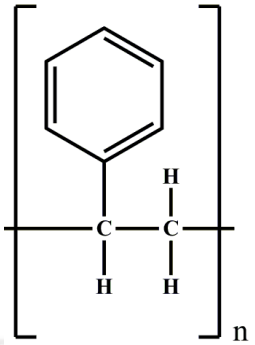

Figure 1.1: Structure of PS.

The structure of PS is illustrated in Figure 1.1. Compared to the PS, PS nanocomposites offer better properties such as higher mechanical and thermal stability, low gas permeability and improved fire retardancy (Hajibeygi et al., 2017; Ray and Okamoto, 2003; Zare, 2016).

1.4 Filler selection

Usually, incorporation of inorganic fillers into organic polymer do enhance brittle nature of composite material. Also, inorganic filler addition with higher loading percentages does not enhance mechanical and other properties of the composite material due to inadequate dispersion of fillers throughout the polymer matrix. This limits upon amount of fillers that can be incorporated into polymers to enhance the characteristics of the composite materials.

From application perspective, numerous inorganic particles are beneficial for incorporation into polymer/metal/ceramics matrices to achieve desired composite materials. Compared to the pure metal, metal matrix constituting fillers have improved high temperature creep characteristics and hardness. For a ceramic matrix, fillers are incorporated to enhance its

toughness and fracture properties. Similarly, for polymer matrix, inorganic fillers improve stiffness, strength, electrical and thermal properties (Garcia et al., 2004).

Nanoscale materials are defined as substances in which at least one dimension is less than approximately 100 nm (nanometers). Nanomaterials are broadly classified into three categories depending on the dimensions of dispersed particles (Chrissafis and Bikiaris, 2011). The first category refers to particle having only one dimension in nanometer scale and these have platelet like structure. Classical examples of this category are clays and LDHs.

The second category refers to those materials in which two dimensions are in the nm range and the third dimension is in the larger range. These materials possess elongated structure. Nanotubes and nanofibers are conventional examples of this category. The third category refers to materials in which all dimensions are in nanoscale. Spherical silica, nanocrystal, metal nanoparticle are examples in this category. The dispersion of nanoparticle in the polymer matrix is strongly influenced by the aspect ratio of nanoparticle (ratio of length and breadth) and filler-polymer phase interactions as contact surfaces.

Besides these, in nanocomposites synthesis, the compatibility of filler and polymer is another important aspect that needs to be considered. The compatibility issues are usually targeted by organic modification of filler to enhance dispersion of filler in the polymer matrix through vigorous stirring.

1.4.1 Layered double hydroxide

LDH is mineral and synthetic materials with positive charged brucite type layers of mixed metal hydroxide (Figure 1.2). LDHs are layered crystalline materials having anionic

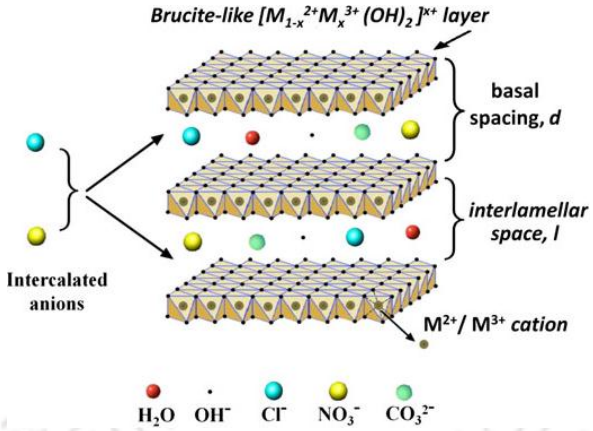

Figure 1.2: Structure of LDH.

counter ions in the gallery space. In general LDH chemical formula is presented as $[M^{2+}_{1-x} M^{3+}_{x}(OH)_2]^{x+}(A^{m-})_{x/m}$ .yH_2O, where, M^{2+} is metallic divalent cations (Ni^{2+}, Mg^{2+}, Zn^{2+}, Cu^{2+}, or Co^{2+}), M^{3+} is a metallic trivalent cations (Al^{3+}, Mn^{3+}, Ga^{3+}, Cr^{3+} or In^{3+}), A^{m-} is anion (with charge m^-) interlayer (NO_3^-, CO_3^{2-}, or OH^-). Also, in the formula, X value varies in the range of 0.20 – 0.33 for pure phase of LDHs (Acharya et al., 2007).

1.4.2 Organic modification of LDH

Organic modification of LDHs is essential prior to its application in the polymer matrix for preparing polymer nanocomposites. The exfoliated or intercalated polymer nanocomposite preparation depends upon the compatibility of LDH with polymer. LDHs are hydrophilic in nature and they must be made organophillic (hydrophobic) to become compatible with most host polymers that are hydrophobic in nature. Therefore, without modification, LDH will only disperse and undergo phase separation in the polymer matrix.

To overcome this problem, organic ions from surfactants or intercalants are substituted for inorganic ions between the clay galleries. In this regard, it is important to note that higher charge density and longer surfactant chain length will enforce clay layers to move further away and provide easier access for polymer chains to penetrate within the LDH layers. Thereby, the nanocomposite structure undergoes exfoliation, which is a desired feature to enhance the properties of the nanocomposite material.

1.4.3 Advantages of LDH

- High purity LDHs with homogeneous structure, known chemical compositions, and desired functionalities can be synthesized in the laboratory using co-precipitation method (Feitkneeht et al., 1942; Miyata, 1977).
- LDHs have been widely studied and suggested materials to serve as catalysts (Choudary et al., 2001), catalyst precursors (Choudary et al., 2002), adsorbents (You et al., 2002), ion exchangers (Kozai et al., 2002), electrode modifiers (Qiu and Villemure, 1997), optical materials (Takagi et al., 1993), precursors for preparing CO_2 adsorbents (Wang et al., 2011a), fire retardant additives (Nyambo et al., 2008), drug delivery hosts (Alcantara et al., (2010), cement additives (Plank et al., 2010) and nanofiller for polymer nanocomposites (Leroux and Besse, 2001) .
- LDH containing magnesium and aluminum are biocompatible and have been used as an antacid and antipepsin agent.
- Endothermic decomposition of LDHs produce metal oxide residues. This principle is explored to improve thermal and flame retardancy of polymers in LDH polymer nanocomposites.

- Ni-Al LDH can be used to assist bacteriophage removal in water treatment and filtration applications.
- Ni-Al LDH modified electrodes have been reported to serve as biosensors (Park et al., 2005).

1.5 Alternate matrix polymers in nanocomposites

1.5.1 Thermoplastic based nanocomposites

Many thermoplastic based nanocomposites were prepared by reinforcing nanoparticle in the polymer matrices. Thermoplastic polymers used for this type of nanocomposites includes polybutylene, polyethylene (PE), polyamide (PA), polyacrylonitrile (PAN), polycarbonate (PC), polymethyl methacrylate (PMMA), polyethylene copolymer, polymethyl pentane, PS, polyphenylene oxide (PPO), polyvinyl chloride (PVC), polypropylene (PP), polyphenylenesulfide, polysulfone (PSF), etc (Chrissafis and Bikiaris, 2011).

1.5.2 Thermoset based nanocomposites

Various thermosetting resins have been used for the preparation of nanocomposites by introducing nanoparticles into the polymer matrix. These include melamine formaldehyde and urea, vinylester, cyanate ester, polyester, bismalemide (BMI), polyurethane (PU), polyimide (PI), epoxy resin, etc (Mittal, 2008; Chrissafis and Bikiaris, 2011).

1.6 Polymer nanocomposite preparation methods

Polymer nanocomposites are multiphase systems in which the dispersed nanofiller in the polymer matrix has atleast one dimension in the nanoscale regime. Various methods exist to prepare polymer nanocomposites. Among these, solvent blending, melt compounding and in-situ polymerization are most widely used. In these methods, the first two methods facilitate direct addition of polymer into LDH galleries and the third method facilitates insertion of monomers followed with polymerization in the galleries.

1.6.1 Solvent blending method

Solvent blending method is a two stage process. The first stage involves LDH exfoliation into single layers using a suitable solvent in which the polymer is soluble. Due to the weak forces that stack LDH layers, relevant solvent addition facilitates easy dispersion. Thereby in the second stage, the polymer addition was facilitated to the LDH solvent mixture which get absorbed onto the delaminated sheets. After subsequent period of processing, evaporation separates into a precipitate by removing the solvent. During this step, sheets reassemble and depending upon the extent of penetration, the sandwiched polymer would have either exfoliated or intercalated structure (Jamshidian et al., 2012; Du et al., 2007; Rahim et al., 2009). The schematic illustration of steps involved in solvent blending method is shown in Figure 1.3 (a).

1.6.2 Melt blending method

This method employs direct mixing of LDH inside the polymer matrix in the molten state or flow conditions. Under high temperature conditions, depending on the compatibility

between layer surface and the chosen polymer, the polymer chains spread from the molten mass, to the LDH galleries. Thereby, depending upon the degree of polymer penetration, the composite either has intercalated or delaminated structure. Due to not using organic solvents that pose environmental hazard issues, this technique is widely used in polymer industries (Wang et al., 2011b; Najafi et al., 2012; Du et al., 2007). A schematic illustration of steps involved in melt blending method is depicted in Figure 1.3 (b).

1.6.3 In-situ polymerization method

In-situ polymerization involves engorging of LDH in liquid monomer or monomer solution. This step facilitates polymer formation inside intercalated sheets. The polymerization is driven by heat or radiation or diffusion of a relevant organic initiator within the interlayer before monomer enlargement occurs. Toyota research team used the method to realize nylon 6 based nanocomposites from caprolactum (Wang et al., 2012; Song et al., 2007). A schematic of the in-situ polymerization method to depict various steps is shown in Figure 1.3 (c).

1.7 Structural classification of polymer nanocomposites

LDHs have received significant attention as nano reinforcements in the polymer matrix, due to its potential in enhancing the mechanical and thermal properties of the polymer. The extent to which the LDHs dispersed in polymer plays a key role in the improvement of the before mentioned properties.

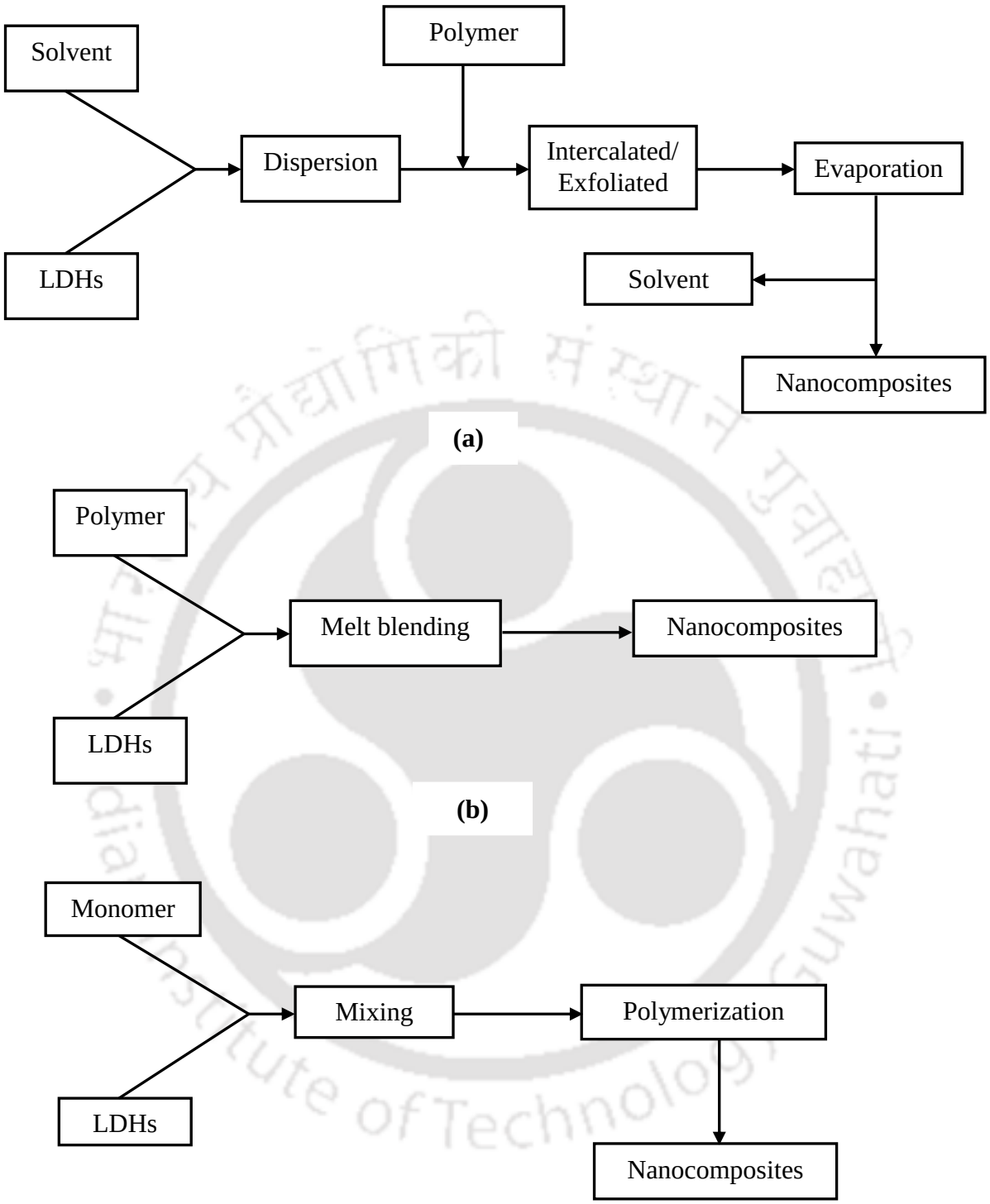

Figure 1.3: Schematic representation of preparation methods for polymer/LDH nanocomposites: (a) solvent blending method, (b) melt blending and (c) in-situ polymerization.

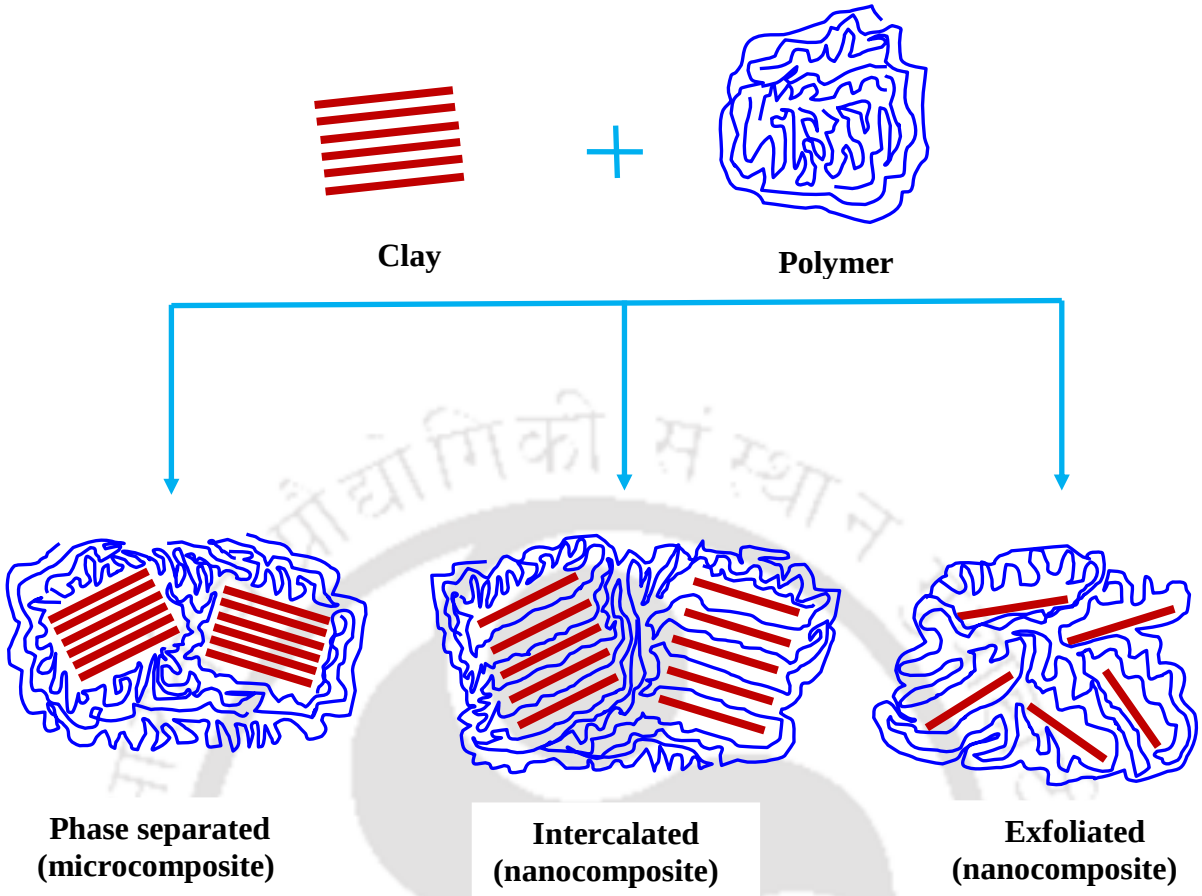

Figure 1.4: Phase dispersion in different types of polymer nanocomposites.

The level of dispersion of layered silicates usually depends upon the (i) interaction between the polymer and LDHs and (ii) preparation method through which the nanocomposite is synthesized. Therefore, based on the variation in the interaction between the polymer and the LDHs, as shown in Figure 1.4, three different structures of polymer nanocomposites are possible.

1.7.1 Exfoliated structure

The exfoliated nanocomposites are formed by extensive polymer penetration between the LDH interlayer's. In such structure, the ordered structure is diminished and the individual

platelets are randomly distributed in the polymer and diffraction peak cannot be detected by X-ray diffraction (XRD). This shows greater phase homogeneity than the intercalated nanocomposites. Usually, the LDH content of an exfoliated nanocomposite is much lower than intercalated nanocomposite. However, achieving exfoliation up to complete level is a challenging task in practical situations. Achieving exfoliated structures can lead to a profound enhancement in the mechanical and thermal properties of the polymer (Mittal et al., 2009; Morgan and Gilman, 2003).

1.7.2 Intercalated structure

Intercalated nanocomposites are formed when both matrix and reinforcing phase are compatible with each other so that few polymer chains penetrate between the LDH galleries. In this type of nanocomposite, ordered structure is preserved and diffraction peak move to left side (the diffraction peak shift to a lower angle ($2\theta^{o}$)) which can be detected by XRD analysis. Thereby, intercalation increases the basal spacing between the LDH layers (Mittal et al., 2009; Morgan and Gilman, 2003).

1.7.3 Phase separated structure

This type of morphology occurs when the interaction between the LDH and the polymer is quite low. Due to this, intercalation of the polymer between the LDH layers will not be achieved. The microcomposite, thus resulting in such circumstances is referred to as phase separated composite. The properties of such phase separated composites are rather hardly ever enhanced or would exhibit downturn after reinforcement (Mittal et al., 2009; Morgan and Gilman, 2003).

1.8 Targeted property enhancements in polymer nanocomposites

Typically, polymer nanocomposites constitute 1 – 10% of nanofiller on a weight basis. However, property enhancements would be similar to the values obtained for traditional composites prepared with 20 – 35% mineral or glass. Typical enhancements in nanocomposite properties are summarized as follows:

- Greater thermal stability.
- Excellent flame retardancy.
- Enhanced electrical conductivity.
- Enhanced mechanical properties such as strength, modulus and dimensional stability.
- Reduced gas, water and hydrocarbon permeability.
- Improved physical properties.
- Lower density and similar recyclability.
- Increased melt strength.

1.9 Applications of polymer nanocomposites

Over the past three decades, polymer composites received wide recognition in applications with a great percentage compared to other materials (Garces et al., 2000; Ahmadi et al., 2004; Kurahatti et al., 2010; Wei et al., 2011). Some of them are mentioned below.

- The major applications of the composite materials are as structures for military aircrafts and commercial airlines. Similarly, they have applications in marine, sports goods, textile and chemical industries.

- Several civil constructions require polymeric composite materials due to specific advantages of the same.
- With high flame retardant characterization parameter values, polymer composites can be used for high temperature applications (example: internal combustion engine).
- Polymer composite materials can be used to reduce fuel loss in the fuel tank and fuel line in cars.
- Various industrial applications of polymer composites have been reported. Apart from these, metallic sandwich panels have also been developed with polymer composites for structural applications.
- Improved gas barrier characteristics have enabled usage of nanocomposites in food packaging industry. Examples include packaging for confectionary, cheese, boil in the bag foods and processed meat. Extrusion coating application with paper board is used in fruit juice and dairy industry.
- Automotive and industrial applications are extensive. Mirror housing on various types of vehicle, engine cover and handles are few examples in this regard.
- Nano-level incorporation of fillers strongly influence transparency and haze characteristics of the polymeric films. For these, additional applications exist.
- Nanocomposites are used as impellers and blades for various applications such as vacuum cleaners. They are also used as cover for portable electronic equipment such as mobile phones.
- LDH based nanocomposites containing magnesium and aluminum is biocompatible and is used as an antacid and anti-pepsin agent.

- LDH based nanocomposites acts as soluble inorganic vector for different genes and deoxyribonucleic acid (DNA) biomolecules.

Figure 1.5 summarizes various potential applications of polymer nanocomposites (Garces et al., 2000; Ahmadi et al., 2004; Kurahatti et al., 2010; Wei et al., 2011).

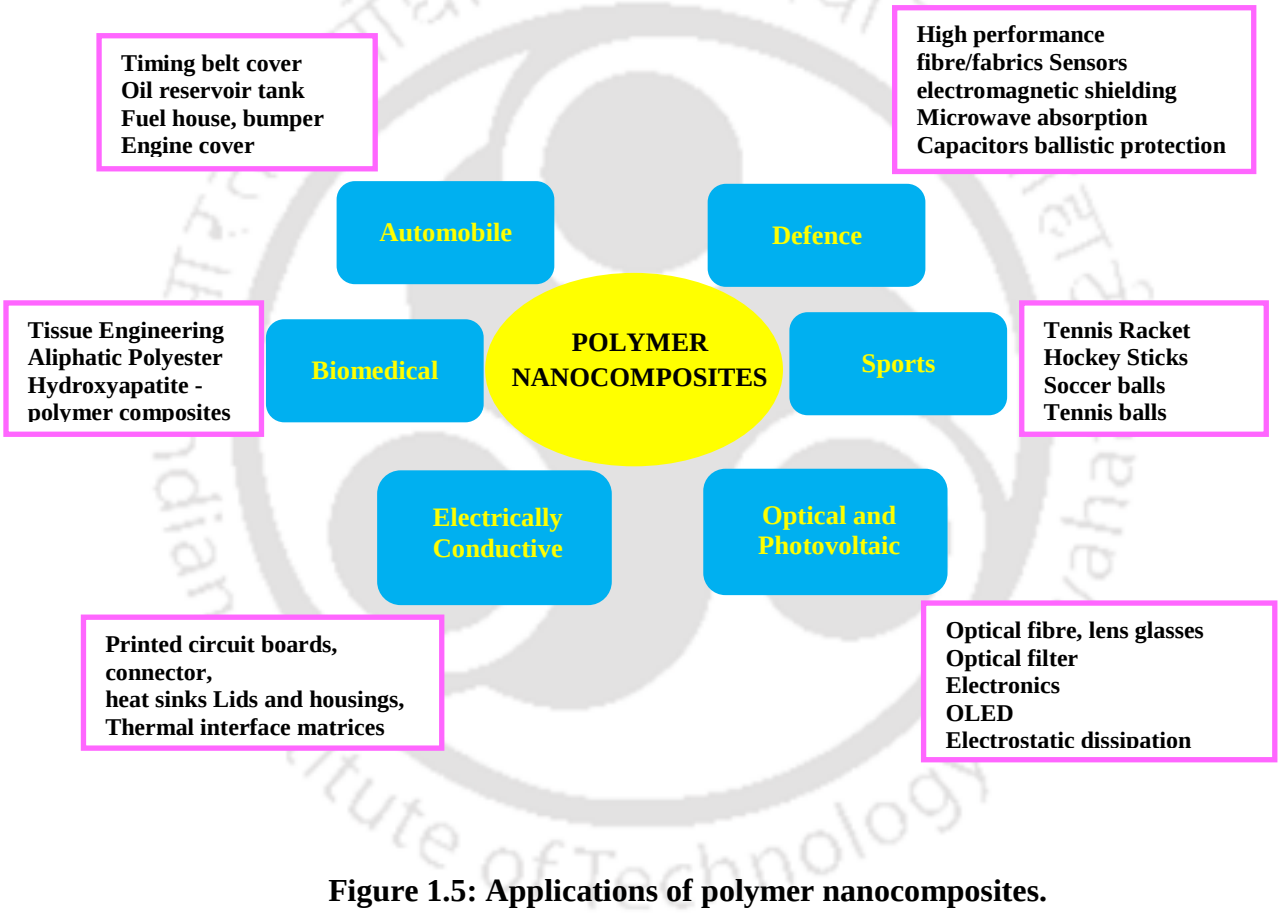

Figure 1.5: Applications of polymer nanocomposites.

1.10 State-of-the-art summary

The available state-of-the-art in polymer nanocomposites has been presented in four sub-sections namely, (a) Rheology of polymer solutions, (b) Polymer/clay nanocomposites, (c) Polymer/LDH nanocomposites and (d) Polymer and polymer nanocomposite gears.

1.10.1 Rheology of polymer solutions

A fundamental understanding of polymer rheology is necessary to develop relevant models for applicability in polymer processing operations to aid in process optimization and predict flow instabilities during process conditions. The available literature in this regard refers to rheology of polymer solutions, blends and other relevant materials.

Using rotational viscometer, Al-Fariss and Al-Zahrani (1993) studied rheological behaviour of dilute aqueous polymer solutions such as pusher 700, Rohagit F600 and Flocon 4800 CT. For the carried out experiments, the concentrations, temperature and applied shear rate were varied from 500 – 3000 ppm, 20 – 65 °C and 5.40 to 692.5 sec^{-1}. For both Newtonian and non-Newtonian liquids, the authors developed a correlation to predict polymer solution viscosity as a function of these independent variables. With a coefficient of fitness of 0.98 – 0.99, the developed model was evaluated to offer an average absolute error of 3.12, 8.54, 9.65% for solutions of pusher 700, Rohagit F600 and Flocon 4800 CT, respectively.

Silva et al. (2000) investigated rheological properties of polymer blend based on ethylene-octane copolymer and PP using an instrument, capillary rheometer and a rheometric dynamic stress rheometer. A non-Newtonian flow behaviour was observed for all polyethylene elastomer (PEE)/PP samples at high shear rates, and a Newtonian flow

behaviour at low shear rates. The rheological measurements indicated that PEE and PEE/PP blends possess different flow behaviour at low and high frequencies.

Ohta et al. (1994) conducted rheological studies of highly dilute solutions of very high molecular weight PE for applicability in gel spinning process. With an emphasis on the shear flow viscosity of the solutions, the authors found that for wider shear rates of 10^{-4} to 10^{3} sec^{-1}, such PE solutions possess shear thinning behaviour. Also, enhanced PE solution concentration indicated expected non-Newtonian behaviour by the system.

For aqueous poly-vinyl alcohol (PVA) solutions, Briscoe et al. (2000) evaluated rheological properties as a function of several factors such as degree of polymer hydrolysis, temperature, pressure and electrolyte concentration. The authors concluded that the rheology of PVA solutions is primarily dependent on relative strength of hydrogen bonding that exists between polymer chains and water molecules but not inter and intra chain hydrogen bonding. It has been further delineated that the variation in the independent variables has brought forward variations in the alternate hydrogen bonding mechanisms and thereby contributes to variations in the rheological properties of the system.

The flow behaviour of urethane oils that were prepared with alternate reactant ratios was investigated by Guner et al. (2004). Their investigations involved determination of polymer solution viscosities at various temperatures. The authors inferred that toluene diisocyanate (TDI) polymer solutions exhibited non-Newtonian behaviour and poly (1,4-butandiol) tolylene 2,4-diisocyanate (PBTDI) terminated prepolymer solutions behaved as Newtonian fluid. For all cases, Erickson's equation has been evaluated to be relevant to predict viscosity variation with concentration. Bingham, Power law and Casson models were tested for their fitness to represent measured viscosity and shear rate data. The authors finally

inferred that for industrial application, polymer solution prepared with higher TDI ratio is applicable as a formulation for high solid coating.

Al-Fariss (1987) studied rheological behaviour of Saudi medium oils using HAKKE (Rotovisco model RV-12) viscometer. The author evaluated that the non-Newtonian fluid viscosity variation is a function of both temperature and shear rates. Power law model provided good fitness with respect to consistency coefficient and flow behaviour index determination for measured shear stress and shear rate data.

The rheological properties of pectin, starch, xanthan, and carrageenan solutions were evaluated by Marcotte et al. (2001) using rotational viscometer in the temperature and shear rate range of 20 – 80 °C and 0 – 300 sec^{-1}. For starch and pectin systems, Power law model was evaluated to fit well with measured shear stress and shear rate data. However, for carrageen and Xanthus systems, Hershel-Bulkley model was relevant to fit well for measured data. Also, the evaluated constants for various models indicated sensitivity of these parameters with respect to variations in temperature and concentration.

1.10.2 Polymer/clay nanocomposites

The vast research carried out till date in the field of polymer/clay nanocomposites primarily targets upon replacing inorganic cations in the interlayers of layered silicate with organic cations possessing alkyl chains (Krikorian et al., 2003; Mittal et al., 2009; Raquez et al., 2013). This step attempts to enhance affinity and bonding between layered silicate and polymer due to presence of organic cations possessing alkyl chain that increase distance between silicate interlayers. With this effect, a superior dissemination of polymeric chains occurs inside the galleries.

Adopting solution intercalation method, Paul et al. (2013) prepared PS/clay laponite nanocomposites. The authors evaluated upon the effect of nanoclay content (2 – 10 wt.%) on structural and thermal properties of the nanocomposite. The XRD studies indicated that 2 and 5 wt.% laponite clay containing PS nanocomposites possessed a combination of both exfoliated and intercalated clay structures. Compared to pure PS, the nanocomposite thermal degradation temperature was 29 °C higher.

Limpanart et al. (2005) used melt intercalation method to fabricate PS/organoclay nanocomposites. Two different kinds of organoclay (D1805 and D1820) were prepared by cation exchange reaction process and were used with constant nanofiller (2 wt.%) loadings. The d-spacing value of the D1805 and D1820 were determined using Bragg's equation as 2.9 nm and 3.8 nm, respectively. The d-spacing enhanced for PS/D1805 nanocomposite (from 2.9 to 4.3 nm) and PS/D1805 nanocomposite (from 3.8 to 3.9 nm). This indicated intercalated and phase separated organoclay layers in the structure. The Transmission electron microscopy (TEM) micrographs indicated that the D1805 and D1805 were intercalated and phase separated in the PS matrix.

The PS/organoclay nanocomposites were investigated by Jang and Wilkie (2005). The authors synthesized PS nanocomposites by adopting bulk polymerization of organoclay modified with dimethylbenzyl hydrogenated tallow chloride. The XRD study conveyed that the d-spacing of clay layer enhanced from 1.1 nm (pristine clay) to 2.1 nm for organically modified clay and reached upto 3.8 nm for bulk polymerized nanocomposite. Thereby, it is apparent that PS nanocomposite possessed intercalated morphology. Also, the peak heat release rate (PHRR) has been evaluated to decrease with increasing clay content (55% reduction in the value for 5% nanofiller loaded nanocomposite in comparison with pristine

PS). The thermo gravimetric analysis (TGA) results also indicated improved thermal degradation temperature for the PS/organoclay nanocomposite in comparison with the virgin PS.

Zhang et al. (2003) incorporated organically modified clay in the PS polymer using γ-ray irradiation technique. Four different organoclay modifiers (three reactive groups and one non-reactive group) were investigated by the authors. The Fourier transmission infrared spectroscopy (FTIR) results exhibited characteristic peaks at 1720 cm^{-1} (C=O stretching) and 2919 cm^{-1} (C-H stretching) for all clays (MSABM, MOABM, MHABM and HABM). Both XRD and TEM analyses confirmed upon the presence of intercalated nanocomposite (PS/HABM) and exfoliated nanocomposites (PS/MSABM, PS/MOABM, PS/MHABM) structures in the PS nanocomposite samples. From the TGA analysis, it was confirmed that PS/MSABM, PS/MOABM, PS/MHABM nanocomposites samples have higher thermal stability than the PS/HABM nanocomposites.

PS/organomodified montmorillonate (OMMT) nanocomposites were fabricated using extruder machine and melt intercalation process by Zidelkheir et al. (2006). In the processes the authors allowed ion exchange of algerian montmorillonite using octadecylammonium cation. Nanocomposite characterization was conducted using XRD, TEM, differential scanning calorimetery (DSC), TGA, rheology and tensile measurements. The XRD spectra and TEM micrographs confirmed micro structure of PS/OMMT composite with 2 wt.% OMMT loading. However, for higher OMMT loading, a partial intercalated structure was existent. In summary, nanocomposite with 5 wt.% nanofiller loading provided highest thermal stability. The storage modulus (G′) and loss modulus (G″) values for the nanocomposites

increased with OMMT loading and indicated higher rheological and mechanical properties of the nanocomposites with respect to pure PS.

Bourbigot et al. (2004) adopted bulk polymerization technique for the preparation of organically modified clay reinforced PS composite materials. The authors observed that the material thermal stability increased with increasing clay content. In comparison with the virgin PS, the degradation temperature enhanced by 50 °C for the nanocomposite. The kinetic analysis of the PS nanocomposite simulated in a cone calorimeter indicated that the PHRR is half of that of virgin PS. There by, the authors conveyed that clay serves as char promoter and reduces degradation rate due to functioning as a protective barrier in the material.

MMT was organically modified with sodium dodecylsulfonate (a-MMT) and octadecylammonium (c-MMT), respectively, and reinforced in the PS matrix through melt compounding method (Wang et al., 2009). The incorporation of a-MMT and c-MMT in the PS matrix enhanced the thermal properties. At 10% weight loss, the PS/c-80MMT and PS/c-100MMT nanocomposites demonstrated 17 °C and 11 °C, enhancement respectively in the thermal degradation temperature as compared to neat PS. It was observed that the addition of modified MMT in the blend exhibited enhanced flammability of the nanocomposites.

Kim et al. (2003) prepared PS/OMMT nanocomposites using solvent casting method and chloroform solvent. XRD studies confirmed intercalation of OMMT in the PS matrix. The onset degradation temperature of the nanocomposite was shifted to a higher temperature due to the incorporation of the clay. Further, glass transition temperature (T_g) value for the nanocomposite increased linearly with nanofiller loading in the nanocomposite. The rheological measurements also confirmed increased viscosity (η) with increasing OMMT

loading. Also, the storage and loss moduli of PS/OMMT nanocomposites increased monotonically with OMMT loading for all frequencies.

Wang and Zhang (2007) carried out investigations to evaluate upon the influence of commercial organophilic montmorillonite (Claytone APA) on the characterization parameters of in-situ polymerization based PS nanocomposites. The XRD analysis confirmed exfoliated and intercalated structures in the nanocomposite material. For 50% weight loss reference point, the thermal decomposition temperatures of PS, 1, 2 and 4 wt.% clay containing PS samples were evaluated as 416, 437, 440 and 444 °C, respectively. Also, G′ and G″ values enhanced with enhanced organoclay content in the nanocomposites.

Uthirakumar et al. (2005a) prepared high impact polystyrene (HIPS) based MMT nanocomposites with 1 – 5 wt.% nanofiller loading. In-situ polymerization was adopted by the authors to prepare nanocomposites which were subsequently analysed for structural and thermal properties. XRD analysis confirmed complete disappearance of MMT layer peaks in the nanocomposites. TEM images exhibited well dispersion of MMT layers in the polymer matrix. HIPS nanocomposite synthesized with 5 wt.% MMT exhibited 18 °C enhancement in thermal stability with respect to pristine polymer. The T_g values for pristine PS and 5 wt.% MMT loaded nanocomposite were 98.8 and 101 °C, respectively. Also, clay content has been analyzed to significantly enhance Young's moduli with 53% enhanced in the Young's modulus for 5 wt.% HIPS/MMT-5 in comparison with the pristine polymer.

Okamoto et al. (2000) prepared PMMA and PS nanocomposites using lipophilized smectic clay by in-situ free radical polymerization method. The clays were modified with two different modifiers i.e. oligo- (oxypropylene)-, diethyl-, methyl-ammonium chloride (SPN), and methyl-trioctil-ammonium chloride (STN). The d-spacing of these nanocomposites was

examined by XRD and TEM analysis. The d-spacing for the solid SPN and STN obtained by XRD measurements were 4.20 and 1.81 nm, respectively. The XRD results conveyed intercalated structures for PMMA nanocomposites, which were further confirmed by the TEM images. It was also noted that the flocculation takes place owing to the hydroxylated edge-edge interaction of silicate layers. In the glassy region below glass transition temperature, compared to pristine PS, the storage modulus was 57% and 34% higher for PS/SPN and PMMA/STN nanocomposites.

Using solvent co-precipitation method, Fu et al. (2006) prepared PMMA/clay nanocomposites that were deployed eventually for microcellular foams. The effect of nanoclay content on the mechanical characterization parameters of nanocomposite foams were focussed by the authors. PMMA nanocomposite containing 0.5 wt.% clay exhibited significant enhancement in mechanical properties such as elastic modulus, tensile strength, elongation at break, which were evaluated to increase by 24, 54 and 97% respectively with respect to the pristine PS. Beyond this extent of nanofiller loading, the mechanical properties reduced. This is possibly due to excessive agglomeration of nanoclay in the PS matrix which enhanced stress concentration in PMMA matrix.

Yamagata et al. (2012) adopted solution intercalation method to prepare PMMA/OMMT nanocomposites. Two different kinds of OMMT (NZ70 and NX) modified with quaternary alkylammmonium ions were reinforced into the PMMA matrix to prepare the nanocomposites. From the XRD results, it was found that the peak related to d_{001} was shifted to lower 2θ value. This conveys partial exfoliation of silicate layers in the structure. The TEM images also exhibited that clay layers were well dispersed in the polymer matrix although some aggregates were also noticed. With increasing OMMT content in the nanocomposite,

the flexural modulus increased and reached a maximum value for 4 wt.% OMMT in the nanocomposite material. Similarly, toughness also enhanced for NX containing nanocomposites and especially for 1 and 2 wt.% OMMT loaded nanocomposites. This is due to stress transfer to the platelets of silicate layers and shear deformation. Thus, NX possessing highly hydrophobic quality has been critically reasoned to contribute towards PMMA/OMMT nanocomposites.

Unnikrishnan et al. (2011) prepared melt-extrusion based organically modified nanoclay PMMA nanocomposites. Three different organoclay modifiers with varying hydrophobicity (single tallow vs. ditallow) were investigated by the authors. Both XRD and TEM analyses affirmed upon the existence of partially intercalated and exfoliated nanocomposites structures in the nanofiller reinforced PMMA matrix. For 50% weight loss reference point, the TGA analyses suggested that thermal stability was enhanced by 3 to 16 °C. Compared to the pure PMMA, the activation energy improved by 23 kJ/m for PMMA/C30B nanocomposite sample. The reinforcement also led to the improvement in the tensile modulus by 36% for PMMA/3% C10A sample. However, lower tensile strength and impact strength were obtained for all the compositions. The order of various materials with respect to burning rate is as follows: PMMA/C93A > PMMA/C10A > PMMA/C30B > PMMA.

Valandro et al. (2013) prepared PMMA/MMT nanocomposites by using in-situ polymerization with ethanol and acetonitrile as solvents. Two kinds of organomontmorillonite (SWy-1-C8-Mt and SWy-1-C16-Mt) were prepared by ion-exchange process and were used with various loadings (1, 3 and 5%). The XRD results demonstrated that intercalated as well as exfoliated structures exist in the prepared nanocomposites. Also, the structural morphology

of the nanocomposites has been evaluated to be strongly influenced with clay loading and used solvent. Various nanocomposites were exposed to Ultra Violet (UV) light at 40 °C for photo-oxidative degradation followed by size exclusion chromatographic (SEC) analysis. After 15 – 20 h of irradiation, significant decrement in number average molecular weight was evaluated for various nanocomposite compositions. The SEC suggested that pure PMMA and nanocomposites underwent degradation due to random chain scissions. It was also found that most of the samples prepared in acetonitrile exhibited lower values of coefficient associated to degradation rate. However, the same value has been six times higher for pure PMMA. Also, nanocomposites with higher nanofiller content exhibited slower oxidation rates.

Using surface modified clay material, Sharma and Nayak (2009) prepared melt intercalation based PP nanocomposites in a twin-screw extruder. The authors examined upon the role of clay content on the thermal and mechanical characterization parameters of the nanocomposites. The PP/OMMT-11 (3 wt.%) displayed an increment in the thermal degradation temperature with a maximum degradation temperature of 33 °C higher than that of the neat PP. Similarly, compared to neat PP, the PP/OMMT-11 nanocomposite indicated 2.3 °C improvement in the T_g value. The reinforcement also led to the improvement in Tensile strength and Tensile modulus by 17% and 32%, respectively, as compared to neat PP.

Goad (2011) adopted two step melt compounding process and prepared PP/clay nanocomposites for rheological investigations. The rheological measurements were carried out using ARES-rheometer in a dynamic mode at 220 °C. The incorporation of clay into the PP matrix enhanced storage modulus and viscosity of the nanocomposite. Due to this, the rheological behaviour of the nanocomposite was significantly different than that of the PP polymer.

Using dimethyldioctadecylammonium modified MMT, PP nanocomposites had been prepared by Mittal (2008). The authors conducted structural, mechanical and gas permeation studies for the prepared nanocomposites. The XRD results elucidated that all nanocomposites exhibited intercalated structures. Compared to the PP, the PP/OMMT nanocomposite possessed 33% higher tensile modulus. The nanocomposite possessed 33% lower permeability coefficient than the PP. These indicated good dispersion of OMMT in the PP matrix as well as high aspect ratio.

Zhao et al. (2005) prepared melt compounding based PE/clay nanocomposites. The TEM analysis confirmed that PE/JS 5 nanocomposites have partially exfoliated nanocomposites. This is due to the fact that while exfoliated clay layers exist, some aggregates of clay layers were still existent in the PE matrix. For various samples such as pure PE, PE/JS 2, PE/JS 10, PE/JS 15, the onset temperatures were 428.0, 461.5, 453.5, 450.5, and 451.0 °C, respectively and these indicate that nanocomposites have higher onset temperature than the PE. The maximum degradation temperature (T_{max}) were 484, 492, 491, 484, and 479 °C for pure PE, PE/JS 2, PE/JS 5, PE/JS 10, and PE/JS 15 samples, respectively. The PE/JS 2 nanocomposite sample exhibited 54% lower peak heat release rate in comparison with pristine PE.

Clay was organically modified with dimethyldialkylammonium halide and reinforced in the PE through melt compounding method by Gopakumar et al. (2002). The XRD analyses identified intercalated structure of PE nanocomposites. The crystallization temperature of PE/clay (5%) sample was also enhanced by 6 °C. The addition of 5 wt.% modified clay to PE resulted in a 9% increase in Young's modulus over unfilled PE.

Organoclay modified with butyltriphenylphosphonium, were synthesized by Suin et al. (2014). Thereafter, the modified clay were dispersed in the PC matrix via solution blending approach and the effect of various loadings of modified clay on the thermal and mechanical properties of PC was investigated. The XRD revealed destruction of the ordered geometry of aluminosilicate layers in the nanocomposites. However, from direct visualization through TEM, a discernible amount of clay was found to be localised in PC matrix. The presence of modified clay in the PC matrix enhanced the T_g by 4 °C as compared to pure PC. The tensile strength and Young modulus of pure PC was increased by 50% and 40%, respectively, on incorporating 0.5 phr clay into the PC polymer. The dynamic mechanical analysis (DMA) revealed that the storage modulus increased in both glassy and rubbery region with an increase in clay loading in the nanocomposites.

Chang et al. (2003) prepared two different organo clays such as MMT and fluorinated mica modified with hexadecylamine (C16-MMT and C16-mica). Thereafter, the respective clays were dispersed in the poly(lactic acid) (PLA) matrix via solution casting approach and the effect of various loadings of clays on the thermal and mechanical properties of PLA was investigated. Considering 2% weight loss as a reference point, it was found that the thermal degradation temperature of the nanocomposites (with 8 wt.% loading) shifted to lower temperature with a maximum offset value of 49 °C for C16-MMT and 16 °C for C16-mica. The enhancement in the tensile strength by 32% and 57% was obtained for C16-MMT and C16-mica reinforced PLA nanocomposites (4 wt.% clay), respectively. With further increase in loading, both nanocomposites exhibited reduced tensile properties. This is due to the agglomeration of clay nanoparticles that resulted in improper dispersion. For the case of tensile modulus, PLA/C16-mica nanocomposites exhibited three fold enhancements in

comparison with the PLA. The possible reasons for the same were good orientation of the filler in the PLA matrix and high aspect ratio of the layered mica.

Ray et al. (2002) investigated upon the effect of variant modified MMT clay loadings in PLA matrix based nanocomposites that were prepared using melt extrusion method. TEM analysis revealed upon intercalation of silicate layers with PLA and random distribution of MMT clay in the PLA matrix. It was evaluated that the storage modulus increased with MMT loading (3 – 7 wt.%). Compared to PLA, the storage modulus of the nanocomposite was higher by about 33 – 140%.

A brief summary of the available state-of-the-art in polymer/clay nanocomposites is presented in Table 1.1.

Table 1.1: Literature summary for polymer/clay nanocomposites.

Authors	Polymer matrix	Nanofiller	Modifier	Method of preparation	Remarks
Paul et al., 2013	PS	clay laponite	cetyltrimethyl ammonium bromide	solution intercalation technique	• Exfoliated and intercalated structure obtained. • Thermal stability was enhanced by 29 °C.
Limpanart et al., 2005	PS	organoclay (D1805 and D1820)	Na-bentonite	melt intercalation method	• Intercalated and separated structure obtained • The total weight loss of D1805 and D1820 organo clay in the temperature range of 100 – 550 °C, due to the surfactant are around 24% and 46%, respectively.
Jang and Wilkie, 2005	PS	organoclay	dimethyl benzyl hydrogenated tallow chloride	bulk polymerization technique	• Intercalated structure as suggested by XRD. • PHRR was reduced for PS nanocomposites containing 5 wt.% organoclay. • Thermal stability found maximum at 5 wt.% loading.
Zhang et al., 2003	PS	clay	hexadecyltrimethyl ammonium bromide (HAB)	γ-ray irradiation technique	• Intercalated and exfoliated strictures were confirmed by XRD and TEM.

Authors	Polymer matrix	Nanofiller	Modifier	Method of preparation	Remarks
Zidelkheir et al., 2006	PS	OMMT	octadecylammine	melt intercalative compounding	• Intercalated and exfoliated structure was confirmed by XRD and TEM. • At 10% weight loss, thermal degradation temperature was enhanced by 4 to 16 °C. • T_g was enhanced by 3.3 to 4 °C.
Bourbigot et al., 2004	PS	clay	N-N-dimethyl-n-hexadecyl (4-vinylbenzyl) ammonium chloride	bulk polymerization technique	• Thermal stability enhanced by 50 °C.
Wang et al., 2009	PS	clay	i) sodium dodecylsulfonate ii) octadecylammonium	melt blending method	• At 10% weight loss, thermal degradation temperature enhanced by 17 °C.
Kim et al., 2003	PS	clay		solvent casting method	• Intercalated structure was confirmed by XRD. • Thermal degradation temperature and T_g enhanced for composites. • The G′ and G″ values increase as the content of clay increase.
Wand and Zhang, 2007	PS	clay		in-situ polymerization	• Intercalated and exfoliated structures were confirmed by XRD. • At 50% weight loss, thermal degradation temperature enhanced by 28 °C.

Authors	Polymer matrix	Nanofiller	Modifier	Method of preparation	Remarks
Uthirakumar et al., 2005a	HIPS	clay	ABTBA	in-situ polymerization	• Exfoliated structure obtained as suggested by TEM. • Thermal degradation temperature was enhanced by 18 °C. • T_g was enhanced by 2.6 °C. • Young modulus was increased by 53%.
Okamoto et al., 2000	PMMA and PS	smectic clay	oligo-(oxypropylene)-, diethyl-, methyl-ammonium chloride (SPN) and methyl-trioctil-ammonium chloride (STN)	free radical polymerization	• Intercalated structure obtained as suggested by XRD and TEM. • G′ was enhanced for PMMA (34%) and PS (57%) based composites.
Fu et al., 2006	PMMA	clay		solvent co-precipitation method	• Elastic modulus, tensile strength, elongation at break increased by 24%, 54% and 97%, respectively.
Yamagata et al., 2012	PMMA	OMMT	quaternary alkylammonium ions	solution intercalation method	• Partially exfoliated structure obtained. • Flexural modulus was found to be maximum at 4 wt.%.
Unnikrishnan et al., 2011	PMMA	Cloisite 30B, Cloisite 10A and Cloisite 93A	methyl tallow bis-2 hydroxyethyl quaternary ammonium salt	melt intercalation	• Partially exfoliated structure obtained by TEM. • Tensile modulus was enhanced by 36% for PMMA/C10A composite. • At 20% weight loss, thermal stability was enhanced by 3 to 16 °C.

Authors	Polymer matrix	Nanofiller	Modifier	Method of preparation	Remarks
Valandro et al., 2013	PMMA	OMMT	octyltrimethylammonium bromide (C8) and hexadecyltrimethylammonium bromide (C16)	in-situ polymerization	• Number average molecular weight was significantly reduced after 15 – 20 h, when exposed to UV light.
Sharma and Nayak, 2009	PP	clay	P-aminobenzoic acid	melt intercalation method	• Thermal stability was enhanced by 33 °C for PP/OMMT-II (3 wt.%). • Maximum degradation temperature increased by 31 °C for PP/OMMT-II (3 wt.%). • Tensile strength and tensile modulus enhanced by 17% and 32%, respectively.
Goad, 2011	PP	clay		melt intercalation method	• The storage modulus and viscosity are found to be increased with the incorporation of clay into PP.
Mittal, 2008	PP	clay	dimethyldioctadecyl ammonium	melt intercalation method	• Intercalated structure obtained. • Tensile modulus was increased by 33%.
Zhao et al., 2005	PE	clay	dio-actadecyldimethyl ammonium chloride	melt compounding method	• Partially exfoliated morphology obtained. • Thermal degradation temperature was improved by 23 °C for PE/JS 15 nanocomposites. • T_{max} improved by 8 °C for PE/JS 2 nanocomposites. • The PHRR of the PE/JS 2 nanocomposite was reduced by 54%.

Authors	Polymer matrix	Nanofiller	Modifier	Method of preparation	Remarks
Gopakumar et al., 2002	PE	clay	dimethyldialkyl-ammonium halide	melt compounding method	• Intercalated structure was confirmed by XRD. • Crystallization temperature enhanced by 6 °C. • Young modulus was increased by 9%.
Suin et al., 2014	PC	clay	butyltriphenyl-phosphonium	solution blending	• Exfoliated structure was confirmed by XRD and TEM. • T_g enhanced by 4 °C. • The Tensile and Young modulus enhanced by 50% and 40%, respectively.
Chang et al., 2003	PLA	C16-MMT, C16-Mica	hexadecylamine	solution intercalation method	• Initial degradation temperature decreased by 49 °C and 16 °C for PLA/C16-MMT-8 and PLA/C16-Mica-8 composites, respectively.
Ray et al., 2002	PLA	OMMT		melt extrusion method	• G′ and G″ of the nanocomposites increased with increasing OMMT content (3 – 7 wt.%).

1.10.3 Polymer/LDH nanocomposites

Using in-situ bulk polymerization method, Tai et al. (2011) reinforced Mg-Al LDH (1 – 5 wt.%) into PS polymer matrix and evaluated their structural and thermal characteristics. XRD results demonstrated that exfoliated and intercalated structures were obtained for different nanocomposites. TGA studies conveyed that, for 10% weight loss reference point, the thermal degradation temperature increased by 19 – 34 °C for the nanocomposites in comparison with the PS polymer. Similarly, the T_g increased by 3 °C for 5 wt.% loaded Mg-Al LDH containing PS nanocomposites in comparison with pristine PS. The LDH loading also reduced marginally the PHRR with increasing LDH loading content in the nanocomposite.

The PS nanocomposites were prepared using Mg-Al LDH by in-situ free radical bulk polymerization (Botan et al., 2012). The Mg-Al LDH were modified with sodium dodecyl sulfate (SDS) modifier. The XRD results elucidated that all nanocomposites exhibit exfoliated structures. At 20% weight loss reference point, the pure PS exhibited a degradation temperature of 391 °C, which increased to 400, 402, 404 and 408 °C for 0.5, 1, 3 and 5% LDH loaded PS nanocomposites, respectively. All nanocomposites exhibited enhanced flammability or fire resistance property in comparison with pure PS. The PS nanocomposite containing 5 wt.% LDH possessed highest percentage of LDH burned 50.61% lower than the pure PS.

Qiu and Qu (2006) prepared PS/LDH nanocomposites using soap-free emulsion polymerization (SFEP) method. XRD and TEM analyses indicated homogeneous inorganic LDH layer distribution in the polymer matrix. For 3 wt.% loss reference point, the PS/LDH

nanocomposite decomposition temperature of 329.6 °C was 53.3 °C higher than that of the virgin PS (276.3 °C).

Qiu et al. (2005) fabricated exfoliated PS/Zn-Al LDH nanocomposites using solution intercalation method. Both XRD and TEM analysis confirmed exfoliated and intercalated structures for PS/Zn-Al LDH 5 and PS/Zn-Al LDH 20 nanocomposites, respectively. For 50% weight loss reference point, the 5 wt.% and 20 wt.% Zn-Al LDH containing nanocomposites possessed respectively 30 °C and 17 °C higher temperature than that of the pure PS. The exfoliated nanocomposites possessed higher thermal stability than intercalated nanocomposites.

The role of N-lauroyl-glutamate (LG) surfactants were examined during exfoliated PS/Zn-Al LDH nanocomposite fabrication by Ding and Qu (2005) via emulsion polymerization. For the different nanocomposites, XRD and TEM analyses affirmed exfoliated and intercalated structures. Zn-Al LDH possessing samples confirmed LG presence by indicating peaks corresponding to C-H stretching vibration at 2957, 2923, 2853 cm^{-1}. For 50 wt.% loss comparison point, the decomposition temperature of exfoliated PS/Zn-Al LDH nanocomposite with 5 wt.% LDH was 28 °C higher than that of the pristine PS.

Matusinovic et al. (2012) prepared Ca-Al LDH based PS nanocomposites using in-situ bulk polymerization method. Both XRD and TEM analysis confirmed exfoliated structure for PS/Ca-Al LDH 5 nanocomposites. Nanocomposite possessing highest Ca-Al LDH loading (10 wt.%) possessed highest thermal decomposition temperature of 434 °C, which is 10 °C higher than the pristine PS. The PHRR for pristine PS and PS/Ca-Al LDH nanocomposites containing 10 wt.% of LDH was found to be 1587 kW/m^2 and 926 kW/m^2, respectively.

Emulsion and suspension polymerization based PS/Zn-Al LDH nanocomposites were prepared by Ding and Qu (2006a). Even for 10 and 20 wt.% Zn-Al LDH loadings, the nanocomposites possessed completely exfoliated morphology. FTIR spectra confirmed upon the existence of various functional groups in the nanocomposites with stretching vibration of sulphate of SDS found at 1218 and 1247 cm^{-1}. For 50 wt.% loss comparison point, the 5 wt.% Zn-Al LDH nanocomposite possessed higher decomposition temperature of 411.8 °C. Incidentally, for pure PS, the corresponding value was 383.8 °C. The thermal degradation temperatures of the PS/LDH samples with 5 wt.% Zn-Al LDH loading is 28 °C higher than that of PS polymer.

Ding and Qu (2006b) studied structural, thermal and mechanical properties of PP/Zn-Al LDH and PP/MMT nanocomposites. These materials were fabricated with melt-intercalation technique. XRD and TEM studies confirmed that PP/LDH nanocomposite possesses exfoliated structure with well dispersed Zn-Al LDH layers at molecular level in the PP polymer. The TGA and DMA analysis indicated higher thermal stability of PP/LDH nanocomposites in comparison with PP/MMT nanocomposites and pristine PP polymer and this was especially relevant in the higher temperature range. The XPS and FTIR analysis confirmed that the photo-oxidation mechanism of PP in the PP/LDH nanocomposite was significantly lower than that existent in the PP/MMT and PP samples and this confirms better UV stability of the former nanocomposite samples.

The thermal degradation behaviour of PP/organically modified Co-Al LDH (PP/Co-Al LDH) was studied via TGA analysis by Wang et al. (2011b). The PP/Co-Al LDH nanocomposites were prepared with melt compounding process. For the samples, Friedman and Flynn-Waal-Ozawa methods were used by the authors to determine thermal degradation

activation energy values. The authors also investigated upon the role of nanofiller content (1.5 – 6 wt.%) on the thermal properties of nanocomposites. For the nanocomposites, it was clearly apparent that activation energy values were higher than that of the pure PP for same weight loss reference points. Both methods have successfully demonstrated similar trends in activation energy variations with variations in conversion (α).

Wang et al. (2012) prepared 0.5 – 16 wt.% LDH containing PP nanocomposites using onstep reverse micro-emulsion method. For 50 wt.% reference point, the thermal stability of Mg-Al-DD LDH loaded PP possessed higher temperature than the pure PP. With respect to nanofiller content, the 50 wt.% decomposition temperature was 336 °C for pure PS which eventually increased to 384 ^{o}C for 1 wt.% nanofiller sample and reduced to 340 °C for 16 wt.% nanofiller sample. For 1 wt.% nanofiller sample, recrystallization and melting temperatures were higher than 6.7 °C and 2.5 °C, respectively than those obtained for the pure PP. Melt rheology studies conveyed that the nanocomposites possess reduced G′ and G″ values for lower LDH loaded samples (less than 2 wt.%). This was due to increased mobility of confined polymer chains at the PP-LDH interface. For further increase in LDH loading from 2 – 16 wt.%, both storage and loss moduli increased consistently. For PP/LDH nanocomposites, upto 1.5 wt.% of LDH, damping factor increased with increasing LDH loading and eventually reduced for further enhancement in LDH loading. This was due to restriction in the relative motion of polymer chains that was brought forward by the LDH nanoparticles in the polymer matrix and making the structure stiffer than the earlier scenario. The complex viscosity trends followed similar trends obtained for storage and loss modulus of PP/LDH nanocomposites.

The disorderly exfoliated PMMA/LDH nanocomposite was prepared by in-situ bulk polymerization (Wang et al., 2006). The nanocomposite tensile modulus increased with increasing LDH-U loading in the sample. An increase of LDH-U content from 3 to 5 wt.% enhanced the tensile modulus from 38% to 80% (1.38 GPa to 1.8 GPa). For 50 wt.% loss as reference point, the thermal decomposition temperatures for PMMA nanocomposite samples containing 5 wt.%, of LDH was about 90 °C higher than that of pristine PMMA. The DSC analysis indicated 22 °C higher T_g for the same sample with respect to pristine PMMA. The degradation process activated energy for pristine PMMA was 160 kJ/mol which increased to 200 – 240 kJ/mol for the disorderly exfoliated nanocomposite samples.

Adopting exfoliation/adsorption process, Li et al. (2003) prepared PMMA/Mg-Al LDH nanocomposites. For 10% weight loss taken as the reference point for comparison, the decomposition temperature was 140 and 288.5 °C for pristine PMMA and PMMA/LDH nanocomposite, respectively. The temperature corresponding to the maximum rate of weight loss of pristine PMMA and PMMA/LDH nanocomposite were 367.2 °C and 337.2 °C, respectively.

The effect of organic modification of LDH on PMMA nanocomposite properties was investigated by Nyambo et al. (2009). The organic treatment of LDH helped to improve structural, thermal and fire retardancy properties of the nanocomposite samples. TEM micrographs conveyed that nanocomposites formation was apparent in modified LDH, whereas unmodified MgAl-CO_3, MgAl-NO_3 and calcined LDH gave micro-composite structure. Unmodified Mg-Al CO_3, Mg-Al NO_3 and calcined LDH gave only 30% reduction in PHRR value of its composites. On the other hand, organic modification of MgAl-CO_3 gave 51% reduction in PHRR value of its nanocomposites. This analysis clearly indicated organic

modification of LDH facilitated improved fire retardant property. The TGA analysis also provided similar trends with higher thermal decomposition temperature value for PMMA/organomodified Mg-Al LDH samples in comparison with PMMA samples.

Manzi-Nshuti et al. (2009) prepared PMMA/LDH nanocomposites using bulk polymerization method. LDHs investigated by the authors include calcium aluminium undecenoate LDH (Ca_3Al LDH) and calcium iron undecenoate LDH (Ca_3Fe LDH) which were prepared by the co-precipitation method. Exfoliated structures of the nanocomposites were confirmed during XRD studies. TEM studies conveyed that at lower magnification, PMMA/Ca_3Fe LDH 5 nanocomposite structure involved agglomeration in polymer matrix. The higher magnification conveyed that LDHs did not exist as individual layers but as groups. The TEM analysis of other PMMA/Ca_3Al LDH nanocomposites conveyed mixed morphology of both intercalated and exfoliated structures. For 50 wt.% loss reference point, in comparison with PMMA, the thermal decomposition temperature of PMMA/Ca_3Al LDH 10 and PMMA/Ca_3Fe LDH 10 nanocomposites were higher by 33 and 38 °C respectively. Compared with pure PMMA, the lowest PHRR was recorded for 10 wt.% containing PMMA/Ca_3Al LDH and PMMA/Ca_3Fe LDH nanocomposites.

Pereira et al. (2009) prepared unsaturated polyester (UP)/LDH nanocomposites and evaluated thermal, mechanical and fire retardancy properties for the samples. The authors used various nanofillers such as Adipate-LDH (A-LDH) and 2-methyl-2-propene-1-sulfonate-LDH (S-LDH). The intercalated structures of different nanocomposites were identified by XRD analysis. From physical observation, A-LDH based nanocomposite exhibited homogeneous distribution of nanofiller which was not the case for UP/S-LDH nanocomposite. Flexural strength for nanocomposites reduced in comparison with the

polymer sample. Compared to the unsaturated polyester, the nanocomposites exhibited a significant reduction in flammability by 46% and 32% for UP nanocomposites containing 1 wt.% A-LDH and 5 wt.% S-LDH, respectively.

Chen and Qu (2005) reported the improved thermal and mechanical properties for poly methyl acrylate (PMA)/Zn-Al LDH nanocomposites over pure polymer. The XRD results suggested that for PMA/Zn-Al LDH nanocomposites, the (001) diffraction peak of Zn-Al LDH component appeared at $2\theta=3.10^{o}$. This indicates that the basal spacing of OZn-Al LDH is expanded to 2.85 nm due to the intercalation of PMA chains into the interlayers of Zn-Al LDH during the in-situ polymerisation. They found that, degradation temperature of PMA/Zn-Al LDH nanocomposites corresponding to 10 wt.% weight loss was 342 °C, which was 17 °C higher than that of pure PMA (325 °C). The tensile strength of PMA/Zn-Al LDH nanocomposite was enhanced to 3.81 MPa, compared to the pure PMA (0.46 MPa).

LDH modification using benzoate anions was targeted by Matusinovic et al. (2009) to enhance polymer matrix compatibility with LDH layers. Thereby, the authors fabricated poly(styrene-co-methyl methacrylate)/LDH nanocomposite (PS-PMMA/LDH-B) using in-situ bulk multistep polymerization. XRD analysis confirmed upon the disappearance of Ca-Al LDH in the nanocomposite due to disordering. However, TEM analysis conveyed partial dispersion of LDH-B in the polymer matrix to form a structure containing alternate matrix-particle regions in which particles appeared to exist in a intercalated structure. For 50 wt.% loss being selected as a reference, the PS-PMMA nanocomposite having 7.5 wt.% LDH-B, displayed about 26 °C higher thermal degradation temperature than that of the PS-PMMA copolymer. The DSC measurements exhibited slightly diminished value of T_g over PS-PMMA copolymer.

Pradhan et al. (2008) incorporated Mg-Al LDH modified with sodium 1-decasulfonate ($C_{10}H_{21}SO_3Na$) into ethylene propylene dieneterpolymer (EPDM) and carboxylated nitrile rubber (XNBR). Both elastomers possessed widely distinct polarities and functional groups. The nanocomposites were compounded by internal mixer followed by compression molding press at 150 °C and 100 kN pressure. The XRD results demonstrated that intercalated structures exist in various nanocomposites. TEM micrographs suggested that the Mg-Al LDH were more efficiently exfoliated in XNBR/LDH samples, while in the EPDM nanocomposites, the LDH layers were distributed in soft cluster form at 5 wt.% loading of the nanofiller material. It was also observed that LDH particle promoted strain-induced crystallization in XNBR/LDH nanocomposites. The XNBR samples (17.83 MPa) exhibited higher tensile strength in comparison with EPDM nanocomposites (3.25 MPa). Similarly, the tensile modulus and elongation were also increased.

Using melt intercalation, Du et al. (2007) prepared Nylon 6/Mg-Al LDH nanocomposites. The XRD analysis demonstrated that high LDH loading made the LDH layer difficult to exfoliate. The thermal decomposition temperature of the Nylon 6/LDH nanocomposites with 5 wt.% of Mg-Al LDH is 19.7 °C lower than that of nylon 6. The same sample indicated an enhancement in the crystallization temperature by 12 °C with respect to nylon 6. The PHRR values of the same sample were significantly lower than that of the nylon 6 sample.

Using solution intercalation method, Kuila et al. (2007) prepared Ethyl vinyl acetate (EVA) nanocomposites with SDS modified Mg-Al LDH. The XRD analysis conveyed that (003) peak corresponding to LDH shifted to lower 2θ value and this confirmed intercalated nanocomposite formation. However, TEM micrograph exhibited existence of partially

exfoliated Mg-Al LDH layers along with the stacked crystallites in the EVA matrix. The tensile strength and elongation at break values for the EVA nanocomposite containing 1 wt.% LDH increased by 42% and 5% with respect to the values obtained for the polymer.

Trujillano et al. (2006) prepared LDH with the hydrotalcite-like structure, containing Cu^{2+} and Al^{3+} in the layers and different alkyl sulphonates in the interlayer. These were characterized by XRD, FTIR and TGA analysis. The LDH synthesis was achieved through co-precipitation using NaOH as precipitation agent. The XRD patterns were acquired for 2θ range of 2 – 20°. The sharp XRD peak recorded at 2θ value of 12^{o} corresponding to (003) plane of a hydrotalcite structure. From the width of the brucite-like, the interlayer spacing calculated was 0.27 nm. This indicated that carbonate anions were located parallel to the molecular plane of layers similar to brucite. After surfactant modification, the diffraction of basal planes shifted towards lower diffraction angle. This was expected with the molecular sizes available for the surfactants.

A broad summary of various LDH based polymer nanocomposite investigations has been presented in Table 1.2.

Table 1.2: Literature summary for polymer/LDH nanocomposites.

Authors	Polymer matrix	Nanofiller	Modifier	Method of preparation	Remarks
Tai et al., 2011	PS	Mg-Al LDH	SDS	in-situ bulk polymerization	• Exfoliated and intercalated structures were confirmed by XRD. • At 10% weight loss, thermal stability was improved by 19 to 34 °C. • T_g was enhanced by 3 °C. • PHRR was reduced for composites.
Botan et al., 2012	PS	Mg-Al LDH	SDS	in Situ free radical bulk polymerization	• Exfoliated structure was confirmed by XRD. • At 20% weight loss, thermal stability was improved by 9 to 17 °C. • Flammability was improved by 50.61% for PS/Mg-Al LDH 5 nanocomposites.
Qiu and Qu, 2006	PS	Mg-Al LDH		soap free emulsion polymerization	• Exfoliated structure was confirmed by XRD and TEM. • At 3% weight loss, thermal stability was improved by 53.3 °C.
Qiu et al., 2005	PS	Zn-Al LDH	SDS	solution intercalation method	• Exfoliated and intercalated structures were confirmed by XRD and TEM. • At 50% weight loss, thermal stability improved by 30 °C for PS/Zn-Al LDH nanocomposite.

Authors	Polymer matrix	Nanofiller	Modifier	Method of preparation	Remarks
Ding and Qu, 2005	PS	Zn-Al LDH	N-lauroyl-glutamate	emulsion polymerization	• Exfoliated and intercalated structures were confirmed by XRD and TEM. • At 50% weight loss, thermal stability improved by 28 °C for PS/Zn-Al LDH 5 nanocomposites.
Matusinovic et al., 2012	PS	Co-Al LDH	benzoate	in-situ polymerization	• Exfoliated and intercalated structures were confirmed by XRD and TEM. • Thermal stability was enhanced by 10 °C.
Ding and Qu, 2006a	PS	Zn-Al LDH	SDS	emulsion and suspension polymerization	• Exfoliated structure was confirmed by XRD. • At 50% mass loss, thermal decomposition temperature was enhanced by 28 °C.
Ding and Qu, 2006b	PP	Zn-Al LDH and MMT	SDS	melt intercalation technique	• Exfoliated structure as suggested by XRD and TEM. • PP/LDH nanocomposites had better thermal stability over PP/MMT nanocomposites.
Wang et al., 2011b	PP	Co-Al LDH	DBS	melt compounding method	• Activation energy was improved with increase in Co-Al LDH content.
Wang et al., 2012	PP	Mg-Al LDH	SDS	micro emulsion polymerization	• G′ and G″ was increased with increase in Mg-Al LDH loading. • Loss factor was reduced with increase in Mg-Al LDH loading.

Authors	Polymer matrix	Nanofiller	Modifier	Method of preparation	Remarks
Wang et al., 2006	PMMA	LDH-U	10 - undecenoate	in-situ polymerization method	• Exfoliated structure. • T_g was improved by 22 °C. • Tensile modulus of 1.38 GPa and 1.80 GPa for PMMA and PMMA nanocomposites, repectively.
Li et al., 2003	PMMA	Mg-Al LDH	glycine	exfoliation/ adsorption process	• Exfoliated structure was confirmed by XRD. • At 5% mass loss, thermal degradation temperature enhanced by 9 °C.
Nyambo et al., 2009	PMMA	MgAl-CO_3 LDH	benzene phosphate	melt blending method	• peak heat release rate was reduced modified MgAl-CO_3 based nanocomposites (51%) and Unmodified LDH based nanocomposites (30%).
Manzi-Nshuti et al., 2009	PMMA	Ca_3Al LDH and Ca_3Fe LDH	10-undecenoate	in-situ polymerization method	• Intercalated and exfoliated morphology is suggested by TEM. • At 10% mass loss, thermal stability of PMMA/Ca_3Al LDH 10 and PMMA/Ca_3Fe LDH 10 composites was improved by 28 and 37 °C, respectively.
Pereira et al., 2009	unsaturated polyester	(A-LDH) and (S-LDH)		sonication followed by curing	• Intercalated structure. • Flammability was reduced by 46%.

Authors	Polymer matrix	Nanofiller	Modifier	Method of preparation	Remarks
Chen and Qu, 2005	Poly methyl acrylate (PMA)	Zn-Al LDH	SDS	in-situ polymerization method	• Intercalated structure. • Tensile strength of 0.46 MPa and 3.81 MPa for PMA and PMA/Zn-Al LDH nanocomposite, respectively.
Matusinovic et al., 2009	poly(styrene-co-methyl methacrylate)	Ca-Al LDH	benzoate anions	in-situ polymerization method	• Intercalated structure as suggested by TEM. • At 50% mass loss, thermal stability was enhanced by 26 °C.
Pradhan et al., 2008	EPDM and XNBR	Mg-Al LDH	1-decasulfonate	compression molding	• Exfoliated and intercalated structure obtained. • Tensile strength was improved for XNBR (17.83 MPa) over EPDM (3.25 MPa) nanocomposites.
Du et al., 2007	Nylon 6	Mg-Al LDH	SDS	melt intercalation method	• Exfoliated and intercalated structure as suggested by XRD. • Crystallization temperature was enhanced by 12 °C. • Thermal stability was improved by 19 °C.
Kuila et al., 2007	EVA	Mg-Al LDH	SDS	solution intercalation method	• Intercalated structure as suggested by XRD and TEM. • Tensile strength was improved by 42%.
Trujillano et al., 2006		Cu-Cl LDH	octylsulphonate, octanebenzenesulphonat, dodecylbenzenesulphonate andoctadecanesulphonate	co-precipitation method	• Interlayer spacing of LDH was increased after modification.

1.10.4 Polymer and polymer nanocomposite gears

The gear tooth surface temperature significantly influences a functional gear and hence its life. Taburdagitan and Akkok (2006) investigated the tooth surface temperature in spur gear meshing due to frictional heat using coupled thermo-elastic finite element analysis (FEA). Based on their studies, the authors concluded that the surface temperature increases maximum on the spur gear teeth pair along with the pressure line at the mesh beginning. Thereby, profile modification at the tooth tip could reduce the surface temperature during initial contact.

Two design modifications have been proposed by Kim (2006) to improve durability of plastic spur gears. Among these, one approach refers to insertion of series of holes at the intersection of base circles and tooth centreline. The other approach involves insertion of steel pins after making holes at the intersection of base circle and tooth centreline. The existence of holes reduced accumulation of heat and existence of pins reduced heat generation due to hysteresis. Thereby, the existence of holes and steel pins reduced surface temperature by about 5 – 10 °C and enhanced gear wear resistance.

Lin and Kuang (2008) carried out studies to understand interactions between tooth profile wear and dynamic loads for polyoxymethylene (POM) and nylon 66 plastic gears. The authors used a dynamic model to incorporate effects of various parameters such as position variant tooth mesh stiffness, damping ratio, load sharing, tooth profile wear and temperature to evaluate upon the alterations in dynamic contact loads. The simulation studies conveyed that tooth profile variation occurring due to cumulative sliding wear significantly affected contact loads and as cycle proceeds further, these interactions increase gradually.

Senthilvelan and Gnanamoorty (2009) studied transmission efficiency of polyamide gears. The gear surface temperature and transmission efficiency have been evaluated to reduce with increasing number of cycles. Further, tooth wear and gear tooth stiffness also contributed to reduction in transmission efficiency.

Karimpour et al. (2010) investigated contact behaviour of polymeric gear using ABAQUS (FEA) and analytical approaches and compared with BS ISO 6336 rating standard. From their investigations, the authors concluded that the contact path extensions that occurred in the beginning (premature contact) and end (extension contact) are responsible for larger tooth deflection. Due to this reason, lower stiffness exists for polymer gears than metallic gears. Also, the authors interpreted that premature contact caused pitch line tooth fractures and extended contact caused extreme wear.

Kim et al. (2012) studied wear and friction performances of polyamide and glass fibre composites. The authors attempted to understand precisely about the orientation of reinforced fibres in the wear and friction performance. It was analysed that 10 - 50 wt.% addition of glass fibers reduced the coefficient of friction by 15 – 30% and hence the wear rate. However, surface temperature measurements conducted with infrared rays thermal sensor conveyed that the composites have enhanced temperature by 10 – 15% due to addition of glass fibers. For these investigations, the test conditions were specified as 100 – 900 N normal load, 23.6 cm/s sliding velocity and 7000 m sliding distance.

Teisuke et al. (2001) studied wear distribution on the gear teeth on various combinations of injection-moulded plastic gears such as Nylon 66, Polyacetal and glass fibre reinforced Nylon, polyacetal, polyphenylene sulphide (PPS). From their investigations, the authors concluded that highest level of wear was obtained for unreinforced Nylon and glass

fibre reinforced polyacetal gears and the lowest wear was obtained for unfilled polyacetal gears.

Wright and Kukureka (2001) experimentally proposed co-ordinate wear measurement techniques for polymer composite gears to evaluate upon the criticality of independent variable such as load, sliding speed, roll angle, and slip ratio. The authors developed a moderate correlation for the measurements conducted with simple test configurations such as dic roll/slide test and pin-on-disc configurations.

The gear performance of injection-moulded carbon fiber reinforced polyamide 12 and carbon fiber reinforced polymide 6, 66 and 46 samples was investigated by Kurokawa et al. (2003) using power absorption test rig. Based on obtained results, the authors inferred that the PA12/carbon fibre (CF) gear possessed best combinations of load capability, noiseless property along with lowest water absorption among all polyamides.

Using three dimensional finite element model, Hossan and Hu (2012) investigated stress-strain behaviour of a 20% short glass fibre reinforced Nylon 66 and unreinforced Nylon 66 gear tooth under various dynamic loads. From the carried out studies, the authors concluded that the tooth root region of the gear usually experience high stress and hence are susceptible to maximum failure.

The transmission efficiency of 3 and 5 wt.% nanoclay reinforced polyamide gears while being paired to a steel gear were investigated by Kirupasankar et al. (2012). The authors concluded that nanoclay addition enhanced stiffness and reduced viscous component of the gear material due to which the transmission efficiency of the gear was higher than that obtained for pristine polyamide gears.

Mertens and Senthilvelan (2016) developed 1 wt.% carbon nanotube containing PP nanocomposites using injection moulding to achieve spur gears for durability studies using in-house developed power absorption gear test rig. The tests enabled measurements of test gears surface temperature and in-line torque of driver and driven shafts. Thereby, transmission efficiency of the test-steel gear pair was evaluated using measured torque values. The gear failure mode was correlated with the measured net surface temperature. Upto failure or upto 8.6×10^{-5} cycles, whichever occurred first was noted during the test gears run up. In comparison with the gear fabricated with PP, carbon nanotube-PP gear provided lower surface temperature, improved service life and higher transmission efficiency.

1.11 Literature summary and possible scope for further research

The available state-of-the-art presented in the previous section reveals upon continuing efforts that focus upon improved thermal, mechanical and flammability properties of PS polymer. In this regard, the Ph.D. thesis focuses towards fabrication of PS based nanocomposites by incorporation of two different nanofillers.

1.11.1 Synthesis of Co-Al LDH and Ni-Al LDH nanofiller materials

The state-of-the-art summary presented in the previous section indicates that Mg-Al LDH nanofiller was targeted by Tai et al. (2011), Botan et al. (2012), Qiu and Qu (2006), Wang et al. (2012), Li et al. (2003), Pradhan et al. (2008), Du et al. (2007) and Kuila et al. (2007). On the other hand, Qiu et al. (2005), Ding and Qu (2005), Ding and Qu (2006a), Ding and Qu (2006b) synthesized Zn-Al LDH. Further, Nyambo et al. (2009), Manzi-Nshuti et al. (2009), Matusinovic et al. (2009), Triujillano et al. (2006) prepared MgAl-CO_3 LDH, Ca_3Al

LDH, Ca-Al LDH and Cu-Cl LDH, respectively. While all LDHs are equally competitive, an earlier research investigation at IIT Guwahati conveyed that among all LDHs (Mg-Al, Co-Al, Ni-Al, Cu-Al, Cu-Fe, Cu-Al and Cu-Cr LDHs), Cu-Cr LDH, Co-Al LDH and Ni-Al LDH provided better thermal properties in comparison with the pristine polymer as well as other polymer/LDH nanocomposites (Sahu and Pugazhenthi, 2010). Among these, Cu-Cr LDH is not compatible for optical property investigations (due to its black colour texture). Therefore, among all LDHs, Co-Al LDH and Ni-Al LDH are relevant for consideration in the Ph.D. thesis research as ideal LDHs to fabricate polymer nanocomposites. Also, as mentioned previously, Co-Al LDH and Ni-Al LDH have specific applications in waste water treatment and antibacterial applications.

Therefore, to better understand the functionality of Co-Al LDH and Ni-Al LDH nanofiller materials in polymer nanocomposites, a fundamental understanding and knowledge of the characterization parameters of these nanofiller materials is important. There upon, their specific contribution towards PS nanocomposite materials can be assessed upon. Therefore, the synthesis and characterization of said nano materials is needed prior to PS nanocomposite fabrication and characterization.

1.11.2 Rheological analysis of PS/Co-Al LDH blend solution

Rheological characterization is very important to utilize polymers and polymer nanocomposites as materials in the operation of various process equipments. Rheological analysis is useful for handling, processing, mixing and transportation of said materials. With respect to Ni-Al LDH polymer blends and their rheological analysis, the available literature (Chakraborty et al. (2014)), conveys that PMMA was considered as base polymer along with solvent blending method.

PS polymer is produced in huge volumes and is available at a lower price compared to many other polymers. PS is clear, hard, brittle thermoplastic polymer in solid glassy state. It offers acceptable resistance towards acids and bases. PS products such as test tubes and petri dishes look similar to glass made products. Further, PS is used for sample storage and transport as well as food grade packaging products. Considering all these, it is worthwhile to investigate the efficacy of PS as a matrix for PS/LDH nanocomposite fabrication.

On the other hand, the rheological analysis of PS/Co-Al LDH nanocomposites is needed to enhance insights into the material properties. Also, LDH loading and temperature effect needs to be targeted in such experimental and theoretical investigations with shear rate variation as dependent variable.

1.11.3 Solvent blending based PS/LDHs nanocomposites fabrication

The solvent blending based polymer nanocomposite fabrication were targeted by Paul et al. (2013) (PS/clay laponite nanocomposites), Kim et al. (2003) (PS/clay nanocomposites), Qiu et al. (2014) (PS/Zn-Al LDH nanocomposites), Yamagata et al. (2012) (PMMA/OMMT nanocomposites), Kumar et al. (2014) (PMMA/OMMT nanocomposites), Suin et al. (2014)

(PC/clay nanocomposites), Kuila et al. (2007) (EVA/Mg-Al LDH nanocomposites). With respect to LDHs, only few authors targeted the same. Among these, Mg-Al LDH, Zn-Al LDH have been studied as effective nanofillers with respect to pristine PS polymers. However, with Co-Al LDH and Ni-Al LDH as important and relevant nanofiller materials, there is a need to evaluate the effectiveness of PS/Co-Al LDH and PS/Ni-Al LDH nanocomposites using solvent blending method.

1.11.4 Melt intercalation based PS/LDHs nanocomposites fabrication

The available literature referred to fewer investigations with respect to melt intercalation method for LDH based polymer nanocomposites fabrication and characterization. The available literature in this regard corresponds to those presented by Limpanart et al. (2005) (PS/organoclay nanocomposites), Zidelkheir et al. (2006) (PS/OMMT nanocomposites), Wang et al. (2009) (PS/clay nanocomposites), Unikrishnan et al. (2011) (PMMA/Cloisite 30 B), Sharma and Nayak (2009) (PP/clay nanocomposites), Goad (2011) (PP/clay nanocomposites), Mittal (2008) (PP/clay nanocomposites), Zhao et al. (2005) (PE/clay nanocomposites), Gopakumar et al. (2002) (PE/clay nanocomposites), Ding and Qu (2006b) (PP/Zn-Al LDH and PP/MMT nanocomposites), Nyambo et al. (2009) (PMMA/MgAl-CO_3 LDH nanocomposites), Du et al. (2007) (Nylon6/Mg-Al LDH nanocomposites). The combination of PS and Co-Al LDH/Ni-Al LDH nanofiller have not been investigated so far using melt intercalation method. Considering the relevance of Co-Al LDH and Ni-Al LDH as important LDHs, there is a need to investigate and identify optimal nanofiller loading in melt intercalation based PS/Co-Al LDH and PS/Ni-Al LDH nanocomposites.

1.11.5 Durability studies of polymer nanocomposite gears

Polymeric materials have gained significant attention to serve as gears. Many researchers investigated the surface effect on the friction and wear performance of polymer materials (Barrett et al., 1992; Wieleba, 2002; Hohn et al., 2006; Tzanakis et al., 2013). Polymer nanocomposites have better characterization parameters than polymers in terms of durability, low sliding friction, etc. Several works have been carried out to understand the effect of reinforcements on gear performance (Kurokawa et al., 1999; Kurokawa et al., 2000a; Kurokawa et al., 2003; Senthilvelan and Gnanamoorthy, 2004a; Senthilvelan and Gnanamoorthy, 2004b; Senthilvelan and Gnanamoorthy, 2009) and directional shrinkage (Weale et al., 1999; Senthilvelan and Gnanamoorthy, 2006a; Hakimian and Sulong, 2012). However, with respect to polymer nanocomposites, durability studies are limited (Mertens and Senthilvelan, 2016). Given the effectiveness of nanocomposites with respect to pristine polymers, durability studies could further enhance their applications in industrial scenarios. Co-Al LDH and Ni-Al LDH are important nanofiller materials to prepare good quality PS nanocomposites and can serve as efficient polymeric gears with improved properties. However, for such application, characterization studies that target the durability of polymer nanocomposite needs to be investigated, which has not been addressed in the available state-of-the-art.

1.12 Objective of the thesis

Based on the lacunae in the above summarized state-of-the-art, the following major objectives have been identified to be of serious concern and address in the Ph.D. thesis:

- ❖ Preparation and characterization of organomodified Co-Al LDH and Ni-Al LDH.
- ❖ Rheological behaviour of PS/Co-Al LDH blend solution obtained through solvent blending routes.
- ❖ Fabrication and characterization of PS/Co-Al LDH and PS/Ni-Al LDH nanocomposites by solvent blending method.
- ❖ Preparation and characterization of PS/Co-Al LDH and PS/Ni-Al LDH nanocomposites via melt intercalation method.
- ❖ Injection-moulded PS/Co-Al LDH and PS/Ni-Al LDH nanocomposite spur gear performance.

1.13 Organization of the thesis

The doctoral thesis is organized in seven chapters as follows:

Along with a brief introduction, **Chapter 1** presents a consolidated review of available state-of-the-art, existing lacunae and possible scope for further research followed with objectives and organization of the thesis.

Chapter 2 addresses synthesis and characterization of modified Co-Al LDH and Ni-Al LDH.

The temperature dependent rheological behaviour of PS/Co-Al LDH blends has been addressed in **Chapter 3**. Relevant rheological models have also been summarized in the chapter to evaluate upon their fitness with the measured experimental data and identify best rheological model.

Chapter 4 addresses the fabrication and characterization of PS/Co-Al LDH and PS/Ni-Al LDH nanocomposites by solvent blending technique. The properties of PS/Co-Al LDH and PS/Ni-Al LDH nanocomposites were evaluated using XRD, TEM, FTIR, TGA, DSC measurements. Also, rheology and thermal degradation kinetics have been addressed.

The development of PS/Co-Al LDH and PS/Ni-Al LDH nanocomposites using melt blending method have been discussed in **Chapter 5**. Thermal, mechanical, rheological, thermal degradation kinetics/mechanisms have been addressed for the said nanocomposites and the obtained trends have been discussed in the context of properties of PS polymer.

The durability of gears fabricated with PS nanocomposites containing 1 wt.% Co-Al LDH or 1 wt.% Ni-Al LDH has been addressed in **Chapter 6.**

Conclusions and possible directions for future research have been summarized in **Chapter 7** of the Thesis.

Chapter 2:

Synthesis and Characterization of Organomodified Co-Al LDH and Ni-Al LDH

Synthesis and Characterization of Organomodified Co-Al LDH and Ni-Al LDH

This chapter presents the procedures adopted for the synthesis of modified Co-Al LDH and Ni-Al LDH via co-precipitation method. Thereafter, XRD and TGA have been conducted to carry out structural and thermal characterization of the prepared LDHs.

2.1 Introduction

LDH can be prepared using known chemical compositions of high purity reagents. This is one of the excellent advantages of this material. LDHs are a class of anionic lamellar or hydrotalcite, which are well characterized and conventionally used as catalysts (Constantino and Pinnavaia, 1994), adsorbents (You et al., 2002) and matrices for biosensors (Choy et al., 2000). In general LDH chemical formula is presented as $[M^{2+}_{1-x} M^{3+}_{x}(OH)_2]^{x+}(A^{m-})_{x/m} .yH_2O$, where, M^{2+} is metallic divalent cations (Ni^{2+}, Mg^{2+}, Zn^{2+}, or Cu^{2+}, Co^{2+}), M^{3+} is a metallic trivalent cations (Al^{3+}, Mn^{3+}, Ga^{3+}, Cr^{3+} or In^{3+}), A^{m-} is anion (with charge m^-) interlayer (NO_3^-, CO_3^{2-}, OH^-). Also, in the formula, x value varies in the range of 0.20 – 0.33 for pure phase of LDHs (Acharya et al., 2007). In the primary structure, pristine LDH systems have less basal spacing and there will be a stronger electrostatic interlayer interaction due to their higher charge density and hydrophilic property. Thereby, it is very difficult to penetrate polymers into layers of pristine LDH because of larger size and hydrophobic character of polymer. For this reason, modification of LDHs by various anionic species (carboxylates, sulfonates, sulfates and phosphates) containing a hydrophobic

aromatic/aliphatic chain is necessary, to make them as promising host for a large number of applications (Kuila et al., 2007). Recent progress in polymer/layered nanocomposites (PLNs) has been a very important mile stone achievement in the polymer technology (Costa et al., 2008; Alansi et al., 2015; Ray and Okamoto, 2003). The PLNs have been used in various applications due to their superior thermal, mechanical and fire retardant properties in comparison with pristine polymer (Ray and Okamoto, 2003).

The objective of this section of the thesis is to preparation of modified LDHs via co-precipitation method. The structural and thermal properties of the prepared LDHs have been evaluated using different techniques.

2.2 Experimental

2.2.1 Materials

Cobalt nitrate ($Co(NO_3)_2.6H_2O$), aluminium nitrate ($Al(NO_3)_3.9H_2O$), nickel nitrate ($Ni(NO_3)_2.6H_2O$), xylene (C_8H_{10}), sodium hydroxide (NaOH) and sodium dodecyl sulfate (SDS) were procured from Merck (I) Ltd., Mumbai, India. Water used for this work was taken from the Millipore water system (ELIX-3).

2.2.2 Preparation of modified Co-Al LDH

Co-Al LDH was prepared using SDS through co-precipitation method by following the procedure described elsewhere (Du et al., 2009). The procedure for the synthesis of modified Co-Al LDH is diagrammatically presented in Figure 2.1.

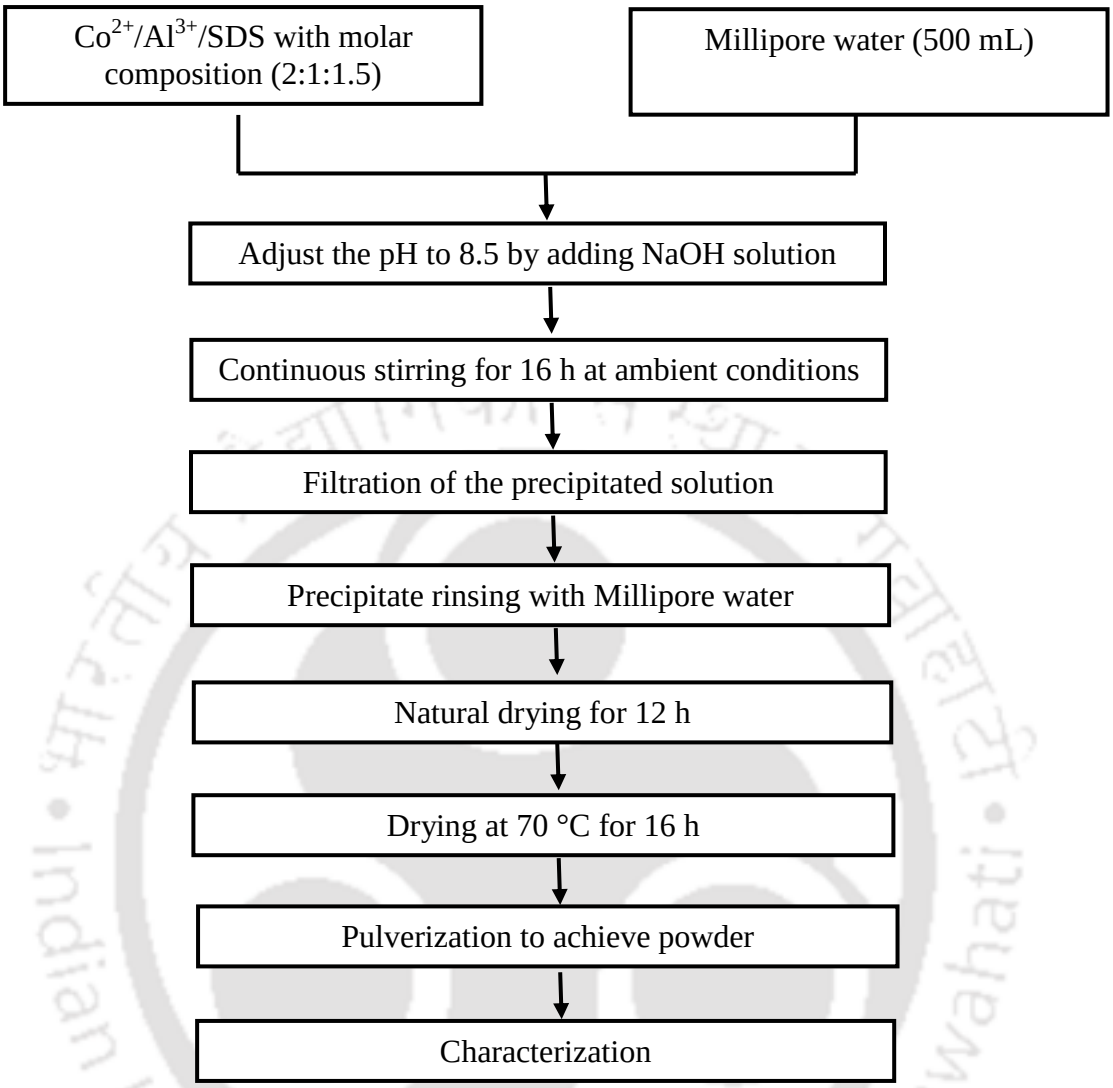

Figure 2.1: Steps involved in modified Co-Al LDH preparation.

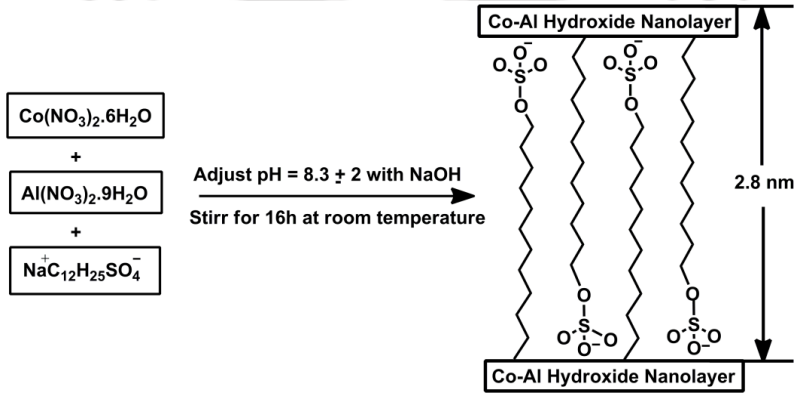

Figure 2.2: Schematic representation for synthesis of modified Co-Al LDH.

Initially, Cobalt nitrate, aluminium nitrate and SDS were dispersed in Millipore water (500 mL) to form a solution containing Co^{2+}/Al^{3+}/SDS with a desirable molar composition (2:1:1.5). Under dynamic stirring condition, an aqueous solution of 2 M NaOH was further added drop by drop upto a solution pH of 8.5. Then, the mixture was stirred further for 16 h to form precipitate at ambient conditions. The thick slurry was collected on the top of the filter paper during the filtration of the precipitated solution. Finally, Millipore water was used to rinse the precipitate, in such a way that the pH of the residual filtrate becomes neutral. This final purified product is called LDH material, which was kept in the atmospheric condition for 12 h and consecutively dried at 70 °C for 16 h in a hot air oven (Make: Reico, Model: ROV/DG). Dried LDH was pulverized into powder form for further use. Figure 2.2 depicts the schematic of synthesis of modified Co-Al LDH.

2.2.3 Synthesis of pristine Ni-Al LDH

Co-precipitation method was adopted to prepare pristine Ni-Al LDH (P-Ni-Al LDH). In this method, firstly, the solution mixture containing nickel nitrate, aluminium nitrate and sodium nitrate was prepared with a 2:1:2 molar ratio, respectively. To this solution, 2 M NaOH solution was added under constant stirring condition to enhance the pH to 10. Thereafter, continuous stirring for 16 h at room temperature facilitated the formation of LDH precipitate. Finally, pristine LDH in powder form was achieved by filtering suspension and washing precipitate until filtrate reached neutral pH followed with drying at 60 °C for 16 h and grinding. Figure 2.3 illustrate procedural steps adopted for P-Ni-Al LDH preparation.

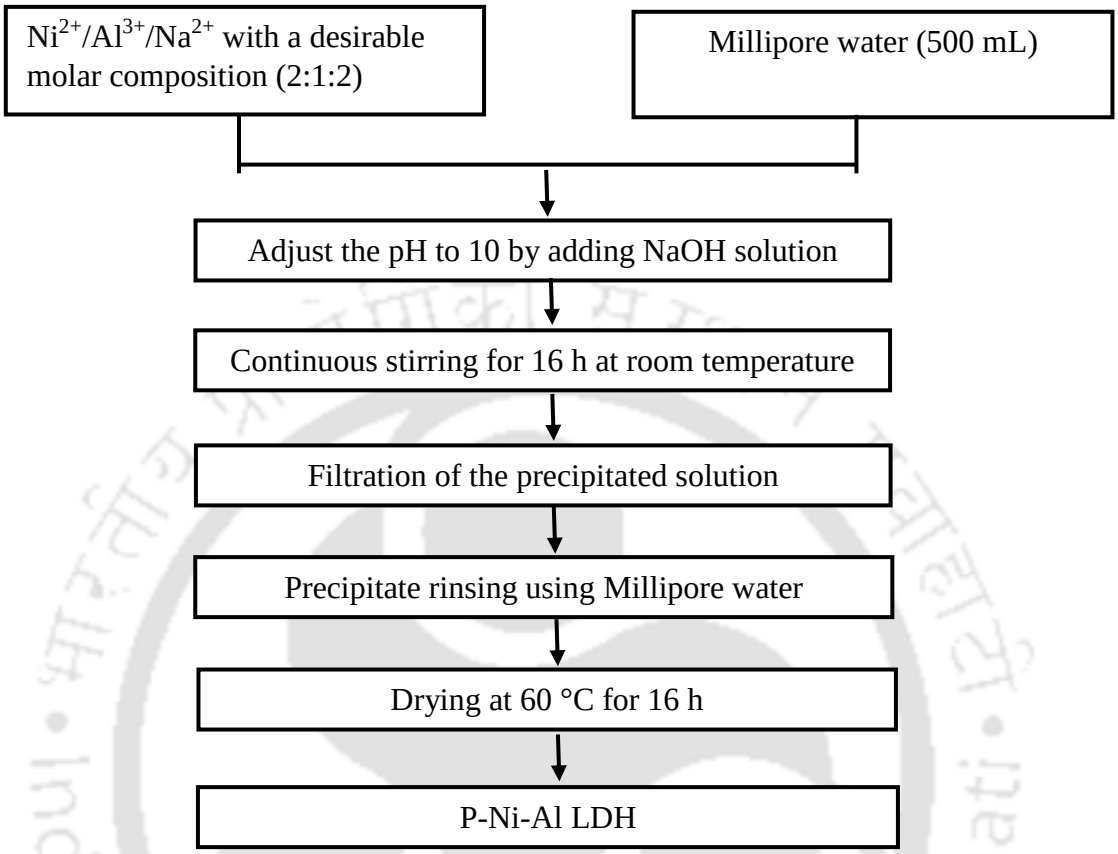

Figure 2.3: Steps involved in P-Ni-Al LDH synthesis.

2.2.4 Preparation of modified Ni-Al LDH

The prepared P-Ni-Al LDH was modified through regeneration method to obtain modified Ni-Al LDH. The procedure for the synthesis of modified Ni-Al LDH is depicted in Figure 2.4. Prior to modification with SDS, P-Ni-Al LDH powder (2.5 g) was subjected to calcination at 500 °C for 5 h in a box furnace (heating rate = 10 °C/min).

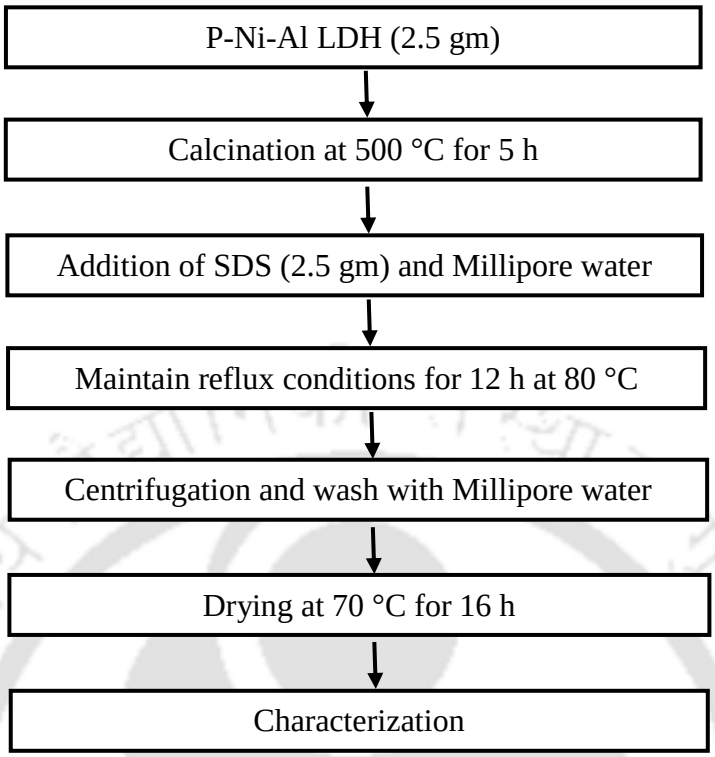

Figure 2.4: Steps involved in modified Ni-Al LDH preparation.

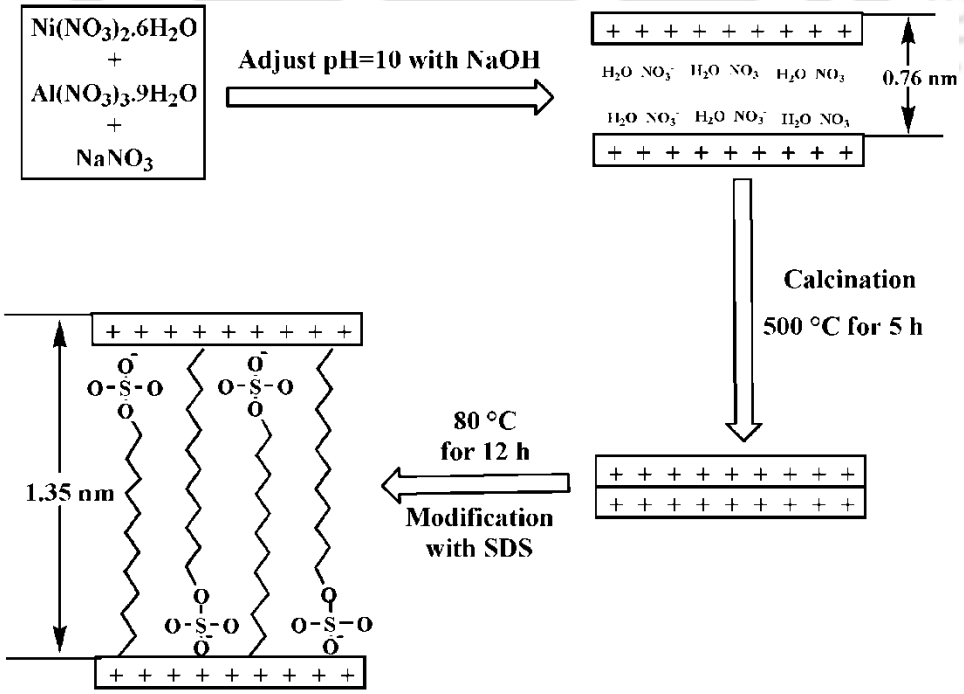

Figure 2.5: Chemical transformations involved during modified Ni-Al LDH preparation.

Then the calcined gray coloured powder was dispersed in 120 mL of aqueous SDS solution (2.5 g) and was subjected to reflux conditions for 12 h at 80 °C. Subsequently, residue was separated with centrifugation and washed for several cycles with Millipore water to remove adhered SDS. Finally, modified Ni-Al LDH was obtained after drying the residue at 70 °C. The dried sample was grinded to make as finer particles and used for the fabrication of PS nanocomposite films. Figure 2.5 shows the schematic of modification of Ni-Al LDH with SDS.

2.3 Characterization

2.3.1 X-ray diffraction analysis

XRD pattern of modified Co-Al LDH and Ni-Al LDH samples were measured at room temperature in air using AXS D8 ADVANCE fully automatic powder X-ray diffractometer (Bruker). The XRD instrument was operated with Cu-Kα radiation (λ = 0.15406 nm) and Ni filter. The patterns were recorded for 2θ range from 2° to 50° with a scan speed of 0.02 sec^{-1}.

2.3.2 Fourier transforms infrared spectroscopy

The FTIR analysis of various samples was performed using Shimadzu Fourier transform infrared spectroscope for the confirmation of functional peaks in modified Co-Al LDH and Ni-Al LDH.

2.3.3 Thermo gravimetric analysis

The thermogravimetric analysis was carried out using Mettler Toledo thermo analyser that was operated with 10 °C/min heating rate from room temperature to 700 °C in nitrogen atmosphere.

2.4 Results and discussion

2.4.1 XRD analysis

2.4.1.1 Modified Co-Al LDH

XRD is a most powerful tool for characterizing the level of crystallinity of materials and assessments of layered structures, i.e. exfoliated and/or intercalated, as the peaks significantly alter with the gallery height of the LDH. Figure 2.6 shows the XRD results of Co-Al LDH in the 2 range of 2° – 50° with a scan speed of 0.02 sec^{-1}. The d-spacing value of the Co-Al LDH is determined as 2.8 nm from the reflection peak (003) at 3.14° (using Bragg's equation, $n\lambda = 2d\sin\theta$; here, λ = 1.5406 Å and n = 1). This value signifies brucite like layer's thickness. It is supposed that a larger space between Co-Al nanolayers endorses intercalation of the polymer molecules and also increases compatibility among modified Co-Al LDH and polymer molecules. This leads to easy exfoliation of the stacking Co-Al layers in the polymer matrix to form well dispersed polymer/LDH blends.

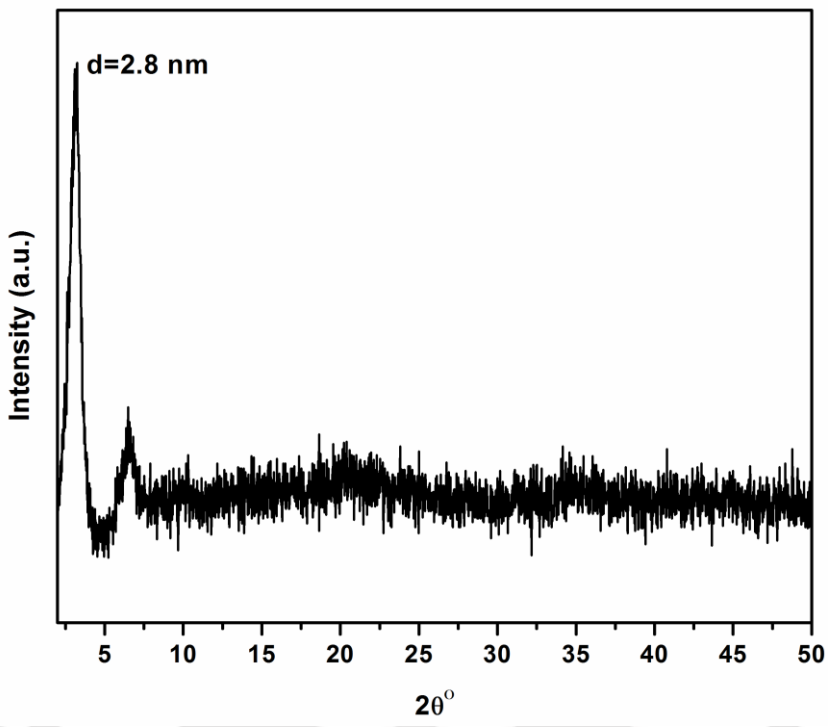

Figure 2.6: XRD pattern of modified Co-Al LDH.

2.4.1.2 P-Ni-Al LDH and modified Ni-Al LDH

The XRD spectra (2θ range of 5 – 50°) of P-Ni-Al LDH and modified Ni-Al LDH have been presented in Figure 2.7. It can be seen in Figure 2.7 (a) that for the P-Ni-Al LDH, the (003) peak obtained at 2θ value of 11.1° corresponds to d-spacing value of 0.8 nm (evaluated using Bragg's law). For the other case (Figure 2.7 (b)), the (003) peak is slightly shifted towards left side at 2θ value of 6.54°. This is due to the modification of pristine LDH with SDS. The increment in d-spacing value (d_{003} = 1.35 nm) for modified LDH is due to the intercalation of SDS in the LDH gallery spaces (see Table 2.1). Further, it corroborates an alteration in the hydrophilic nature of the LDH surface into organophilic nature. This helps to enhance the compatibility between modified LDH and PS matrix. This also leads to easy exfoliation of modified Ni-Al LDH stacking layers into matrix to form a better LDH dispersed PS nanocomposites.

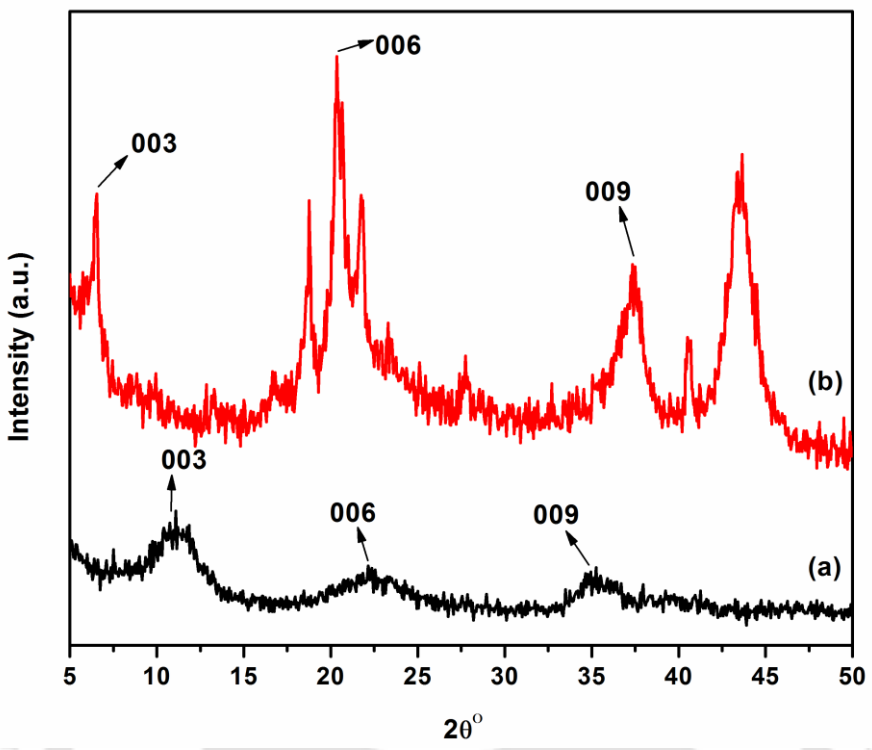

Figure 2.7: XRD diffractogram of (a) P-Ni-Al LDH and (b) modified Ni-Al LDH samples.

Table 2.1: XRD result summary for P-Ni-Al LDH and modified Ni-Al LDH.

Sample	(003)		(006)		(009)	
	2θ°	d (nm)	2θ°	d (nm)	2θ°	d (nm)
P-Ni-Al LDH	11.1	0.80	22.15	0.40	35.22	0.25
Ni-Al LDH	6.54	1.35	20.31	0.44	27.75	0.32

2.4.2 FTIR analysis

2.4.2.1 Modified Co-Al LDH

The surface functional groups of the LDH were further revealed by FTIR spectrum. Figure 2.8 illustrates the FTIR spectrum of modified Co-Al LDH. The peak obtained at 3500 cm^{-1} is accredited to the O-H stretching of hydroxyl group of LDH (Costa et al., 2008). A broader

peak at wavenumber of 1630 cm^{-1} represents to the existence of δ (H-OH) (Qiu et al., 2005). An intense peak is observed at 1218 cm^{-1} which is assigned as symmetric vibration of sulfate from dodecyl sulfate anion (Kumar et al., 2015). The peak at wavenumber of 1063 cm^{-1} is designated as asymmetric vibration of sulfate from dodecyl sulfate. Three prominent peaks attained in the region of 2848, 2920 and 2957 cm^{-1} are designated for C-H stretching vibration (Guo et al., 2011). Guo et al. (2011) also achieved C-H stretching vibration at these particular wavenumbers. The bands seen at lower frequency region signify lattice vibration modes and it can be attributed to M-O and M-O-M from 800 to 450 cm^{-1} (where M = Co, Al) in the LDH sheets (Kanan and Swamy, 1992; Mallakpour and Dinari, 2015).

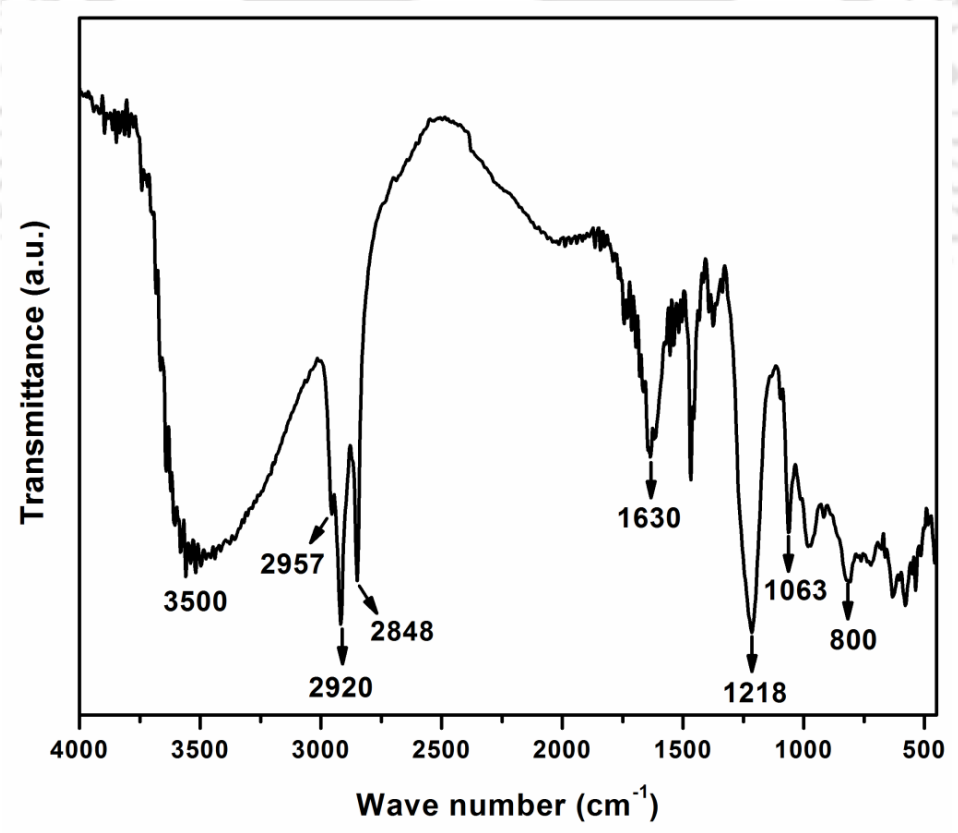

Figure 2.8: FTIR spectrum of modified Co-Al LDH.

2.4.2.2 P-Ni-Al LDH and modified Ni-Al LDH

Figure 2.9 depict FTIR spectra of both P-Ni-Al LDH and modified Ni-Al LDH samples. For P-Ni-Al LDH (Figure 2.9 (a)), it can be noticed that a broad band appeared for a wave number of 3480 cm^{-1}. This is due to O-H stretching vibration of interlayer water molecules (Alansi et al., 2015). P-Ni-Al LDH containing NO_3^- anions have characteristic vibration bands. An intense broader peak at 1385 cm^{-1} affirms existence of nitrate ion. The peak obtained at 822 cm^{-1} is designated as NO_3^- ion. The medium sharp peak at 1632 cm^{-1} is associated to bending mode of interlayer water molecules i.e. δ (H-OH). The lattice vibration bands from O-M-O and M-O (M=Ni, Al) groups have been recorded at lower frequency around 400 – 800 cm^{-1} (438 cm^{-1}).

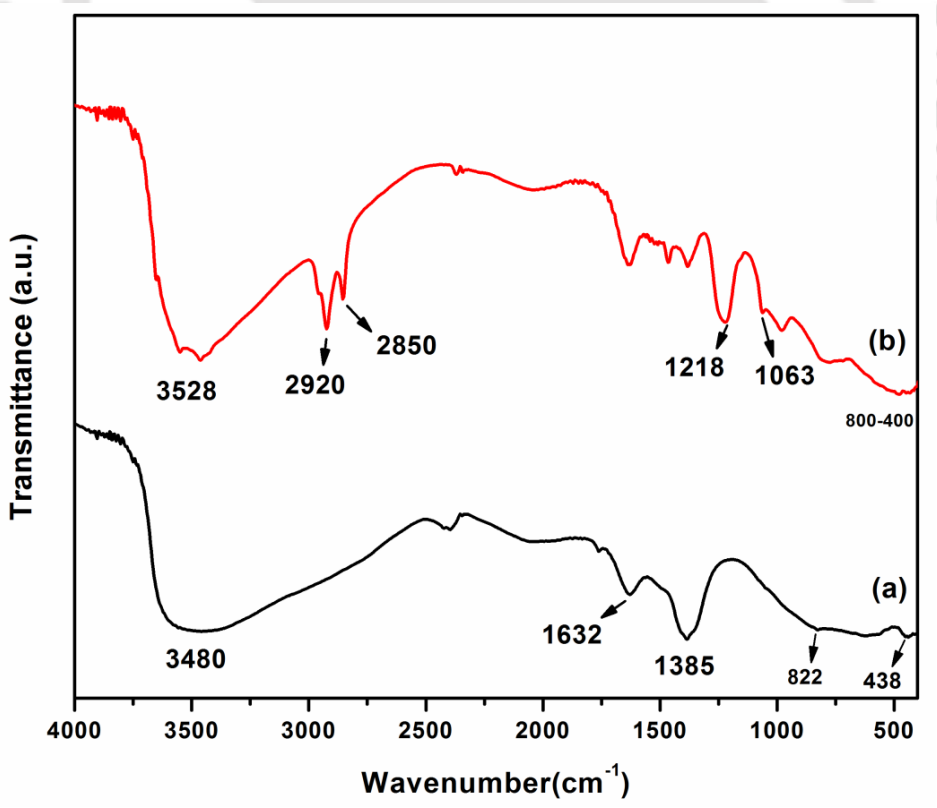

Figure 2.9: FTIR spectra of (a) P-Ni-Al LDH and (b) modified Ni-Al LDH.

FTIR spectrum of modified Ni-Al LDH is also shown in Figure 2.9 (b). O-H stretching vibration of hydrogen-bonded metal hydroxide layer and lattice water have been attained at 3528 cm^{-1}. The two characteristic peaks at 2850 and 2920 cm^{-1} are designated for stretching vibration of CH_3 and CH_2 of the modifier (SDS), respectively. The two peaks at 1218 cm^{-1} and 1063 cm^{-1} have been assigned to symmetric vibration ($\nu_{S=O}$) and asymmetric vibration ($\nu_{o\ S=O}$) of sulfate from dodecyl sulfate anion, respectively (Costa et al., 2008).

2.4.3 TGA analysis

2.4.3.1 Modified Co-Al LDH

TGA analysis is primarily carried out to examine the degradation temperature as well as thermal stability of the polymer matrix. The TGA curve of modified Co-Al LDH is presented in Figure 2.10. TGA profile of modified Co-Al LDH shows a complex thermal degradation behavior. For modified Co-Al LDH, the mass loss before 200 °C is attributed to the loss of physically adsorbed and interlayer water (Alansi et al., 2015). The mass loss between 200 and 350 °C corresponds to the decomposition of the interlayer dodecyl sulfate (Xie et al., 2001). The mass loss above 350 °C is attributed to the decomposition of LDH sample up to the formation of Co-Al oxides.

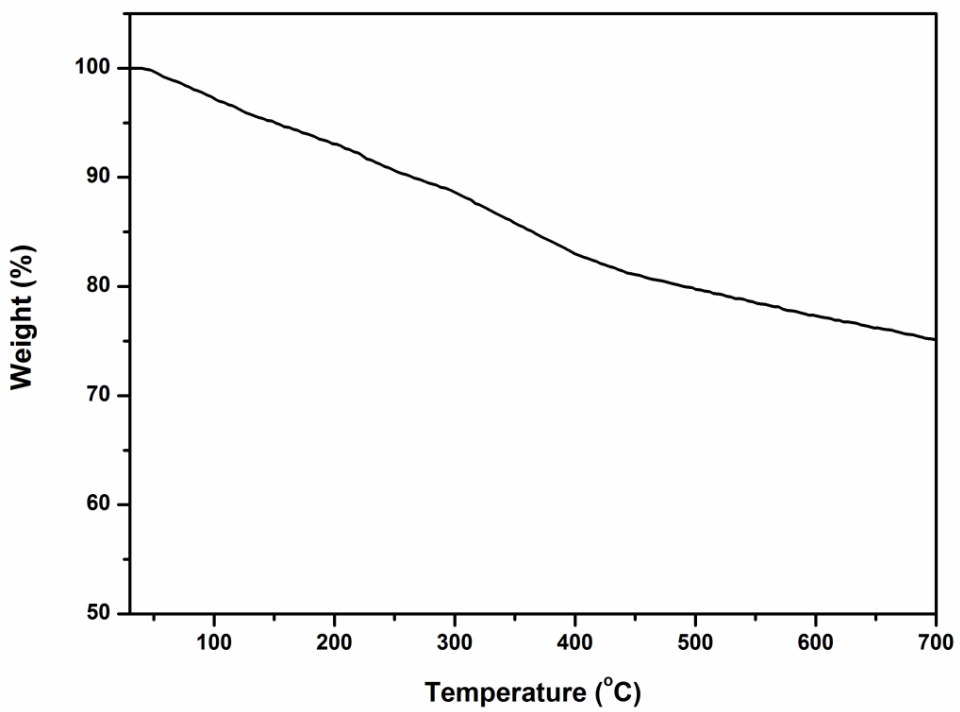

Figure 2.10: TGA profile of modified Co-Al LDH.

2.4.3.2 P-Ni-Al LDH and modified Ni-Al LDH

The TGA analysis provides insights with respect to thermal stability of LDHs. The thermal stability mainly depends on various factors such as cationic (brucite-like layer), anionic and crystalline nature of the LDH material. Figure 2.11 depicts the TGA curve for P-Ni-Al LDH and modified Ni-Al LDH. It is clearly seen that the thermal decomposition of P-Ni-Al LDH takes place at three different stages (Palmer et al., 2009). At low temperature (up to 200 °C), P-Ni-Al LDH mass loss is due to the loss of physically adsorbed and interlayer water. Loss in the range of 270 – 450 °C is due to dehydroxylation and nitrate anions loss. At higher temperature range (450 – 700 °C), thermal decomposition of mixed metal oxides occurs (Ding and Qu, 2005). A similar TGA profile was also reported by Alansi et al. (2015) for Mg-Al LDH. In the present work, 10% weight loss is obtained at the temperature of 133.4 °C for P-Ni-Al LDH and the final residue at 700 °C is 57.8%. Thermal behaviour of the LDH is varied

significantly after modification with SDS (see Figure 2.11 (b)). While weight loss below 200 °C is due to water loss from adsorbed and interlayer states, weight loss between 200 and 350 °C is due to SDS degradation in the LDH layer (Leroux et al., 2001). At higher temperature (350 – 700 °C), the LDH sample degrades to yield Ni-Al oxides. The residue obtained at 700 °C is 83.67% for the modified Ni-Al LDH. The comparative thermal properties of the P-Ni-Al LDH and modified Ni-Al LDH are enlisted in Table 2.2. The outcomes of the thermal decomposition of P-Ni-Al LDH and modified Ni-Al LDH demonstrate the extent of the thermal stability of prepared LDHs and are in agreement with reported values in the literature (Lv et al., 2009).

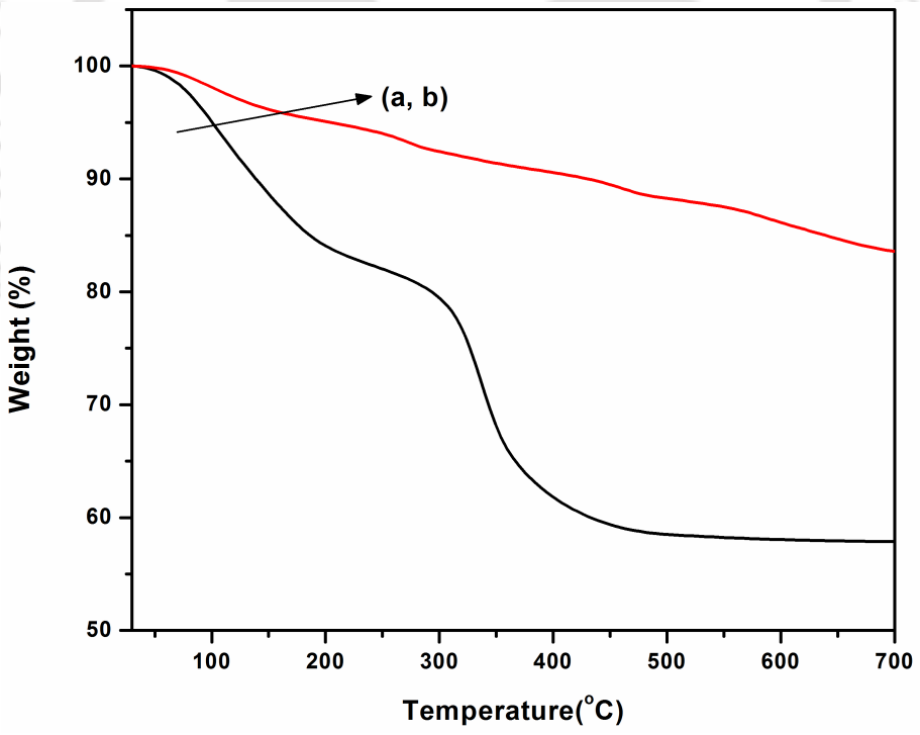

Figure 2.11: TGA thermograms of (a) P-Ni-Al LDH and (b) modified Ni-Al LDH.

Table 2.2: Thermal characterization parameters of P-Ni-Al LDH and modified Ni-Al LDH.

Sample	Temperature at 10% weight loss (T_{10}) °C	Residue (wt.%) obtained at 700 °C
P-Ni-Al LDH	133.4	57.8
Ni-Al LDH	430.1	83.67

2.5 Summary

Modified Co-Al LDH and Ni-Al LDH was successfully synthesized using co-precipitation method. It is found from XRD analysis that the d-spacing value of the modified Co-Al LDH is determined as 2.8 nm (obtained from the reflection peak (003) at 3.14°). It has been analyzed that for the P-Ni-Al LDH, the basal spacing (d_{003}) of (003) peak at 2θ value of 11.1° is evaluated to be 0.8 nm. Further, in the XRD pattern of modified Ni-Al LDH, a characteristic peak corresponding to (003) plane is observed at 2θ value of 6.54° and corresponding basal spacing (d-spacing) of 1.35 nm. Considering 10% mass loss as a reference, the degradation temperature of modified Co-Al LDH and Ni-Al LDH is found to be 266.4 and 430.1 °C, respectively. The residue obtained at 700 °C was evaluated to possess 70.5 wt.% and 83.67 wt.% of original samples weight for modified Co-Al LDH and Ni-Al LDH samples, respectively. Among the investigated modified LDHs, modified Co-Al LDH exhibit lower residue content due to enhanced presence of modifier content in the modified Co-Al LDH.

Chapter 3:

Rheological Behaviour of PS/Co-Al LDH Blend Solution Obtained Through Solvent Blending Route

Rheological Behaviour of PS/Co-Al LDH Blend Solution Obtained Through Solvent Blending Route

This chapter addresses rheological behaviour of solvent blending method based PS/Co-Al LDH solutions. PS blends with variant Co-Al LDH content (3, 5 and 7 wt.% with respect to pristine PS) were synthesized with the said method. The rheological characterization studies were carried out at various temperatures (20, 30 and 40 °C) and shear rates (0.1 to 100 sec^{-1}). Rheological studies clearly depict that shear rate, solution concentration and testing temperature are responsible for rheological behaviour of the chosen system. For the considered temperature range, the PS blend solution viscosity decreases with shear rate. Compared to pristine PS, all PS/Co-Al LDH blends exhibit increment in their shear viscosity.

3.1 Introduction

In the last few decades, several researchers have performed interesting studies on the behavior of polymers solutions and also contributed important information on the non-Newtonian behavior and classification of the fluids formed by these polymers (Diaz and Navaza, 2004). Numerous polymers have been used in various industries that includes pharmaceutical, textile, cosmetics and food (Sandford and Baird, 1983). In biotechnology, polymers are used as immobilization material for living cells due to their property to form gels with cations (Voilley, 1995). Due to enhanced economic prominence to polymer manufacture, it is essential to take note and optimize the operational and equipment design parameters of processes. In this regard, rheological properties are critically required during

required during handling, processing, transporting and mixing (Alvarez et al., 2000; Bueno and Cruz, 2001; Rawase et al., 1997). The experiments with polymer blends are motivating because, the addition of different polymers can give different characteristics. The significant alteration in rheological characteristics is largely due to temperature and concentration (Rao and Steffe, 1992). Besides the technology, complexity of producing, processing, and handling materials require a more extensive knowledge of their physical properties. Thus, the rheology is an ultimate quality control issue (Zakaria and Rahman, 1996). Rheology involves study on the deformation of matter due to application of force. It is most commonly applied in the study of liquids and liquid-like materials such as paints, polymer solutions, blood, molten plastics and oil well drilling mud. The rheological properties vary with the consistency index (K) and flow index (n) used in the Power-law model. The index, K varies radically with the temperature and solution concentration (Wanchoo et al., 1996). Several researchers have found that microscopic and mesoscopic clay particles influence rheological properties of the polymer nanocomposites (Solomon et al., 2001; Mitchell and Krishnamoorti, 2002).

A polymer can drastically modify the rheological properties of the fluid. Therefore, selection of appropriate polymer and polymer concentration is necessary to get optimal performance. For example, PMMA is added to motor oil for the reduction of oil property dependency on the temperature (Al-Shammari et al., 2011). The viscosity of the polymer solution depends on a number of factors and the solution viscosity depends on the concentration of the dissolved polymer. Krevelen (1990) mentioned that some of these factors include molecules shape, molecular weight, hydrophilic nature and interaction of polymers with the solvents. Al-Zaharani (1990) explained that in good solvents, polymer segments prefer to be surrounded by solvent molecules unlike the poor solvents where the polymer molecules try to minimize the area of contact with the solvent molecules, which directly

affects its size and the viscosity of the solution. Gutierrez et al. (2014) demonstrated use of a quartz crystal viscometer to determine the viscosity of PS/limonene solutions in the presence of high pressure carbon dioxide. Matsumoto et al. (1975) measured the dynamic and steady flow properties of disperse systems of styrene-divinylbenzene copolymer particles in a PS solution over wide ranges of frequency, shear rate, and strain amplitude. Their system showed Newtonian behavior at extremely low rates of shear, which results approximately constant apparent viscosity.

Ohta et al. (1994) studied rheological behavior of PE for its utilization in the gel spinning technology. The authors primarily investigated on the shear flow viscosity of these solutions and found that such PE solutions exhibit a shear thinning behavior ranging a shear rate of 10^{-4} to 10^{3} sec^{-1}. Moreover, non-Newtonian behavior was more apparent with increasing PE content in their solutions. Briscoe et al. (2000) concluded upon the influence of hydrogen bonding on the rheological behaviour of PVA solutions. Their work revealed that the rheological behavior primarily depends on the relative strength of H_2 bonding present among the polymer chains along with water molecules. Perez et al. (2005) studied rheology of metallocene linear low density polyethylene (m-LLDPE) with linear density polyethylene (LDPE), and they used extrusion rheometry to analyze miscibility effect on practical rheology. Al-Fariss et al. (1988) studied viscosity behavior of three types of Saudi Arabian crude oils as a function of shear rate at certain temperatures. The modified correlation proposed in this study has been found to fit well with the experimental data for crude oils as well as the polymer. Kundu and Kundu (2001) demonstrated that the gelation depends on the wt.% ratio of methyl cellulose and surfactants which were present in the solution. Costa et al. (2006a) examined linear viscoelastic characteristics of Mg-Al LDH nanocomposites with

LDPE and HDPE and also studied upon the effect of LDH loading in the temperature range of 180 – 260 °C.

In this chapter of the thesis, studies conducted on the rheological behavior of PS/Co-Al LDH blend solutions at various temperatures using rotational rheometer with parallel plate geometry have been presented. The obtained experimental results were evaluated for their fitness with various rheological models such as Power law, Herschel-Bulkley, Carreau, Sisko, Casson and Cross model. Shear stress and viscosity were determined as a function of shear rate. Depending on the combination of regression co-efficient, bias factor and standard error values, the best rheological model in this study has been identified.

3.2 Experimental

3.2.1 Materials

PS was procured from National Chemicals Ltd., Gujarat India. All other materials were same as those discussed in section 2.2.1.

3.2.2 Preparation of modified Co-Al LDH

Section 2.2.2 summarizes synthesis procedure for modified Co-Al LDH material.

3.2.3 Synthesis of PS/Co-Al LDH blend solution

PS/Co-Al LDH blend was prepared in xylene (Table 3.1). Prior to synthesis, PS and modified Co-Al LDH were dried for 12 h at 60 and 70 °C, respectively in a hot air oven to

Table 3.1: Nomenclature and sample composition for various PS/Co-Al LDH blend solutions.

Sample Name	LDH loading (wt.%)	LDH (g)	Solvent (mL)	PS (g)
PS	0	0	109	5
PSCL 3	3	0.15	109	4.85
PSCL 5	5	0.25	109	4.75
PSCL 7	7	0.35	109	4.65

remove the adsorbed moisture content. Firstly, a required amount of LDH was added in 109 mL of xylene and continuously allowed to stir for 24 h. Further, calculated quantity of PS was added in the prepared LDH solution and again allowed to stir for 12 h at atmospheric conditions. The pristine PS solution was synthesized by following the similar process in the absence of Co-Al LDH. The resultant PS and PS/Co-Al LDH blend solution was taken immediately for rheological analysis. The prepared solution have been designated as pristine PS, PSCL 3, PSCL 5 and PSCL 7 for polystyrene, PS/Co-Al LDH (3 wt.%), PS/Co-Al LDH (5 wt.%) and PS/Co-Al LDH 7 (wt.%), respectively.

3.3 Characterization

Rheological measurements were conducted on a rotational rheometer, Physica MCR 301 (Anton Paar), by parallel plate geometry with 50 mm of radius. The parallel plate rheometer comprises two parallel with circular plates, in which one of them is stationary, and the other one rotates. Rheological studies were carried out in the shear rate ranging between

0.1 sec^{-1} and 100 sec^{-1}. Fresh samples were used for each measurement at temperatures of 20, 30 and 40 °C.

3.4 Rheological models

Majority of polymer solutions are non-Newtonian i.e., the viscosity of the polymer mixture and solution varies with factors besides shear rate. Mostly polymeric solutions are shear thinning in nature or the viscosity of the polymer solution and blends decrease with increasing shear rate. This can be elaborated by the arrangement of polymeric chain on applying a shear force. At a higher shear rate, viscosity decreases because of easier flow of molecules owing to alignment of the polymer molecules. Various mathematical models have been used to explain the shear rate versus shear stress of non-Newtonian fluids.

Power law (Reiner, 1926) and Bingham plastic model are the most common two parameter models. The power law model is stated as:

$$\tau = K \gamma^{n} \quad (3.1a)$$

$$\eta = K. \gamma^{n-1} \quad (3.1b)$$

where, γ is the shear rate, τ is the shear stress, η is the apparent viscosity, K is the consistency index, and n is the power law parameter or flow behavior index. For a Newtonian fluid n is equal to 1, for shear thickening fluid, n is more than 1 and for shear thinning fluid, n is less than 1.

Herschel–Bulkley model is expressed as (Herschel and Bulkley (1926)):

$$\tau = \tau_{o} + K \gamma^{n} \quad (3.2)$$

Bingham plastic model is expressed as (Bingham (1922)):

$$\tau = \tau_o + \gamma.\mu_p \quad (3.3)$$

were, τ_o is the yield stress and μ_p is the plastic viscosity. There are numerous models that include three or more parameters. Third parameter helps to describe the flow of fluid in the upper and lower Newtonian region as well as in the power law region.

Sisko model is a three parameter model (Sisko, 1958). It is used to articulate the flow behavior in Power law region and upper Newtonian region.

$$\eta = \eta_\infty + K\gamma^{n-1} \quad (3.4)$$

Casson model is also used to express the non-Newtonian behavior (Casson, 1989)

$$\tau = \tau_o^{1/2} + \eta_\infty \gamma^{1/2} \quad (3.5)$$

where, η_α is the viscosity at infinite shear stress.

Both Cross and Carreau models are used to express the flow characteristics of polymer solution, blood flow, activated sludge and food. They are four parameter models.

Cross model is expresses as (Cross, 1965):

$$\eta = \eta_\infty + [(\eta_o - \eta_\infty) / (1+ (C \times \gamma)^m)] \quad (3.6)$$

where, C, m, η_o and η_α are time constant, dimensionless exponent, initial viscosity (measured at zero shear rate) and final viscosity (measured at infinite shear rate), respectively.

Carreau model is expressed as (Carreau et al., 1968):

$$\eta = \eta_\infty + [(\eta_o-\eta_\infty) \times (1+ (\lambda \times \gamma)^2)^{(n-1)/2}] \quad (3.7)$$

In the above expression, viscosity at infinite/final shear rate and viscosity at initial/zero shear rate are denoted as η_α and η_o, respectively. λ is the relaxation time. n is the gauge of shear thinning properties.

The standard error (SE) formula is used to fit the model with the experimental data (Nindo et al., 2007)

$$SE= (\sum(y_m - y_c)^2 / (n-1))^{1/2} \quad (3.8)$$

where, calculated value is denoted as y_c, measured value is as y_m at each data point and number of data point as n. Bias factor gives us additional information about variance of measured from calculated values. Bias factor (B_f) of 1 signifies that measured values coincide with calculated values.

The B_f is described as follows (Betts and Walker, 2004):

$$B_f = 10^{[\sum \log (y_c / y_m) / n)]} \quad (3.9)$$

The parity plot (measured vs. calculated viscosity graph) and standard error/bias factor values need to be consistent with one another.

3.5 Results and discussion

3.5.1 Effect of modified Co-Al LDH

The polymer solution viscosity mainly relies on various factors that include molecular weight, molecular shape and polymer molecules interaction with the solvents. Furthermore, the viscosity of solution depends on the dissolved polymer concentration. The prepared PS and PS/Co-Al LDH blend solutions were considered to examine the effect of Co-Al LDH content at various temperatures on the shear stress and viscosity by changing the shear rate. The influence of LDH content on shear stress versus shear rate for pristine PS and PS/LDH solution is illustrated in Figures 3.1 – 3.3. The trends obtained from the rheological analysis

convey that at low shear rate (0.1 – 10 sec^{-1} and 0.1 – 20 sec^{-1} for PS and PS/Co-Al LDH blend solutions, respectively) the viscosity of PS and PS/Co-Al LDH blend solutions rapidly decrease with increasing shear rate (see Figures 3.1 – 3.3). At higher shear rates ranging between 30 and 100 sec^{-1}, the viscosity remains almost constant. The trends in rheological analysis demonstrate that the investigated pristine PS and PS/LDH solutions behave in a non-Newtonian manner (revealed with a reduction in solution viscosity with increasing shear rate as in Figures 3.1 – 3.3). It is also observed that as the content of LDH increases, solution viscosity also increases due to the increased LDH particle interaction with PS matrix and subsequent difficulty for flow. When the content of Co-Al LDH increases, the viscosity of PS solution also increases due to enhancement in intermolecular association. Most theories related to viscosity of polymer solutions are formulated around dilute solutions but, for real polymer solutions, viscosity prediction are often more complex than those predicted with simple theories.

3.5.2 Effect of temperature

Similar to the procedures associated to studies conducted to evaluate upon the effect of modified Co-Al LDH concentration, the prepared PS/Co-Al LDH blend and PS solutions were investigated to evaluate the effect of temperature (20, 30, 40 °C) on the shear stress and viscosity. To do so, shear rate has been varied in the carried out investigations. As presented in Figures (3.4 – 3.7), an increase in temperature reduces dispersion shear stress. This observation is similar to the data of Graziano et al. (1979) and had been explained either due to reduction in the interactive forces or disappearance of the water bridges due to evaporation.

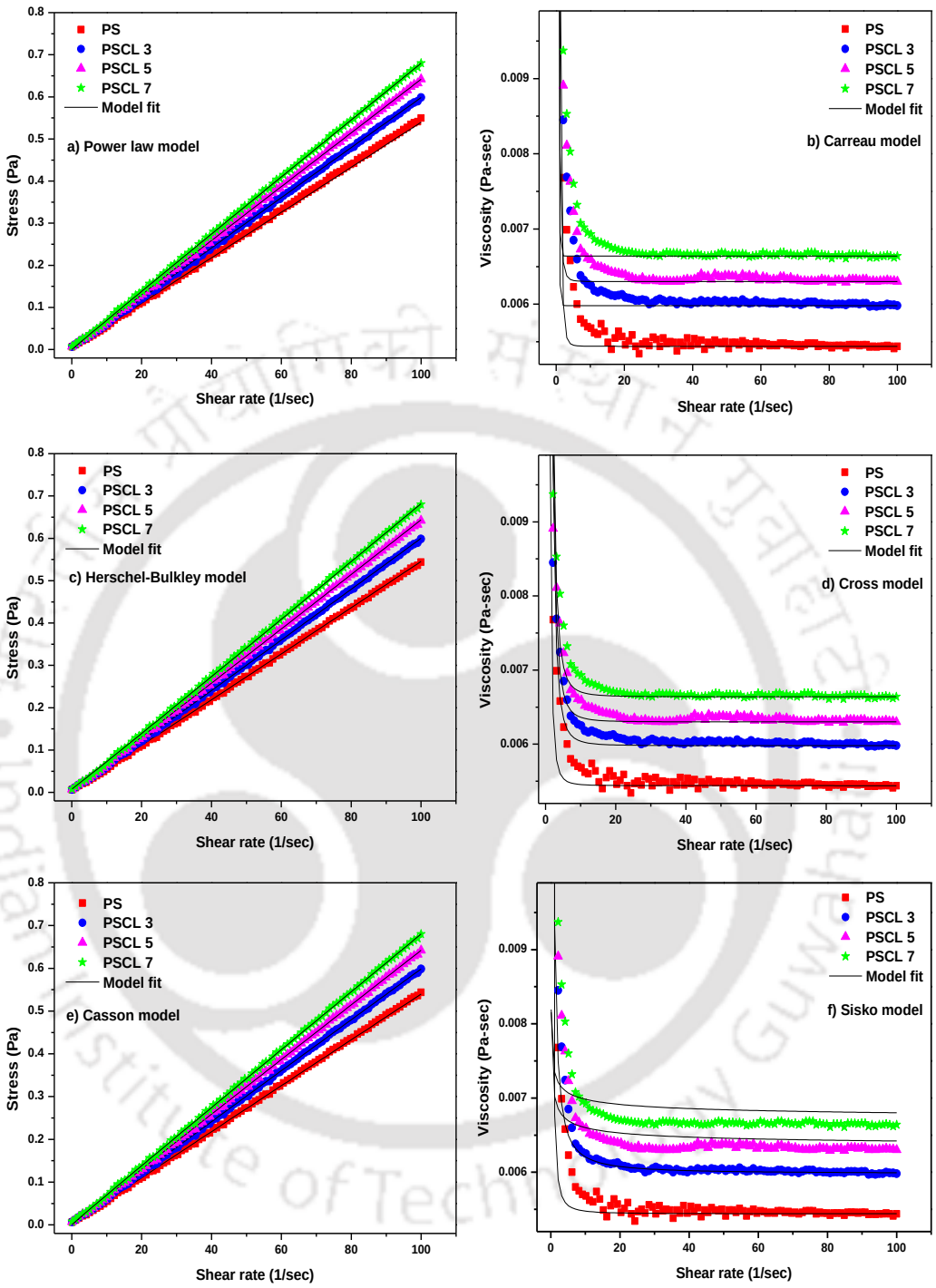

Figure 3.1(a-f): Model fitness plots of PS and PS/Co-Al LDH blend solution rheological data measured at 20 °C.

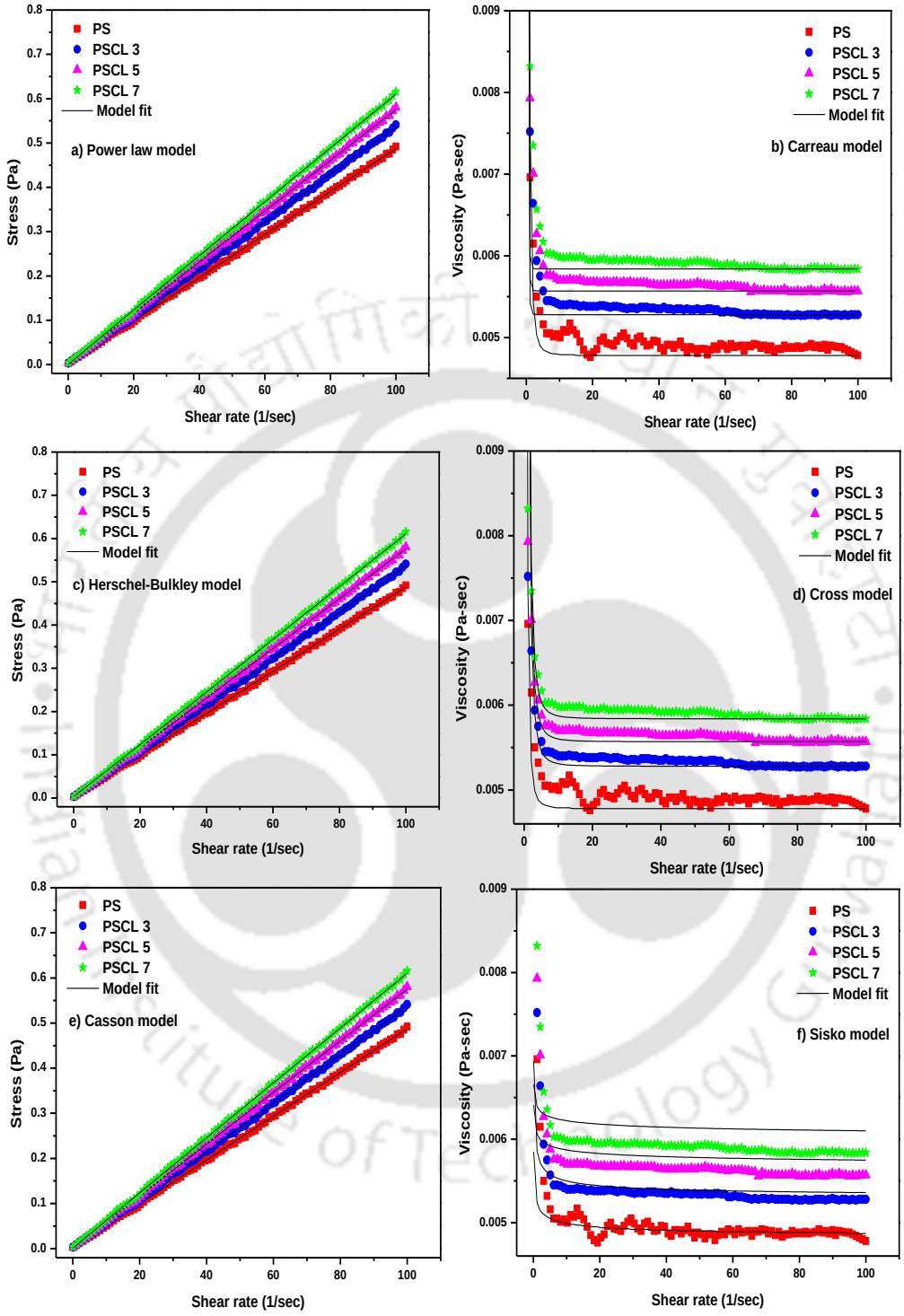

Figure 3.2 (a-f): Model fitness plots of PS and PS/Co-Al LDH blend solution rheological data measured at 30 °C.

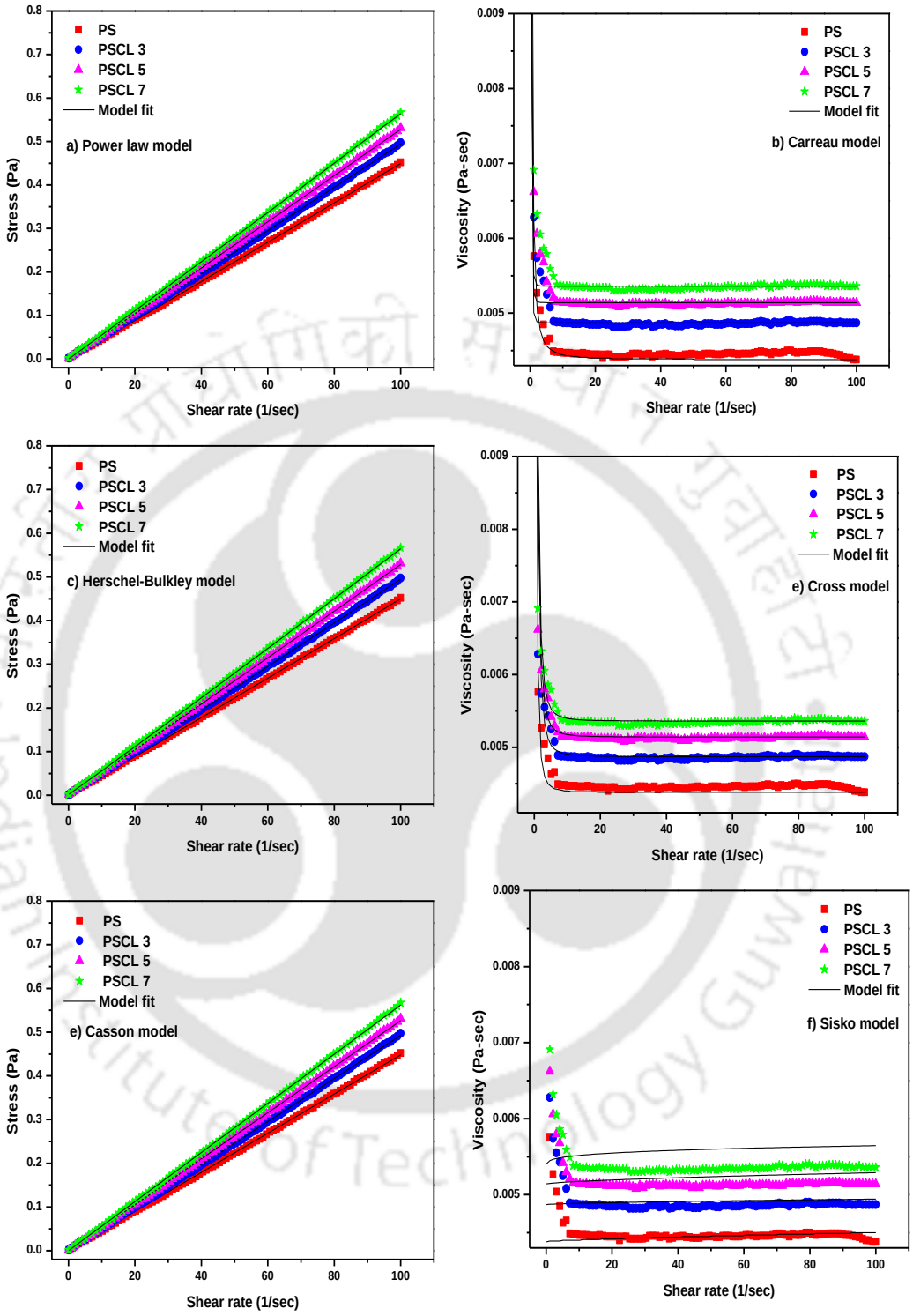

Figure 3.3 (a-f): Model fitness plots of PS and PS/Co-Al LDH blend solution rheological measured data at 40 °C.

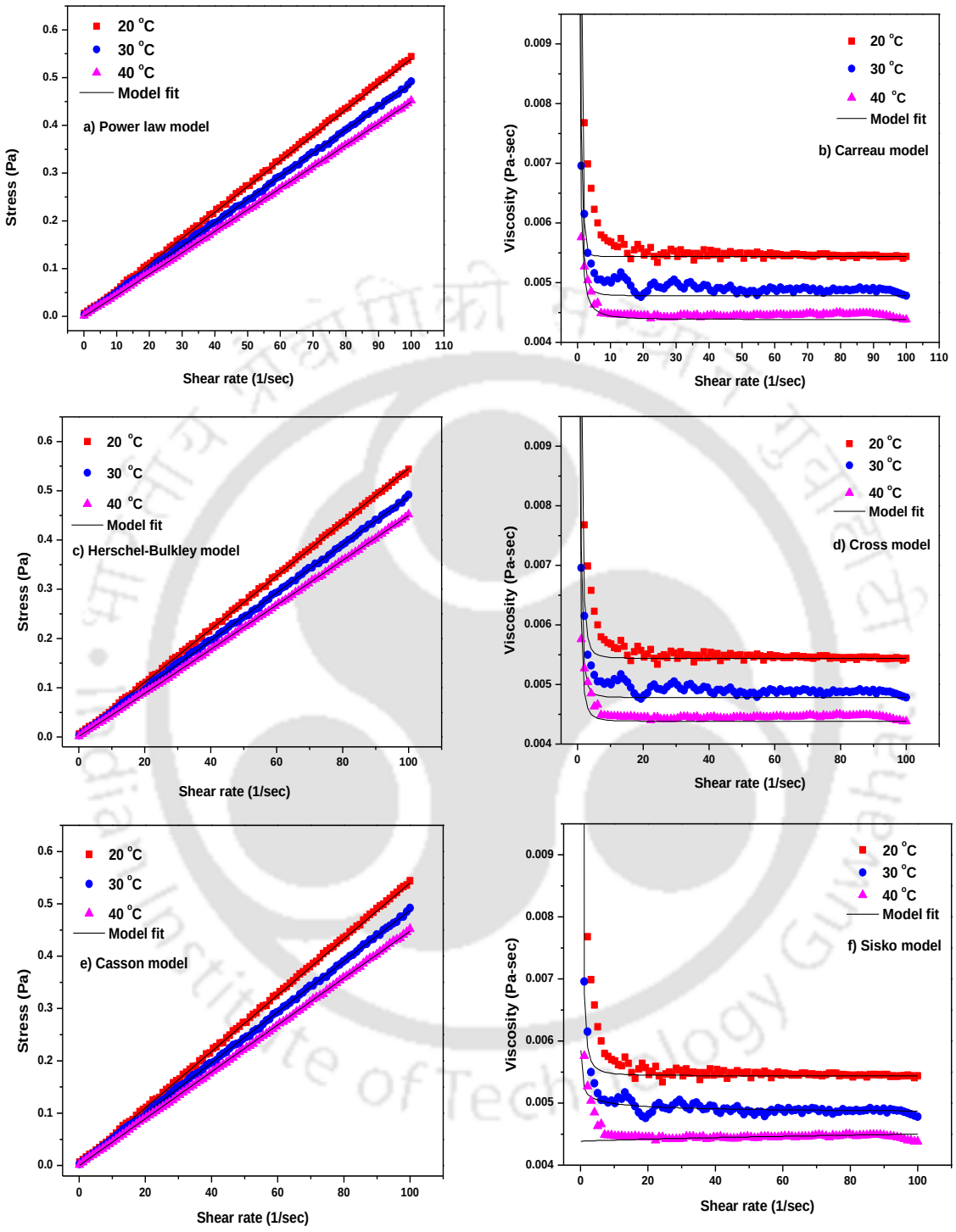

Figure 3.4 (a-f): Model fitness plots of pristine PS solution rheological data measured at various temperatures.

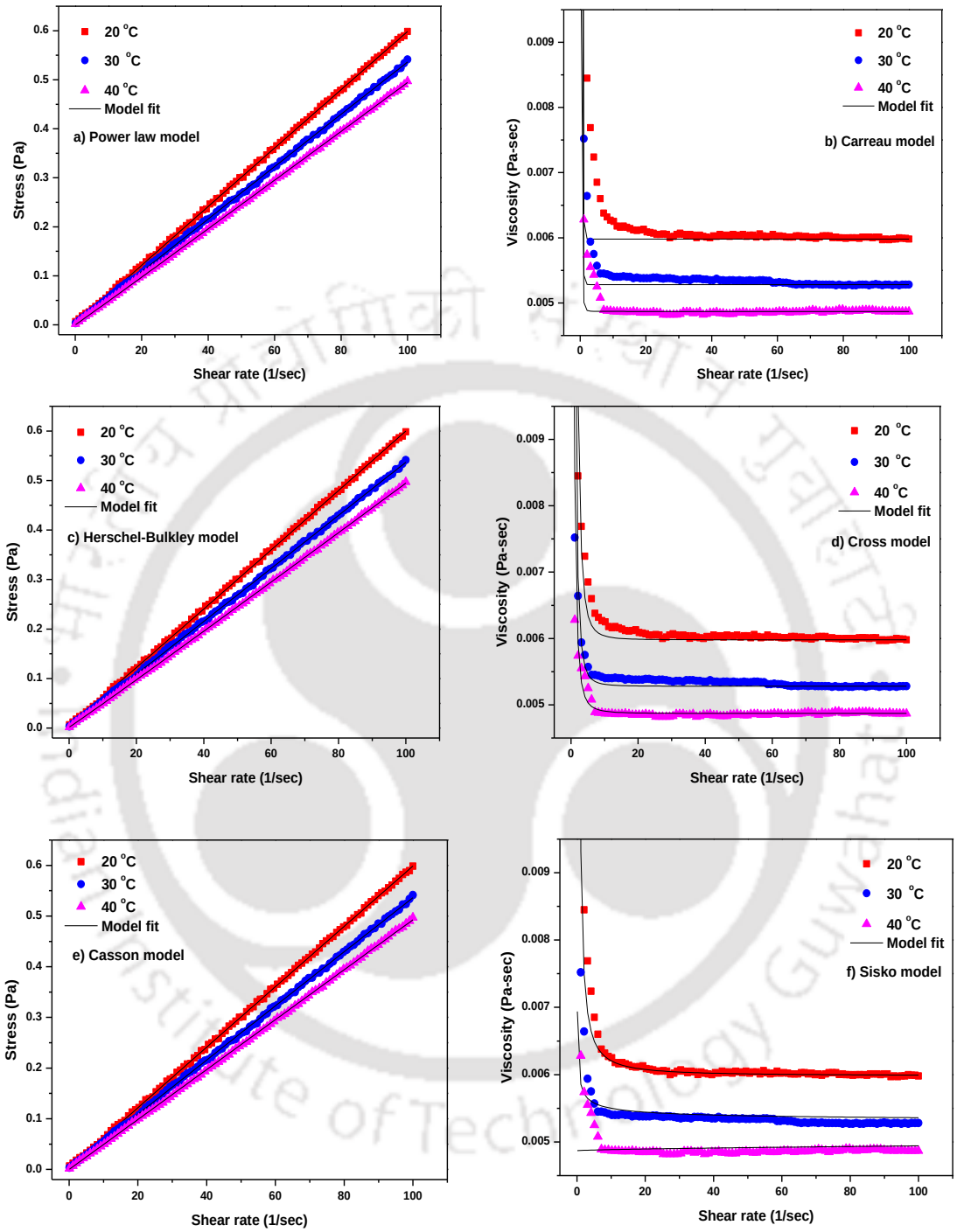

Figure 3.5 (a-f): Model fitness plots of PSCL 3 solution rheological data measured at various temperatures.

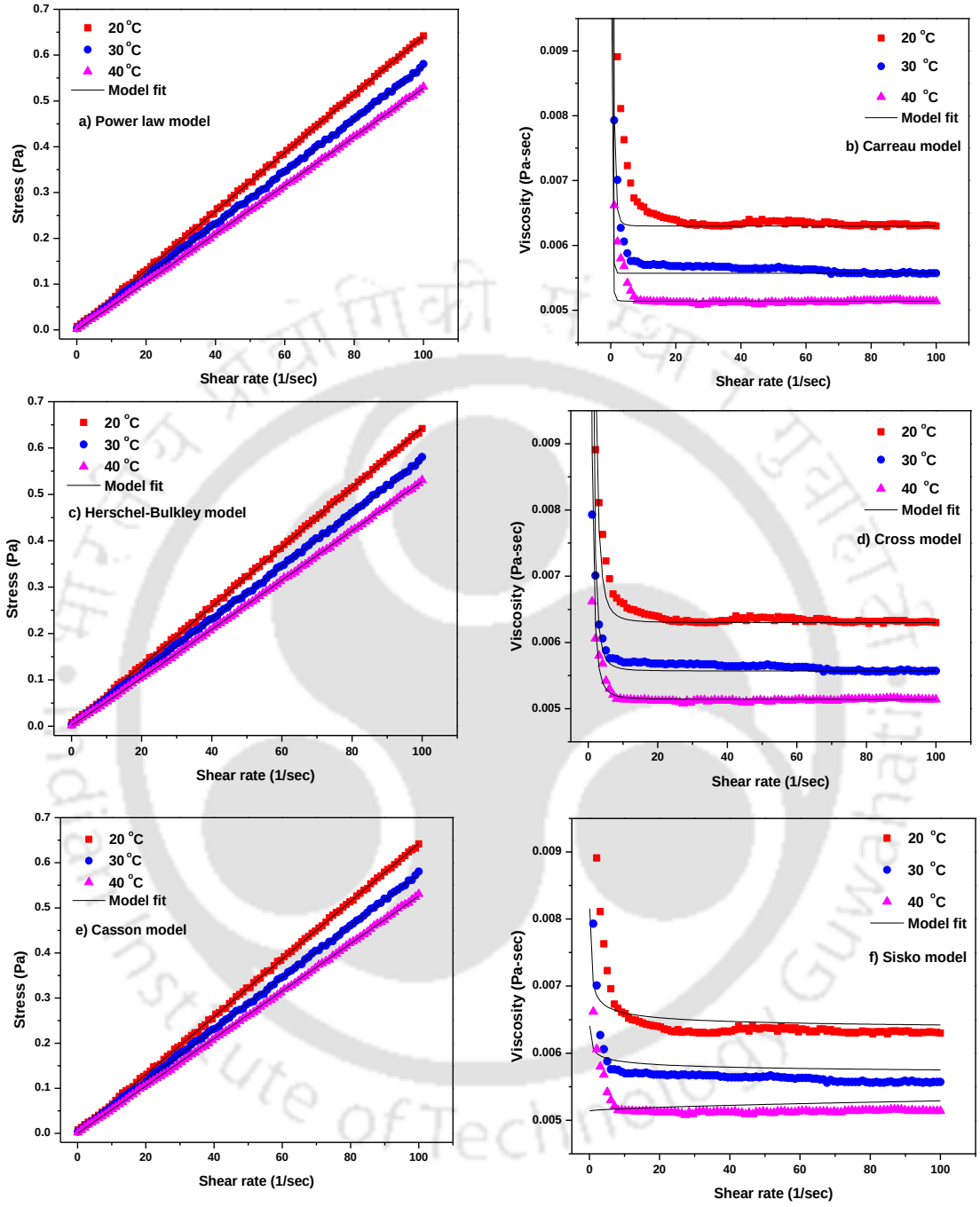

Figure 3.6 (a-f): Model fitness plots of PSCL 5 blend solution rheological data measured at various temperatures.

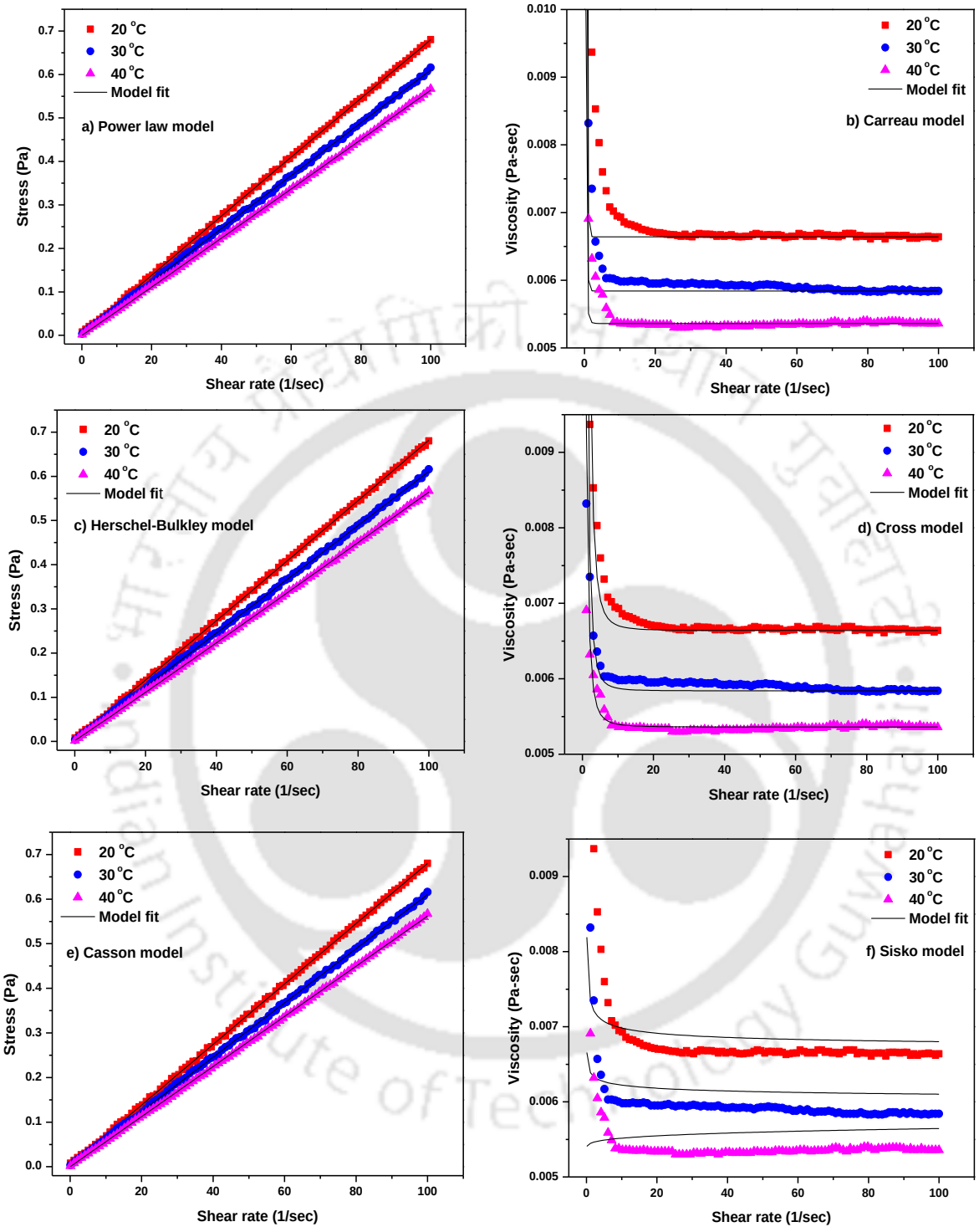

Figure 3.7 (a-f): Model fitness plots of PSCL 7 blend solution rheological data measured at various temperatures.

According to the traditional concepts used in establishing time rate temperature reduced variables (Graziano et al., 1979), an increase in temperature corresponds to a shift to lower effective shear rates. This is consistent with the trend shown in figures, as far as the shapes of the curves are concerned. The level of the curves decreases at higher temperatures, indicating that a different generalized Ostwald curve must be considered at each temperature for any given material. While the modified Co-Al LDH content increases, the polymer blend solution viscosity also increases. Similarly, at higher loading (> 7 wt.% LDH), the polymer solution flow decreases regardless of its temperature. As seen from the figures, there is a jump in viscosity as the concentration was increased for all temperatures.

3.5.3 Rheological models

Models described earlier have been used to fit experimental data obtained from the rheological study of pristine PS and PS/Co-Al LDH blend solutions at three different temperatures. In this investigation, we have taken η_o, η_∞ as known quantity by considering them as viscosity at initial and final shear rate, respectively. The calculated parameters for all models are listed in Table 3.2. The regression coefficient (R^2) values of the estimated τ, η indicate that the Herschel-Buckley, Power law and Casson model are the best fit among all the models followed by Cross model. Other models, Carreau and Sisko predictions are not good as per n value. Analysis of Figures 3.8 – 3.11 give us more information about best fitted models. Models such as Power law and Casson model (R^2 nearby 1) are deviating from the line of equivalence (45° line). To justify our analysis, Bias factor and standard error values are calculated as presented in Table 3.3. Figures (3.8 – 3.11) obtained for different rheological model with respect to each solution convey whether the model predicted data is under

predicted or over predicted. Bias factor, B_f >1 signifies over prediction; B_f < 1 signifies under prediction and B_f = 1 means perfect model fitting with the experimental data. As illustrated in Figures 3.8 – 3.11, the pristine PS solution closely followed the trend given by Herschel-Bulkley model at temperature of 20 °C and Cross model best fits with measured data of 30 and 40 °C. Consequently, for the PS with variant concentration of modified Co-Al LDH, low temperature (20 °C) and high temperature (30 and 40 °C) data fit well with Herschel-Buckley and Cross model, respectively. B_f analysis demonstrates that the Herschel-Bulkley and Cross model fit data are under predicting the measured value. Two models were suggested to relate the apparent viscosity to modified Co-Al LDH content, shear rate and temperature, which evidently affect the flow properties of the PS solution. The viscosity of the PS enhances with an increase in modified Co-Al LDH content and decreases with increasing temperature and shear rate.

Table 3.2: Linear regression model parameters for rheological behaviour of PS/Co-Al LDH blend solutions.

Model	LDH loading (wt.%)	Temperature (°C)	Parameters		R^2
			K	n	
Power law	0	20	0.0056	0.9891	0.9999
		30	0.0050	0.9928	0.9998
		40	0.0042	1.0098	0.9999
	3	20	0.0062	0.9905	0.9998
		30	0.0055	0.9928	0.9998
		40	0.0047	1.0098	0.9999
	5	20	0.0067	0.9905	0.9998
		30	0.0059	0.9928	0.9998
		40	0.0051	1.0098	0.9999
	7	20	0.0071	0.9905	0.9998
		30	0.0063	0.9928	0.9998
		40	0.0054	1.0098	0.9999

Model	LDH loading (wt.%)	Temperature (°C)	Parameters		R^2
			C	**m**	
Cross	0	20	2.1061	2.7013	0.9979
		30	2.1222	2.5165	0.9941
		40	2.0623	2.1430	0.9901
	3	20	2.1065	2.6993	0.9980
		30	2.1123	2.6213	0.9972
		40	2.0689	2.2454	0.9938
	5	20	2.1061	2.6973	0.9980
		30	2.1140	2.6199	0.9971
		40	2.0620	2.2792	0.9948
	7	20	2.1059	2.7032	0.9981
		30	2.1130	2.6185	0.9971
		40	2.0646	2.2655	0.9944
			λ	**n**	
Carreau	0	20	1.2234	-3.5079	0.9963
		30	1.8874	-1.5653	0.9924
		40	2.7341	-0.5848	0.9906
	3	20	1.2324	-3.4630	0.9963
		30	1.5675	-2.2424	0.9955
		40	2.3546	-0.8725	0.9933
	5	20	2.0099	-0.6444	0.9738
		30	1.5716	-2.2338	0.9954
		40	2.2669	-0.9540	0.9941
	7	20	1.2175	-3.5386	0.9964
		30	1.5749	-2.2231	0.9954
		40	2.3085	-0.9150	0.9938
			K	**n**	
Sisko	0	20	1.57×10^{-3}	-0.6408	0.9999
		30	4.75×10^{-4}	0.6467	0.9998
		40	4.86×10^{-6}	1.6999	0.9999
	3	20	0.0037	-0.2239	0.9998
		30	0.0006	0.5623	0.9998
		40	3.72×10^{-6}	1.6436	0.9999
	5	20	0.0007	0.6046	0.9998
		30	0.0005	0.7778	0.9998
		40	7.57×10^{-6}	1.6477	0.9999
	7	20	0.0007	0.6725	0.9998
		30	0.0005	0.8356	0.9998

Model	LDH loading (wt.%)	Temperature (°C)	Parameters		R^2
		40	8.56×10^{-5}	1.2606	0.9999
			K	**n**	
Herschel-Bulkley	0	20	5.0×10^{-3}	1.0163	0.9998
		30	4.70×10^{-3}	1.0064	0.9998
		40	4.12×10^{-3}	1.0181	0.9999
	3	20	0.0055	1.0162	0.9998
		30	0.0052	1.0064	0.9998
		40	0.0045	1.0181	0.9999
	5	20	0.0059	1.0162	0.9998
		30	0.0055	1.0064	0.9998
		40	0.0048	1.0181	0.9999
	7	20	0.0062	1.0162	0.9998
		30	0.0058	1.0064	0.9998
		40	0.0052	1.0181	0.9999
			τ_o	η_∞	
Casson	0	20	3.49×10^{-5}	5.30×10^{-3}	0.9999
		30	1.59×10^{-5}	4.82×10^{-3}	0.9998
		40	1.52×10^{-15}	4.47×10^{-3}	0.9998
	3	20	2.68×10^{-5}	0.0059	0.9998
		30	1.75×10^{-5}	0.0053	0.9998
		40	6.78×10^{-19}	0.0049	0.9998
	5	20	2.88×10^{-5}	0.0063	0.9998
		30	1.87×10^{-5}	0.0056	0.9998
		40	2.38×10^{-16}	0.0052	0.9998
	7	20	3.05×10^{-5}	0.0067	0.9998
		30	1.99×10^{-5}	0.0060	0.9998
		40	1.81×10^{-20}	0.0056	0.9998

In other rheological studies, Diaz and Navaza (2003) studied the rheological properties of carboxymethyl cellulose and alginate sodium salts. In their study, the apparent viscosity and the influence of shear rate on different polymers concentration and temperature on rheological behaviour have been reported. To fit the experimental data, the power law (Ostwald de Waele model) was chosen for its simplicity and the good fit was obtained for this model. Hamed and Belhadri (2009) evaluated the rheological behaviour of different samples and determined the effect of components such as clay, calcium carbonate and potassium chloride.

Table 3.3: Bias factor and standard error of various viscosity models for PS/Co-Al LDH system.

Model	Sample	Temperature (°C)	B_f	SE
Power law	PS	20	0.9540	0.0057
		30	0.9704	0.0024
		40	0.9570	0.0012
	PSCL 3	20	0.9603	0.0062
		30	0.9872	0.0026
		40	0.9861	0.0013
	PSCL 5	20	0.9793	0.0066
		30	1.0027	0.0027
		40	0.9985	0.0014
	PSCL 7	20	0.9866	0.0069
		30	1.0145	0.0029
		40	1.0224	0.0014
Cross	PS	20	0.9984	0.0012
		30	0.9720	0.0002
		40	0.9820	0.0001
	PSCL 3	20	0.9967	0.0011
		30	0.9964	0.0004
		40	1.0043	0.0002
	PSCL 5	20	0.9982	0.0012
		30	0.9952	0.0005
		40	1.0045	0.0002
	PSCL 7	20	1.0004	0.0013
		30	0.9951	0.0005
		40	1.0043	0.0003
Carreau	PS	20	0.9690	0.0031
		30	0.9730	0.0002
		40	0.9850	0.0001
	PSCL 3	20	0.9679	0.0034
		30	0.9769	0.0014
		40	0.9893	0.0007
	PSCL 5	20	0.9719	0.0035
		30	0.9758	0.0015
		40	0.9897	0.0007
	PSCL 7	20	0.9716	0.0037
		30	0.9756	0.0016
		40	0.9894	0.0008

Model	Sample	Temperature (°C)	B_f	SE
Sisko	PS	20	0.9824	0.0013
		30	0.9782	0.0024
		40	0.9790	0.0012
	PSCL 3	20	0.9927	0.0002
		30	0.9922	0.0025
		40	0.9901	0.0013
	PSCL 5	20	0.9830	0.0064
		30	1.0045	0.0027
		40	0.9989	0.0014
	PSCL 7	20	0.9893	0.0068
		30	1.0158	0.0028
		40	1.0225	0.0014
Herschel-Bulkley	PS	20	1.0030	0.0005
		30	1.0023	0.0005
		40	1.0090	0.0004
	PSCL 3	20	1.0035	0.0005
		30	1.0173	0.0006
		40	1.0091	0.0007
	PSCL 5	20	1.0233	0.0007
		30	1.0333	0.0007
		40	1.0219	0.0008
	PSCL 7	20	1.0309	0.0008
		30	1.0454	0.0008
		40	1.0463	0.0008
Casson	PS	20	0.9590	0.0054
		30	0.9784	0.0023
		40	0.9830	0.0012
	PSCL 3	20	0.9658	0.0060
		30	0.9926	0.0024
		40	0.9913	0.0013
	PSCL 5	20	0.9848	0.0063
		30	1.0081	0.0026
		40	1.0050	0.0014
	PSCL 7	20	0.9922	0.0066
		30	1.0201	0.0027
		40	1.0291	0.0014

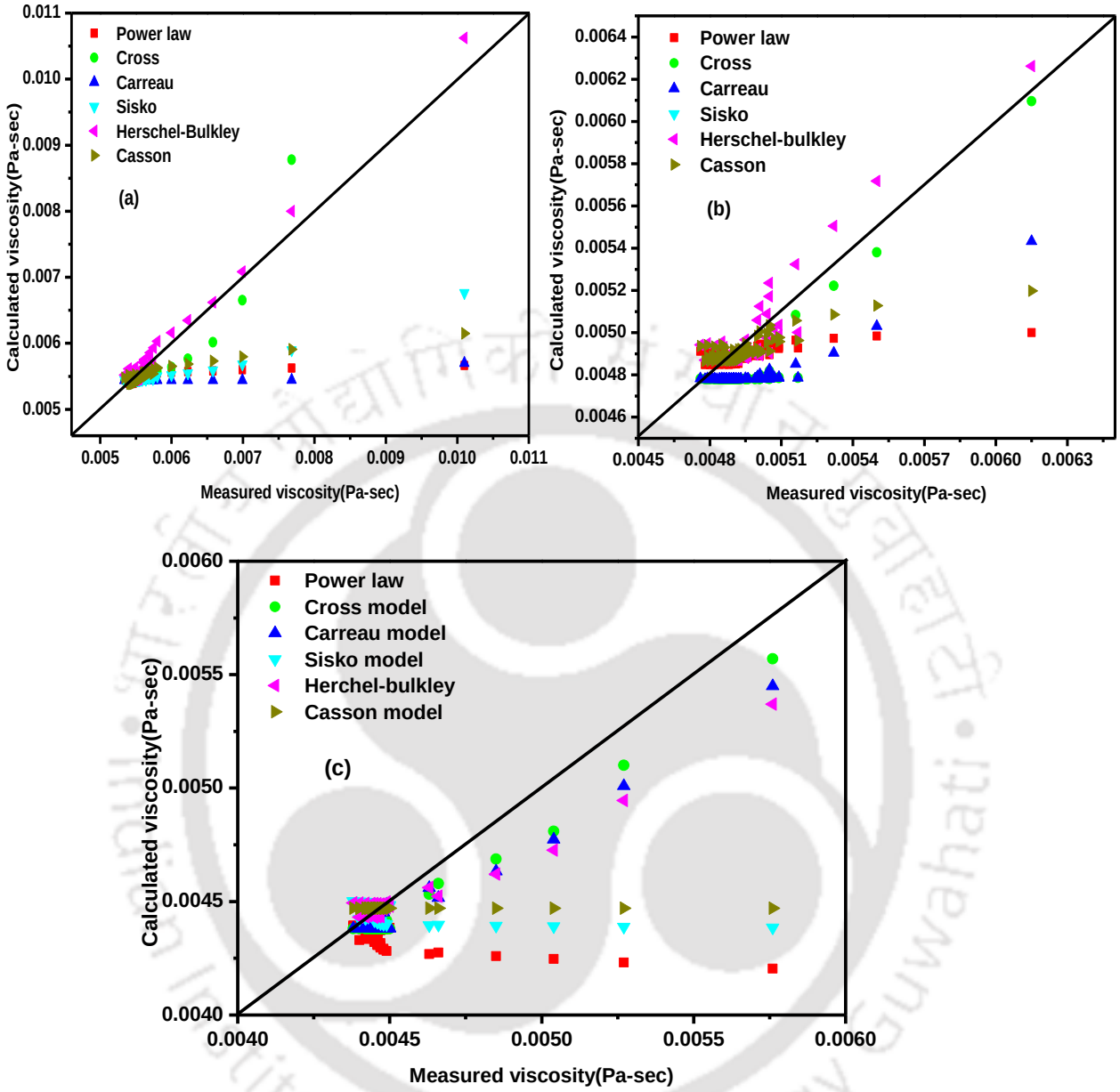

Figure 3.8 (a-c): Viscosity parity plots for pristine PS solution data measured at (a) 20 °C, (b) 30 °C and (c) 40 °C.

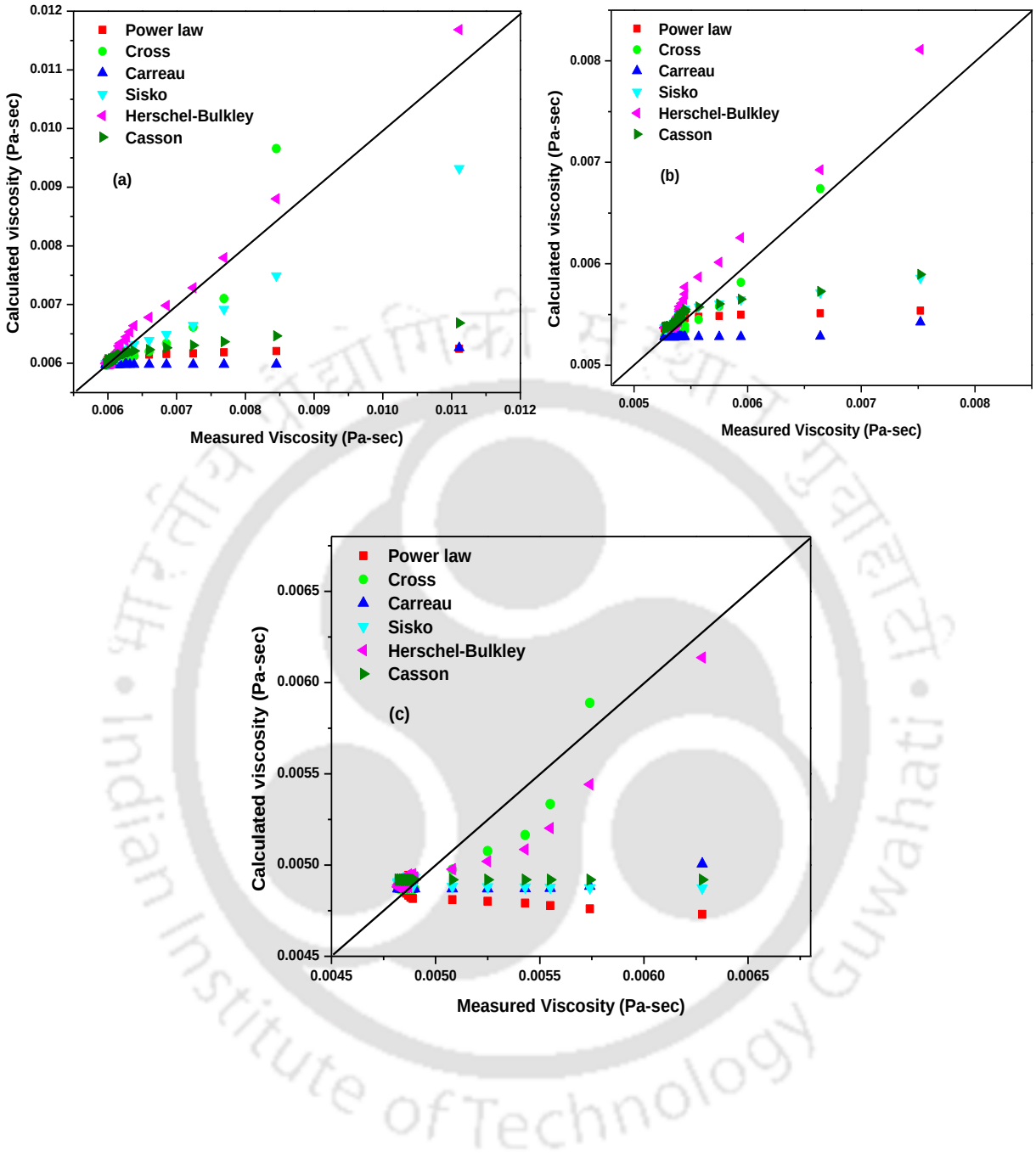

Figure 3.9 (a-c): Viscosity parity plots for PSCL 3 solution data measured at (a) 20 °C, (b) 30 °C and (c) 40 °C.

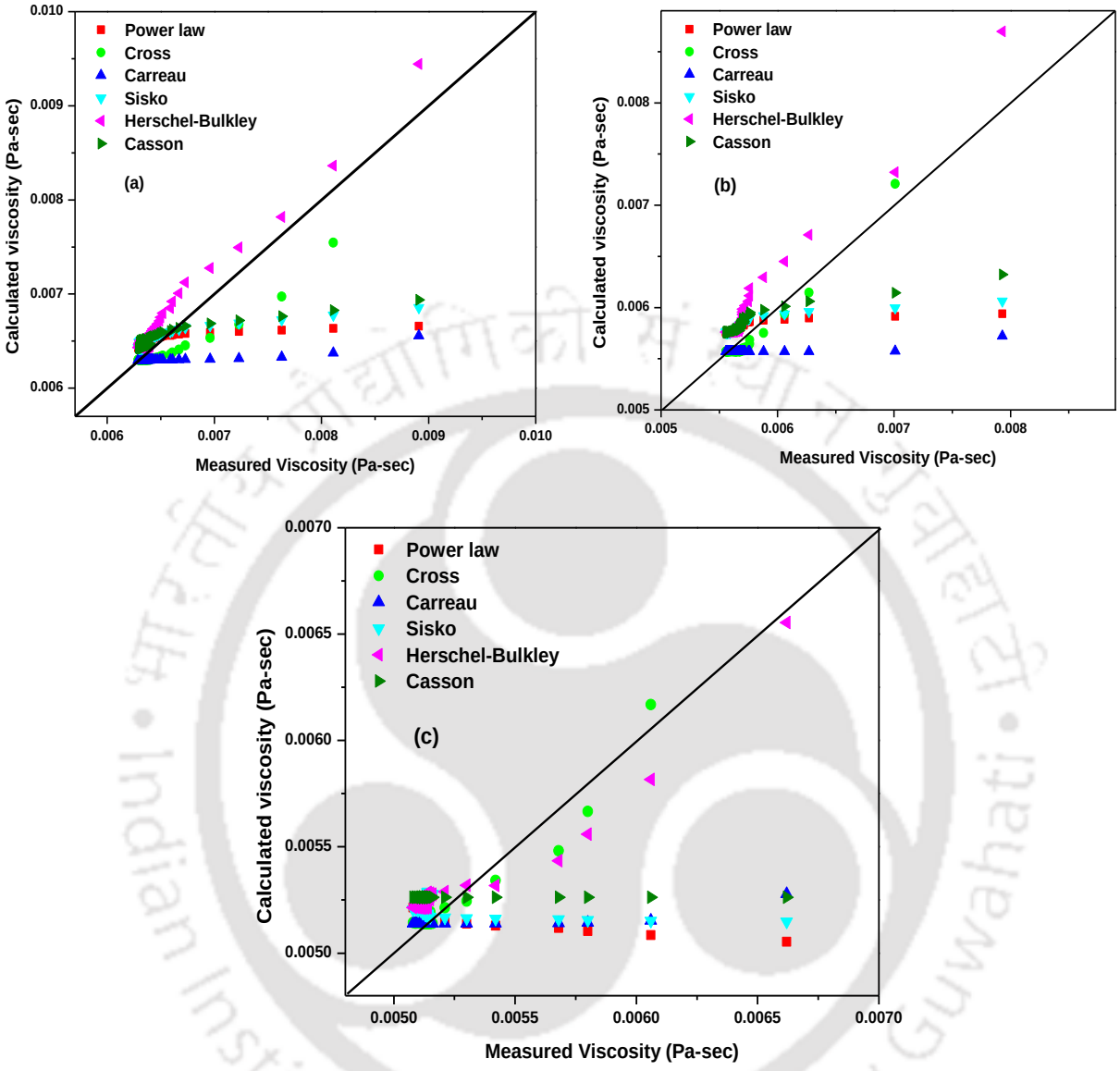

Figure 3.10 (a-c): Viscosity parity plots for PSCL 5 solution data measured at (a) 20 °C, (b) 30 °C and (c) 40 °C.

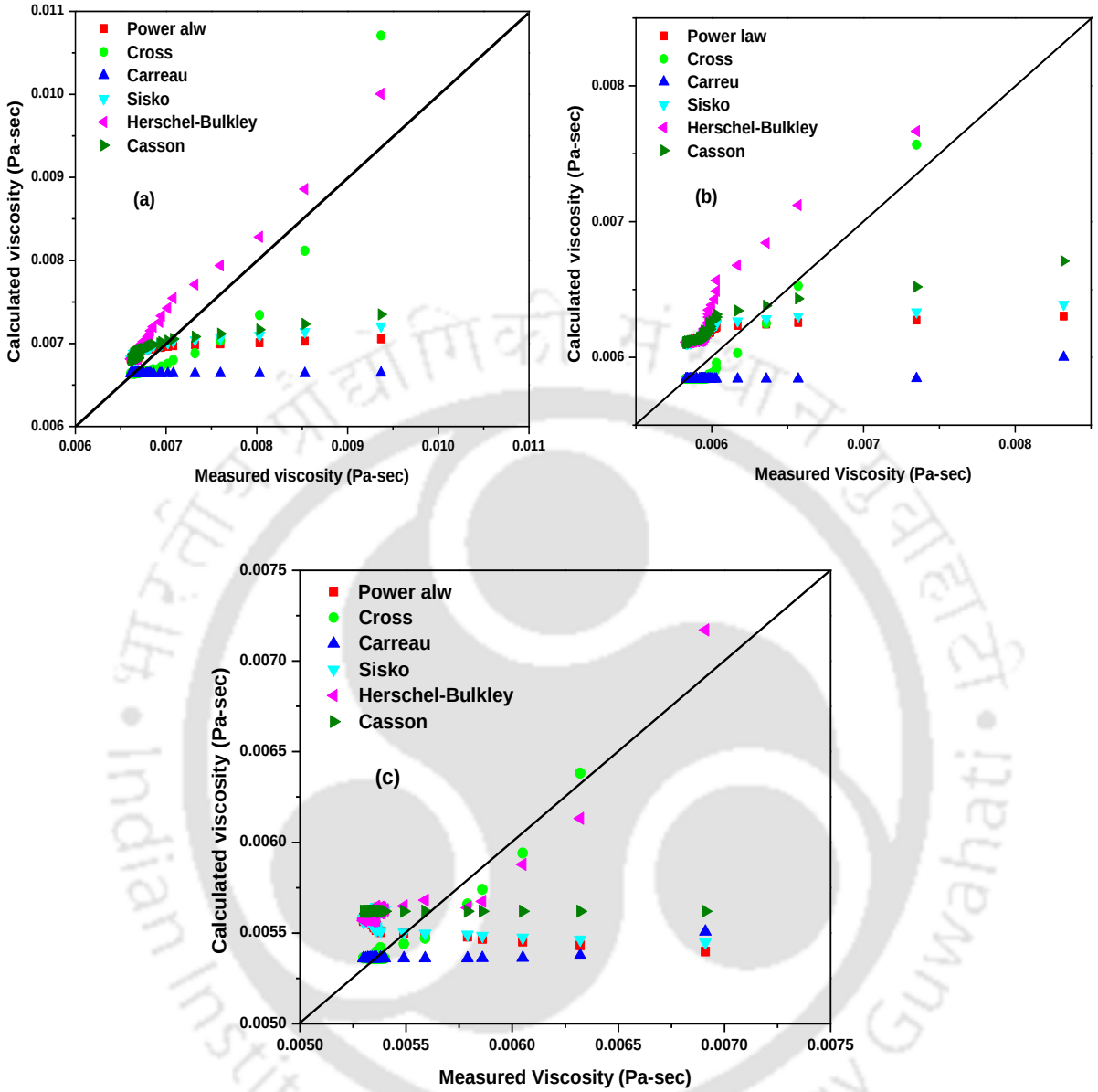

Figure 3.11 (a-c): Viscosity parity plots for PSCL 7 solution data measured at (a) 20 °C, (b) 30 °C and (c) 40 °C.

These formulations exhibited non-Newtonian rheological behaviour, which were described well by the three parameter, Herschel-Bulkley rheological model.

Figures 3.8 – 3.11 justify that the correlations given in this work fit better with experimental values than that of Rosenberger et al. (2002) in the entire range of parameters (LDH (0 – 0.35 g), temperature (20, 30 and 40 °C) and shear rate (0.1 – 100 sec^{-1}). Hence, these models could be especially useful in hydrodynamic optimization and also computational fluid dynamic (CFD) simulation of airlift where viscosity plays a major role on the hydrodynamic regime, oxygen transfer and mass transport and consequently influences the system performance (Garakani et al., 2011).

3.6 Summary

The effect of LDH loading with temperature on the rheological behaviour of PS/Co-Al LDH blends has been effectively studied, which is crucial for polymer manufacturing industries. Rheological studies demonstrated enhancement in viscosity with increasing LDH loading in the polymer solution. The viscosity of PS and PS/Co-Al LDH solution decreased with increasing the shear rate for all applied temperatures. To assess upon the flow behaviour of the PS solution, rheology data of PS and PS/Co-Al LDH solution were validated with various rheological models such as Herschel-Bulkley, Power law, Sisko, Casson, Carreau and Cross model. From regression coefficient and B_f analysis, Herschel-Bulkley model fit well with rheological data obtained at 20 °C and cross model fit well for data obtained at 30 and 40 °C. Similarly, for the PS loaded with variant concentrations of Co-Al LDH, Hershel-Buckley and Cross model fit well to represent rheological behaviour existent at lower (20 °C) and higher (30 and 40 °C), respectively.

Chapter 4:

Preparation and Characterization of PS/CO-Al LDH and PS/Ni-Al LDH Nanocomposites by Solvent Blending Method

Chapter 4

Preparation and Characterization of PS/Co-Al LDH and PS/Ni-Al LDH Nanocomposites by Solvent Blending Method

This chapter summarizes procedures adopted and subsequent characterization analysis of PS/LDH nanocomposites prepared with solvent blending method and variant content (1 – 7 wt.%) of modified Co-Al LDH and Ni-Al LDH. Structural, thermal and viscoelastic properties of the prepared PS/LDHs nanocomposites were evaluated using XRD, TEM, FTIR, TGA, DSC and rheometer. Moreover, the activation energy of the degradation process of both pristine PS and PS nanocomposites was evaluated using Coats-Redfern method. Criado model was deployed to evaluate reaction mechanism associated to thermal decomposition of PS/LDHs nanocomposites. Integral procedural decomposition temperature (IPDT) was also determined to analyse upon the improvement of thermal stability in the nanocomposites. Finally, rheological properties were measured for PS nanocomposites under molten state and water vapor transmission rate (WVTR) analysis was conducted to determine water vapor permeability of the nanocomposite films.

4.1 Introduction

In this chapter, an attempt has been made to fabricate and investigate characterization parameters associated to solvent blending based PS nanocomposites prepared with modified layered double hydroxides (Co-Al LDH and Ni-Al LDH). LDHs can be easily synthesized by co-precipitation method. LDHs are well characterized anionic clays and have been utilized in

several applications such as catalysts, adsorbents, separation techniques and ion-exchangers (Costa et al., 2008). The preparation of various types of polymer nanocomposites was reported in numerous literatures (Liu et al., 2006; Guo et al., 2011; Qiu et al., 2005; Paul et al., 2013; Botan et al., 2012; Penga et al., 2010; Alansi et al., 2015; Noh and Lee, 1999; Limpanart et al., 2005; Zhang et al., 2003; Uthirakumar et al., 2005b; Bourbigot et al., 2004; Chen and Wang, 2007). Liu et al. (2006) synthesized Co-Al LDH using various anions (acetate, chlorate and nitrate) and found that the NO_3-LDH provides greater degree of exfoliation in comparison with other modifiers. Guo et al. (2011) prepared PU/Co-Al LDH composites by in-situ polymerization technique. The authors reported that the decomposition temperature of PU/Co-Al LDH nanocomposite with 5 wt.% LDH was found to be 36.4 °C lower than the pristine PU. Qiu et al. (2005) incorporated Zn-Al LDH nanoparticle in the PS matrix by solution intercalation method. The authors reported that the thermal decomposition temperature of the nanocomposites is 17 °C more than that of pristine PS. In another study, Paul et al. (2013) prepared PS/O-laponite nanocomposites using solution intercalation technique and attained improvement in the thermal stability (425 °C for pristine PS and 454 °C for PS/O-laponite composites) due to the presence of O-laponite in PS matrix. PS/MgAl LDH nanocomposites containing 5 wt.% LDH prepared by in-situ free radical bulk polymerization method exhibited about 18 °C enhancement in thermal stability over pristine PS (Botan et al., 2012). A simple solution intercalation technique was adopted for the preparation of polycaprolactone/Co-Al LDH nanocomposites (Penga et al., 2010). TGA results confirmed that the nanocomposites had around 18 °C lower thermal degradation temperature as compared to pure polycaprolactone. The synthesis of PS/LDH nanocomposites via direct intercalation method was reported by Alansi et al. (2015) and the improvement of

T_{max} by 2 °C was noticed for 2 wt.% MgAl LDH loaded PS nanocomposites. Noh and Lee (1999) demonstrated that the T_g of PS nanocomposites with 30 wt.% MMT was improved by about 5 °C over pristine PS and the material was synthesized with emulsion polymerization method. Limpanart et al. (2005) followed melt compounding technique to synthesize PS/clay nanocomposites. Depending upon the modification of the organoclay, two major types of composites namely, conventional and intercalated nanocomposites could be fabricated. Zhang et al. (2003) synthesised PS/clay nanocomposites by γ-ray irradiation technique. They found that the incorporation of clay greatly improved the thermal properties of the PS nanocomposites. The formation of exfoliated PS/clay nanocomposites via in-situ polymerization was demonstrated by Uthirakumar et al. (2005b). They reported that a delaminated structure was obtained due to the anchored radical initiator within the clay layers. The inclusion of clay nanoparticles in PS through bulk polymerization conveyed low PHRR (520 kW/m^2) in nanocomposite when compared to pure PS (1025 kW/m^2) (Bourbigot et al., 2004). Chen and Wang (2007) prepared PP composites by melt blending method and studied thermal decomposition kinetics of the nanocomposites. They utilized Coats-Redfern and Criado model to measure the activation energy and determine the reaction mechanism of PP nanocomposites, respectively.

From the available state-of-the-art, it is apparent that experimental investigations have not targeted upon the fabrication and characterization of modified Ni-Al LDH and Co-Al LDH based PS nanocomposites through solvent blending method. Henceforth, the chapter targets solvent blending based synthesis of PS/Co-Al LDH and PS/Ni-Al LDH nanocomposites to examine upon the effect of variant LDH content on structural, thermal and rheological characterization parameters. Further, characterization also attempts to evaluate upon the

kinetics and reaction mechanism associated to thermal decomposition of the prepared samples.

4.2 Materials and methods

4.2.1 Materials

The polymer matrix utilized for the manufacturing of nanocomposites was polystyrene. This was supplied by National Chemical Ltd., Gujarat, India. All other chemicals including Cobalt nitrate ($Co(NO_3)_2.6H_2O$), aluminum nitrate ($Al(NO_3)_3.9H_2O$), nickel nitrate ($Ni(NO_3)_2.6H_2O$), sodium nitrate ($NaNO_3$), sodium hydroxide (NaOH), xylene (C_8H_{10}) and sodium dodecyl sulfate ($NaC_{12}H_{25}SO_4$) were obtained from Merck (India) Ltd, Mumbai. Water used for this work was taken from the Millipore water system (ELIX-3).

4.2.2 Preparation of modified Co-Al LDH and Ni-Al LDH

The procedure for the preparation of modified Co-Al LDH and Ni-Al LDH is discussed in sections 2.2.2 – 2.2.4.

4.2.3 Preparation of PS/LDHs nanocomposites

A series of nanocomposites (PS/LDH) with variant content of LDH was synthesized by solvent blending route as follows. Firstly, PS and LDHs (Co-Al LDH and Ni-Al LDH) were dried at 60 °C and 70 °C for 12 h to remove the adsorbed moisture. Desired content of Co-Al LDH material (1, 3, 5 and 7 wt.%) samples were dispersed in 109 mL of xylene (in each beaker) and stirred for 24 h. The subsequent step in the procedure involves addition of required amount of dried PS (Table 4.1) to stirred Co-Al LDH solution and the stirring

continued for another 12 h. Thereafter, the PS/Co-Al LDH solution was smeared on a flat petridish and was kept for 16 h to allow formation of film under natural drying condition. Eventually, after drying the films in a vacuum oven at 60 °C to eliminate residual solvent, PS/ Co-Al LDH nanocomposite films were obtained. Following similar procedure, pristine PS sample was also prepared without adding Co-Al LDH and Ni-Al LDH. The prepared films were kept in desiccators for further characterizations. The nomenclature for PS nanocomposite samples with various composition of Co-Al LDH were PS, PSCL 1, PSCL 3, PSCL 5 and PSCL 7 for 0, 1, 3, 5 and 7 (wt.%) LDH content, respectively. Similarly, a series of PS/Ni-Al LDH nanocomposites containing (1 – 7 wt.% of LDH) have been as well prepared using above described procedure for comparison with PS/Co-Al LDH nanocomposites. For Ni-Al LDH based nanocomposites, the samples nomenclature refers to PSNL 1, PSNL 3, PSNL 5 and PSNL 7 for PS/Ni-Al LDH 1 (wt.%), PS/Ni-Al LDH 3 (wt.%), PS/Ni-Al LDH 5 (wt.%), and PS/Ni-Al LDH 7 (wt.%), respectively. The experimental procedure followed for the preparation of nanocomposites is schematically represented in Figure 4.1.

4.2.4 Characterization

X-ray diffractometer (Make: Bruker, Model: D8 ADVANCE) equipped with Cu-Kα - radiation and Ni filter was used to record spectra of various samples at room temperature.

Table 4.1: Nomenclature and sample preparation conditions for various PS nanocomposites.

Sample	LDH Loading (wt.%)	LDH (g)	PS (g)	Solvent (mL)
PS	0	0	5	109
PSCL 1	1	0.05	4.95	109
PSCL 3	3	0.15	4.85	109
PSCL 5	5	0.25	4.75	109
PSCL 7	7	0.35	4.65	109
PSNL 1	1	0.05	4.95	109
PSNL 3	3	0.15	4.85	109
PSNL 5	5	0.25	4.75	109
PSNL 7	7	0.35	4.65	109

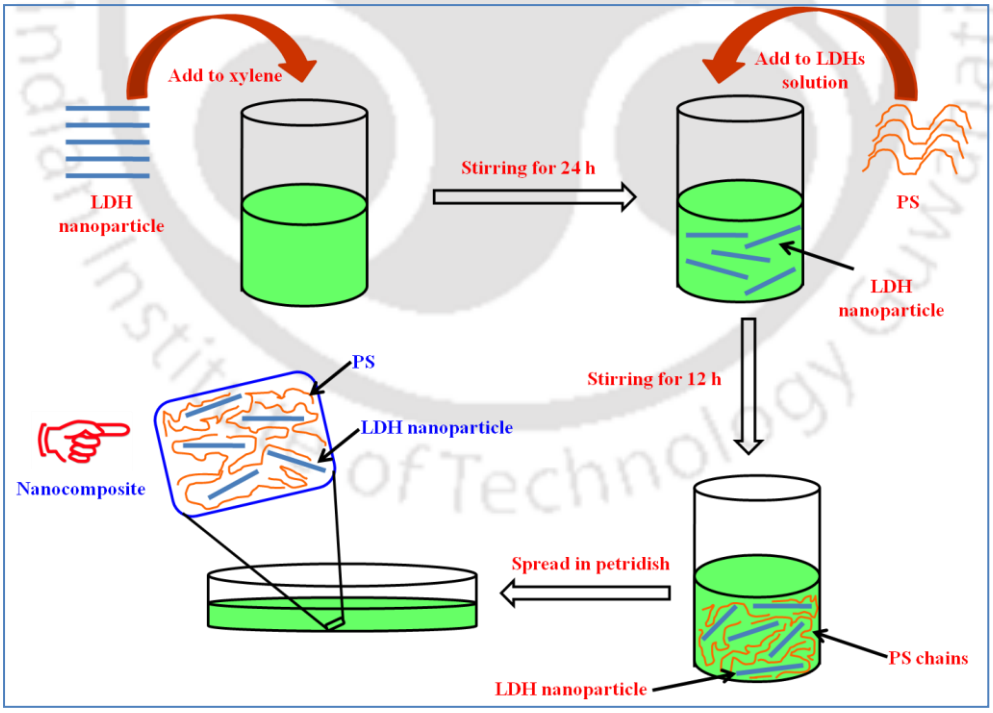

Figure 4.1: Schematic of PS nanocomposite preparation using solvent blending method.

Transmission electron microscope (Make: JEOL, Model: JEM 2100) operated at 200 kV accelerating voltage was adopted to analyze the extent of LDH dispersion in the PS nanocomposites. FTIR spectra of the LDH and PS nanocomposite samples were carried out using a Shimadzu (FTIR) spectroscope (Model: IRAffinity-1) with wavenumber range of 4000 – 400 cm^{-1} at room temperature. The test for WVTR was performed using PERMATRAN-W instrument (Make: Mocon USA, Model: 1/50 G) and according to ASTM E 398. TGA data for both LDH and nanocomposite samples were recorded using high temperature thermogravimetric system (Make: M/s Mettler Toledo, Switzerland; Model: TGA 851e/LF/1100) that was operated with nitrogen at a scan rate and temperature range of 10 °C/min and 30 – 700 °C, respectively. The DSC analysis (Make: M/s mettle Toledo, Switzerland; Model: 1) was performed with nitrogen for a heating rate and temperature range of 5 °C/min and 25 – 200 °C, respectively. A rheometer (Make: Anton Paar; Model: MCR 301) facilitated with parallel plate geometry (diameter and gap of 50 mm and 1 mm, respectively) was employed in an oscillatory mode to evaluate viscoelastic properties of the PS nanocomposites. Dynamic frequency sweep measurements were performed in the angular frequency range of 0.01 to 100 sec^{-1} using strain amplitude within the linear viscoelastic region at a temperature of 190 °C.

4.2.5 Thermal degradation kinetics

The LDH layers incorporated in the polymer matrix increases thermal stability of the polymer nanocomposite. This is primarily due to the barrier effect of the LDH platelets distributed throughout the matrix. The effect of the LDH loading can be observed by evaluating the activation energy of pure polymer and polymer nanocomposites (using Coats-

Redfern method) and appropriate kinetic models. The calculation procedure involves determination of the kinetic parameters such as activation energy, pre-exponential factor, and order of the reactions of different polymer nanocomposites by adopting Coats-Redfern method. The reaction mechanism of thermal decomposition of nanocomposites with different fillers was obtained using Criado method.

Kinetic studies of the degradation process were performed for better understanding of the thermal degradation behaviour of PS, PS/Co-Al LDH and PS/Ni-Al LDH nanocomposites. Isothermal rate of conversion has been assumed to be a linear function of rate constant (k) and fractional weight loss (α).

$$\frac{d\alpha}{dt} = kf(\alpha) \tag{4.1}$$

Arrhenius equation is given by following expression:

$$k = Ae^{\frac{-E_a}{RT}} \tag{4.2}$$

Coupling equation 4.1 and 4.2 yields,

$$\frac{d\alpha}{dt} = kf(\alpha) = Ae^{\left(\frac{-E_a}{RT}\right)} f(\alpha) \tag{4.3}$$

where, T denotes the temperature, t indicates reaction time, A signifies pre-exponential factor, E_a refers to apparent activation energy, R represents gas constant, f(α) symbolizes reaction model and α refers to fractional weight loss or conversion degree. α is expressed as:

$$\alpha = \frac{(w_0 - w_t)}{(w_0 - w_\infty)} \tag{4.4}$$

where, w_0 denotes initial weight, w_t represents actual weight and w_α signifies final weight of the samples during TGA analysis.

$$\frac{d\alpha}{dt} = \frac{d\alpha}{dT}\frac{dT}{dt} = \beta\frac{d\alpha}{dT} \tag{4.5}$$

where, $\beta = \frac{d\alpha}{dT}$ = heating rate. Now by combining equations 4.3 and 4.5, we get:

$$\frac{d\alpha}{dT} = \frac{A}{\beta}e^{\frac{-E_a}{RT}}f(\alpha) \tag{4.6}$$

Integrating both sides and reorganizing, we get the following expression:

$$g(\alpha) = \int_0^\alpha \frac{d\alpha}{f(\alpha)} = \frac{A}{\beta}\int_0^T e^{\frac{-E_a}{RT}}dT \tag{4.7}$$

Here, g(α) is the integral function of conversion degree α. The polymer decomposition processes, mainly obey the deceleration or sigmoidal functions. For various solid reaction mechanisms, g(α) has various relationships which are summarized in Table 4.2.

4.2.5.1 Coats-Redfern method

The method was given by Coats and Redfern (1964). The following procedure summarizes the method.

Using equation 4.7 and substituting $f(\alpha) = (1-\alpha)^n$ and $x = E_a/RT$ rearranging, we get:

$$g(\alpha) = \frac{ART^2}{\beta E_a}\left(1 - \frac{2RT}{E_a}\right)\exp\left(\frac{E_a}{RT}\right) \tag{4.8}$$

g(α) can be expressed in various ways for various n values:

when n = 1, $\quad g(\alpha) = -\ln(1-\alpha)$ (4.9a)

when n≠1, $$g(\alpha) = \frac{1}{n-1}[(1-\alpha)^{1-n} - 1] \quad (4.9b)$$

The combination of equation 4.8 and 4.9 after rearrangement yields:

n=1 $$\ln\left(-\frac{\ln(1-\alpha)}{T^2}\right) = \ln\left[\frac{AR}{\beta E_a}\left(1-\frac{2RT}{E_a}\right)\right] - \frac{E_a}{RT} \quad (4.10a)$$

n≠1 $$\ln\left(\frac{1-(1-\alpha)^{1-n}}{(1-n)T^2}\right) = \ln\left[\frac{AR}{\beta E_a}\left(1-\frac{2RT}{E_a}\right)\right] - \frac{E_a}{RT} \quad (4.10b)$$

For plots with good fitness, plotting the left hand side term in above expressions versus 1/T indicates a straight line plot whose slope refers to the activation energy. The constant value of the plot enables the evaluation of pre-exponential factor, by considering the relationship involving $\left(1-\frac{2RT}{E_a}\right)$ in the parenthesis as 1. The advantage of the method is that investigation can be performed with only single heating value which is not the case for other kinetic methods that require several heating values.

4.2.5.2 Criado method

Criado et al. (1989) proposed a method which can accurately determine the reaction mechanism in the solid phase reaction process using the activation energy value obtained from Coats-Redfern method. This method is used for the study of the mechanism of thermal degradation at a particular heating rate. The values of E_a, A and the apparent order of the reaction (n) are evaluated using Coats-Redfern method.

Criado introduced a new function, Z(α), given as:

$$Z(\alpha) = \frac{\frac{d\alpha}{dt}}{\beta}\pi(x)T \quad (4.11)$$

where, $x = E_a / RT$ and π(x) is an estimated relationship acquired by integration with temperature that cannot be articulated by straight forward investigation formula. Paterson (1971) suggested a sensible expression between π(x) and P(x)

$$\pi(x) = xe^{x}P(x) \tag{4.12}$$

Senum and Yang (1977) and Flynn (1997) projected an estimated biquadratic rational relation of P(x):

$$P(x) = \frac{e^{-x}}{x}\frac{x^3 + 18x^2 + 86x + 96}{x^4 + 20x^3 + 120x^2 + 240x + 120} \tag{4.13}$$

$$Z(\alpha) = f(\alpha)g(\alpha) \tag{4.14}$$

For x > 20, equation (4.13) can give negligible inaccuracy, based on the analyses of the thermogravimetric value. Merging equation (4.6) and (4.14), the following expression is achieved:

$$Z(\alpha) = \frac{\beta}{A} g(\alpha)\frac{d\alpha}{dt} e^{\frac{E_a}{RT}} \tag{4.15a}$$

Combining equations (4.11) and (4.13), the following relationship is obtained:

$$Z(\alpha) = \frac{d\alpha}{dt}\frac{E_a}{R} e^{\frac{E_a}{RT}} P(x) \tag{4.15b}$$

Using equation (4.15 b), Z (α) versus α experimental plots are obtained and are subsequently compared to the master plot between Z (α) versus α using the equation (4.15a) for various mechanism functions, g(α) and precisely the best fit refers to the reaction mechanism of the thermal degradation reaction.

Table 4.2: g(α) expressions for alternate reaction mechanisms associated to solid state process.

Mechanism	g(α)	Solid state process
Sigmoidal function		
A2	$-[\ln(1-\alpha)]^{1/2}$	Nucleation and growth
A4	$-[\ln(1-\alpha)]^{1/3}$	Nucleation and growth
A3	$-[\ln(1-\alpha)]^{1/4}$	Nucleation and growth
Deceleration Functions		
R2	$[1-(1-\alpha)^{1/2}]$	Phase boundary controlled reaction: contraction area
R3	$[1-(1-\alpha)^{1/3}]$	Phase boundary controlled reaction: contraction volume
D1	α^{2}	One-D diffusion
D2	$(1-\alpha)\times\ln(1-\alpha)+\alpha$	Two-D diffusion
D3	$[1-(1-\alpha)^{1/3}]^{2}$	Three-D diffusion, Jander equation
D4	$(1-2/3\alpha)-(1-\alpha)^{2/3}$	Three-D diffusion, Ginstlinge Brounshtein equation
F1	$-\ln(1-\alpha)$	Random nucleation having one nucleus on individual particle
F2	$1/(1-\alpha)$	Random nucleation having two nucleus on individual particle
F3	$1/(1-\alpha)^{2}$	Random nucleation having two nucleus on individual particle

4.3 Results and discussion

4.3.1 XRD analysis

The structural properties of the nanocomposites are highly influenced with the degree of dispersion of LDH in the PS matrix. Generally, layered nanofillers in reinforcing material facilitate either intercalated or exfoliated structure. This primarily depends on the synthesis method, content of the filler and chemical nature of the organic modifier used in the filler. If

an intercalated composite is formed, there will be an increment in the d-spacing value as compared to original LDH. The exfoliated nanocomposite is produced for the case in which LDH layers are well separated from one to another, well distributed in the polymer and no peak corresponding to basal plane (003) of LDH is observed. Generally, in the polymer/clay nanocomposite systems, the state of dispersion and the interlayer spacing of the clay platelets are typically examined by XRD and TEM. TEM is time demanding, and merely provides qualitative information on the sample in total, where as XRD gives quantification of changes in layer spacing, however, without providing information on high layer spacing (>7 nm) and/or relatively disordered structures. Hence, both these techniques (XRD and TEM) are generally used to assess upon the nanocomposite structures (Morgan and Gilman (2003)). Figure 4.2 (i) depicts XRD diffraction patterns of Co-Al LDH, PS and PS nanocomposites. The d-spacing value of the Co-Al LDH is determined as 2.8 nm from the reflection peak (003) at 3.14° through Bragg's equation. For pristine PS (Figure 4.2 i (a)), it is observed that the presence of two small halos centered at 2θ value between 10 and 20° is owing to amorphous characteristic of PS. In Figure 4.2 i (b-e), the characteristic peak (003) of Co-Al LDH layers got completely disappeared in the PS nanocomposites. This conveys that LDH layers might be exfoliated or delaminated in the PS matrix.

Figure 4.2 (ii) depicts XRD diffraction patterns of Ni-Al LDH, PS and PS nanocomposites. The Ni-Al LDH (003) reflection obtained at 2θ value of 6.54° corresponds to the d-value of 1.35 nm. Similarly, it is also noticed that (003) diffraction peak is absent in PS/Ni-Al LDH nanocomposites (Figure 4.2 (ii) (b-e)). As mentioned, XRD technique alone is not sufficient to conclude upon the prevalent nanocomposite structure and it should be used along with TEM to obtain insights on the dispersion of nanofiller (Morgan and Gilman (2003)).

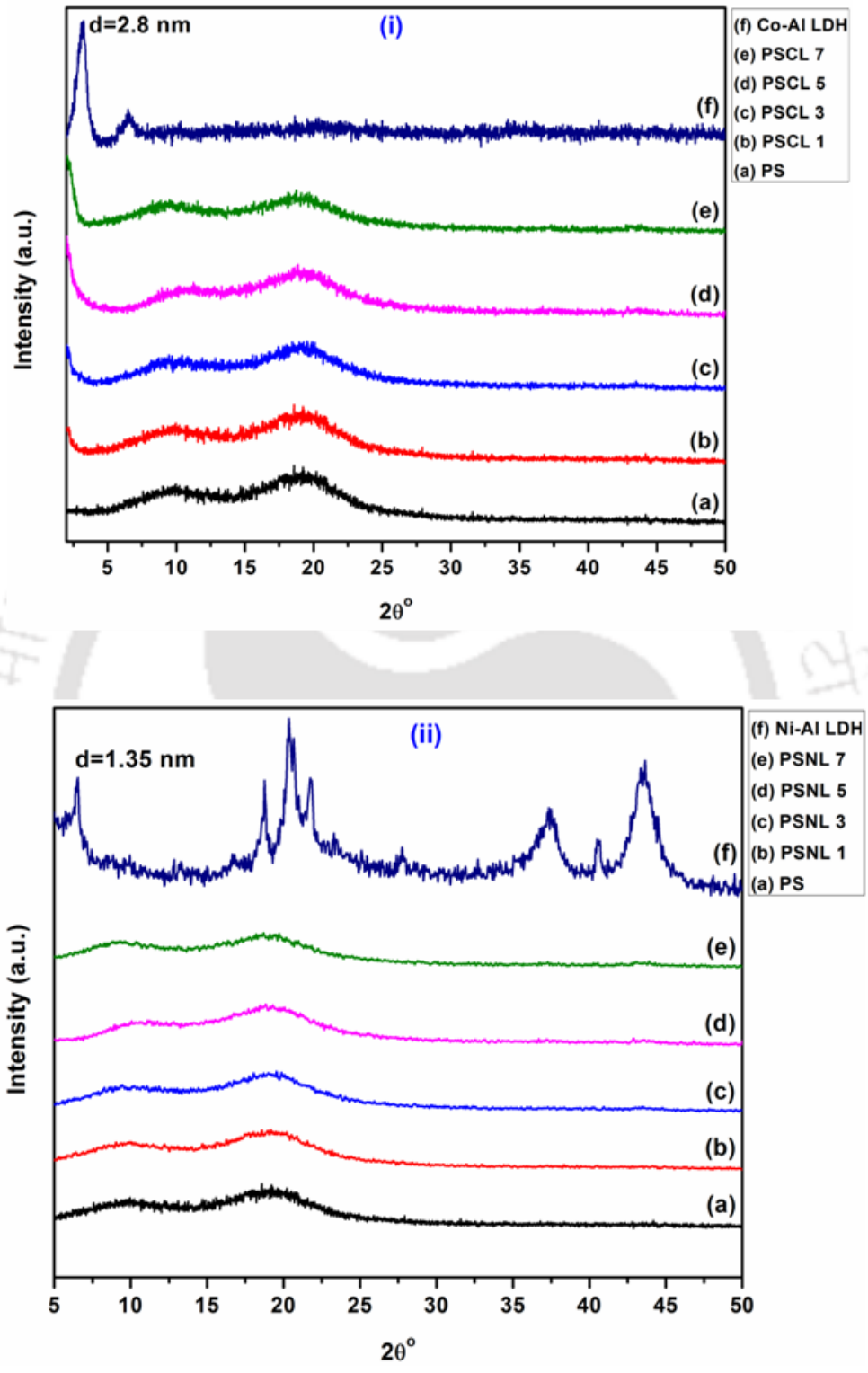

Figure 4.2: XRD patterns of (i) PS/Co-Al LDH and (ii) PS/Ni-Al LDH nanocomposites.

4.3.2 TEM analysis

TEM is a more useful technique for the evaluation of LDH distribution in the polymer matrix. Figure 4.3 (i) and 4.3 (ii) present the TEM images of prepared PS/Co-Al LDH and PS/Ni-Al LDH nanocomposites, respectively. TEM images of PSCL 1, PSCL 3, PSCL 5 and PSCL 7 nanocomposites are presented in Figure 4.3 i (a-d). The TEM images can provide a qualitative understanding of dispersion of the LDH and the type of nanocomposites formed in the context of either intercalated or exfoliated structure. One can see from Figure 4.3 i (a-b) that in the case of PSCL 1 and PSCL 3 samples, a better dispersion of Co-Al LDH layers in PS matrix is noticed. The dark lines show LDH galleries and the bright region signifies the PS matrix. These images (Figure 4.3 i (a) and (b)) indicate that the LDH layers have lost their ordered stacking structure, and are totally delaminated in the PS matrix. The galleries lines are illustrated by arrow marks. However, the PS nanocomposite with 5 wt.% Co-Al LDH is found to have partially exfoliated and intercalated structure (see Figure 4.3 i (c)). The arrow and circle marks represent the exfoliated and intercalated structure, respectively. Similar observations were reported by Alansi et al. (2015) for PS/Mg-Al LDH nanocomposite. Figure 4.3 i (d) illustrates the intercalated morphology of PS nanocomposites at higher loading of LDH (7 wt.%) in the PS matrix. A similar behaviour was also reported for PS/MgAl LDH nanocomposites prepared by solution intercalation route (Zhu et al., 2001). Ding and Qu (2005) also achieved intercalated structure of PS nanocomposites with higher content of Zn-Al LDH synthesized by emulsion polymerization. Similarly, it is also noticed that Ni-Al LDH layers are dispersed in PS/Ni-Al LDH nanocomposites [see Figure 4.3 ii (a-d)]. Based on the these trends in the results, it can be confirmed that the delaminated PS/LDHs nanocomposites are formed at lower loading of nanofiller (<3 wt.%).

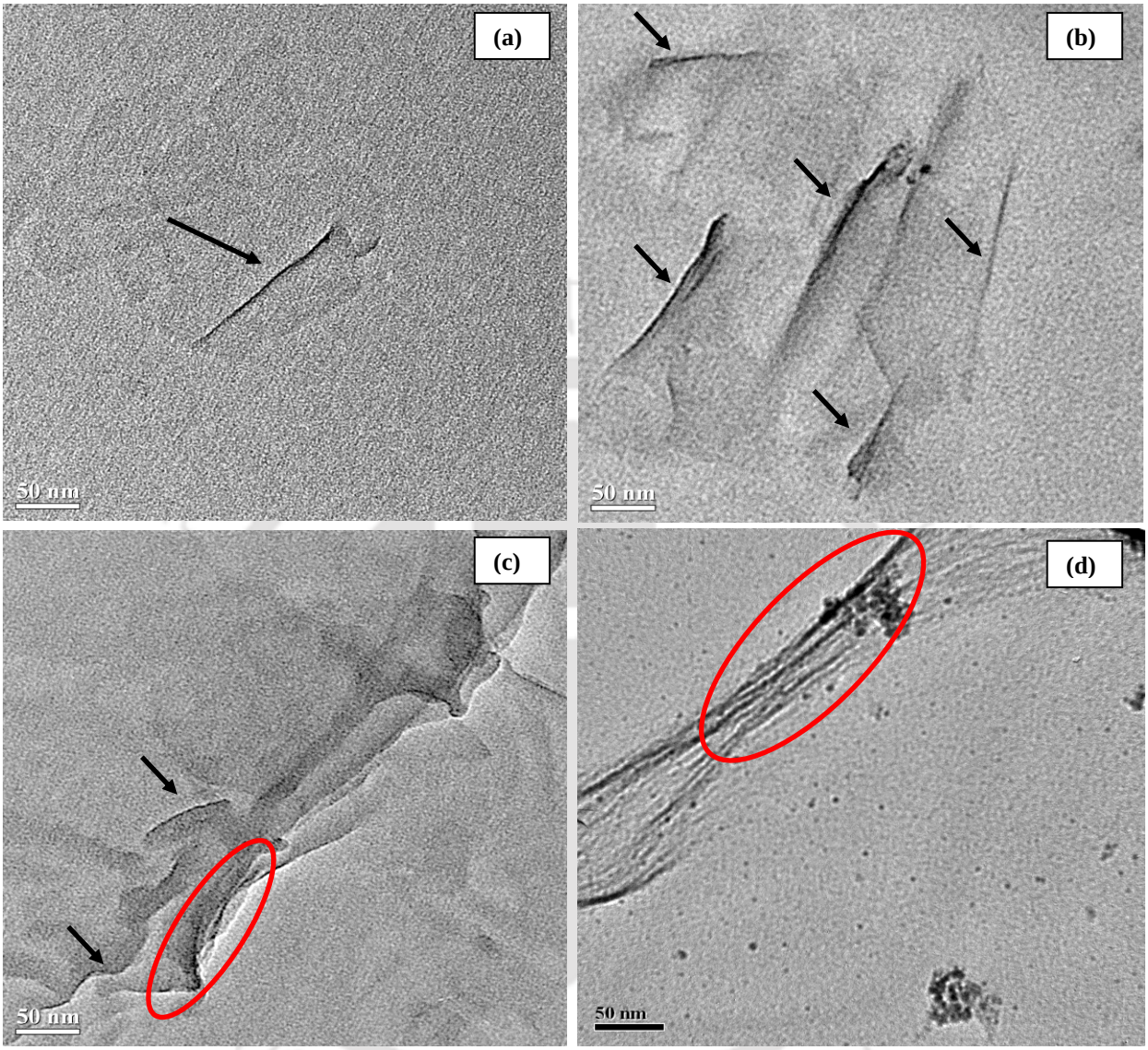

Figure 4.3. (i): TEM images of (a) PSCL 1, (b) PSCL 3, (c) PSCL 5 and (d) PSCL 7 nanocomposites.

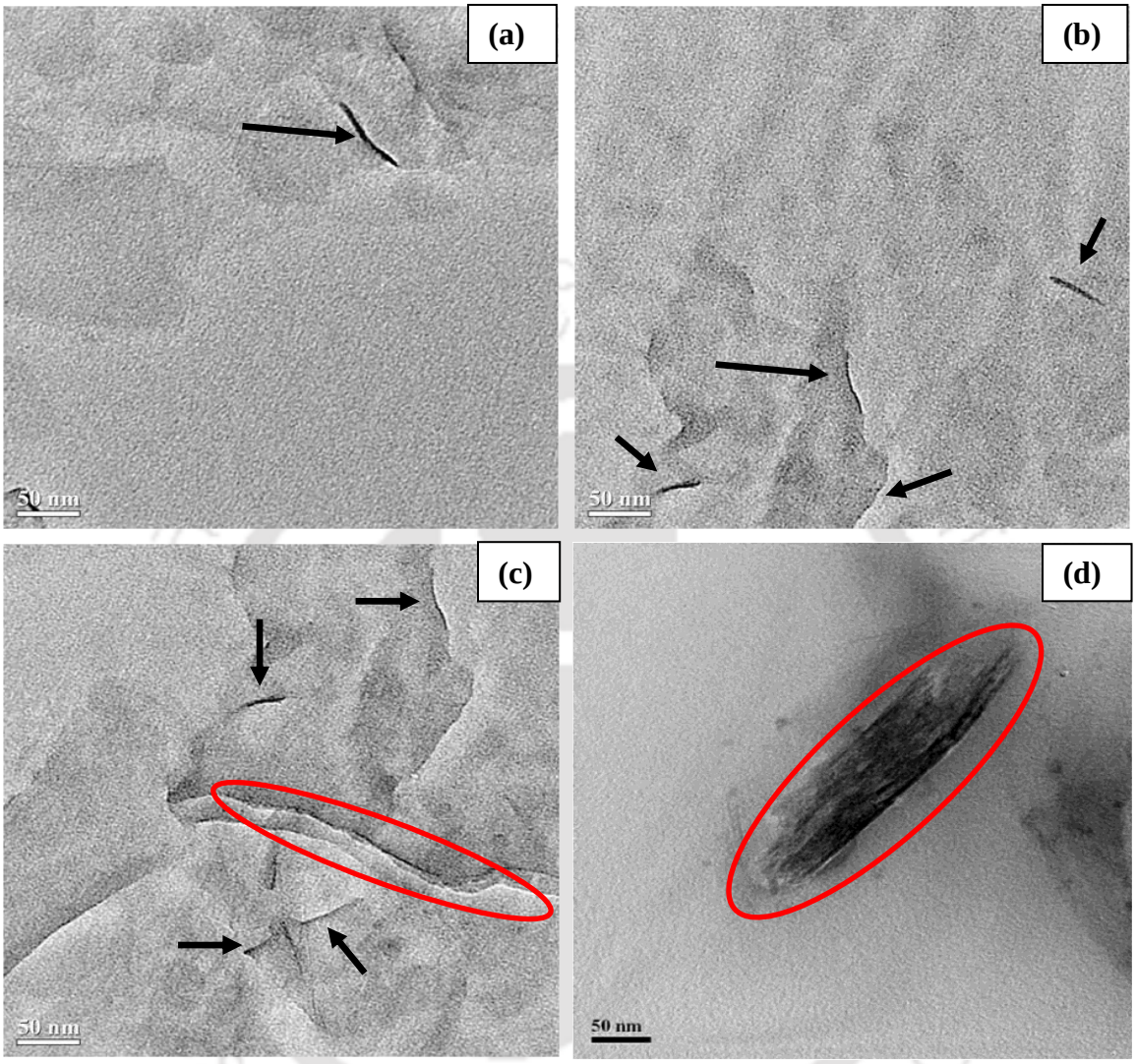

Figure 4.3. (ii): TEM images of (a) PSNL 1, (b) PSNL 3, (c) PSNL 5 and (d) PSNL 7 nanocomposites.

4.3.3 FTIR analysis

The FTIR spectra for pristine PS and its various nanocomposites are presented in Figure 4.4. The FTIR analysis has been performed to identify various functional groups that exist in the Co-Al LDH, Ni-Al LDH and PS nanocomposites.

A typical FTIR spectrum of Co-Al LDH, pristine PS and PS nanocomposite is illustrated in Figure 4.4 (i). Apparently, for Co-Al LDH sample (Figure 4.4 i (a)), the medium sharp peak at 1063 cm^{-1} and an intense peak at 1218 cm^{-1} are designated as asymmetric and symmetric vibration of sulfate from dodecyl sulfate anion, respectively. The characteristic peaks at 2957 cm^{-1}, 2920 cm^{-1} and 2848 cm^{-1} are ascribed to C-H stretching vibration. Bending mode of water molecule is found through a prominent peak at 1630 cm^{-1}. A very strong and broader peak attained at 3500 cm^{-1} is attributed to the O-H stretching of the metal hydroxide layer and interlayer water molecules of Co-Al LDH. For pristine PS sample (Figure 4.4 i (b)), an intense peak appeared at 698 cm^{-1}, which is assigned as that corresponding to mono-substituted benzene. Vibrational mode of CH_2 bending is located at 1453 cm^{-1} and 1368 cm^{-1}. There are two peaks at 1504 cm^{-1} and 1496 cm^{-1} which refer to C=C bending vibration (Du et al., 2009). The medium sharp peak at 2930 cm^{-1} and 3070 cm^{-1} correspond to aliphatic C-H stretching vibration and aromatic C-H stretching vibration, respectively. In comparison with pristine PS sample (Figure 4.4 i (b)), FTIR spectra of PS nanocomposites (Figure 4.4 i (c-f)) possess few new additional absorption prominent peaks. Among these, one is at 1218 cm^{-1} and corresponds to symmetric vibration of sulfate from dodecyl sulfate anion and the other is at 1630 cm^{-1} and this has been assigned to bending mode of water molecules. Also, a broader peak attained at 3500 cm^{-1} indicates existence of O-H stretching modes of interlayer water molecules. These peaks elucidate the occurrence of Co-Al LDH in the PS

nanocomposites. Wang et al. (2004) also obtained similar results with an increase in MMT loading in polymer nanocomposites.

Figure 4.4 (ii) depicts FTIR spectra of Ni-Al LDH, PS and PS/Ni-Al LDH samples. For Ni-Al LDH (Figure 4.4 ii (a)), O-H stretching vibration of hydrogen-bonded metal hydroxide layer and lattice water are attained at 3528 cm^{-1}. The two characteristic peaks at 2850 and 2920 cm^{-1} are designated as the stretching vibration of CH_3 and CH_2 of the modifier (SDS), respectively. The two peaks at 1218 cm^{-1} and 1063 cm^{-1} are assigned to symmetric vibration ($\nu_{S=O}$) and asymmetric vibration ($\nu_{o\ S=O}$) of sulfate from dodecyl sulfate anion,

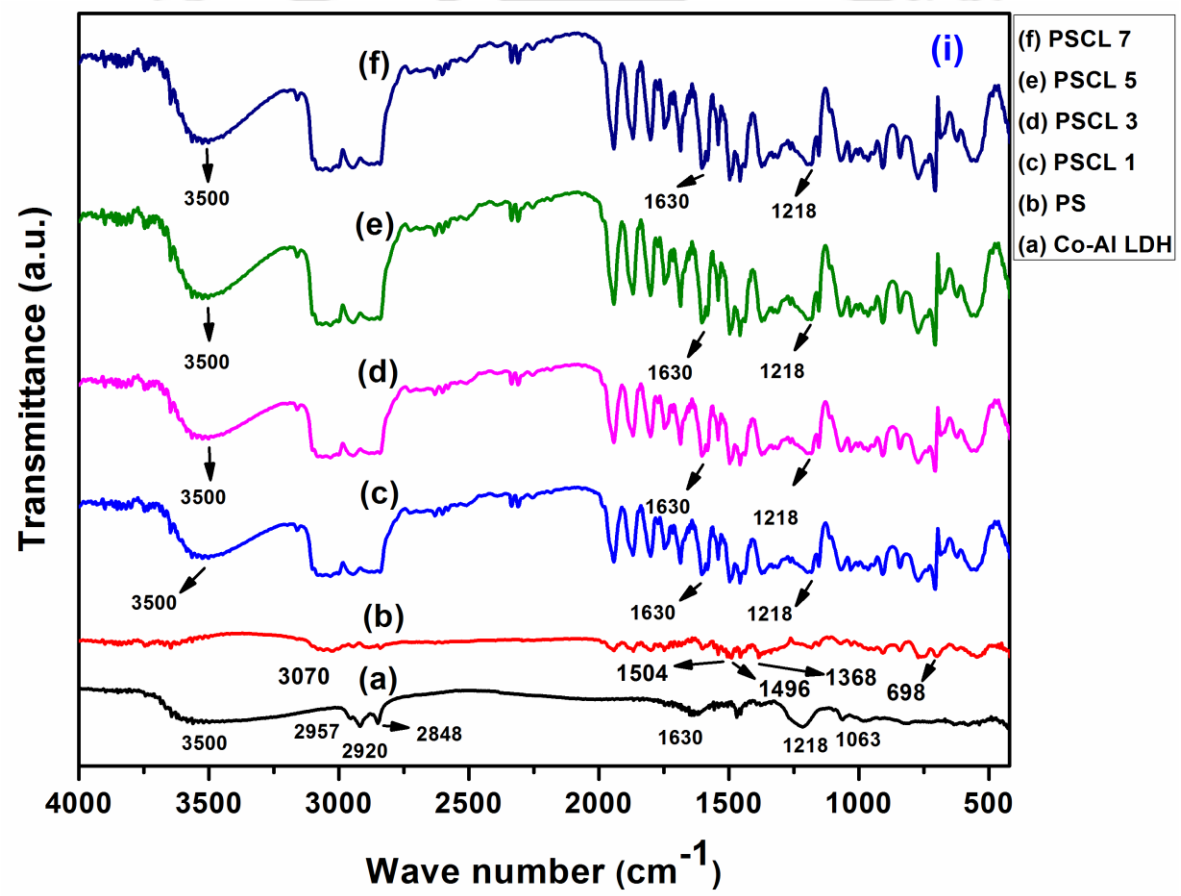

Figure 4.4. (i): FTIR spectra of (a) Co-Al LDH, (b) pristine PS, (c) PSCL 1, (d) PSCL 3, (e) PSCL 5 and (f) PSCL 7 nanocomposites.

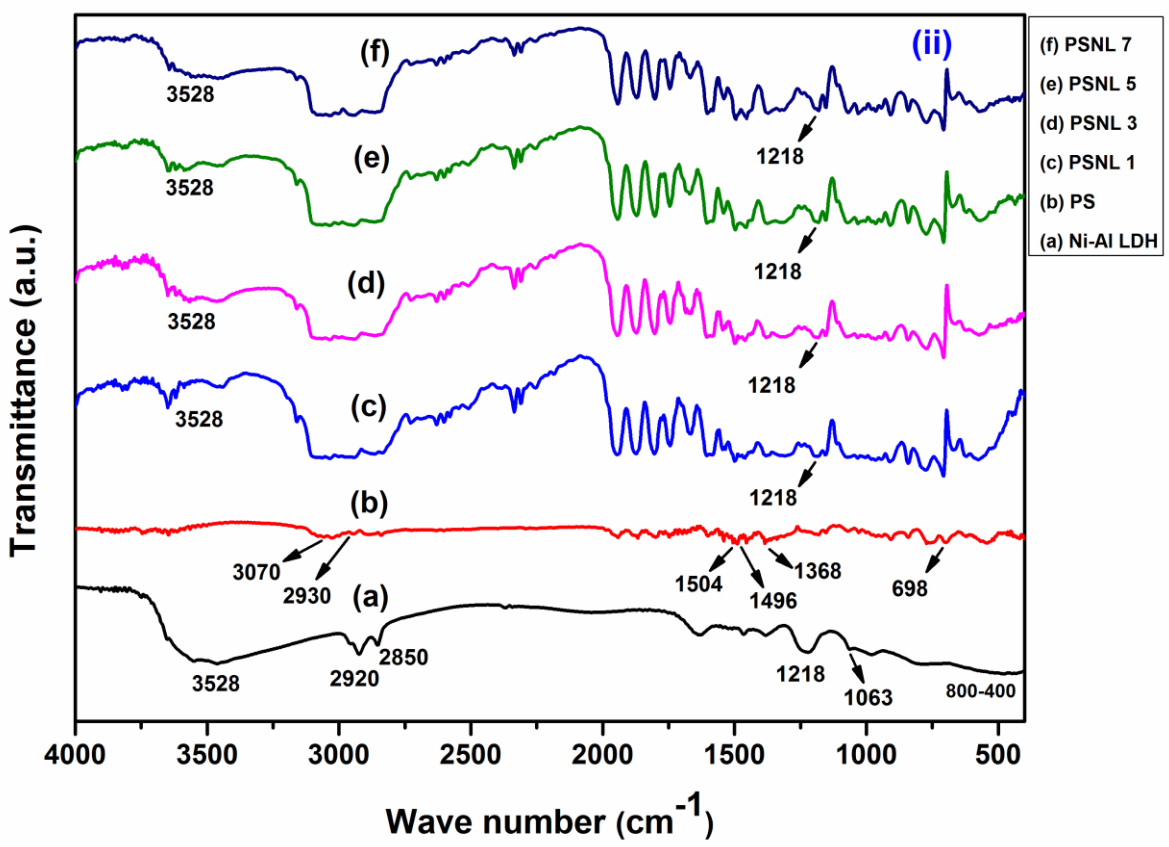

Figure 4.4. (ii): FTIR spectra of (a) Ni-Al LDH, (b) pristine PS, (c) PSNL 1, (d) PSNL 3, (e) PSNL 5 and (f) PSNL 7 nanocomposites.

respectively (Costa et al. 2008). The lattice vibration bands observed at 400 – 800 cm^{-1} correspond to Ni-O, Al-O, O-Al-O modes (Wang et al., 2009). Considering pristine PS ((Figure 4.4 ii (b)) for comparison, the PS nanocomposites (Figure 4 ii (c-f)) possess few new absorption peaks. Among these, the peak located at 1218 cm^{-1} corresponding to symmetric vibration of sulfate from dodecyl sulfate anion and the peak at 3528 cm^{-1} refers to O-H stretching vibration. The lattice vibration bands can also be seen in the region of 400 – 800 cm^{-1} (Qiu et al., 2005). These FTIR assignments reveal that the modified Ni-Al LDH is doped into the PS matrix by the solvent blending method and thereby facilitates nanocomposite structure in the material.

4.3.4 WVTR analysis

The WVTR is considered as an important parameter for food packaging applications. It is quantified by the water vapor permeability coefficient (WVPC), which indicates the amount of water vapor that permeates per unit area and time in a packing material. It is well known that LDHs are able to reduce the transmission rate of packing film.

The WVTR for pristine PS, PSCL 1, PSCL 3, PSCL 5 and PSCL 7 nanocomposites are determined as 18, 17.2, 15.3, 13.6 and 12.45 gm/m^2.day, respectively (see in Figure 4.5 (i)). Similarly, the water vapour transmission rate for PS/Ni-Al LDH nanocomposites having 1 wt.%, 3 wt.%, 5 wt.% and 7 wt.% of LDH are determined as 16.7, 14.5, 12.8 and 11.9 gm/m^2.day, respectively (see in Figure 4.5 (ii). These suggest that the transmission rate reduces with increasing content of LDH. Figure 4.5 (iii) demonstrates how LDH layers hinder the permeation of vapor through the nanocomposite film that leads to reduction in the transmission rate. A similar behaviour of water vapor transmission rate was reported by Yeh et al. (2004) for PS/clay composites. The reduced transmission rate is influenced by several factors such as shape and aspect ratio of nanofiller and loading of nanofiller.

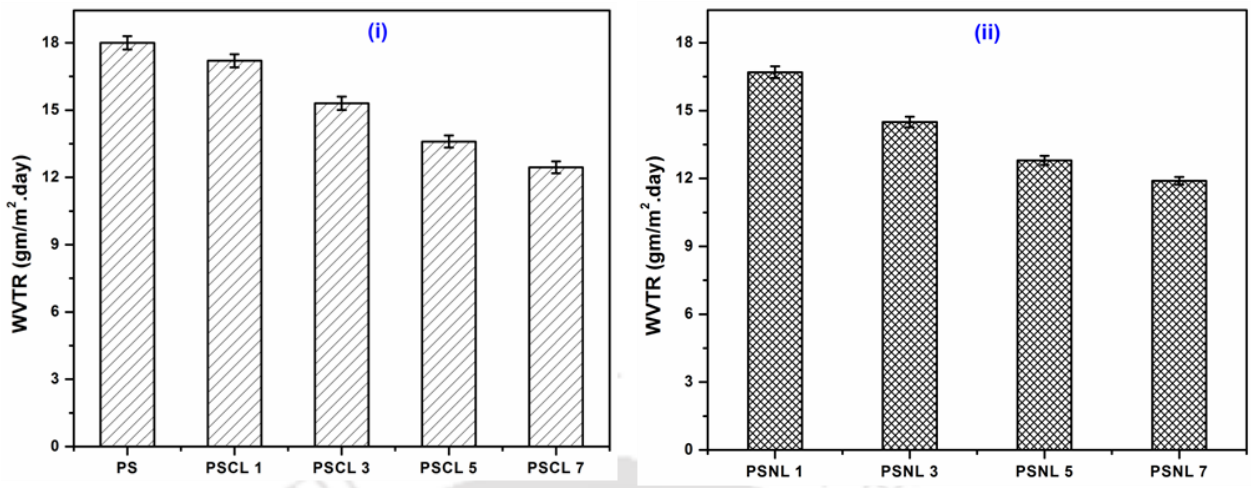

Figure 4.5: WVTR of (i) PS/Co-Al LDH and (ii) PS/Ni-Al LDH nanocomposites.

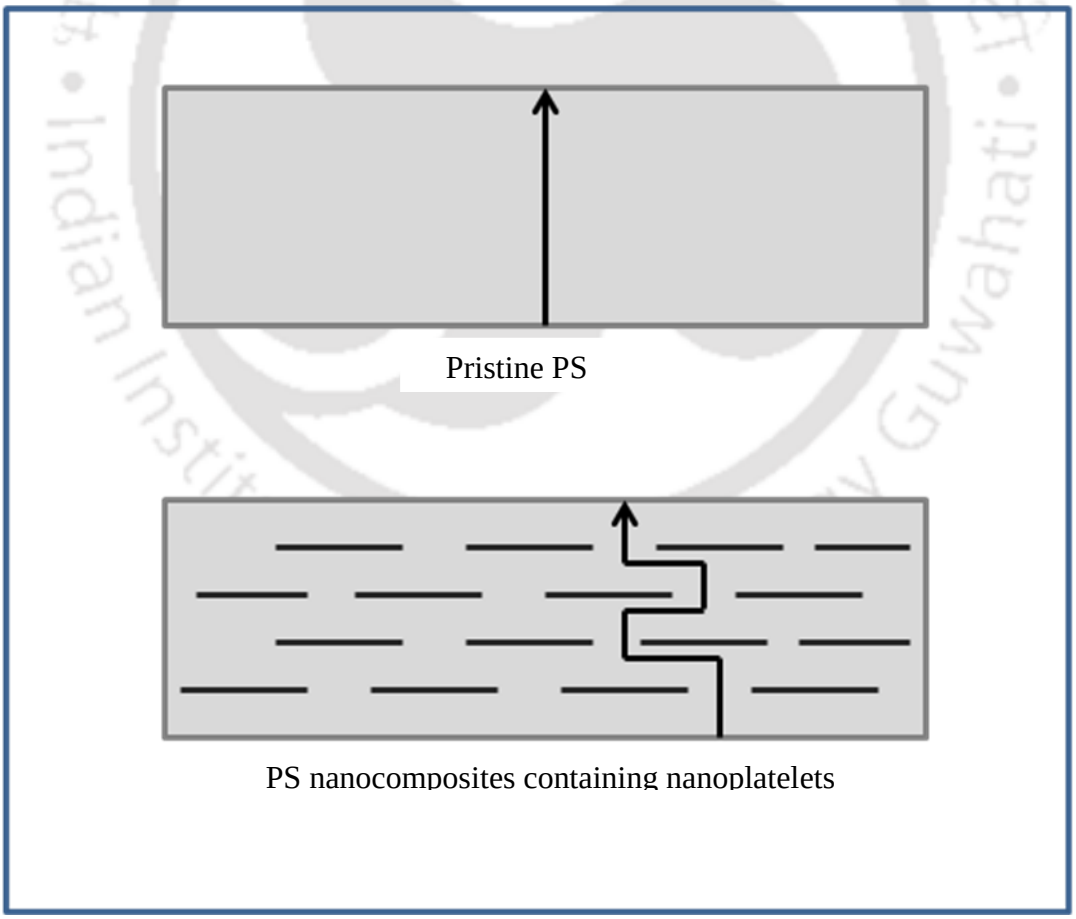

Figure 4.5 (iii): Permeation path imposed by nanoparticles embedded in polymer films.

4.3.5 DSC analysis

To examine upon the movement of PS macromolecular chains in the clay galleries in terms of its T_g, DSC analysis of PS/Co-Al LDH, PS/Ni-Al LDH nanocomposites and PS sample without LDHs was performed and the obtained results have been presented in Figure 4.6. The T_g is evaluated at the inflection point between the onset and the end set temperatures. The T_g value have been found to be 69.3, 71.8, 73.3, 74.4 and 74.8 °C, for pristine PS, PSCL 1, PSCL 3, PSCL 5, PSCL 7 sample, respectively (see Figure 4.6 (i)). The highest enhancement of T_g (5.5 °C more than pristine PS) is achieved for PS nanocomposite containing 7 wt.% Co-Al LDH content. Similarly, the T_g values for PS/Ni-Al LDH nanocomposites samples having 1, 3, 5 and 7 wt.% of LDH are evaluated as 72.2, 73.5, 74.8 and 75.0 °C, respectively (see Figure 4.6 (ii)). Overall, the T_g of PS is improved with the addition of LDHs. This is due to the strong linkages between LDH and PS, which hinders the supportive movement of the PS primary chain fragments. Similar phenomenon was also observed for PS/O-laponite nanocomposites by Paul and co-workers (2013). The PS/Ni-Al LDH nanocomposites exhibit T_g enhancement of 2.9 – 5.7 °C with respect to corresponding value of pristine PS. It was reported in the literature (Zidelkheir et al., 2006) that PS nanocomposite prepared with 10 wt.% MMT content via melt compounding method possessed 4 °C higher T_g value than that obtained for pristine PS.

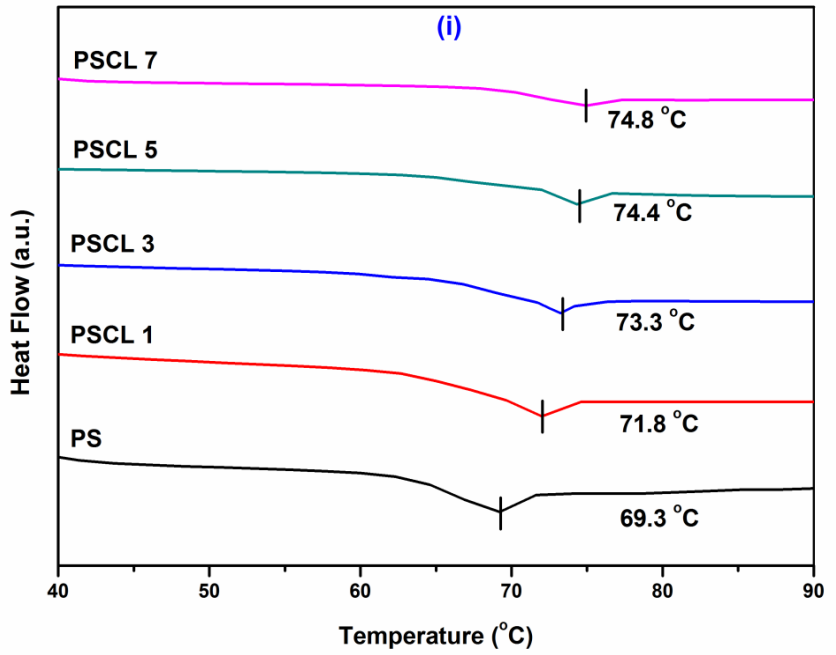

Figure 4.6 (i): DSC curves of PS and PS/Co-Al LDH nanocomposites.

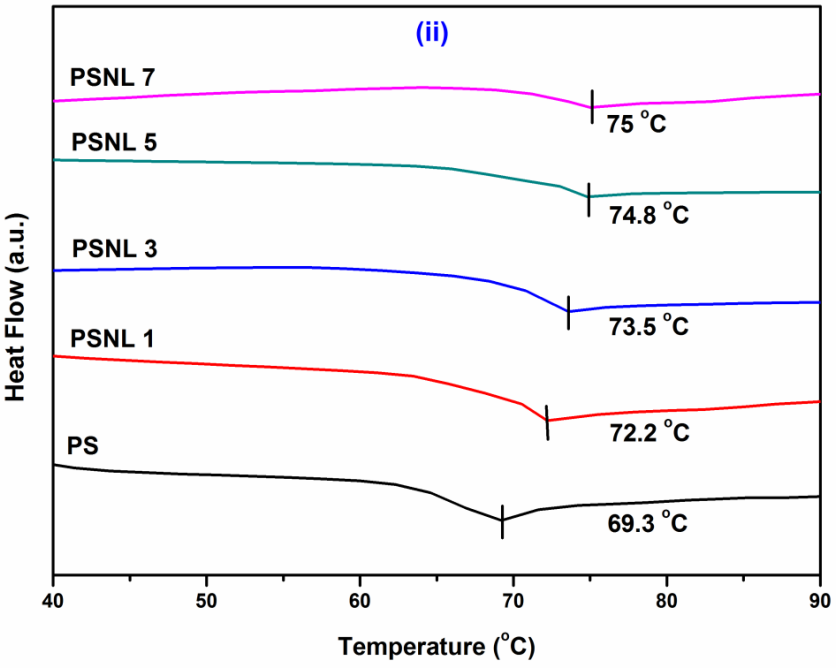

Figure 4.6 (ii): DSC curves of PS and PS/Ni-Al LDH nanocomposites.

4.3.6 TGA analysis

TGA analysis is primarily utilized to examine the degradation temperature as well as thermal stability of the polymer matrix. The TGA curve of pristine PS and PS/Co-Al LDH nanocomposites are presented in Figure 4.7 (i). The main degradation of pristine PS takes place in the temperature range of 350 – 450 °C (see Figure 4.7 i (a)). For the case of PS/Co-Al LDH nanocomposites, two types of degradation profiles can be observed (see Figure 4.7 i (b-e)). The first stage profile that exists for the weight decrement in the temperature range of 140 - 330 °C is due to the vaporization of physisorbed water molecules in the intercalated galleries and thermal degradation of alkyl chains of surfactant molecules (Botan et al., 2012). The TGA profile that exists in the second stage decrement at 330 - 460 °C is due to thermal decomposition of PS macromolecules and creation of black char. Only inorganic residues are present beyond 460 °C. From these TGA results, it is evident that the thermal stability of the PS nanocomposites is enhanced by the incorporation of LDH nanofiller. This is attributed to the barrier effect of LDH layers that hinder heat and diffusion of volatile components generated by thermal degradation. Considering mass decrement of 15% as a reference point, the decomposition temperature (T_d) for pristine PS and PS/Co-Al LDH nanocomposites containing 1, 3, 5 and 7 wt.% of LDH is found to be 360, 370.5, 378.2, 384.6 and 388.5 °C, respectively. The T_d value for PS/Co-Al LDH samples with 1, 3, 5 and 7 wt.% LDH loading is 10.5, 18.2, 24.6 and 28.5 °C higher in comparison with the value obtained for pristine PS, respectively (see Table 4.3). Figure 4.8 (i) demonstrates the thermal behaviour of pristine PS and PS/Ni-Al LDH nanocomposites. Similarly, selecting 15% mass loss as a reference point, the thermal degradation temperatures for pristine PS and PS/Ni-Al LDH nanocomposites having 1, 3, 5 and 7 wt.% of LDH are determined as 360, 372.3, 381.5, 387.7 and 389.1 °C,

respectively. In other words, the thermal stability of nanocomposites improved with respect to pristine PS. The thermal degradation values for PSNL 1, PSNL 3, PSNL 5, and PSNL 7 are 12.3, 21.5, 27.7 and 29.1°C, respectively, higher than that of pristine PS (see Table 4.3).

Among all investigated nanocomposites, the nanocomposite with 7 wt.% LDH content has better thermal stability. The improvement in thermal stability is observed even with small (1 wt.%) addition of LDH and the effect is more pronounced in the nanocomposites samples with higher loading of LDH (>5 wt.%) (Wang et al., 2004). It is also noticed in Figure 4.7 and 4.8 i (b-e) that the char residue content of nanocomposites gradually increases with increasing LDH concentration in the polymer matrix. Interestingly, similar trend was noticed for PS/O-laponite nanocomposites by Paul and co-workers (2013). In their work, thermal stability enhanced gradually for PS/O-laponite composites with increment in the nanofiller loading. It is noteworthy to mention that the addition of Co-Al LDH in polyurethane (PU) (Guo et al., 2011) and polycaprolactone (Penga et al., 2010) decreased thermal stability of the polymer.

In the first derivative of TGA graph (Figure 4.7 (ii) and 4.8 (ii)), the peaks indicate temperature corresponding to the maximum rate of mass decrement. It is apparent that all derivative curves of the nanocomposites (T_{max}) are shifted to the right hand side of pristine PS, which conveys better thermal stability of the composites. With only 7 wt.% nanofiller loading, for PSNL 7 and PSCL 7 nanocomposite, the T_{max} values are 424.5 ^{o}C and 424.6 °C respectively, which are 7.5 and 7.6 °C higher than that obtained for pristine PS (417 °C). Table 4.3 presents the TGA results of pristine PS and its nanocomposites. Generally, around

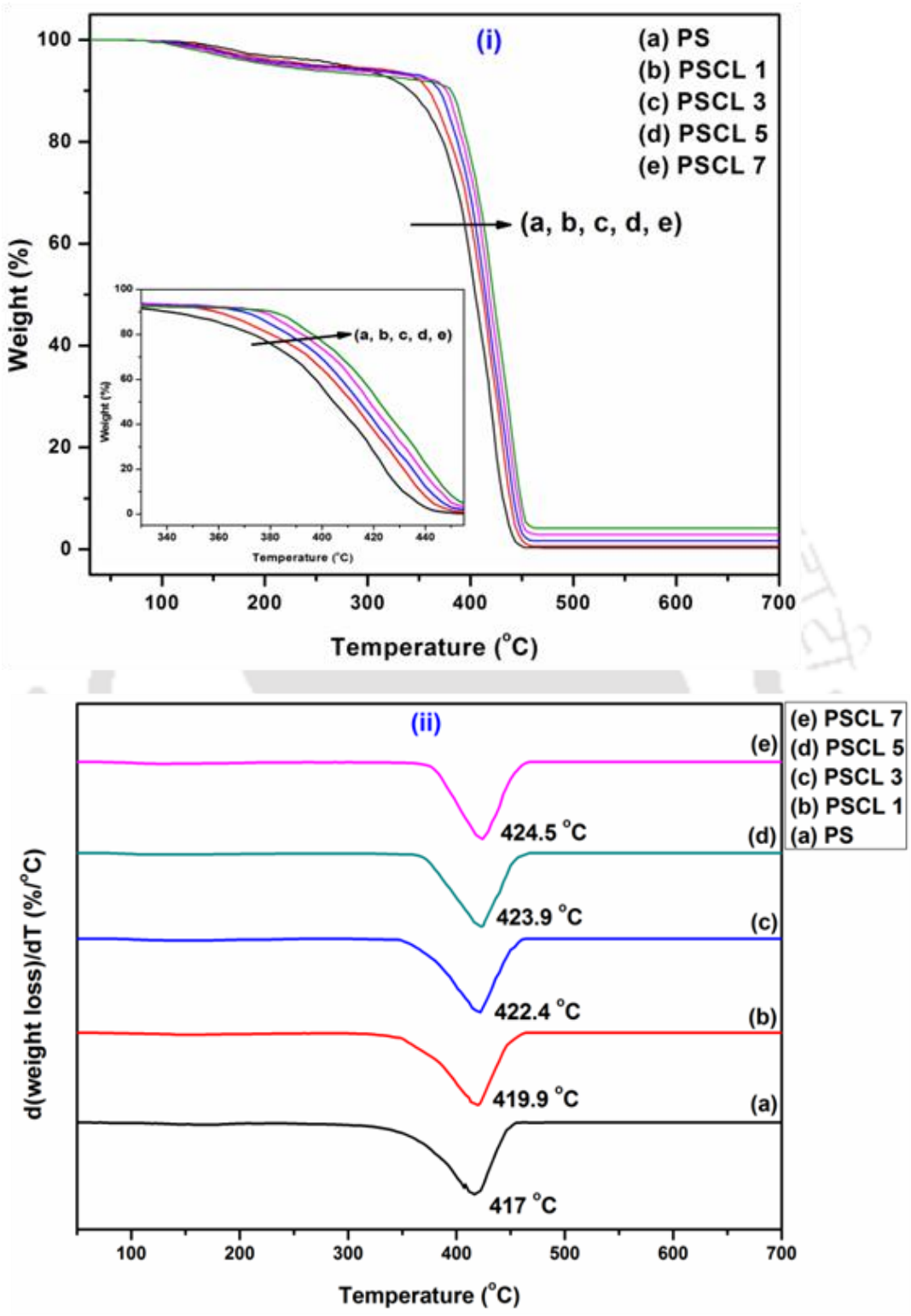

Figure 4.7: (i) TGA and (ii) DTG curves of PS and PS/Co-Al LDH nanocomposites.

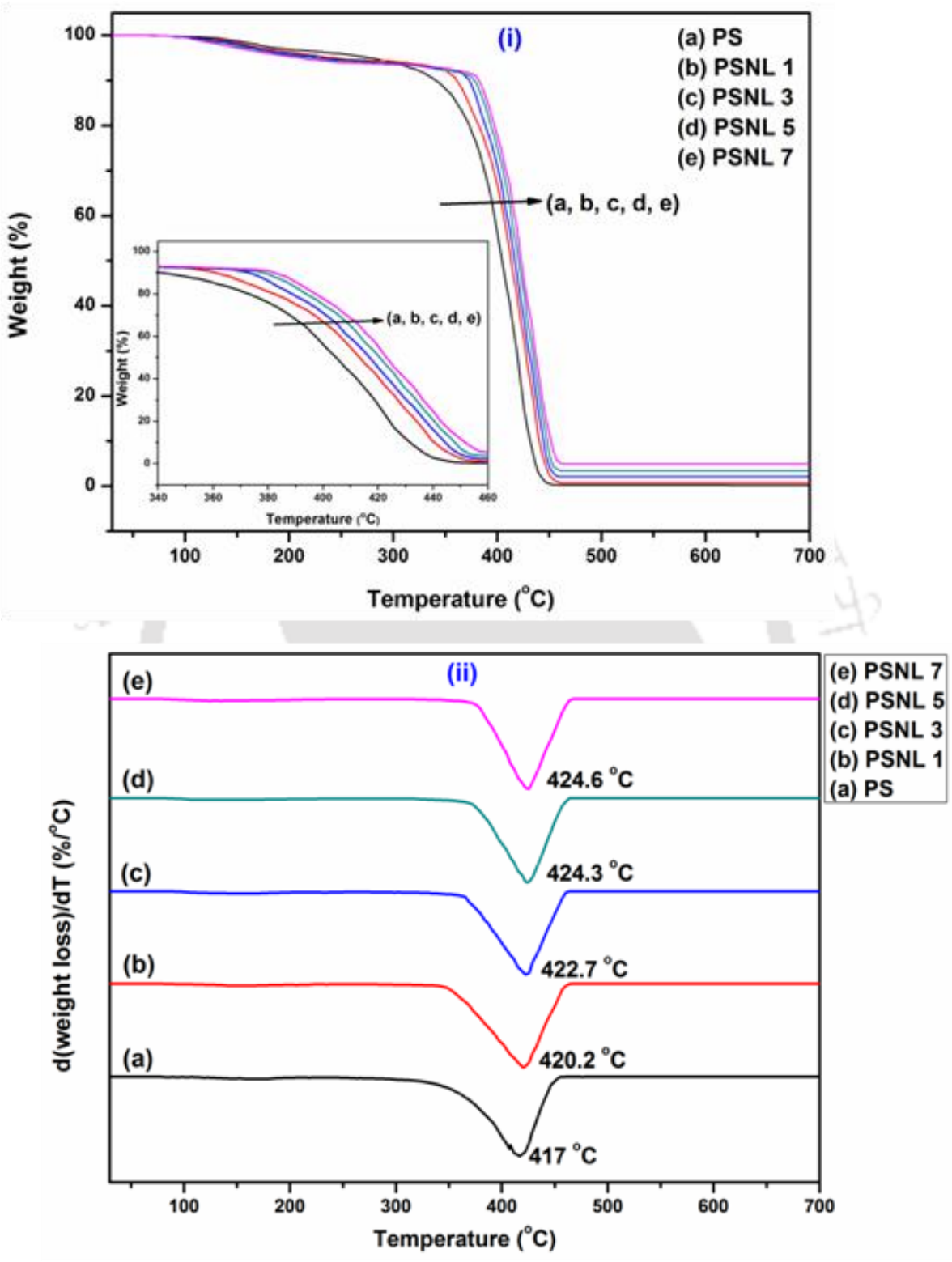

Figure 4.8: (i) TGA and (ii) DTG curves of PS and PS/Ni-Al LDH nanocomposites.

10 – 30 wt.% of inorganic materials (such as glass fiber) are used to reinforce the polymer in order to enhance polymer properties (Kumar and Kumar, 2014). However, it is noticed that a small quantity (even 1 wt.%) of LDH is sufficient to augment the properties of PS due to molecular level dispersion as well as high aspect ratio of the LDH. It is well documented in the literature (Yano et al., 1997) that the effect of improving nanocomposite properties is predominant for higher aspect ratio of the filler.

Table 4.3: Thermal degradation temperatures of PS, PS/Co-Al LDH and PS/Ni-Al LDH nanocomposites.

Sample	Temperature at 15% weight loss (T_{15}) °C	T_{max} (°C)
PS	360.0	417.0
PSCL 1	370.5	419.9
PSCL 3	378.2	422.4
PSCL 5	384.6	423.9
PSCL 7	388.5	424.5
PSNL1	372.3	420.2
PSNL 3	381.5	422.7
PSNL 5	387.7	424.3
PSNL 7	389.1	424.6

4.3.7 Kinetic analysis

4.3.7.1 Coats-Redfern method for kinetic analysis

Coats-Redfern method (Coats and Redfern, 1964), also called as integral method, is generally applied to study the kinetics of solid state system. The order of reaction (n) is evaluated by linear fitting of the left hand side of equation (4.10) versus 1/T. The value of n obtained at the best correlation coefficient (R) is the actual order of reaction, and E_a and A can also be evaluated for the best fit plot.

Coats-Redfern method deals with major decomposition stage of the thermal behaviour of the PS nanocomposites. The thermal degradation data at a single heating rate is sufficient to calculate the respective parameters (A, E_a, and n). Initially, it is assumed that a thermal decomposition reaction comprises a specific order of reaction and it is substituted in equation (4.10). To evaluate the best correlation coefficient (R), the graph of left hand side of equation (4.10) is fitted against to 1/T. The stated route is replicated for various n values to obtain the best R value. Consequently for the best fit plot, A and E_a are evaluated from the intercept and slope of the plotted linear line, respectively. Figure 4.9 and 4.10 illustrates the linearly fitted plot of pristine PS and various PS nanocomposites. The obtained kinetic parameter values including n, E_a and A for the prepared samples are enlisted in Table 4.4. The E_a of pristine PS, PSCL 1, PSCL 3, PSCL 5 and PSCL 7 nanocomposites is determined as 89, 109, 126, 134 and 138 kJ/mol, respectively. The E_a of PSCL 7 is found to be 49 kJ/mol higher than the pristine PS (see Table 4.4). Similarly, the E_a of PSNL 1, PSNL 3, PSNL 5 and PSNL 7 nanocomposites is determined as 112, 128, 136 and 139 kJ/mol, respectively. It can be observed from the Table 4.4 that the E_a of PS/Ni-Al LDH nanocomposites is 23 – 50 kJ/mol

higher than that of pristine PS. The obtained results are in good agreement with TGA data. The E_a and A values for nanocomposites increase with increasing LDH content (see Table 4.4). Chen and Wang (2007) conveyed that PP nanocomposites have enhanced E_a in comparison with pristine polymer.

Table 4.4: Thermal degradation kinetics of pristine PS, PS/Co-Al LDH and PS/Ni-Al LDH nanocomposites obtained from Coats-Redfern method.

Sample	E_a(kJ/mol)	A	n	R^2
PS	89	8.88×10^5	0.2	0.993
PSCL 1	109	5.09×10^7	0.5	0.998
PSCL 3	126	6.19×10^8	0.5	0.998
PSCL 5	134	2.84×10^9	0.5	0.997
PSCL 7	138	4.05×10^9	0.5	0.997
PSNL 1	112	6.12×10^7	0.5	0.998
PSNL 3	128	7.82×10^8	0.5	0.997
PSNL 5	136	3.55×10^9	0.5	0.997
PSNL 7	139	5.03×10^9	0.5	0.996

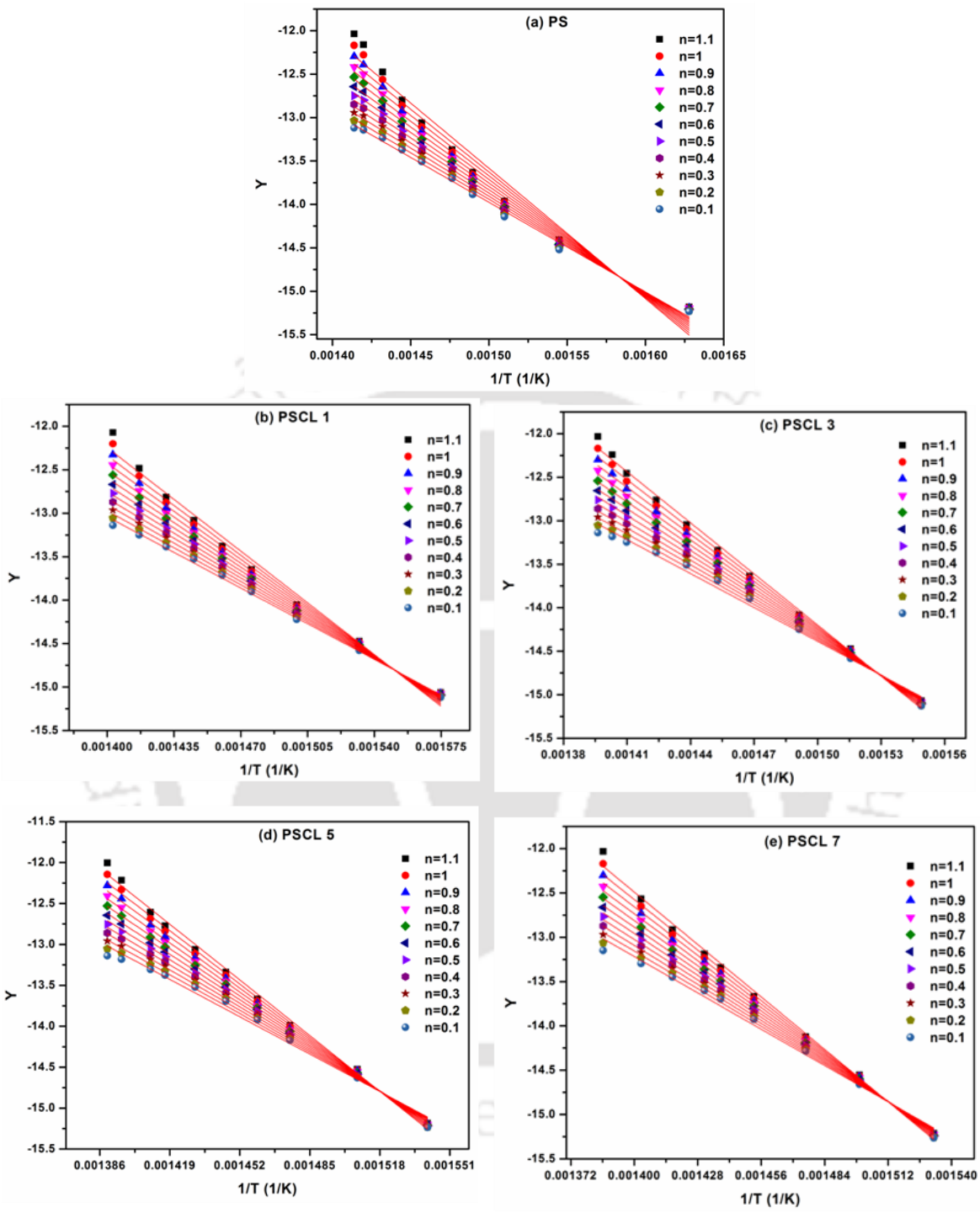

Figure 4.9: Coats-Redfern model fitness plots for (a) pristine PS, (b) PSCL 1, (c) PSCL 3, (d) PSCL 5 and (e) PSCL 7 nanocomposites.

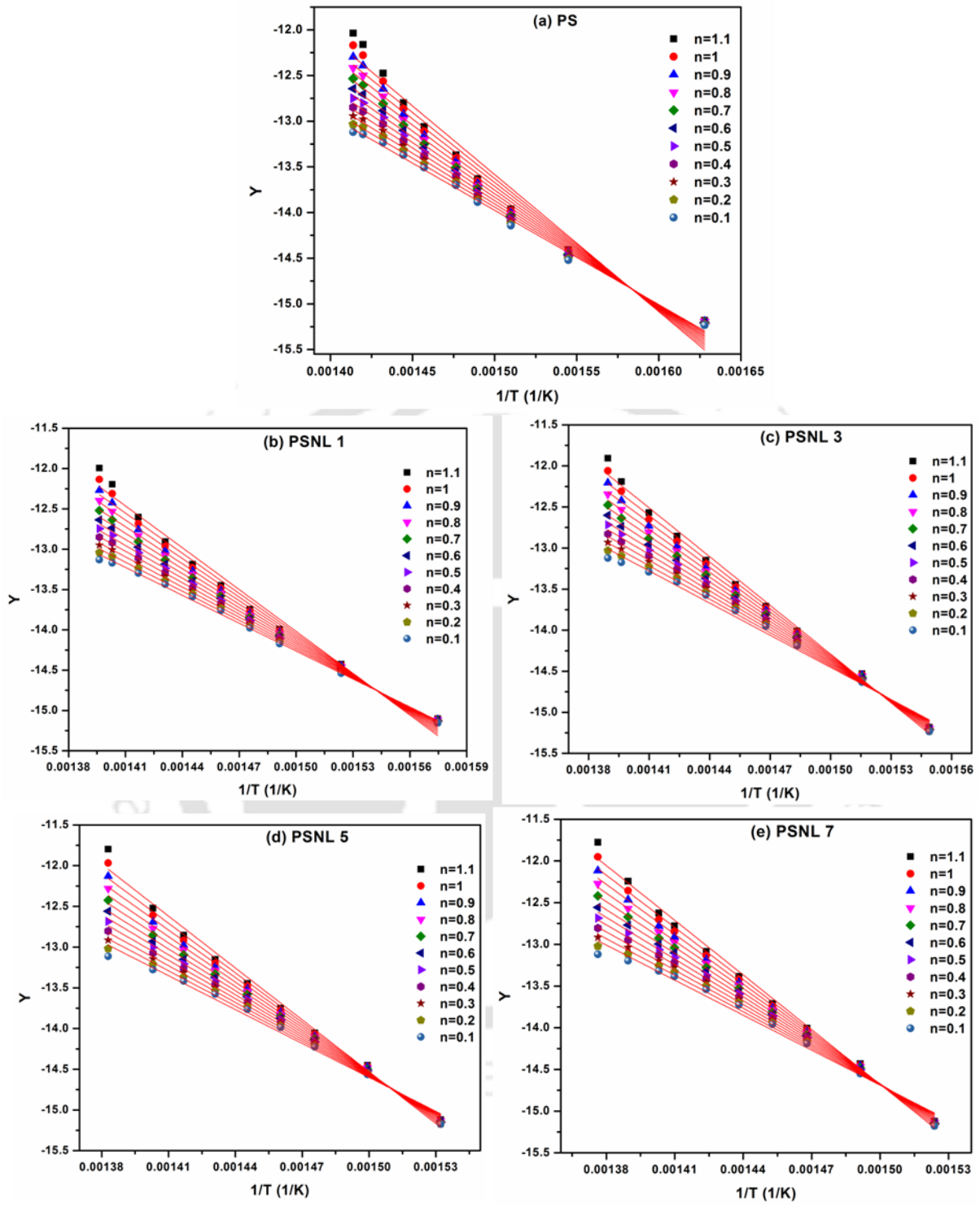

Figure 4.10: Coats-Redfern model fitness plots for (a) pristine PS (b) PSNL 1, (c) PSNL 3, (d) PSNL 5 and (e) PSNL 7 nanocomposites.

4.3.7.2 Criado method for the reaction mechanism analysis

The degradation reaction mechanism was evaluated by Criado model with the help of kinetic variables (*A*, E_a, and *n*) obtained from Coats-Redfern method (Criado et al., 1989). This method can precisely allow determination of reaction mechanism in the solid reactions. The master Z(α)-α curve can be plotted using equation (4.15a) according to the various reaction mechanisms (see Table 4.1). The equation (4.15b) is used to plot the experimental Z(α)-α curve. By comparing these two curves, the type of mechanism involved in the thermal degradation process can be identified. The Z(α)-α master and experimental curve of pristine PS and its nanocomposites is shown in Figure 4.11 and 4.12. It is apparent that the pristine PS nearly follows the master curve of $Z(F_1)$, demonstrating that the thermal decomposition process of pristine PS is associated to F1 reaction mechanism. According to literature, this degradation mechanism refers to random nucleation with one nucleus on the individual particle (Ma et al., 1991). In this type of mechanism, the degradation is initiated from random points, which act as growth centre for the progress of the degradation reaction. After adding Co-Al LDH, for all PS/Co-Al LDH nanocomposites samples, F1 reaction mechanism exists at lower α value (α = 0.15 – 0.4). Nevertheless, at higher conversion (α = 0.7 – 0.9), the thermal degradation reaction tends towards A4 mechanism, which corresponds to nucleation and growth (see Figures 4.11 and 4.12).

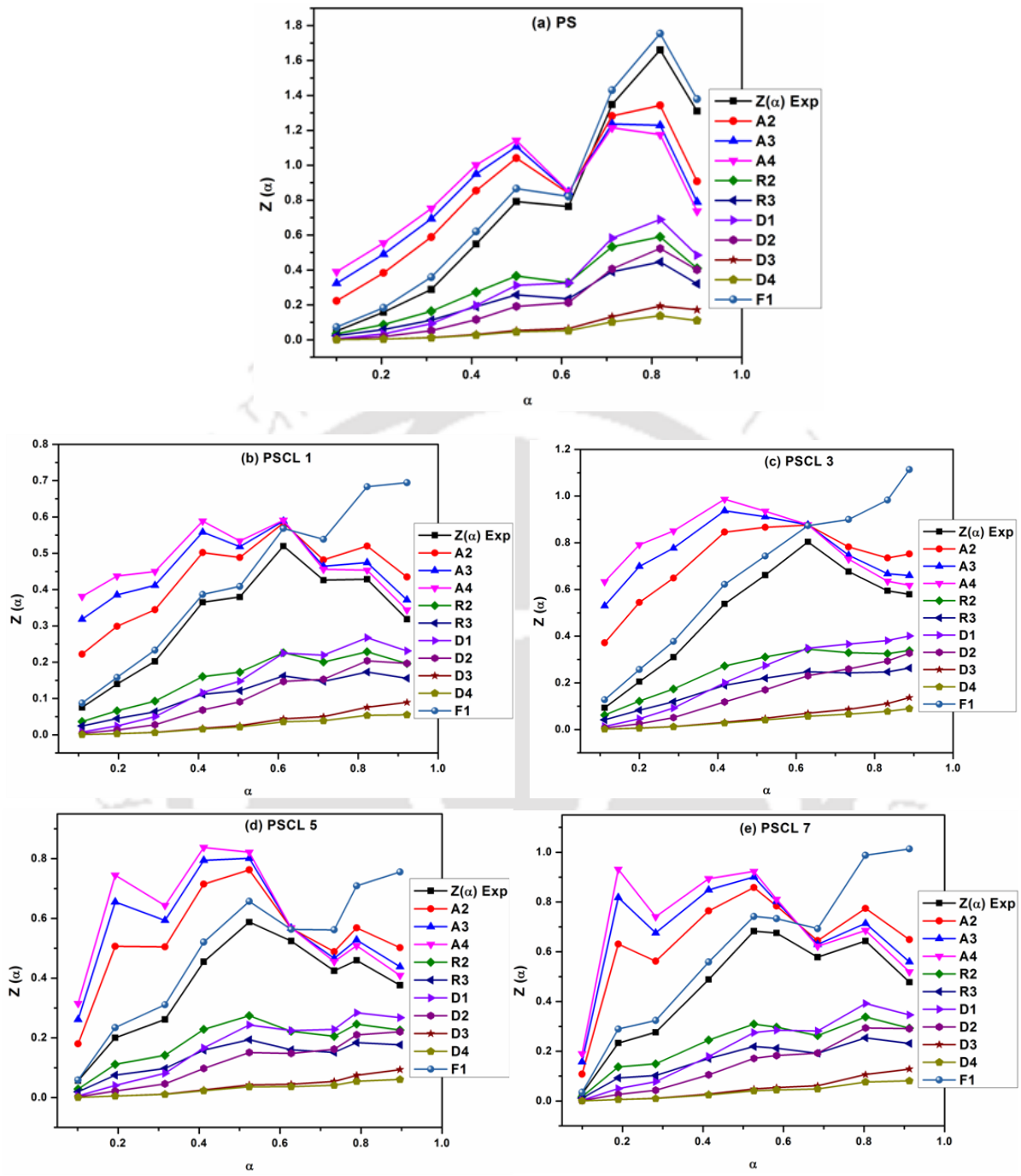

Figure 4.11: Z(α) versus α plots for various cases (a) pristine PS, (b) PSCL 1, (c) PSCL 3, (d) PSCL 5 and (e) PSCL 7 nanocomposites.

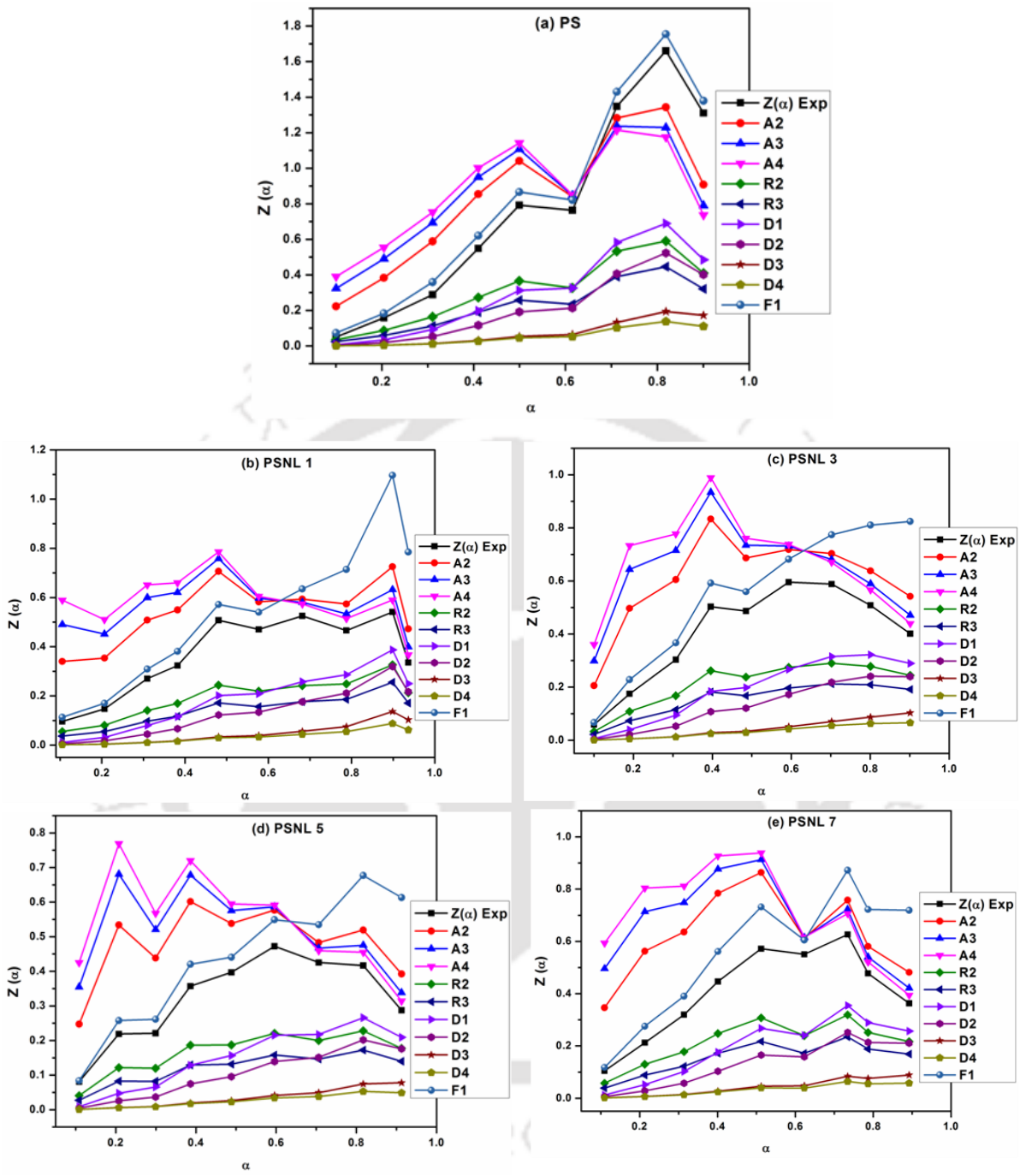

Figure 4.12: Z(α) versus α plots for various cases (a) pristine PS, (b) PSNL 1, (c) PSNL 3, (d) PSNL 5 and (e) PSNL 7 nanocomposites.

4.3.8 Integral procedural decomposition temperature

To evaluate nanocomposites thermal stability, IPDT method was employed by considering the overall shape of the TGA curve. According to Doyle's method (Doyle 1961), the IPDT value is estimated using the following expression:

$$IPDT(^{o}C) = K \times S \times (T_f - T_i) + T_i \tag{4.16}$$

where, $S = \frac{(A_1 + A_2)}{(A_1 + A_2 + A_3)}$; $K = \frac{(A_1 + A_2)}{(A_1)}$; S is the area ratio of total experimental curve specified by the total TGA thermogram. T_f and T_i are the final and initial experimental temperature. As shown in Figure. 4.13, A_1, A_2, and A_3 are partitions of three different areas of the typical TGA thermogram graph. For all prepared samples, the IPDT values are determined using equation (4.16). The IPDT value of pristine PS and PS/Co-Al LDH nanocomposites containing 1, 3, 5 and 7 wt.% of LDH is found to be 380.4, 388.5, 402.6, 410.7 and 415.8 °C, respectively (see Table 4.5). Similarly, the IPDT values of PSNL 1, PSNL 3, PSNL 5 and PSNL 7 nanocomposites is 390.3, 404.1, 412.5 and 417.0 °C, respectively.

As expected, the IPDT value of nanocomposites increases with increasing LDH concentration, which confirms increment of thermal stability of nanocomposites. The IPDT values of PS nanocomposites with 7 wt.% LDH is higher than that of other samples indicating better thermal stability. Similarly, Kim et al. (2010) conveyed enhancement in IPDT values for nanocomposites in comparison with pristine polymer.

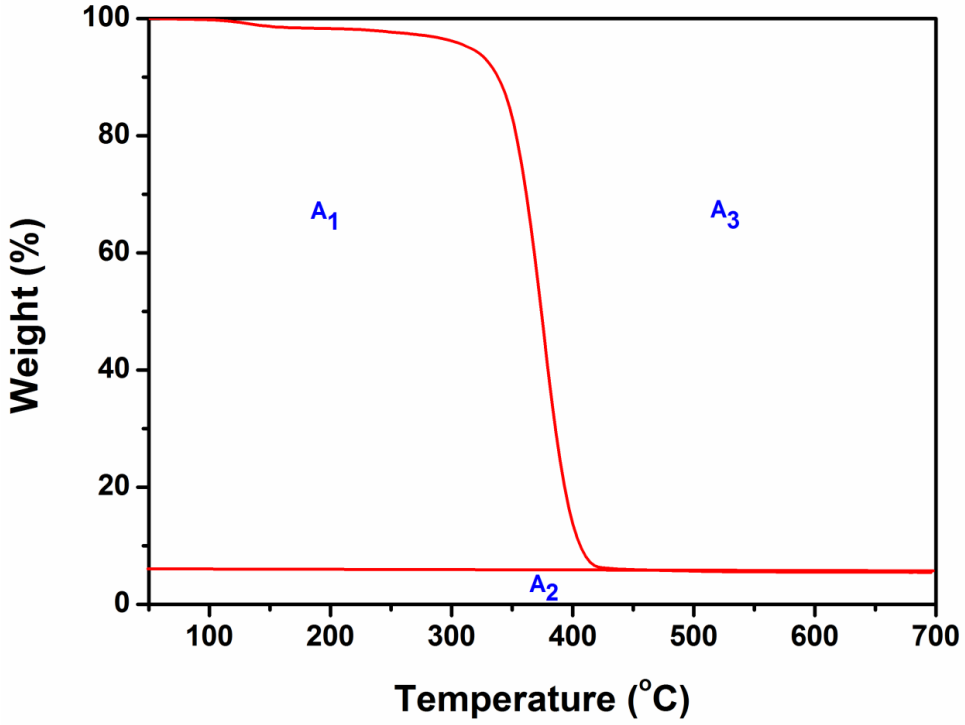

Figure 4.13: Schematic diagram of Doyle's method to determine IPDT.

Table 4.5: IPDT values for pristine PS, PS/Co-Al LDH and PS/Ni-Al LDH nanocomposites samples.

Sample	Initial Temperature (T_i) °C	Final Temperature (T_f) °C	IPDT (°C)
PS	50	700	380.4
PSCL 1	50	700	388.5
PSCL 3	50	700	402.6
PSCL 5	50	700	410.7
PSCL 7	50	700	415.8
PSNL 1	50	700	390.3
PSNL 3	50	700	404.1
PSNL 5	50	700	412.5
PSNL 7	50	700	417.0

4.3.9 Rheological properties

Rheological analysis of polymer nanocomposites are useful to understand the fundamental characteristics of the nanofiller and for varying processing conditions. The storage modulus facilitates insights into the elastic *i.e.* solid like behavior. The loss modulus represents for the viscous *i.e.* liquid like behavior of the polymer melts. The rheological characteristics of polymer and its composites melts are a subject of concentrated research and are highly desired essentials for injection and extrusion process. In addition, the relaxation and mobility of polymer matrix chains are impeded by the geometric confinement of the nanofiller system. Hence, it is necessary to examine the viscoelastic characteristics of polymer and its composites, which are vital factors in preparation processes.

4.3.9.1 Storage and loss moduli

Rheological analysis of the polymer composites is very effective tool to study the variation of microstructure and an interactive force between the polymer and nanofiller. The analysis was carried out with varying frequency between 0.01 and 100 sec^{-1} at a constant temperature of 190 °C. Figure 4.14 demonstrate the frequency dependence of storage molulus of PS/Co-Al LDH and PS/Ni-Al LDH nanocomposites. As depicted in Figure 4.14, the storage modulus of pristine PS is the lowest among all nanocomposite samples (including both type of nanocomposites) in the entire range of frequency and the storage modulus increases with increasing LDH concentration. An increase of storage modulus at lower frequency is a characteristic of pseudo-solid like behaviour due to the formation of network percolating LDH lamellae. At higher frequency, the storage modulus curves overlap with each other for all nanocomposite samples (including both type of nanocomposites). The increment of filler content in the nanocomposites transforms the structure from liquid-like nature to

solid-like nature. The transition concentration for the same is termed as rheological percolation threshold. The appearance of rheological percolation threshold in the nanocomposite samples can be attributed to the formation of continuous network of LDH and polymer chain. The same phenomenon has been reported for PE/Mg-Al LDH nanocomposites (Costa et al., 2006b) and polymer/layered silicate nanocomposites (Lim and Park, 2001).

The rheological parameter used to indicate the viscous effect of the given viscoelastic material is 'loss modulus'. Figure 4.15 shows the plots of loss modulus versus frequency in the range of 0.01 – 100 sec^{-1} at a temperature of 190 °C. Upon comparison with the storage modulus of various samples, it is apparent that the loss modulus is always higher than the storage modulus at lower frequency. This indicates upon the dominance of the viscous part. In the lower frequency region, the rise of loss modulus for the nanocomposite samples is more than the enhancement observed at higher frequency region, despite observing that the nature of all curves is similar.

It is apparent that with the addition of LDH, the loss modulus is altered especially at lower frequency region, since it is quite resistive to flow (Costa et al., 2006b). In the higher frequency region, the relaxation time for the polymer nanocomposites is reduced. It signifies a more flowing situation in which resistance cause by LDH gets cancelled out and the curves come closer to that of pristine PS.

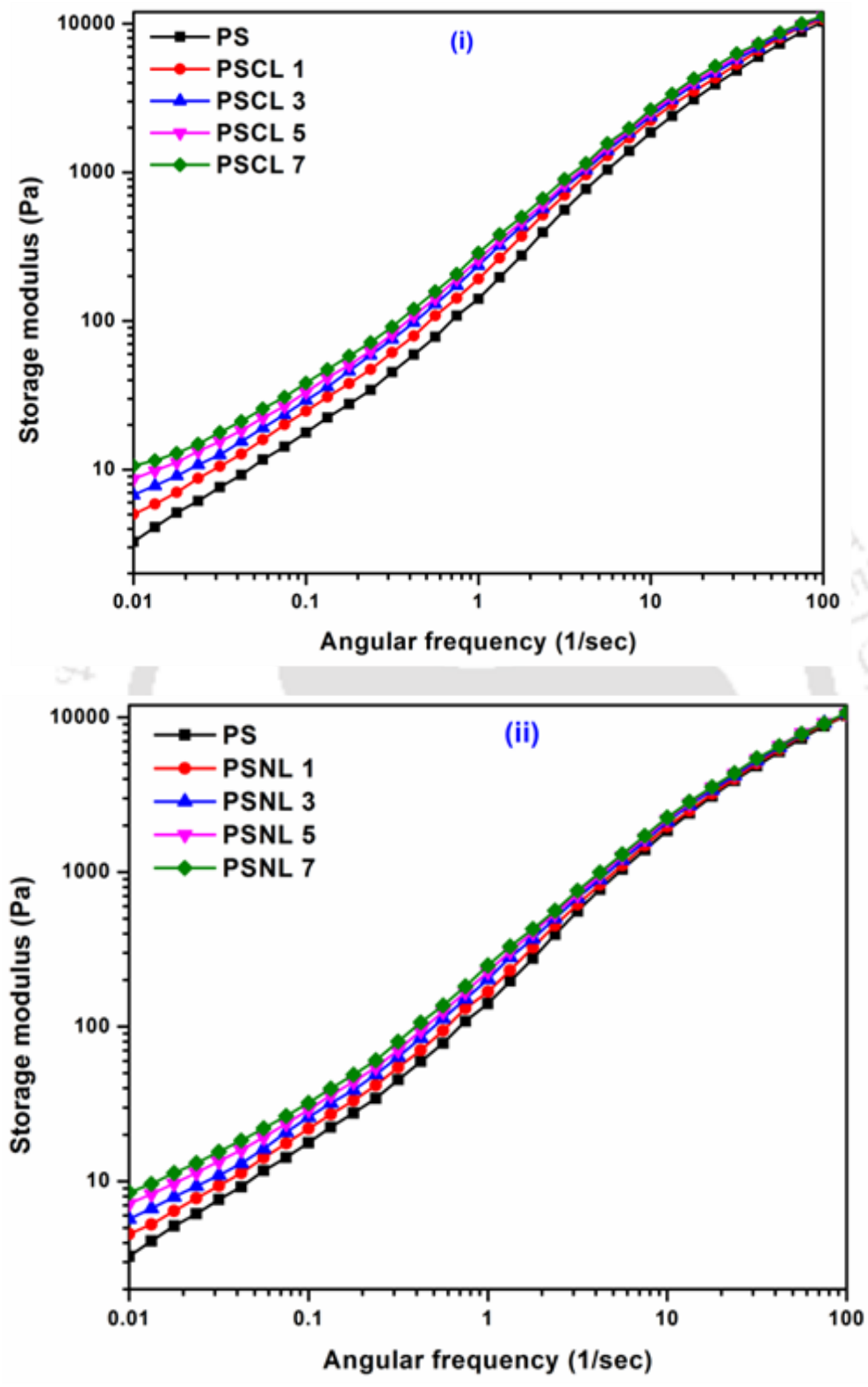

Figure 4.14: Storage modulus profiles of (i) PS/Co-Al LDH and (ii) PS/Ni-Al LDH nanocomposites at 190 °C.

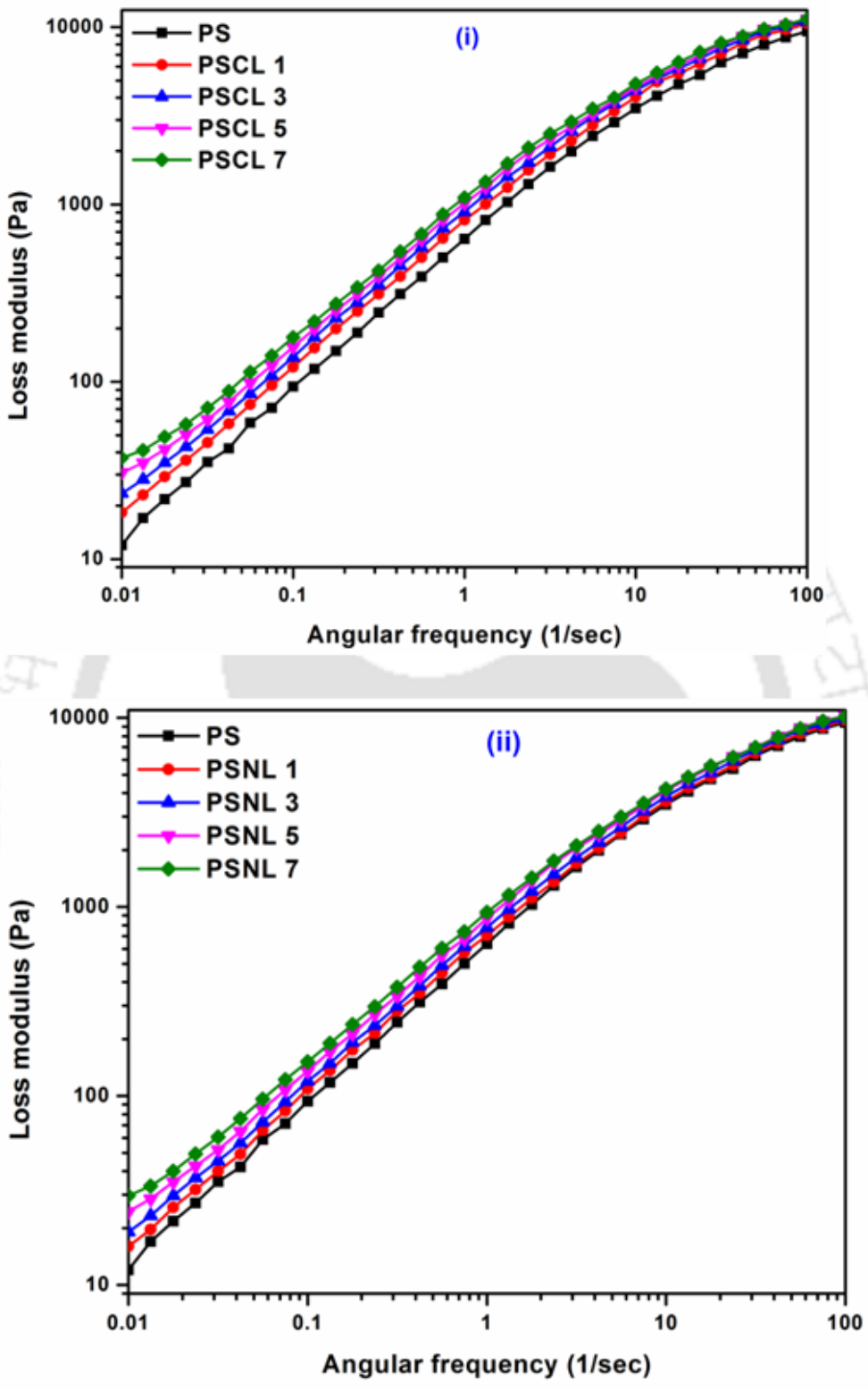

Figure 4.15: Loss modulus profiles of (i) PS/Co-Al LDH and (ii) PS/Ni-Al LDH nanocomposites at 190 °C.

The G′ has slopes of 0.93, 0.89, 0.877, 0.84 and 0.82 for pristine PS, PSCL 1, PSCL 3, PSCL 5 and PSCL 7, respectively. However, G″ has slopes of 0.74, 0.718, 0.699, 0.675 and 0.650, respectively, for pristine PS, PSCL 1, PSCL 3, PSCL 5 and PSCL 7 in log plots. Similarly, the G′ has slopes of 0.90, 0.88, 0.86 and 0.84 for PSNL 1, PSNL 3, PSNL 5 and PSNL 7, respectively and G″ has slopes of 0.72, 0.71, 0.69 and 0.67 for PSNL 1, PSNL 3, PSNL 5 and PSNL 7, respectively in log plots. For the lowest frequencies, the system response affirms to liquid-like behaviour (with G′ less than G″). However, at higher frequencies, both moduli became equal and displayed near plateau region with higher value of G′ than G″. This confirms to glassy solid like behaviour of the PS/LDH nanocomposites (Choi and Ray, 2011).

The crossover points occur at 73.0, 69.8, 65.9, 62.6 and 60.5 sec^{-1} for pristine PS, PSCL 1, PSCL 3, PSCL 5 and PSCL 7, respectively (see Figure 4.16). Further, the crossover points occur at 68, 64.5, 61.8 and 59.9 sec^{-1} for PSNL 1, PSNL 3, PSNL 5 and PSNL 7, respectively (see Figure 4.17). The nanocomposites loaded with LDH exhibit more rapid solid-like behaviour (G′ greater than G″) (Hoffmann et al., 2000). This solid-like behaviour can be explained with a reduction in the slope of G′. The G′ *versus* G″ plot conveys variations in the microstructure of the system due to incorporation of LDH (see Figure 4.18).

For these plots, the slope values for pristine PS, PSCL 1, PSCL 3, PSCL 5 and PSCL 7 nanocomposites have been determined as 1.23, 1.216, 1.213, 1.21 and 1.20, respectively. Further, the corresponding slope values for pristine PS, PSNL 1, PSNL 3, PSNL 5 and PSNL 7 nanocomposites are 1.23, 1.226, 1.224, 1.22 and 1.21, respectively. Potschke et al. (2002) also reported similar behaviour for nanocomposites prepared with multiwalled carbon nanotubes (MWCNT) and polycarbonate polymer.

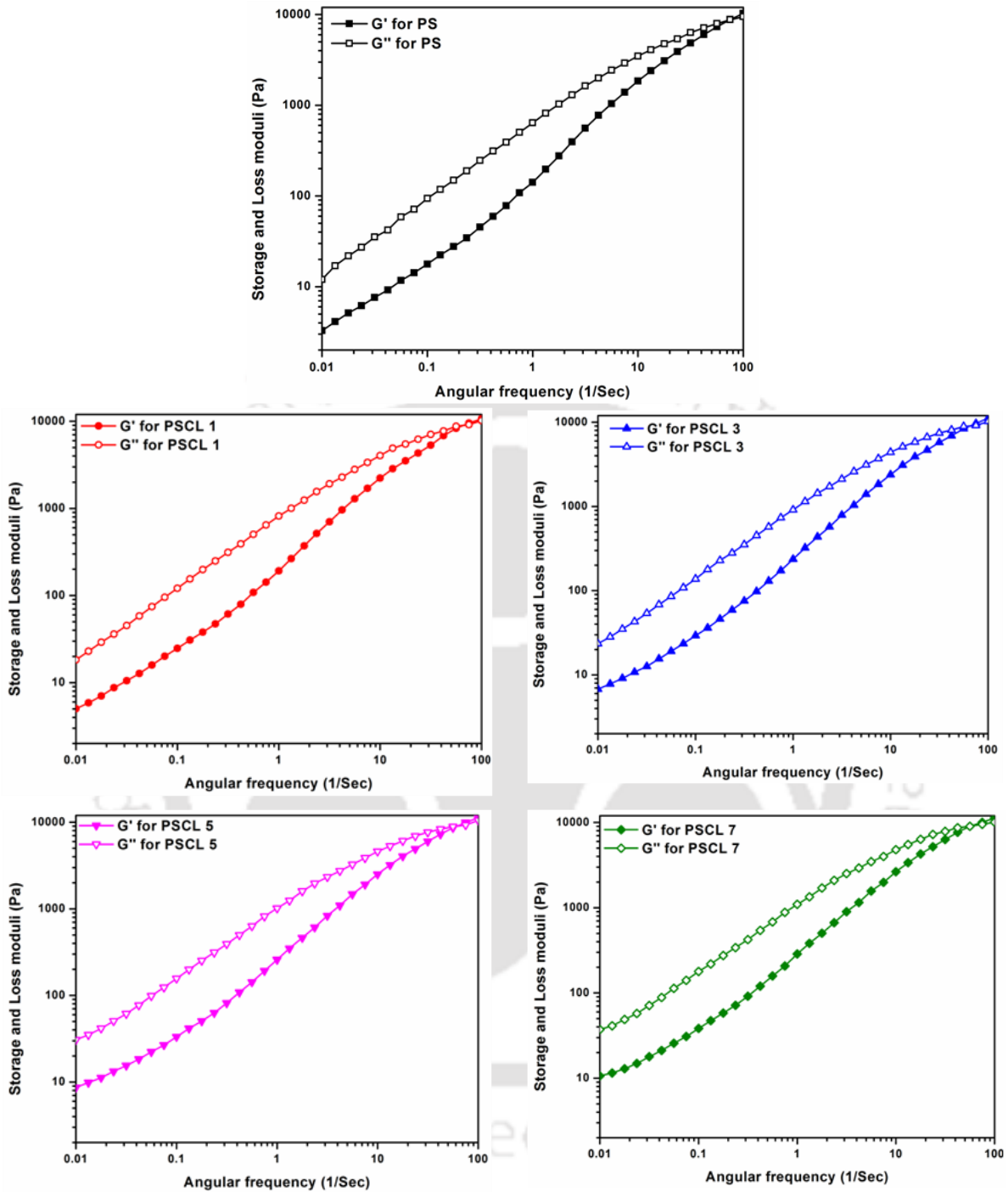

Figure 4.16: Comparison of the storage (G′) and loss (G″) moduli for pristine PS and PS/Co-Al LDH nanocomposites at 190 °C.

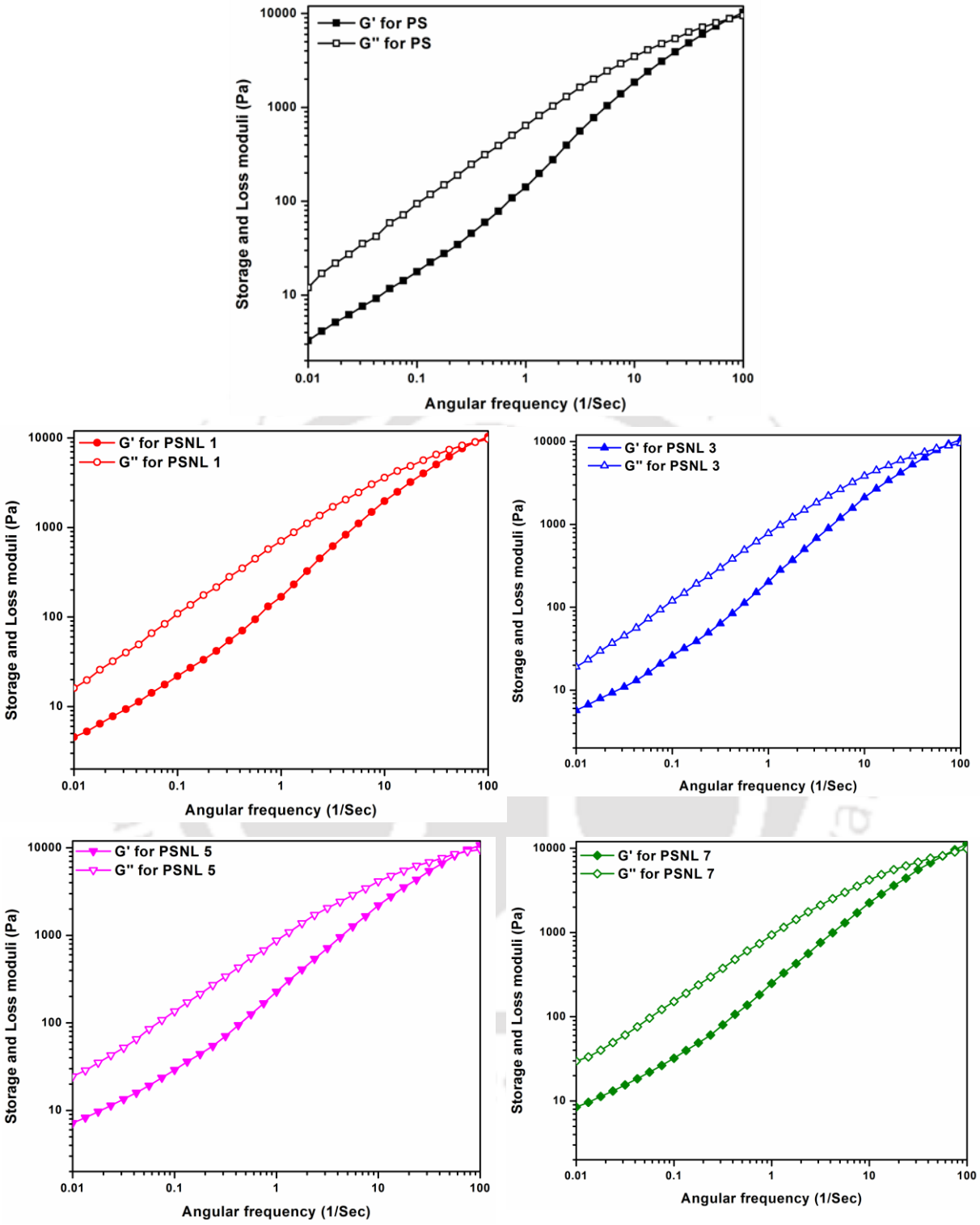

Figure 4.17: Comparison of the storage (G′) and loss (G″) moduli for pristine PS and PS/Ni-Al LDH nanocomposites at 190 °C.

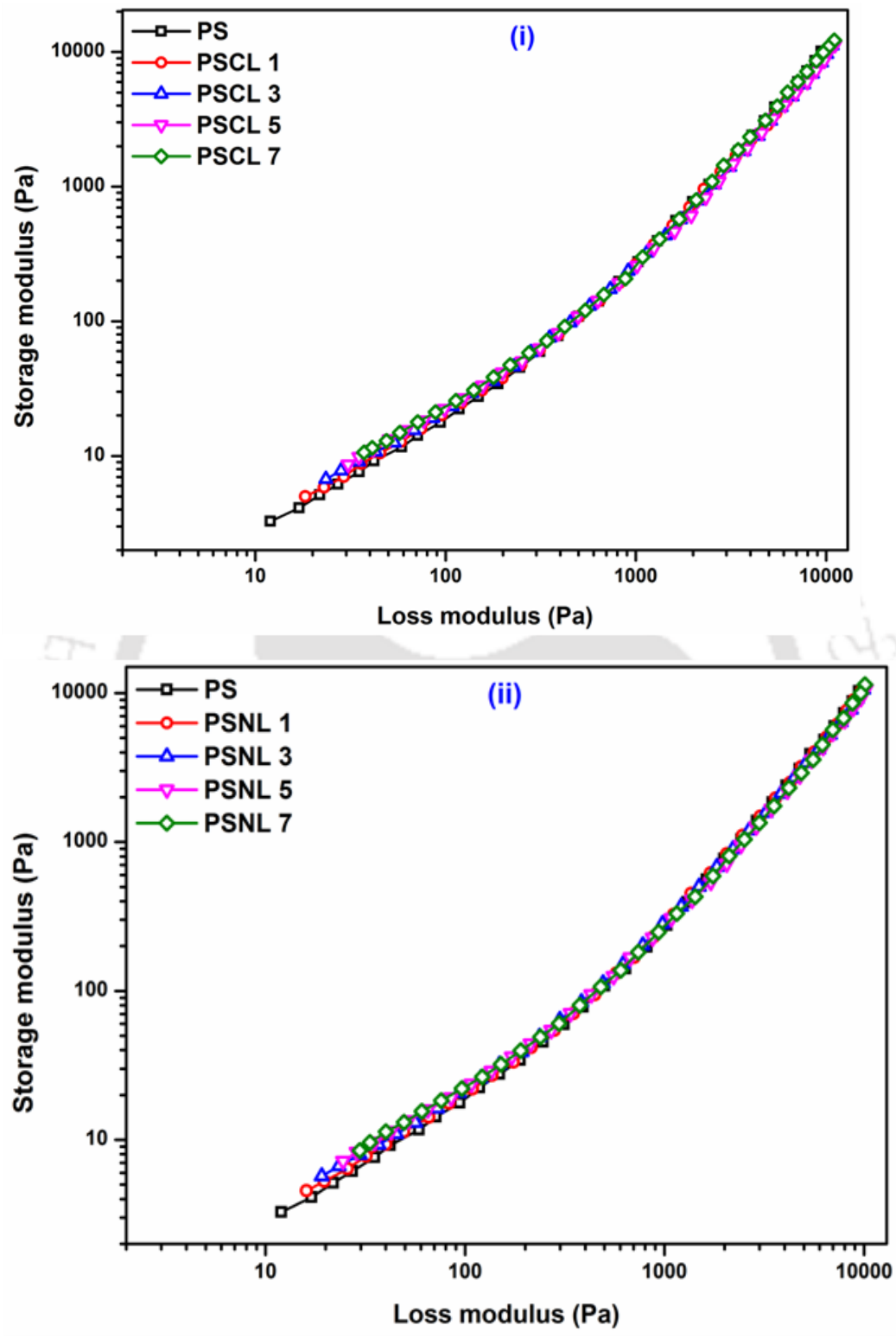

Figure 4.18: Plot of log G′ versus log G″ for (i) PS/Co-Al LDH and (ii) PS/Ni-Al LDH nanocomposites at 190 °C.

4.3.9.2 Loss factor

Figure 4.19 depicts the loss factor as a function of frequency in the range of 0.01 – 100 sec^{-1} at 190 °C. It is observed that the loss factor for both types of nanocomposites is lower than that of pristine PS. Further, it decreases with increasing LDH concentration in the polymer matrix. This is due to the fact that elastic nature of the nanocomposites increases with increasing LDH content (Costa et al., 2006b). Majid et al. (2011) also obtained a similar trend of loss factor for PP nanocomposites with ZnO nanofiller. The reduction of loss factor in the high frequency region is attributed to shear deformation based partial orientation of polymer chain and LDH (Motahari et al., 2012).

4.3.9.3 Complex viscosity

Figure 4.20 portrays the behaviour of complex viscosity with angular frequency in the range of 0.01 – 100 sec^{-1} at 190 °C. The PS/Co-Al LDH and PS/Ni-Al LDH nanocomposites illustrate a rise in complex viscosity values with increasing LDH concentration in the lower frequency region, which is slowly quenched as the frequency increases. The primary cause for this trend is adhesion between the LDH and PS and the cohesive interactions in the LDH layers. This also explains that the addition of LDH influences more frictional interactions. A transition from Newtonian behaviour to a shear thinning nature is also observed with increasing frequency. This is due to the fact that polymer chains have less time to entangle and the direction of randomly dispersed nanofiller is also turned according to the macromolecular chains at higher frequency. As a result, PS/Co-Al LDH and PS/Ni-Al LDH nanocomposites profiles move near to PS curve and all samples exhibit similar trend at higher frequency (see Figure 4.20).

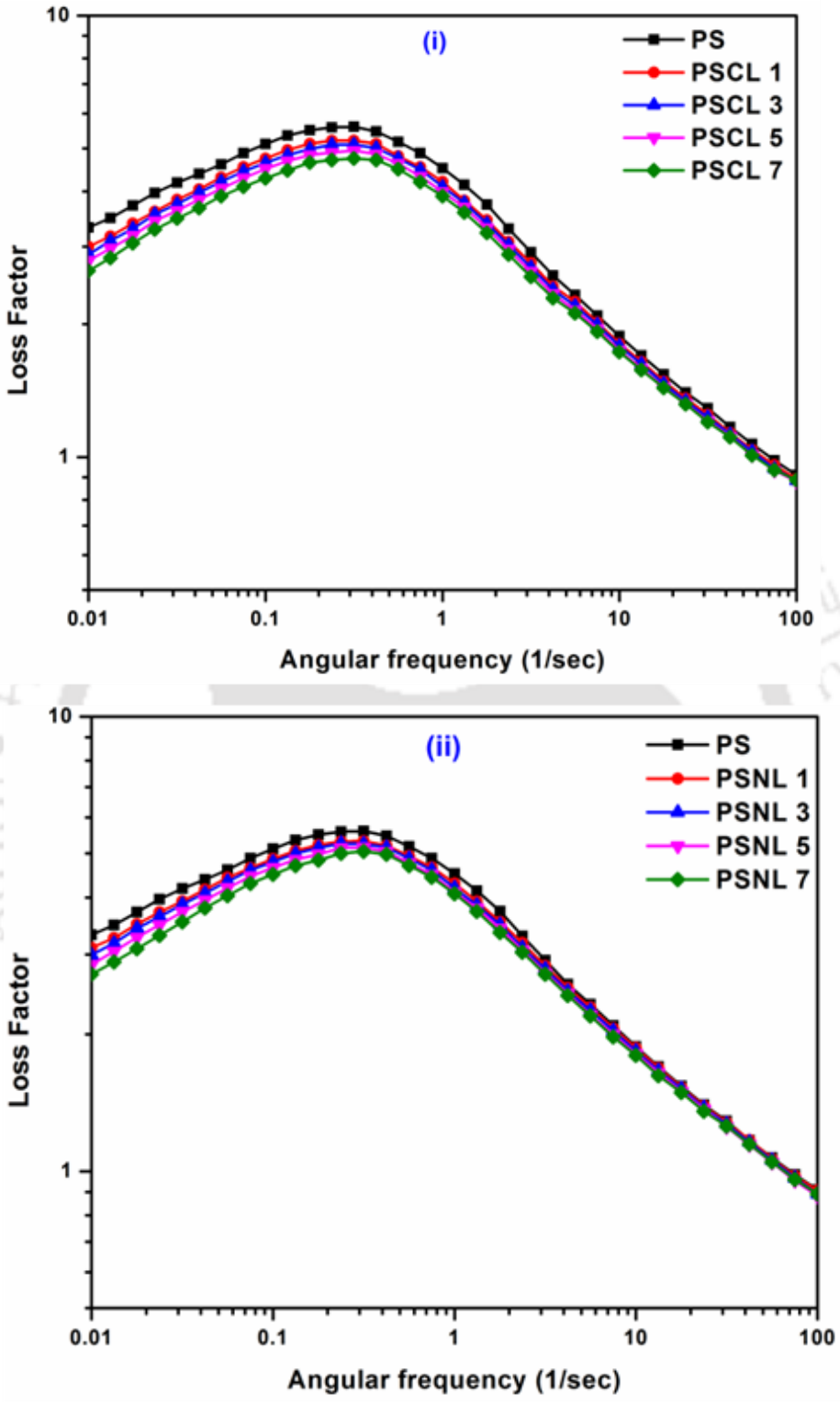

Figure 4.19: Loss factor of (i) PS/Co-Al LDH and (ii) PS/Ni-Al LDH nanocomposites at 190 °C.

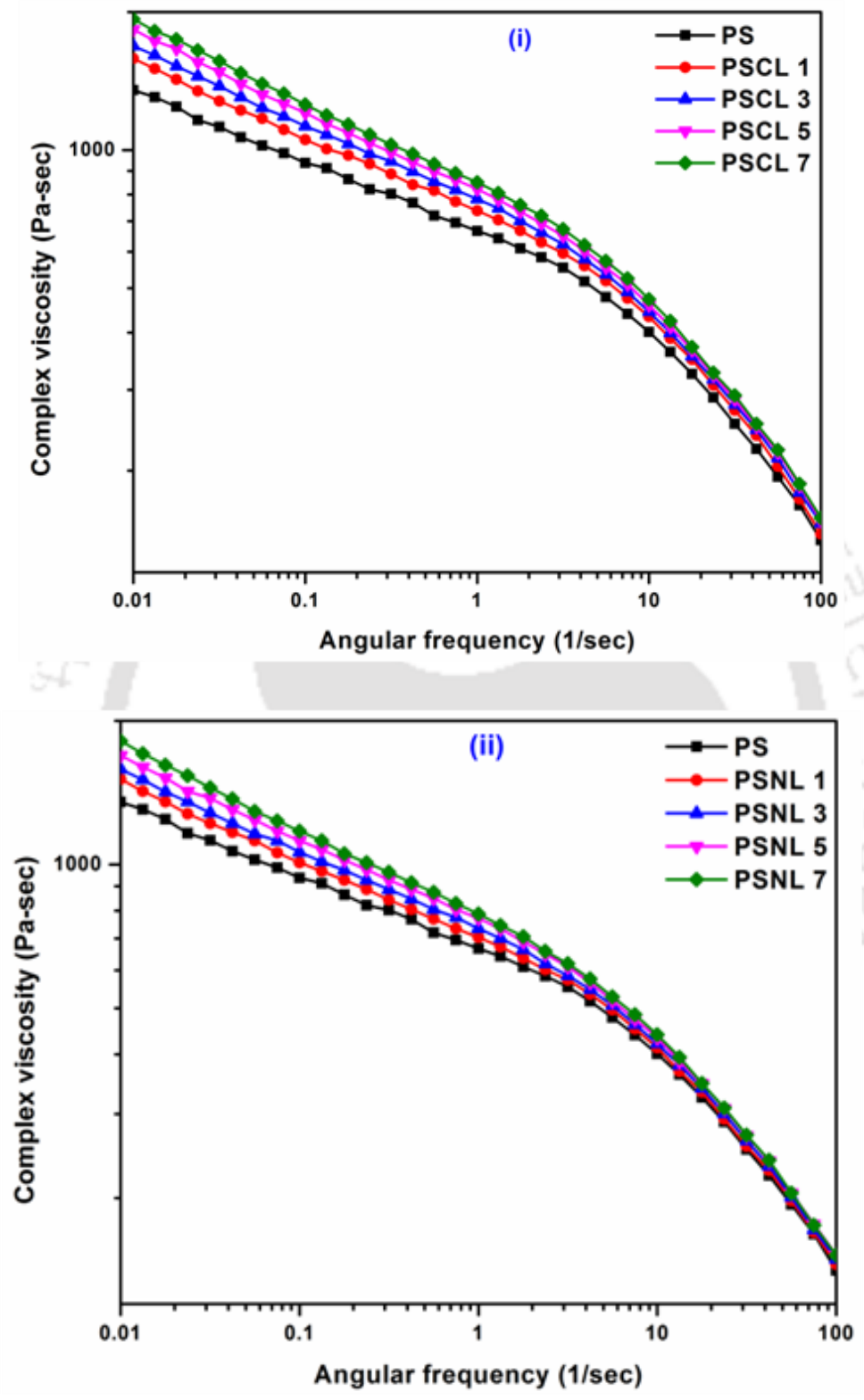

Figure 4.20: Complex viscosity of (i) PS/Co-Al LDH and (ii) PS/Ni-Al LDH nanocomposites at 190 °C.

4.3.9.4 Theoretical prediction of storage modulus and loss factor values

For predicting the theoretical values of storage modulus, many researchers developed correlations based on their modeling effort to represent inclusion based reinforcement of a material. A simplest model equation suggested by Einstein (Majid et al., 2011) is given below:

$$G_c = G_m (1+1.25V_f) \quad (4.17)$$

In the above expression, G represent storage modulus, subscript m and c signifies matrix and nanocomposite. Correspondingly, volume fraction of the nanoparticle inclusions is denoted by V_f. Einstein also provided the following expression:

$$G_c = G_m (1+V_f) \quad (4.18)$$

Based on Einstein equation, Guth (1945) modified the above expressions to provide a correlation presented as follows:

$$G_c = G_m (1+ 1.25V_f + 14.1V_f^2) \quad (4.19)$$

The mixture equation (Majid et al., 2011) is used to indicate upon the damping of rigid fillers using tan δ expression:

$$\tan\delta_c = V_f \tan\delta_f + V_m \tan\delta_m \quad (4.20)$$

For rigid inclusion, the first term can be neglected and the equation is written as (Drzal et al., 1983)

$$\tan\delta_c = V_m \tan\delta_m \quad (4.21)$$

Further, the equation (Equation 4.21) can be modified as (Tung and Dynes, 1987)

$$\tan\delta_c = V_m(G_m/G_c)*\tan\delta_m \quad (4.22)$$

where V_m is the volume fraction of the polymer matrix, the subscript m and c represent matrix and composite.

The graph of theoretical and experimental storage modulus values at 190 °C for nanoparticle loading by wt.% are shown in Figure 4.21. It was found from all models used (Einstein equation (4.17, 4.18) and Guth equation (4.19)) that there was a minor positive deviation from the experimental values (see Figure 4.21 (i) and (ii)). However, the Guth model (Equation (4.19)) strongly agrees with experimental values whereas the Einstein model (Equation (4.18)) shows significant deviation. Karamipour et al. (2011) have obtained similar results for PP/$CaCO_3$ nanocomposites.

For various nanoparticle loadings (as wt.%), the plot of theoretical and experimental tan δ values of PS/Co-Al LDH and PS/Ni-Al LDH composites are shown in Figure 4.22. For low nanoparticle concentration, both equations fit with the experimental data. However, equation (4.21) fits better than equation (4.22) with experimental data. Both equations show departure in case of higher concentration of LDHs, as evidenced from Figure 4.22. The deviation shown by the models from the experimental values might have been due to the reason that localized constraints imposed by the dispersed phase on deformation of PS polymer were ignored by both equations.

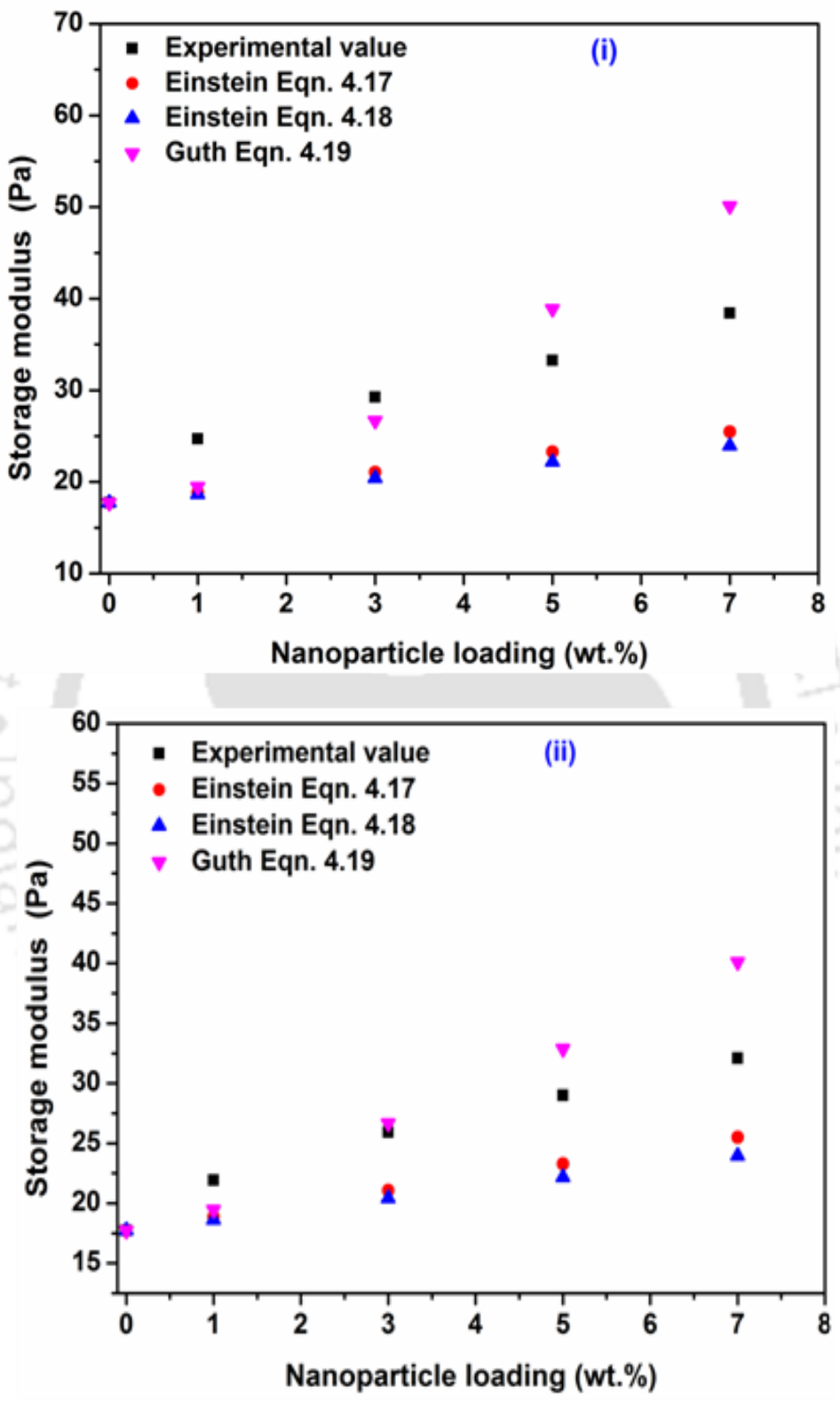

Figure 4.21: Comparison of experimental and theoretical storage modulus values of (a) PS/Co-Al LDH and (b) PS/Ni-Al LDH nanocomposites at 190 °C.

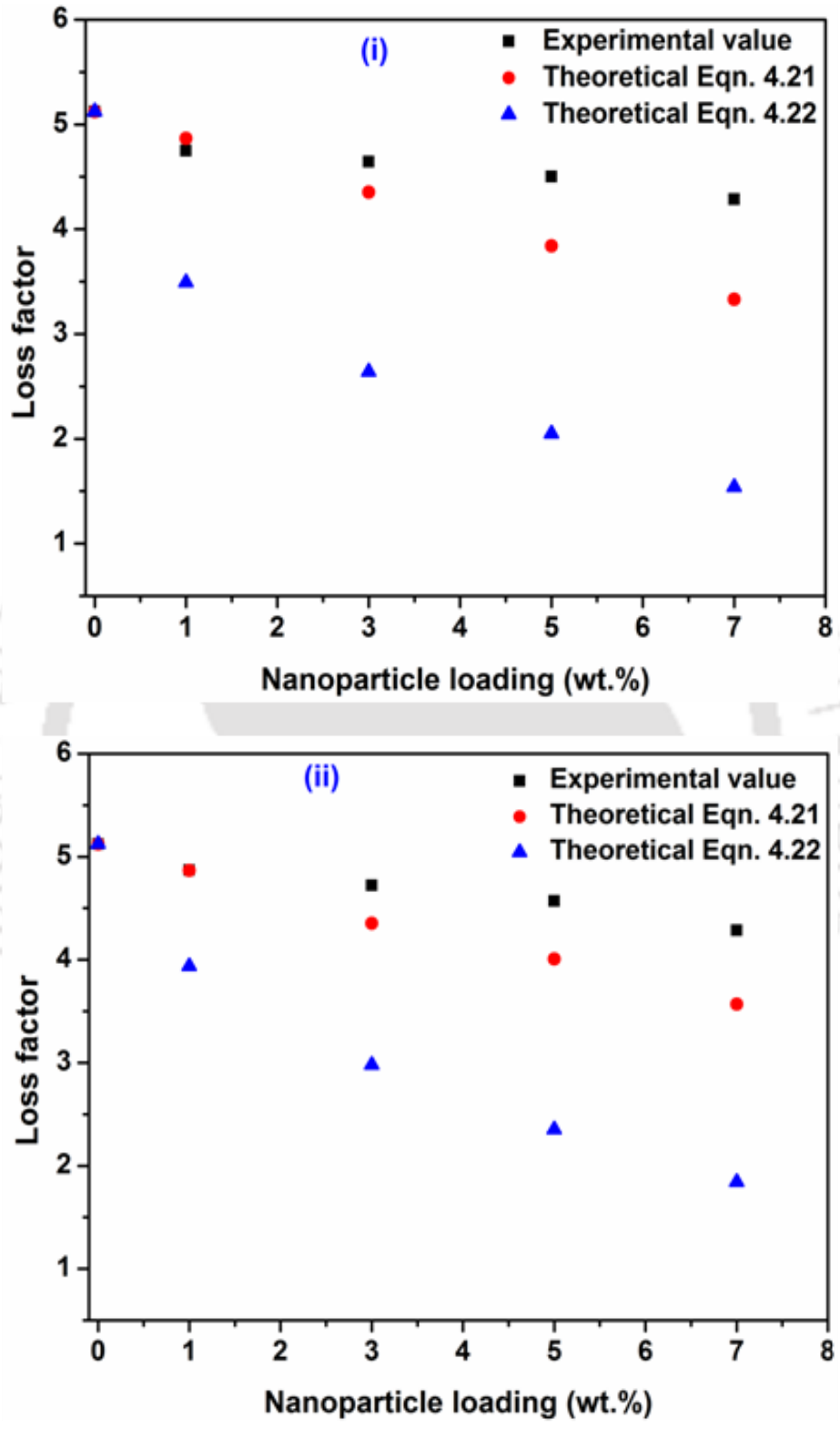

Figure 4.22: Comparison of experimental and theoretical loss factor values of (i) PS/Co-Al LDH and (ii) PS/Ni-Al LDH nanocomposites at 190 °C.

4.4 Summary

Several PS composites were synthesized successfully by dispersing the inorganic nanolayers of Co-Al LDH and Ni-Al LDH in PS polymer via solvent blending method. XRD profiles of PS nanocomposites showed no diffraction peak corresponding to basal plane (003) of Co-Al LDH and Ni-Al LDH, indicating the formation of exfoliated PS/Co-Al LDH and PS/Ni-Al LDH nanocomposite. TEM micrographs exhibited that the LDHs platelets were disseminated well within PS matrix. The FTIR results verified existence of Co-Al LDH and Ni-Al LDH in the PS/Co-Al LDH and PS/Ni-Al LDH nanocomposites, respectively. The WVTR values are 18, 12.45 and 11.9 $gm/m^2/day$ for pristine PS, PSCL 7 and PSNL 7 nanocomposites, respectively.

Also, the PS/Ni-Al LDH nanocomposites possessed enhanced glass transition temperature than those obtained for PS/Co-Al LDH nanocomposites. At 15% mass loss reference point, the thermal decomposition temperature of PS nanocomposites was 10.5 – 28.5 °C higher than the pristine PS, while PS/Ni-Al LDH nanocomposites was 12.3 – 29.1 °C more than the degradation temperature of pristine PS.

The activation energy of PS/Co-Al LDH nanocomposites (20 – 49 kJ/mol) and PS/Ni-Al LDH nanocomposites (23 – 50 kJ/mol) is higher than that of pristine PS. The obtained IPDT and activation energy data is in complete agreement with the thermal stability improvement analysed for PS/LDH nanocomposites using TGA data. Thermal degradation mechanism analysis conveyed that the thermal degradation of nanocomposites followed F1 reaction mechanism initially followed with A4 mechanism at higher temperature. Rheological studies conveyed that the storage modulus and loss modulus increased with increasing content of

LDH and is less dependent on frequency variation at higher frequency. However, the complex viscosity reduces with increasing angular frequency.

In summary, the Ni-Al LDH based nanocomposites demonstrated better properties than Co-Al LDH based nanocomposites. This might be due to two step fabrication process for Ni-Al LDH nanocomposite which was not the case for the single step process adopted for Co-Al LDH nanocomposites. Further research in this direction could be useful to provide deeper insights with respect to improvements in the procedures involved in solvent blending method.

Chapter 5:

Fabrication and Characterization of PS/Co-Al LDH and PS/Ni-Al LDH Nanocomposites via Melt Blending Method

Fabrication and Characterization of PS/Co-Al LDH and PS/Ni-Al LDH Nanocomposites via Melt Blending Method

This chapter addresses the preparation and characterization of melt blending based PS/Co-Al LDH and PS/Ni-Al LDH nanocomposites in the nanofiller loading range of 1 – 7 wt.%. Twin screw extruder was deployed to fabricate 1, 3, 5 and 7 wt.% nanofiller containing nanocomposites using melt intercalation method. Structural, mechanical and thermal properties of the prepared nanocomposites were investigated. The structural properties of the polymer nanocomposites were evaluated using XRD and TEM. The mechanical properties of various nanocomposites were evaluated with tensile, flexural and impact tests. The thermal characterizations were carried out with DSC and TGA. The activation energy and reaction mechanism associated to thermal degradation of pristine PS and its nanocomposites were evaluated with Coats-Redfern and Criado model, respectively. IPDT determination as well confirmed upon thermal stability enhancement in nanocomposites. Overall, among all samples, PS/Ni-Al LDH samples possess improved thermal and mechanical properties.

5.1 Introduction

In the recent past, polymer nanocomposites received significant research interest in both industry and academia. This is due to their ability to provide a further improvement of material properties such as thermal stability, mechanical strength, fire retardancy and gas barrier performance (Nyambo et al., 2008; Realinho et al., 2009; Mallakpour and Dinari,

2014). These property enhancements are due to the layered distribution of inorganic material in the polymer matrix.

The available literature is affirming upon several approaches for polymer nanocomposites preparation (Moet and Akelah, 1993; Ding and Qu, 2005; Du et al., 2007; Paul et al., 2013; Yeh et al., 2004; Qiu and Qu, 2006; He et al., 2006; Majoni, 2015; Tai et al., 2011; Zhang et al., 2008; Wu et al., 2002; Zhao et al., 2003; Chen and Wang, 2007). Using acetonitrile as a solvent, Moet and Akelah (1993) fabricated PS nanocomposites. The authors reported intercalation in PS/clay composites with a maximum basal spacing of 2.54 nm. Ding and Qu (2005) prepared PS/Zn-Al LDH nanocomposites through emulsion polymerization with N-lauroyl-glutamate surfactants. For 10 wt.% Zn-Al LDH loading, the authors achieved completely exfoliated PS/LDH nanocomposites. Du et al. (2007) obtained nylon 6/Mg-Al LDH nanocomposites via melt intercalation of nylon 6 with interlayers of organomodified Mg-Al LDH. Their XRD results demonstrated that too high LDH loading makes it difficult for LDH layers to undergo exfoliation. Paul et al. (2013) and Yeh et al. (2004) prepared clay based PS nanocomposites using solution intercalation technique and in-situ thermal polymerization method, respectively. The authors inferred that the nanocomposites possessed enhanced thermal stability due to nanofiller incorporation in the polymer matrix. Adopting emulsion polymerization, Qiu and Qu (2006) prepared PS/Mg-Al LDH composites and observed that for 50% mass loss reference point, the thermal stability of PS/Mg-Al nanocomposites with 5 wt.% LDH loading is 19 °C higher than that of pristine PS. In another study, the crystallisation temperature enhanced (upto 2 °C) for PS/Zn-Al LDH composites prepared by solvent blending technique with 3 wt.% loading of Zn-Al LDH (He et al., 2006). Enhanced thermal and flammability properties for the PS/LDH composites have also been conveyed by other researchers (Majoni, 2015; Tai et al., 2011). Zhang et al. (2008)

synthesized ethylene-vinyl acetate copolymer (EVA)/Zn-Al LDH nanocomposties via melt and solution intercalation technique. The mechanical test demonstrated that the tensile strength of the nanocomposites is 2.5 – 4.8 MPa higher than pure EVA. Poly (ethylene terephthalate)/clay composite was fabricated and precisely examined for its thermal oxidative degradation behavior by Wu et al. (2002) and Zhao et al. (2003). Chen and Wang (2007) studied thermal degradation kinetics and reaction mechanism of PP nanocomposites that were fabricated with twin-screw extruder.

An elaborate review of the carried out work till date indicates that the synthesis of PS/Co-Al LDH and PS/Ni-Al LDH nanocomposites using melt compounding method has not been conducted and reported. Hence, this chapter aims to fulfill this objective i.e., to analyze the influence of LDHs on the properties of melt compounding based PS nanocomposites. Structural, thermal and mechanical characterization studies have been targeted for the analyses of the PS nanocomposites. For the nanocomposites, based on the TGA data, thermal degradation kinetics and reaction mechanism have also been analyzed using Coats-Redfern and Criado model, respectively.

5.2 Materials and methods

5.2.1 Material

The chemicals used for the synthesis of PS/Co-Al LDH and PS/Ni-Al LDH nanocomposites have been discussed in section 4.2.1 of the thesis.

5.2.2 Preparation of modified Co-Al LDH and Ni-Al LDH

The procedure for the synthesis of modified Co-Al LDH and Ni-Al LDH has been summarized in sections 2.2.2 and 2.2.4, respectively in the Ph.D. thesis.

5.2.3 Preparation of PS/LDHs nanocomposites

A co-rotating twin-screw extruder was used to prepare PS/Co-Al LDH and PS/Ni-Al LDH nanocomposites using melt compounding method. Initially, moisture from pristine PS and Co-Al LDH was removed by drying the samples for 16 h at 60 °C and 70 °C, respectively. Further, the Co-Al LDH (1, 3, 5 and 7 wt.% with respect to pristine PS) was dispersed in 100 mL methanol. The solution was sprayed on a precise quantity of pristine PS pellet for ensuring uniform distribution of Co-Al LDH on the pristine PS matrix. Subsequent drying step for 24 h facilitated methanol evaporation from the samples. The coated PS pellets were fed to the extruder (Model: ZV-20 HI-Torque; Make: Specifiq Engineering and Automats, India) that was operated at a temperature of 185, 195, 210 and 200 °C, for feed, metering, compression and adaptor zones, respectively. After operation, extrudate was thoroughly quenched with water at ambient condition and was cut into pellets and dried using hot air oven at 60 °C for 24 h. Thereafter, dried pellets were fed to injection molding equipment (Model: 180 High Pressure; Make: JSW, Japan) that was operated at 195 – 210 °C. This step was followed to achieve samples for mechanical characterization studies. As controls and reference set, a clean PS sample was also prepared using similar procedure without LDH. In summary, the experimental investigations allowed fabrication of samples designated as Co-Al LDH, PS, PSNL 1, PSNL 3, PSNL 5 and PSNL 7 to represent cobalt-aluminum LDH, polystyrene, PS/Co-Al LDH 1 (wt.%), PS/Co-Al LDH 3 (wt.%), PS/Co-Al LDH 5 (wt.%), and PS/Co-Al LDH 7 (wt.%), respectively. Similarly, a series of PS/Ni-Al LDH nanocomposites containing (1 – 7 wt.% of LDH) were also prepared using above described procedure for comparison with the properties of PS/Co-Al LDH nanocomposites.

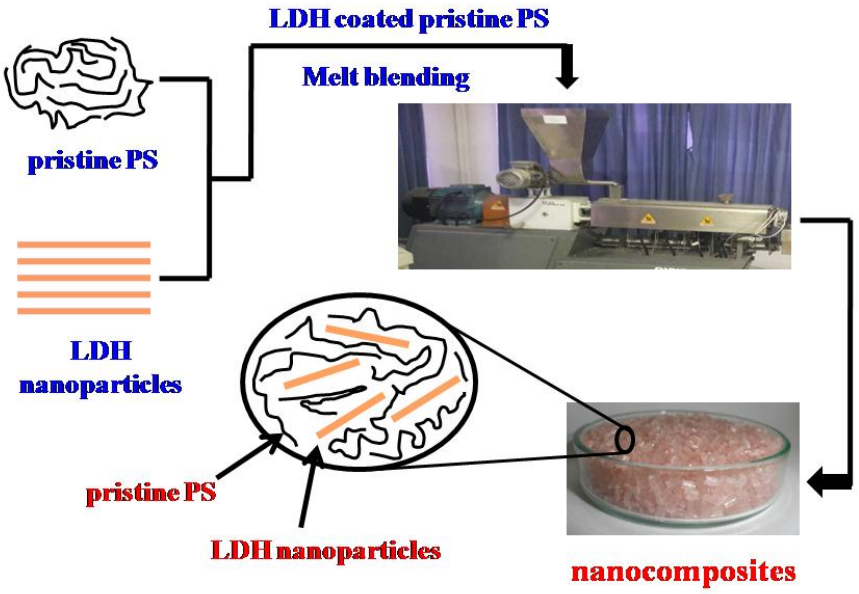

Figure 5.1: Schematic preparation of PS/LDHs nanocomposites.

For Ni-Al LDH based nanocomposites, the sample nomenclature refers to PSNL 1, PSNL 3, PSNL 5 and PSNL 7 for PS/Ni-Al LDH 1 (wt.%), PS/Ni-Al LDH 3 (wt.%), PS/Ni-Al LDH 5 (wt.%), and PS/Ni-Al LDH 7 (wt.%) samples respectively. The experimental procedure followed for the preparation of nanocomposites is presented in Figure 5.1.

5.2.4 Characterization

X-ray diffractometer (Model no: D8 Advance; Make: Bruker, Germany) facilitated with Cu-Kα radiation (0.15406 nm wavelength) and Ni filter was used to obtain XRD profiles at room temperature for Ni-Al LDH, pristine PS and PS nanocomposites. Further, the structural morphology of the PS nanocomposites was evaluated with transmission electron microscopy analysis, using TEM instrument (Model: JEM 2100; Make: JEOL, Japan)

operated at 200 kV accelerating voltage. Fourier transform infrared analyser (Model: IRAffinity1; Make: Shimadzu, Japan) was used to record FTIR spectra at room temperature in the range of 400 – 4000 cm^{-1}. Mechanical characterization studies involved evaluation of impact strength, tensile, and flexural properties of the nanocomposites. Specimens having dimensions of 168×13×3 mm^3 of pristine PS and the nanocomposites were evaluated for tensile strength and modulus using ASTM D 638 method and INSTRON (M 3382, UK) universal testing machine. The nanocomposites along with pristine PS specimens of dimension of 126×13×3 mm^3 were taken for flexural tests which were carried out using universal testing machine INSTRON (M 3382, UK) and ASTM D790 test method. Impactometer (M/s Tinius Olsen, USA) was used to conduct impact strength measurements (specimens having dimension of 62×13×3 mm^3). For each case, six specimens were tested and average value has been reported. Thermal stability of the prepared samples was determined under nitrogen atmosphere with a flow rate of 60 mL/min using high temperature thermo-gravimetric analyser (Model no: TGA 851e/LF/1100; Make: Mettler Toledo, Switzerland) at 10 °C/min heating rate and 30 – 700 °C temperature range. DSC instrument (Model no: 1; Make: Mettle Toledo, Switzerland) operated at 5 °C/min heating rate under nitrogen environment (and 40 mL/min) was used to determine glass transition temperature of pristine PS and other nanocomposite samples.

5.3 Results and discussion

5.3.1 XRD analysis

XRD analysis facilitates evaluation of the degree of intercalation and exfoliation in LDHs based nanocomposites. In such materials, these features are dependent upon several

factors such as LDH composition, organic modifier's chemical nature and method of fabrication. For intercalated nanocomposites, d-spacing (defined as d_{003} or 003 peak is shifted to lower angle) is higher than that of the original LDH. The exfoliated nanocomposites exhibit well separated inorganic layer from one another with no peaks corresponding to basal plane (003) and good distribution of nanofillers in the polymer matrix. The intercalation extent of LDH in PS is based on the LDH interlayer spacing evaluated using Bragg's law (gallery height or d_{003} spacing determined using expression $n\lambda = 2d\sin\theta$, where n = 1 and λ correspond to X-ray wave length (1.5406 Å)) (Hwu et al., 2004).

Figure 5.2 depicts XRD diffractograms of Co-Al LDH, Ni-Al LDH, pristine PS, PS/Co-Al LDH and PS/Ni-Al LDH nanocomposites. The XRD patterns convey that for Co-Al LDH, d_{003} peak exists at 3.14° with a basal spacing of 2.8 nm (see Figure 5.2 i (a)). The amorphous nature of pristine PS is characteristically reflected in two small halos that are centered at 2θ values of 10 and 20^{o} (Botan et al., 2012). No peaks corresponding to d_{003} at lower angles can be observed for PS/Co-Al LDH nanocomposite samples (Figure 5.2 i (c-f)). Similarly, it is also noticed that (003) peak is absent in PS/Ni-Al LDH nanocomposites [see Figure 5.2 (ii)]. Two extreme cases can explain the disappearance of the diffraction peaks in XRD: (a) complete exfoliation of the LDH layers in the polymer matrix, and/or (b) disordering of the LDH layers within the polymer matrix with no change in the d-spacing.

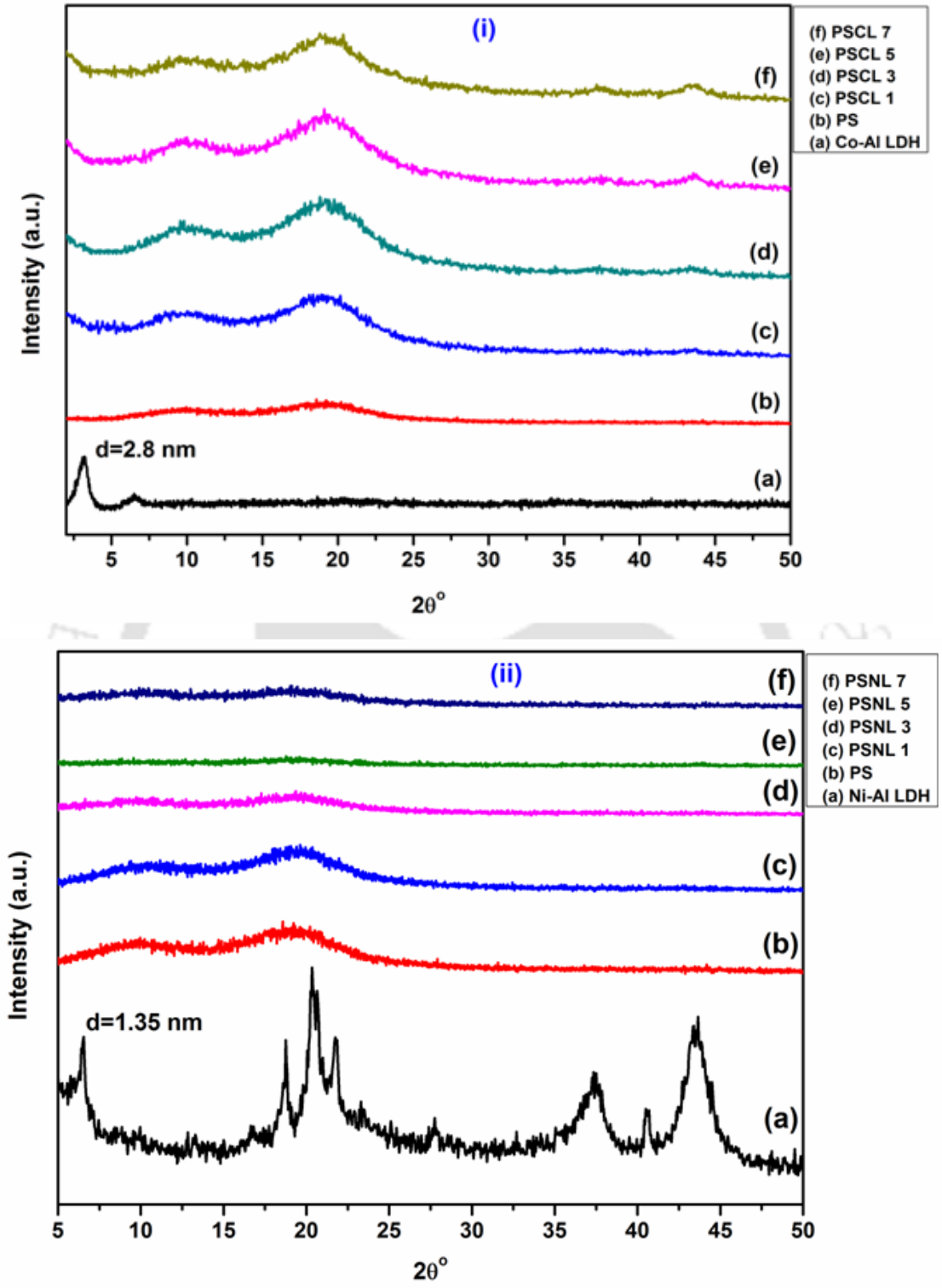

Figure 5.2: XRD patterns of (i) PS/Co-Al LDH and (ii) PS/Ni-Al LDH nanocomposites.

Qiu et al. (2005) also obtained exfoliated structure for PS/Zn-Al LDH 10 (10 wt.% LDH loading) nanocomposites. Similar intercalated and exfoliated nanostructures have been reported for melt blending based PMMA/OMMT (Kumar et al., 2014) and PP/Ni-Al LDH (Kakati et al., 2012) samples, respectively. Also, it is apparent that the results obtained from XRD analysis cannot be considered on their own and additional analysis using TEM is required to assess upon the extent of dispersion (Morgan and Gilman, 2003).

5.3.2 TEM analysis

For the PS nanocomposites, the extent of dispersion and distribution of LDH fillers in the polymer matrix has been investigated using TEM microscopy. The TEM images of prepared PS/Co-Al LDH and PS/Ni-Al LDH nanocomposites are shown in Figure 5.3 (i) and 5.3 (ii), respectively. Figure 5.3 (i) depict the Co-Al LDH layers microstructure in the PS matrix. Figure 5.3 i (a) depicts TEM image for PSCL 1 sample and the pertinent dark lines and bright region signify LDH galleries and PS matrix, respectively. Black arrows have been presented in the figure to indicate LDH layers. Based on the image analysis, it can be inferred that LDH layers got totally exfoliated in the matrix and do not exhibit ordered stack structure. The TEM image of PSCL 3 sample depicted in Figure 5.3 i (b) involves arrows and circle mark to signify exfoliated and intercalated structure, respectively. Thus, the TEM image of the sample conveys that the sample refers to the partially exfoliated structure. Similar morphology with mixed exfoliation characteristics was reported by Alansi et al. (2015) for PS/LDH nanocomposites with 4% loading of inorganic filler (Mg-Al LDH). The TEM image of PSCL 5 and PSCL 7 nanocomposites depicted in Figure 5.3 i (c) and (d), respectively constitute circles indicating intercalated regions and stacked LDH layers. This conveys that the intercalated structure is attained at higher loading of the nanofiller.

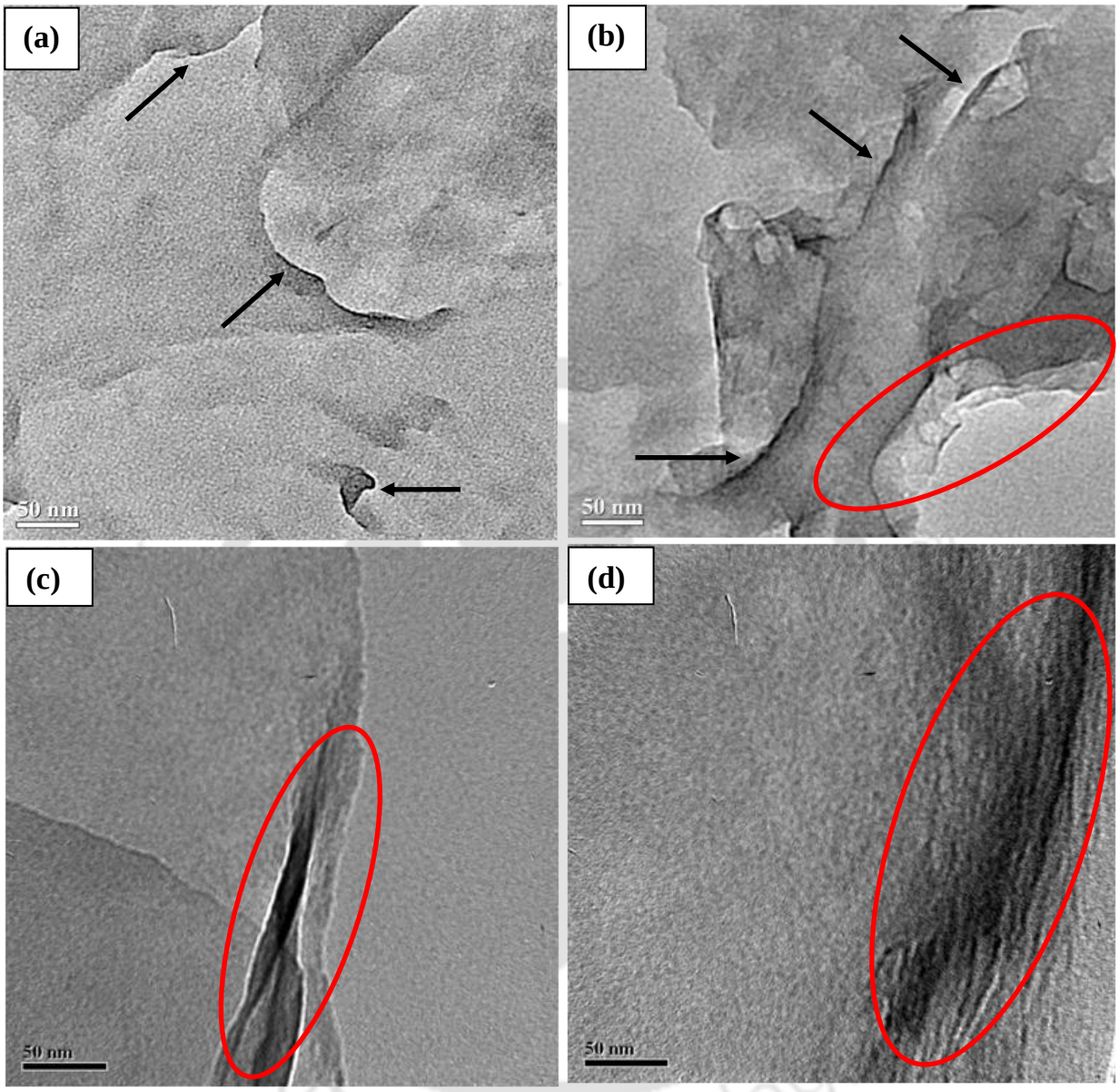

Figure 5.3 (i): TEM images of (a) PSCL 1, (b) PSCL 3, (c) PSCL 5 and (d) PSCL 7 nanocomposites.

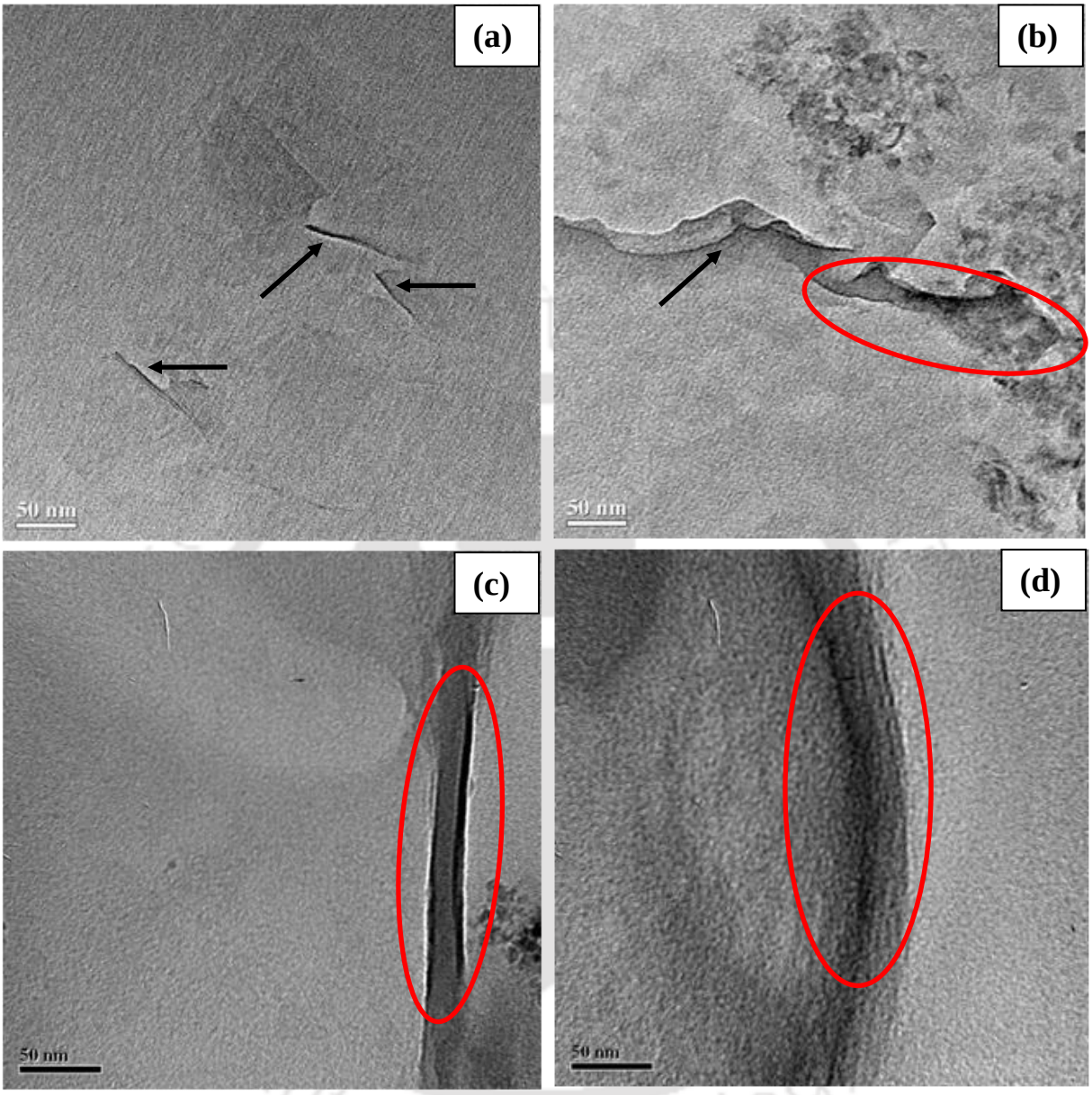

Figure 5.3 (ii): TEM images of (a) PSNL 1, (b) PSNL 3, (c) PSNL 5 and (d) PSNL 7 nanocomposites.

Similar intercalated structures have been reported by Qiu et al. (2005) for PS/Zn-Al LDH nanocomposites for higher values of inorganic filler loading. It can be observed from Figure 5.3 ii (a) that Ni-Al LDH layers are dispersed in exfoliated form in polymer matrix for PSNL 1 sample. While the mixed morphology i.e partially intercalated and exfoliated, is exhibited in PSNL 3 sample (see Figure 5.3 ii (b)), intercalated structure is attained for PSNL 5 and PSNL 7 nanocomposites (Figure 5.3 ii (c and d)).

5.3.3 FTIR analysis

FTIR analysis was performed to evaluate upon the extent of nanofiller incorporation in the PS polymer. Absorption bands characterizing modified Co-Al LDH, pristine PS and PS nanocomposites are presented in Figure 5.4 (i). For Co-Al LDH (Figure 5.4 i (a)), a broader peak at 3500 cm^{-1} affirms upon O-H stretching of hydrogen-bonded metal hydroxide and interlayer water molecules of Co-Al LDH. The peaks at 2848 cm^{-1}, 2920 cm^{-1} and 2957 cm^{-1} are ascribed to C-H stretching vibration. The prominent peak at wavenumber of 1630 cm^{-1} is designated as the bending mode of water molecule. The two peaks at 1063 cm^{-1} and 1218 cm^{-1} signify asymmetric and symmetric vibration of sulfate from dodecyl sulfate anion, respectively (Qiu et al., 2005). The FTIR of pristine PS (Figure 5.4 i (b)) indicates characteristic absorption bands due to aromatic C-H and aliphatic C-H stretching vibration at 3070 cm^{-1} and 2930 cm^{-1}, respectively. Peaks observed at 1504 cm^{-1} and 1496 cm^{-1} have been analyzed due to C=C bending vibration (Wang et al., 2004). Vibrational mode of CH_2 bending is located at 1453 cm^{-1} and 1368 cm^{-1}. The characteristic peak at 698 cm^{-1} is designated to mono-substituted benzene. Incidentally, the FTIR spectra of PS nanocomposites (Figure 5.4 i (c-f)) convey few new peaks in comparison with Figure 5.4 i (b). In these, the

absorption band at 3500 cm^{-1} is designated for the existence of O-H stretching modes of interlayer water molecules. The medium sharp peak at 1630 cm^{-1} indicates bending mode of water molecules. The characteristic peak at 1218 cm^{-1} indicates symmetric vibration of sulfate from dodecyl sulfate anion. The FTIR spectra confirm that Co-Al LDH have been included in the PS polymer and melt intercalation enables the formation of PS/Co-Al LDH nanocomposites.

Figure 5.4 (ii) depicts spectra obtained from FTIR analysis for Ni-Al LDH, pristine PS and PS nanocomposites. For Ni-Al LDH (Figure 5.4 ii (a)), lattice vibration bands have been observed at 400 – 800 cm^{-1} (Ni-O, Al-O, O-Al-O modes) (Wang et al., 2009). The Ni-Al LDH has a characteristic peak at 1063 cm^{-1} (asymmetric vibration ($\nu_{o\ S=O}$) of sulfate from dodecyl sulfate anion), 1218 cm^{-1} (symmetric vibration ($\nu_{S=O}$) of sulfate from dodecyl sulfate anion) (Costa et al., 2008), 2850 cm^{-1} (stretching vibration of CH_3 found in the modifier SDS), 2920 cm^{-1} (stretching vibration of CH_2 found in the modifier SDS), 3528 cm^{-1} (O-H stretching vibration of metal hydroxide layer and interlayer water molecules) (Alansi et al., 2015). Figure 5.4 ii (b) affirmed existence of several absorption bands in pristine PS. These refer to the wavelengths of 698 cm^{-1} (mono-substituted benzene), 1368, 1453 cm^{-1} (vibrational mode of CH_2 bending), 1496, 1504 cm^{-1} (C=C bending vibration), 2930 cm^{-1} (aliphatic C-H stretching vibration), 3070 cm^{-1} (aromatic C-H stretching vibration). Compared with Ni-Al LDH (Fig. 5.4 ii (a)) and pristine PS (Figure 5.4 ii (b)), the PS nanocomposite (PSNL 1, PSNL 3, PSNL 5 and PSNL 7) samples (Figure 5.4 ii (c-f)) exhibit fewer new absorption peaks at 1218 cm^{-1} (symmetric vibration of sulfate from dodecyl sulfate anion), 3528 cm^{-1} (O-H stretching vibrations) and 400 – 800 cm^{-1} (lattice vibration bands (Ni-O, Al-O, O-Al-O modes)).

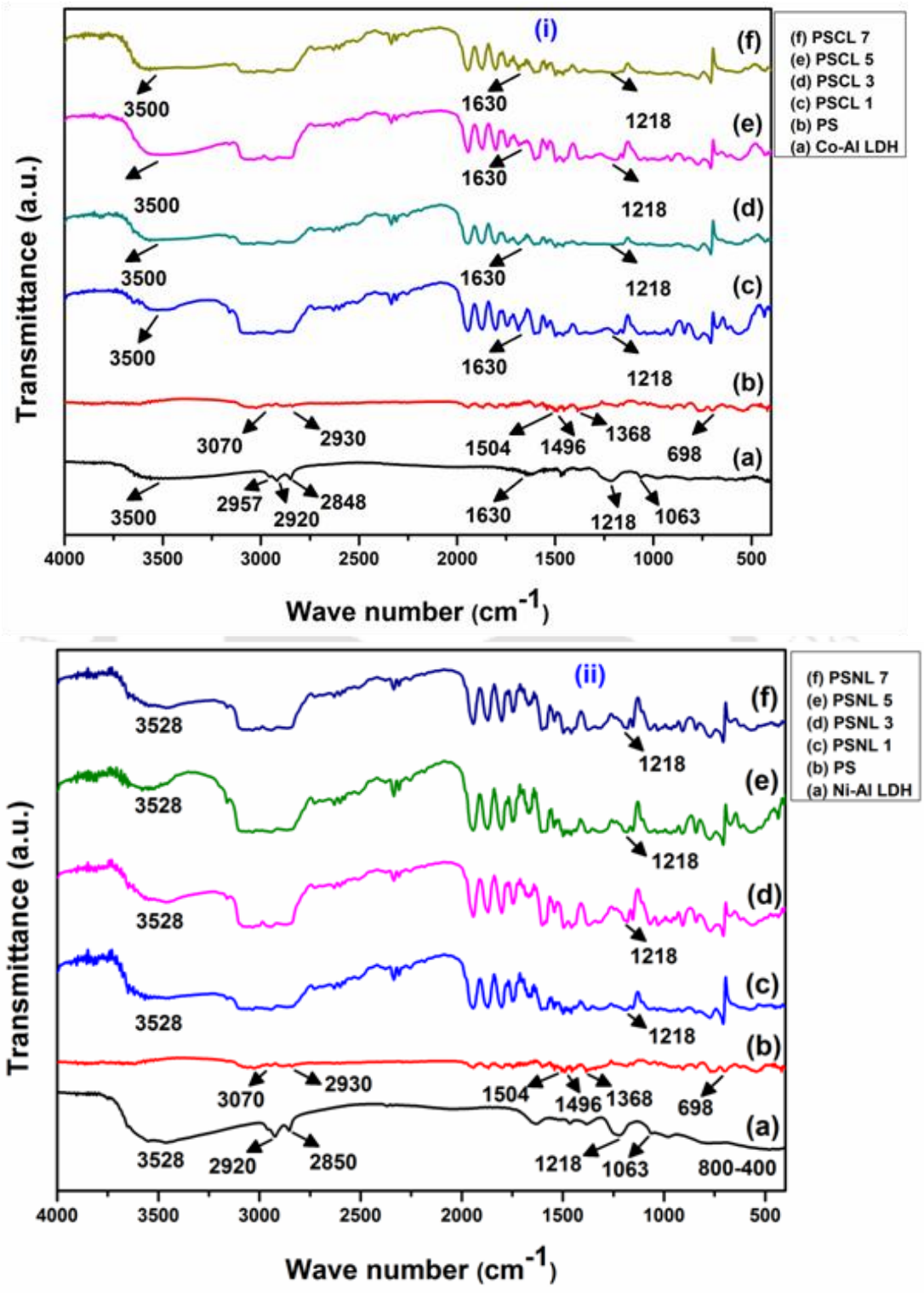

Figure 5.4: FTIR spectra of (i) PS/Co-Al LDH and (ii) PS/Ni-Al LDH nanocomposites.

The FTIR analysis of various samples and their comparative assessment indicates that LDH layers are well dispersed in the PS polymer matrix. Similar trends have been reported by Wang et al. (2004) for MMT dispersed in PS polymer matrix.

5.3.4 Tensile properties

A primary goal of LDH nanofiller reinforcement into the PS matrix is to enhance mechanical properties of the nanocomposites in conjunction with the pristine PS. As LDH loading increases, tensile strength and modulus of nanocomposites increases (see Figure 5.5). This is due to the incorporation of LDH into the composite system, which enhances stiffness and rigidity of polymer nanocomposites. A sharp enhancement in tensile modulus for very small LDH loading (1 wt.%) can be observed in the figure. However, the subsequent enhancement in tensile modulus was not significant upto 7 wt.% LDH loading (see Figure 5.5). In this regard, it can be observed that Genity et al. (1992) conveyed that filler modulus, filler loading and filler aspect ratio are three main factors to enhance the composite modulus.

The tensile strength and modulus of pristine PS and PS/Co-Al LDH nanocomposites have been presented in Figure 5.5 (i). The tensile strength for pristine PS and PS nanocomposites containing 1, 3, 5 and 7 wt.% Co-Al LDH is found to be 29.01, 38.5, 35.62, 31.91 and 30.02 MPa, respectively. Similarly, Figure 5.5 (ii) depicts the tensile strength and modulus profiles of PS and PS/Ni-Al LDH nanocomposites. Compared to pristine PS and all other nanocomposites, PSNL 1 sample exhibited highest tensile strength of 39.01 MPa (36.29 MPa for PSNL 3, 32.30 MPa for PSNL 5, 30.22 MPa for PSNL 7 and 29.01 MPa for pristine PS samples). Stronger interfacial interactions (between LDH and PS) facilitated due to maximum exfoliation in the structure are responsible for maximum tensile strength values at

lower LDH loading (1 wt.%). Similar trends have been reported by Li et al. (2009) for ZnO nanoparticles embedded polyurethane polymer composites. The marginal reduction in tensile strength for higher loading of inorganic nanofiller (3 – 7 wt.%) is possibly due to non-uniform distribution of LDH layers in the polymer along with agglomeration and segregation to thereby allow formation of weak spots in the nanocomposites. Similar behaviour has been reported by Uthirakumar et al. (2005b) for clay loaded PS polymer nanocomposites. Further, Tanniru et al. (2006) elaborated that clay filler aggregation in polyethylene nanocomposites facilitates concentration of stress field at the aggregates thereby triggering easy crack propagation and rapid premature failure.

The tensile modulus profiles of pristine PS and its nanocomposites have been demonstrated in Figure 5.5. The tensile modulus value obtained for PSCL 1 nanocomposite (1 wt.% Co-Al LDH loading) is 20% more than that obtained for PS polymer. In comparison with pristine PS, the tensile modulus for PS/Ni-Al LDH nanocomposites exhibit significant enhancement with the highest tensile enhancement for PSNL 1 sample (23% higher value). This conveys that the incorporation of LDH nanofiller in PS polymer significantly improved its tensile modulus.

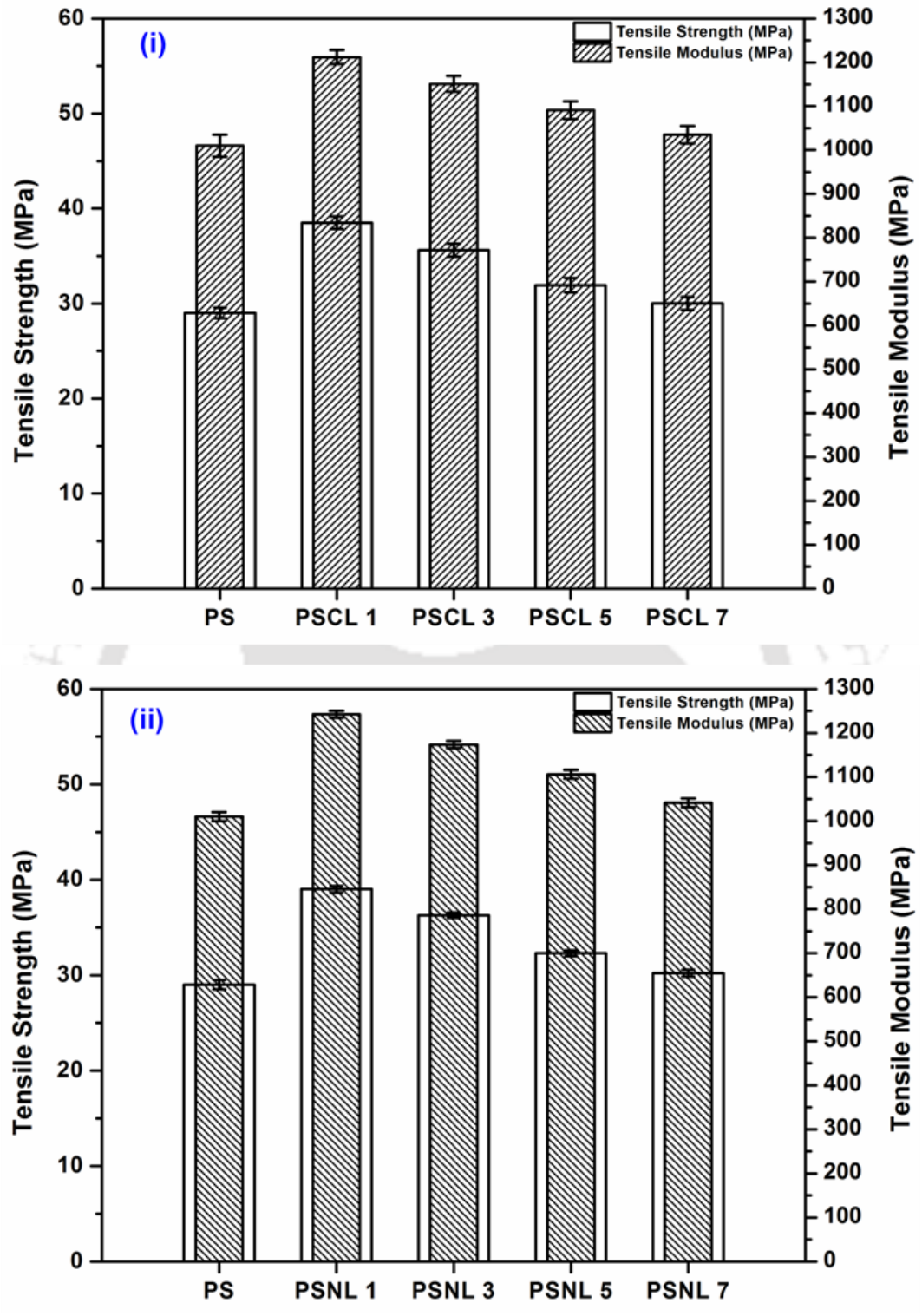

Figure 5.5: Tensile properties of (i) PS/Co-Al LDH and (ii) PS/Ni-Al LDH nanocomposites.

For further increase of LDH loading from 3 to 7 wt.%, the improvement in tensile modulus value is found to be lower as compared to the value obtained for PS nanocomposite with 1 wt.% LDH. This is due to the defects induced by LDH agglomeration and subsequent enhancement in the brittleness of the PS.

5.3.5 Flexural properties

The Co-Al LDH content effect on the flexural strength and flexural modulus of PS nanocomposites is illustrated in Figure 5.6 (i). The pristine PS exhibits a flexural strength of 54.08 MPa. The PSCL 1 (1 wt.% Co-Al LDH loading) nanocomposite possesses a maximum flexural strength of 65.57 MPa. Composites with higher content of Co-Al LDH loading (3, 5 and 7 wt.%) indicate reduction in the flexural strength. The flexural strength of PSCL 3, PSCL 5 and PSCL 7 nanocomposites is 63.81, 58.40 and 55.16 MPa, respectively. Figure 5.6 (ii) depicts trends in flexural strength and modulus of pristine PS and PS nanocomposites (1 – 7 wt.% Ni-Al LDH). The trends confirm that PS/Ni-Al LDH nanocomposites exhibit improved tensile strength in comparison with pristine PS. While pristine PS possessed 54.08 MPa flexural strength, PSNL 1 possessed highest flexural strength of 68.95 MPa followed by PSNL 3 (64.46 MPa), PSNL 5 (59 MPa) and PSNL 7 (55.59 MPa) samples. This is due to homogeneous and uniform distribution of LDH in the polymer matrix that resulted in maximum exfoliation in the nanocomposite structure at 1 wt.% loading of the inorganic nanofiller. At higher loading, LDH agglomeration might have reduced the flexural strength.

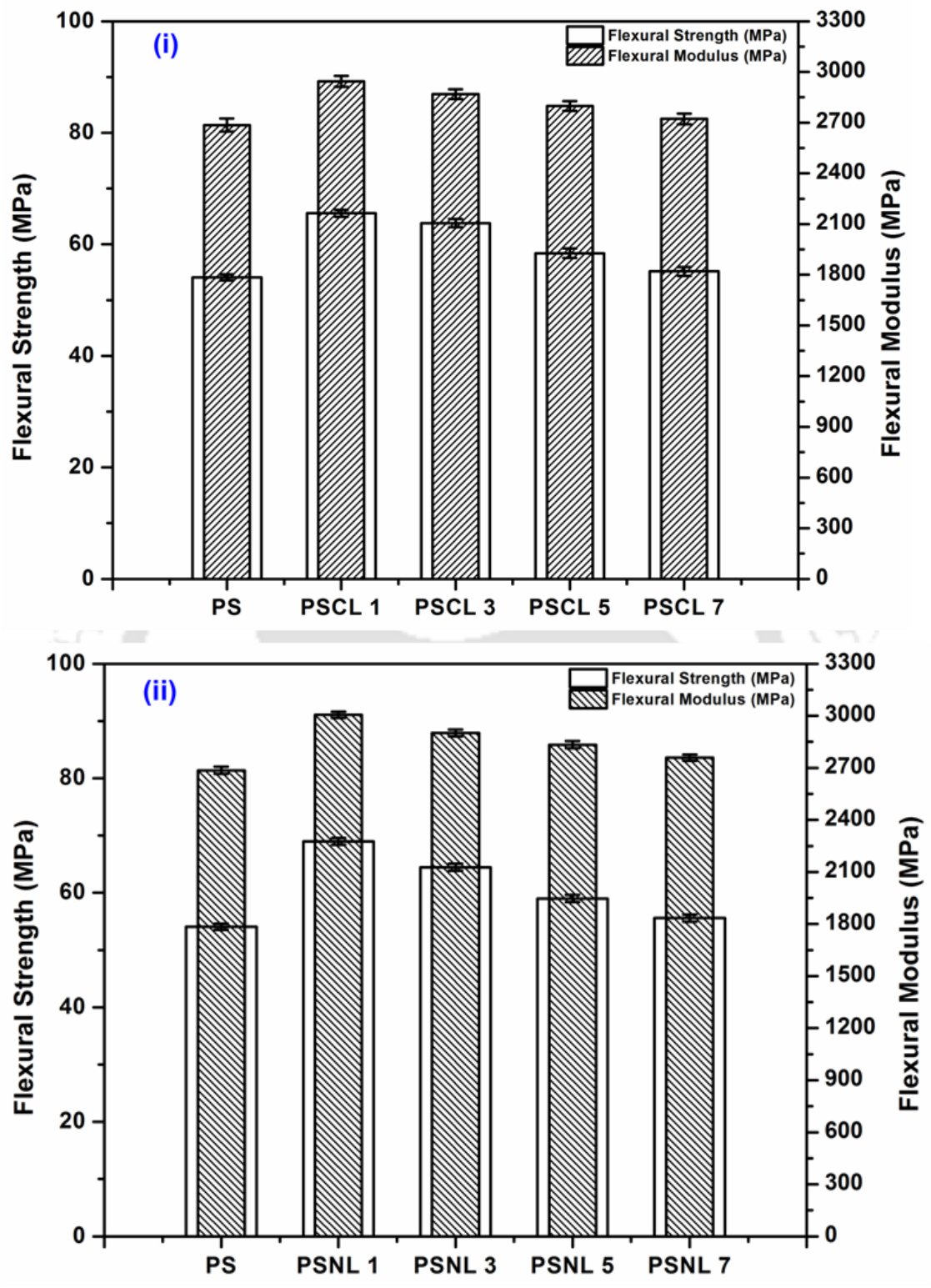

Figure 5.6: Flexural properties of (i) PS/Co-Al LDH and (ii) PS/Ni-Al LDH nanocomposites.

Also, several factors such as extent of intercalation, orientation and distribution of LDH platelets in stress/load direction have been reasoned to influence the flexural properties of polymer nanocomposite materials. Chow et al. (2008) also inferred upon the enhancement in flexural strength for nanocomposites compared with pristine polymer.

Figure 5.6 depicts trends in flexural modulus of PS and PS nanocomposite. Similar trends have been obtained for flexural modulus, given the fact that flexural strength of both pristine PS and PS nanocomposites underwent similar variations with variant concentration of nanofiller loading. Compared to pristine PS, the flexural modulus of PSCL 1 and PSNL 1 samples are 10% and 12% higher, respectively. For higher content of LDH loading (3 – 7 wt.%), the flexural modulus enhancement is not significant. Reasons for such trends are similar to those presented for the flexural strength.

5.3.6 Impact strength

The effect of Co-Al LDH content on the impact strength of the nanocomposites is shown in Figure 5.7 (i). The incorporation of Co-Al LDH progressively enhances the impact strength of the PS composites. It can be easily seen from the plot that the PSCL 1 nanocomposite has the highest impact strength (7.95 kJ/m^2) in comparison with pristine PS (6.68 kJ/m^2). Figure 5.7 (ii) shows impact strength profiles for PS and PS/Ni-Al LDH nanocomposites. Compared to pristine PS, the impact strength for all PS nanocomposites enhanced significantly. The impact strength for PS/Ni-Al LDH sample with 1 wt.% LDH loading is 22% higher in comparison with pristine PS. Yuan et al. (2009) reported 50% enhancement in impact strength for 0.32 wt.% nanofiller loaded PS-m-MWCNT nanocomposites.

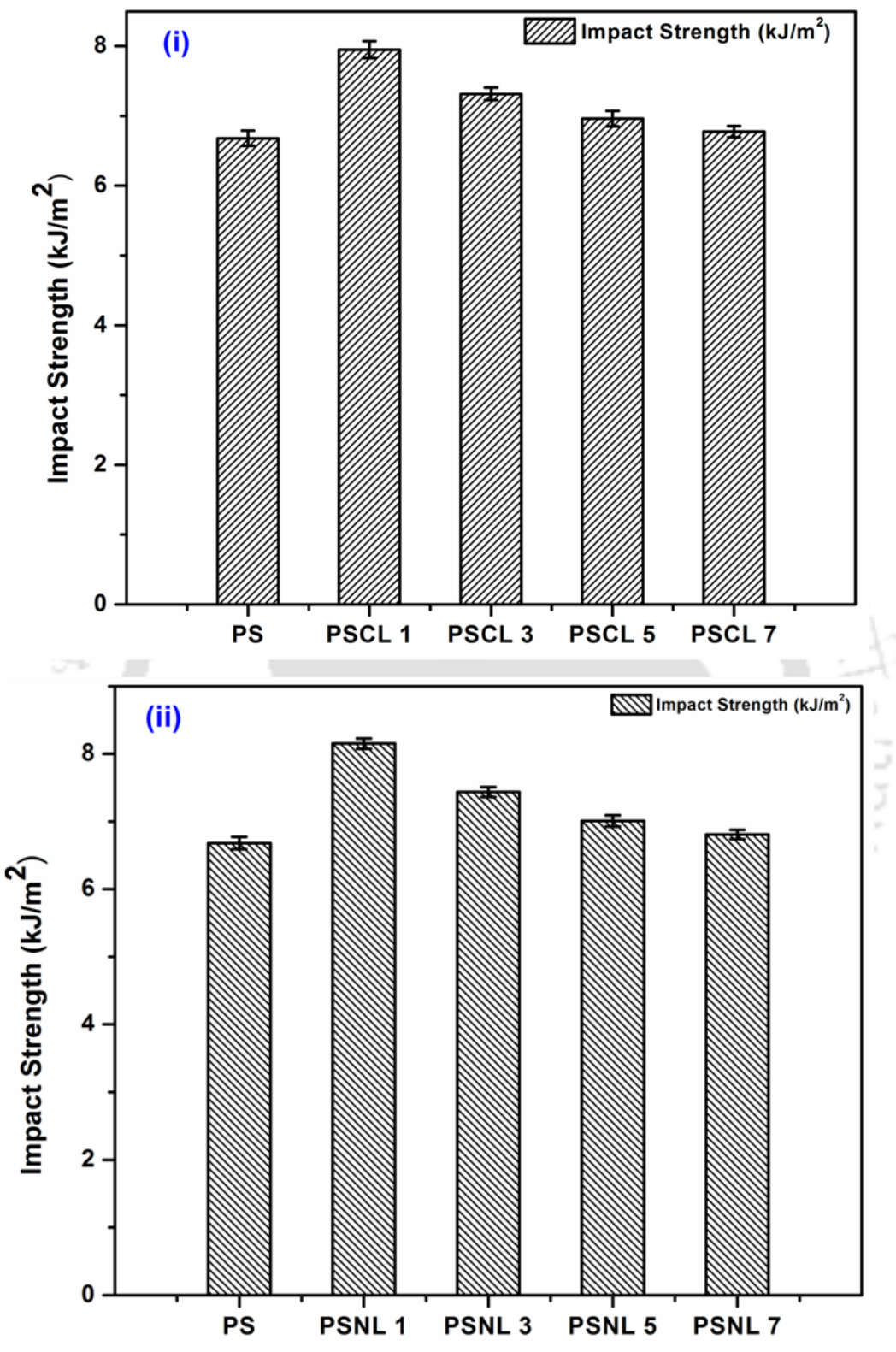

Figure 5.7: Impact strength of (i) PS/Co-Al LDH and (ii) PS/Ni-Al LDH nanocomposites.

Similarly, Yilmazer and Ozden (2006) opined that 1.6 wt.% organoclay loaded PS nanocomposites possessed 4% higher impact strength than that of pure PS. This is attributed to the fact that LDH is homogenously distributed at lower loading in the PS. For higher loading of LDH cases (3, 5 and 7 wt.%), the impact strength did not enhance significantly compared to PS samples and was lower than that of the PS sample with 1 wt.% LDH loading. The addition of LDH to polymer matrix contributed to an enhancement in the immobilization of macromolecular chains. This increases brittleness of PS and thereby decreases impact strength. Further, it is to be noted that nanoparticle migration in polymer nanocomposites is restricted and hence energy dissipation is as well reduced. Therefore, during impact test, it is hypothesized that nanocomposites have a tendency to absorb less energy and undergo deformation and break easily (Mohanty and Nayak, 2010). This is attributed to the fact that exfoliated layers of Ni-Al LDH are homogenously distributed at lower loading in the PS polymer. It is also noticed that Ni-Al layers are more effectively dispersed in PSNL 1 nanocomposite and therefore it exhibits higher impact strength as compared to pristine PS and other nanocomposites samples.

5.3.7 DSC analysis

The DSC analysis was conducted to evaluate the effect of nanofiller on the molecular mobility of PS chains in the polymer nanocomposite. This is typically reflected in the T_g of the sample. For various samples including pristine PS and PS nanocomposites, results obtained from DSC analysis have been presented in Figure 5.8 and the T_g has been evaluated as the value corresponding to inflection point of onset and end-set temperature profiles.

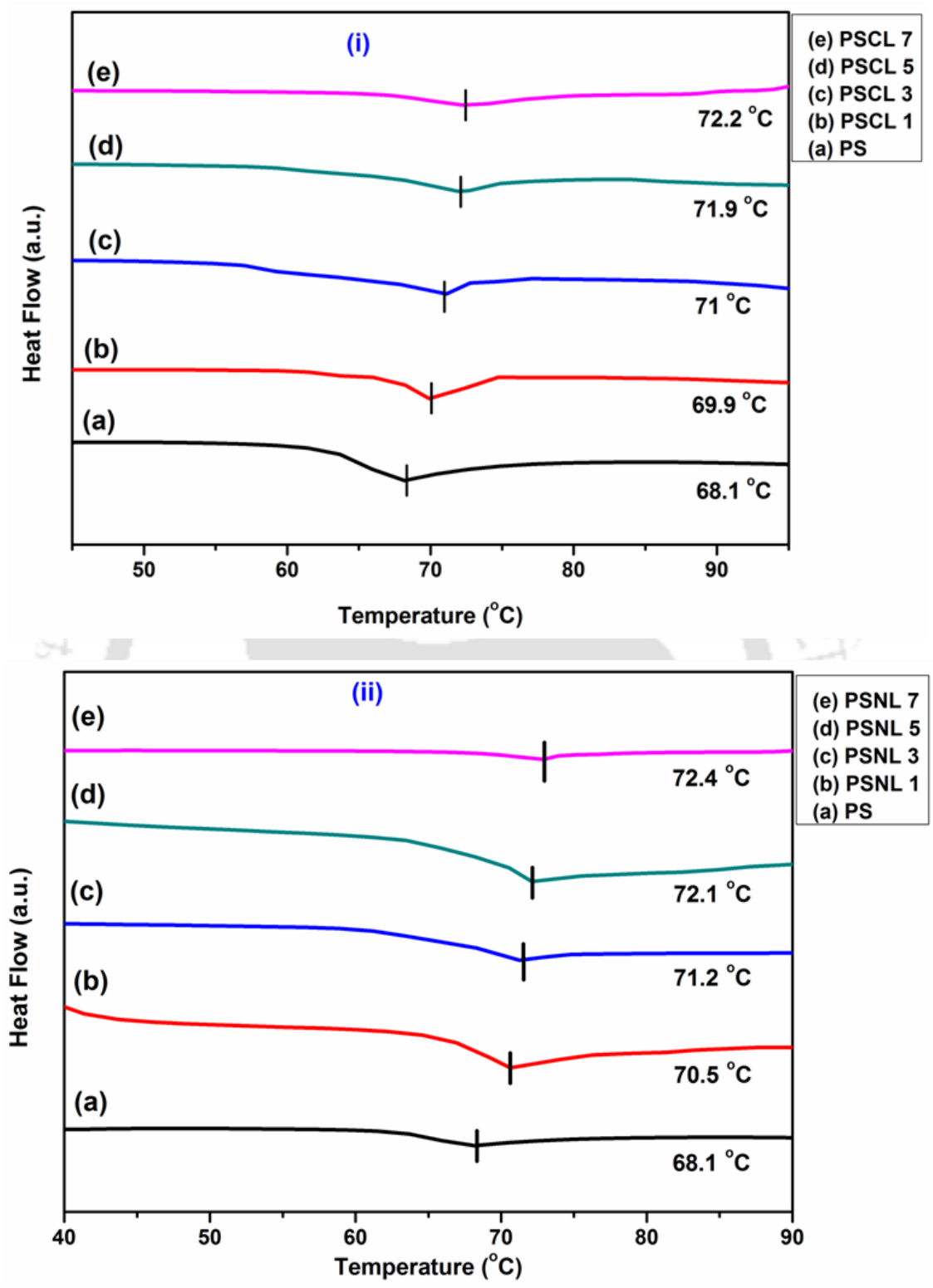

Figure 5.8: DSC curves of (i) PS/Co-Al LDH and (ii) PS/Ni-Al LDH nanocomposites.

For pristine PS, PSCL 1, PSCL 3, PSCL 5 and PSCL 7, the T_g values are 68.1, 69.9, 71, 71.9 and 72.2 °C, respectively (see Figure 5.8 (i)). This indicates that Co-Al LDH addition into the PS matrix enhanced T_g gradually with increasing inorganic filler content. From the DSC analysis, it can be noticed that T_g of PSCL 7 is 4.1 °C more than the T_g of pristine PS (see Figure 5.8 (i)). Similarly, for pristine PS, PSNL 1, PSNL 3, PSNL 5 and PSNL 7, the T_g values are 68.1, 70.5, 71.2, 72.1 and 72.4 °C, respectively. For the PSNL 7 sample, the T_g value is 4.3 °C higher that of the pristine PS sample (see Figure 5.8 (ii)).

This is probably due to the restriction or hindrance of polymer chain motion in the nanocomposite that has been brought forward due to inclusion of the inorganic nanofiller. Similar insights have been presented by Zidelkheir et al. (2006) who inferred that the 10 wt.% PS/clay nanocomposites possessed 4 °C higher T_g values than the pristine PS polymer. Kumar et al. (2014) prepared PMMA/clay nanocomposites using solvent blending method. They reported that the T_g of nanocomposites is 0.9 – 2.6 °C more than that of pristine PMMA. In the work of Kuila et al. (2011), around 2 °C enhancement in T_g was observed for PMMA/graphene nanocomposites with 0.1 wt.% graphene loading.

5.3.8 Thermogravimetric analysis

TGA analysis was conducted to evaluate the comparative thermal degradation/stability of PS/LDHs nanocomposites in comparison with pristine PS. Figure 5.9 (i) depicts TGA profiles of pristine PS, and PS/Co-Al LDH nanocomposite samples. While the shape of the TGA curves of nanocomposite and parent polymer are similar, the thermal stability of the nanocomposite is evaluated to be higher. This is due to the fact that LDH only undergoes degradation at higher temperature. The data obtained from these curves is enlisted in Table

5.1. Choosing 15% mass loss as a reference, the thermal degradation temperatures for pristine PS and its nanocomposites samples having 1, 3, 5 and 7 wt.% of Co-Al LDH have been evaluated as 358, 367.4, 375.3, 380.8 and 384.1 °C respectively. Hence, all nanocomposites exhibited higher thermal degradation temperatures than those obtained for pristine PS. Thermal degradation temperature of PS nanocomposites with 1, 3, 5 and 7 wt.% Co-Al LDH loading is 9.4, 17.3, 22.8 and 26.1 °C higher in comparison with pristine PS, respectively. Also, the PSCL 7 nanocomposite (7 wt.% Co-Al LDH loading) possesses highest thermal stability. Similarly, Figure. 5.10 (i) illustrates TGA curves of pristine PS and PS/Ni-Al LDH nanocomposites. Quantitative information with respect to mass loss at various temperature values has been presented in Table 5.1 for pristine PS and all polymer nanocomposite samples. It could be inferred from Table 5.1 that the degradation temperature corresponding to 15% mass loss ($T_{15\%}$) of PS nanocomposites samples depicts significant enhancement with respect to pristine PS, thereby indicating increased thermal stability. Moreover, the enhancement can be observed to be proportional to Ni-Al LDH content in the PS polymer. The $T_{15\%}$ for pristine PS is 358 °C, which got further enhanced by 11, 20.1, 25.3 and 27.4 °C for PSNL 1, 3, 5 and 7 samples, respectively. The observed enhancement in higher degradation temperature is due to the incorporation of the inorganic nanofiller in PS polymer matrix (Bhanvase et al., 2012). Among all nanocomposites, PSNL 7 exhibited highest thermal stability (Table 5.1). Such behaviour is reasoned due to the presence of barrier effect of LDH lamellar layers which limit emission of produced degradation gases and heat transmission. This eventually contributes to improved thermal stability of nanocomposite materials.

Figure 5.9 (ii) and 5.10 (ii) illustrates DTG curves of PS and PS/LDHs nanocomposites. The peaks in Figure 5.9 (ii) and 5.10 (ii) convey T_{max} of the prepared samples.

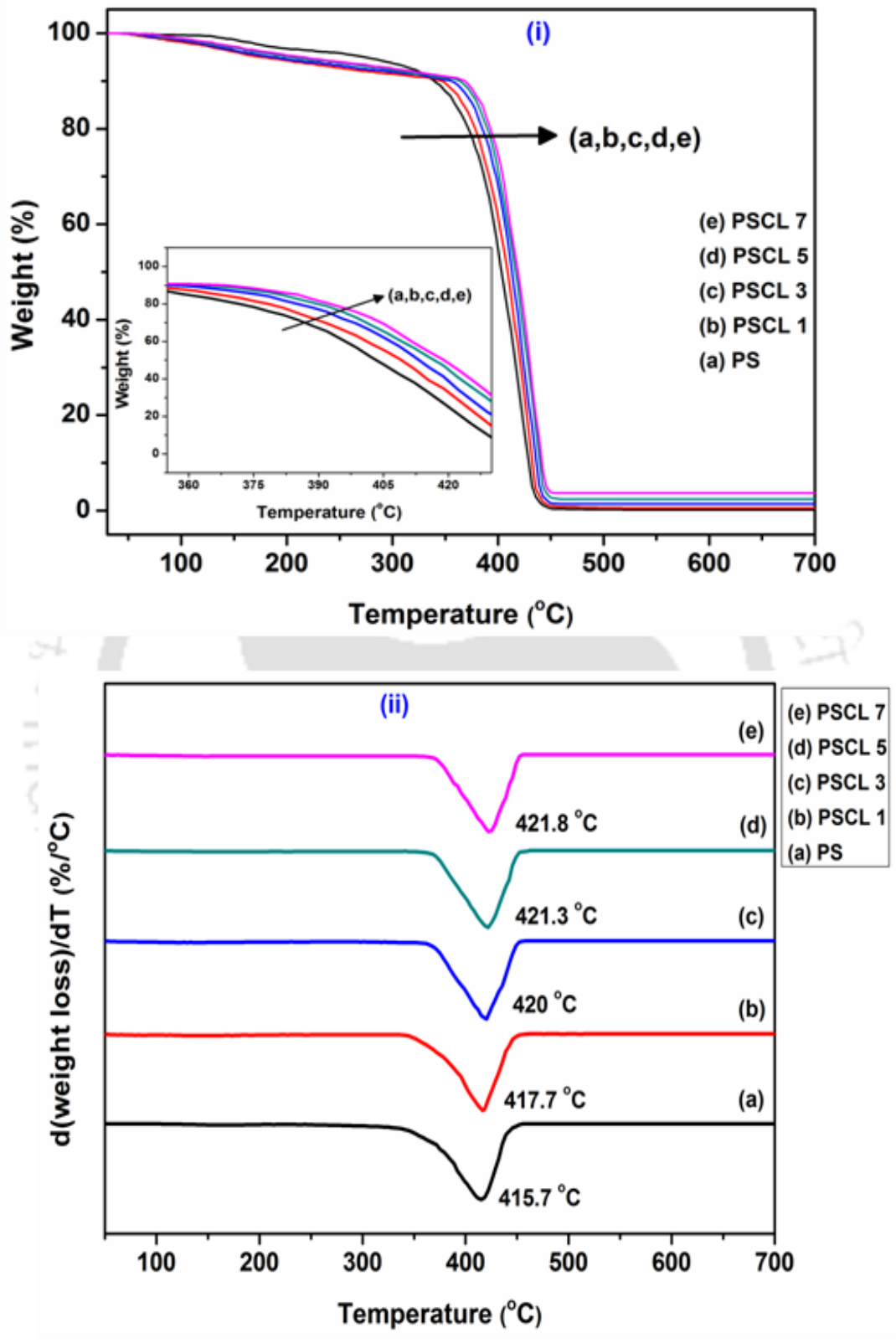

Figure 5.9: (i) TGA and (ii) DTG curves of PS and PS/Co-Al LDH nanocomposites.

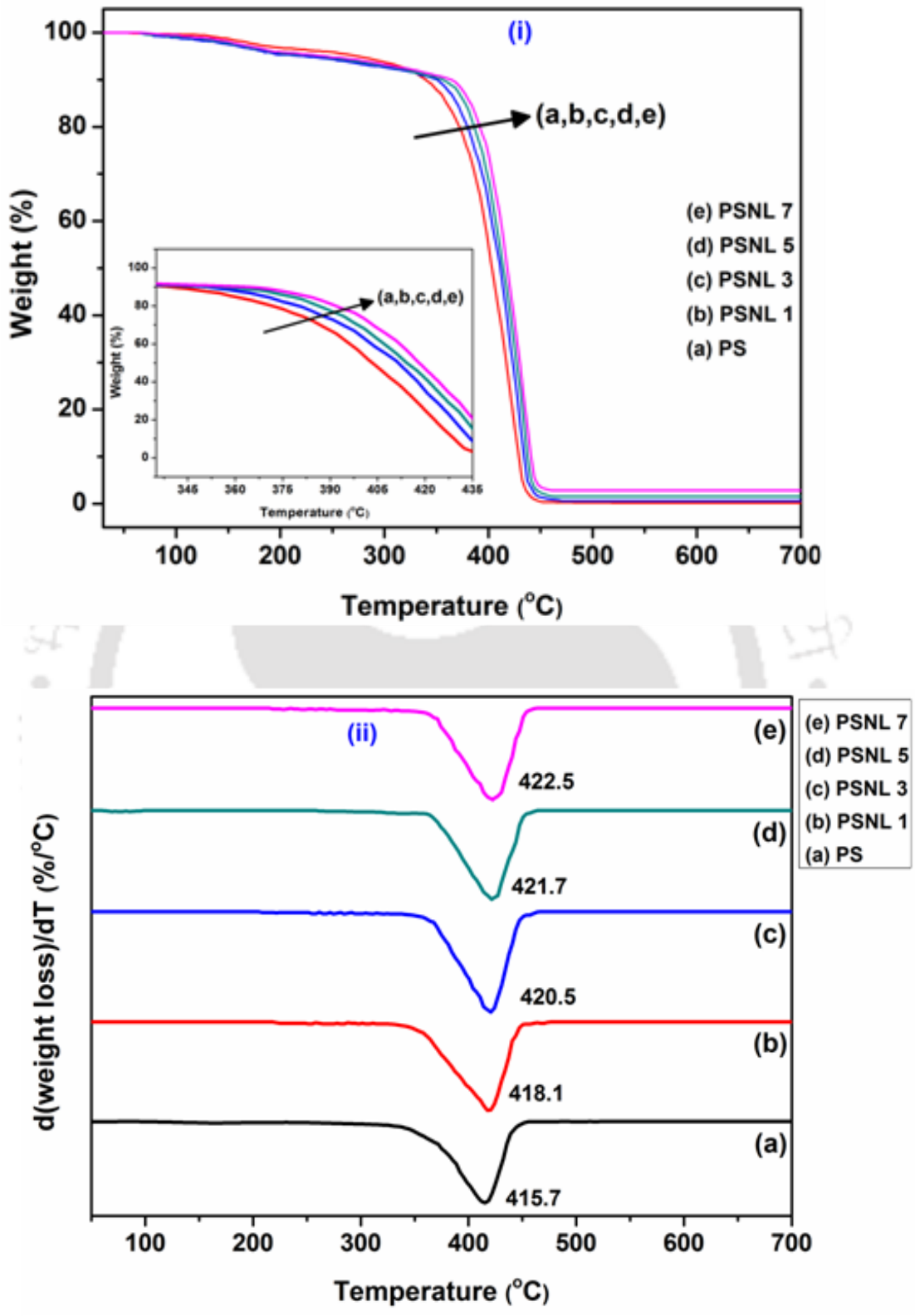

Figure 5.10: (i) TGA and (ii) DTG curves of PS and PS/Ni-Al LDH nanocomposites.

It could be inferred from Figure 5.9 (ii) and 5.10 (ii) that T_{max} peaks of the DTG curves of PS nanocomposites exhibit shift towards higher temperature as compared to pristine PS, thus indicating enhancement in thermal stability. The T_{max} for pristine PS, PSCL 1, PSCL 3, PSCL 5 and PSCL 7 nanocomposites have been obtained to be 415.7, 417.7, 420, 421.3, and 421.8 °C, respectively. Similarly, the PS/Ni-Al LDH nanocomposites possess an enhancement in T_{max} by about 2.4 – 6.8 °C over pristine PS. The improved thermal stability is attributed to the 'tortuous path' effect of LDH layers, which deferments the diffusion pathway of the degradation by-products and hinders the diffusion of the volatile decomposition products. Thus, both TGA and DTG analysis based trends essentially confirm upon enhanced thermal stability of the polymer due to the incorporation of LDH layers in the polymer matrix.

Table 5.1: Thermal degradation temperatures of pristine PS, PS/Co-Al LDH and PS/Ni-Al LDH nanocomposites.

Sample	Temperature at 15% weight loss (T_{15}) °C	$\Delta T_{15\%}$ (°C)	T_{max} (°C)
PS	358.0	-	415.7
PSCL1	367.4	9.4	417.7
PSCL 3	375.3	17.3	420
PSCL 5	380.8	22.8	421.3
PSCL 7	384.1	26.1	421.8
PSNL1	369.0	11.0	418.1
PSNL 3	378.1	20.1	420.5
PSNL 5	383.3	25.3	421.7
PSNL 7	385.4	27.4	422.5

5.3.9 Kinetics analysis

5.3.9.1 Coats-Redfern method

The kinetic analysis of thermal degradation process for pristine PS and PS/LDH nanocomposites has been conducted to understand degradation behaviour of composites in comparison with pristine PS. Coats-Redfern method (Coats and Redfern, 1964) was deployed for the kinetic analysis. Compared to other kinetic models, the method requires only single but not multiple heating data. Using the Coats-Redfern method, for each thermogravimetric curve corresponding to a precise heating rate, kinetic parameters (E_a, n and A) can be obtained. To do so, the left side expressions in equation (4.10 a and 4.10 b) have been plotted with respect to $\frac{1}{T}$ for visualization as a straight line plot with slope and intercept as activation energy and pre-exponential factor, respectively. In this regard, it is important to note that the intercept is determined by considering the expression containing the term $\left(1-\frac{2RT}{E_a}\right)$ as 1. To determine the value of n, different values of n have been assumed and regression coefficient of plots corresponding to various n values have been compared and the n value for which best regression coefficient value was obtained has been inferred as the n value for the measured data. Figure 5.11 depicts linear fitness plots of Coats-Redfern model for pristine PS, PSCL 1, PSCL 3, PSCL 5 and PSCL 7 nanocomposites and different n values. The obtained kinetic parameter values including A, E_a and n for the prepared samples are enlisted in Table 5.2. The evaluated E_a values for pristine PS, PSCL 1, PSCL 3, PSCL 5 and PSCL 7 are 88.1, 106.2, 122.3, 130.3, and 133.4 kJ/mol.

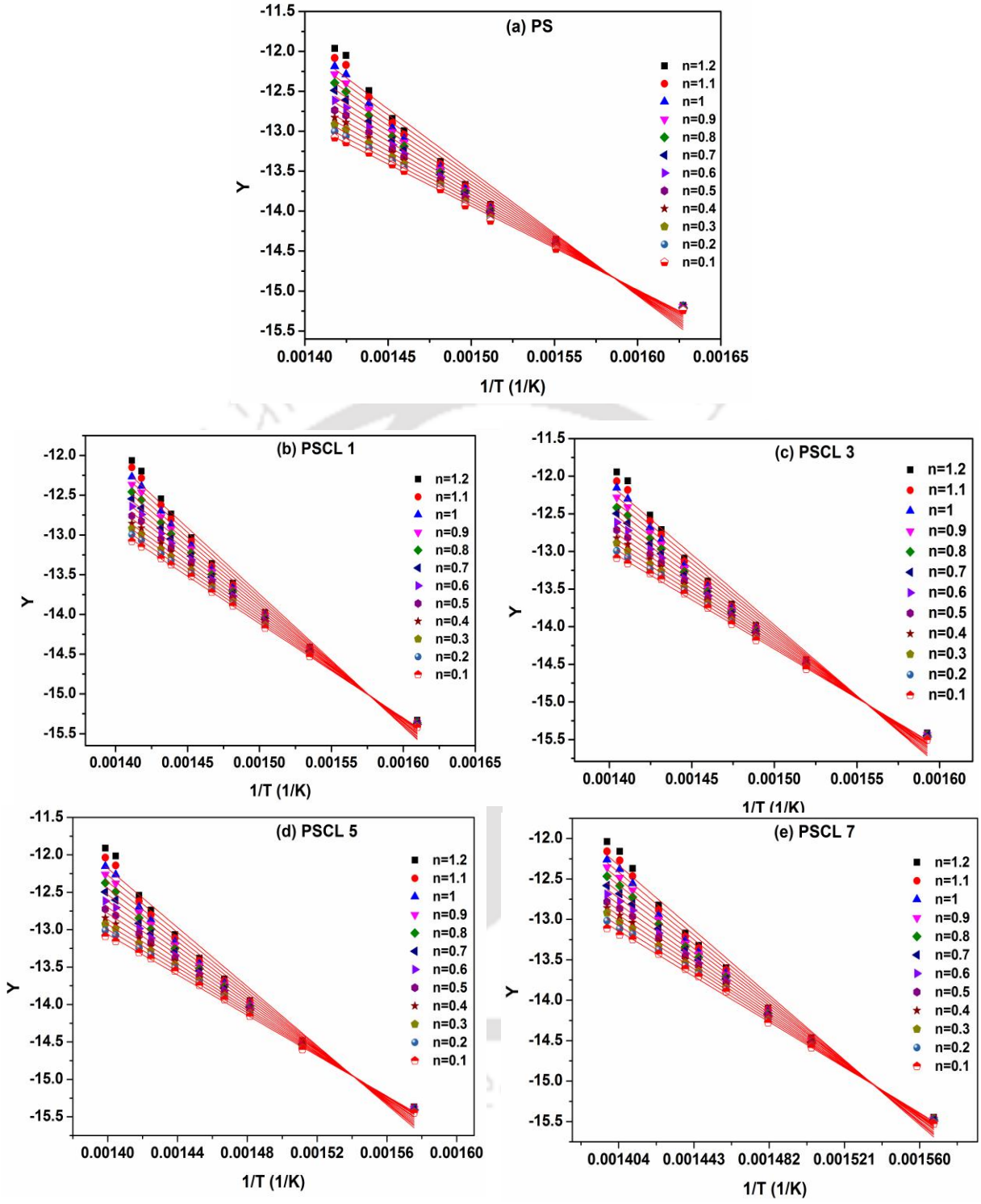

Figure 5.11: Coats-Redfern model fitness plots for (a) pristine PS, (b) PSCL 1, (c) PSCL 3, (d) PSCL 5 and (e) PSCL 7 nanocomposites.

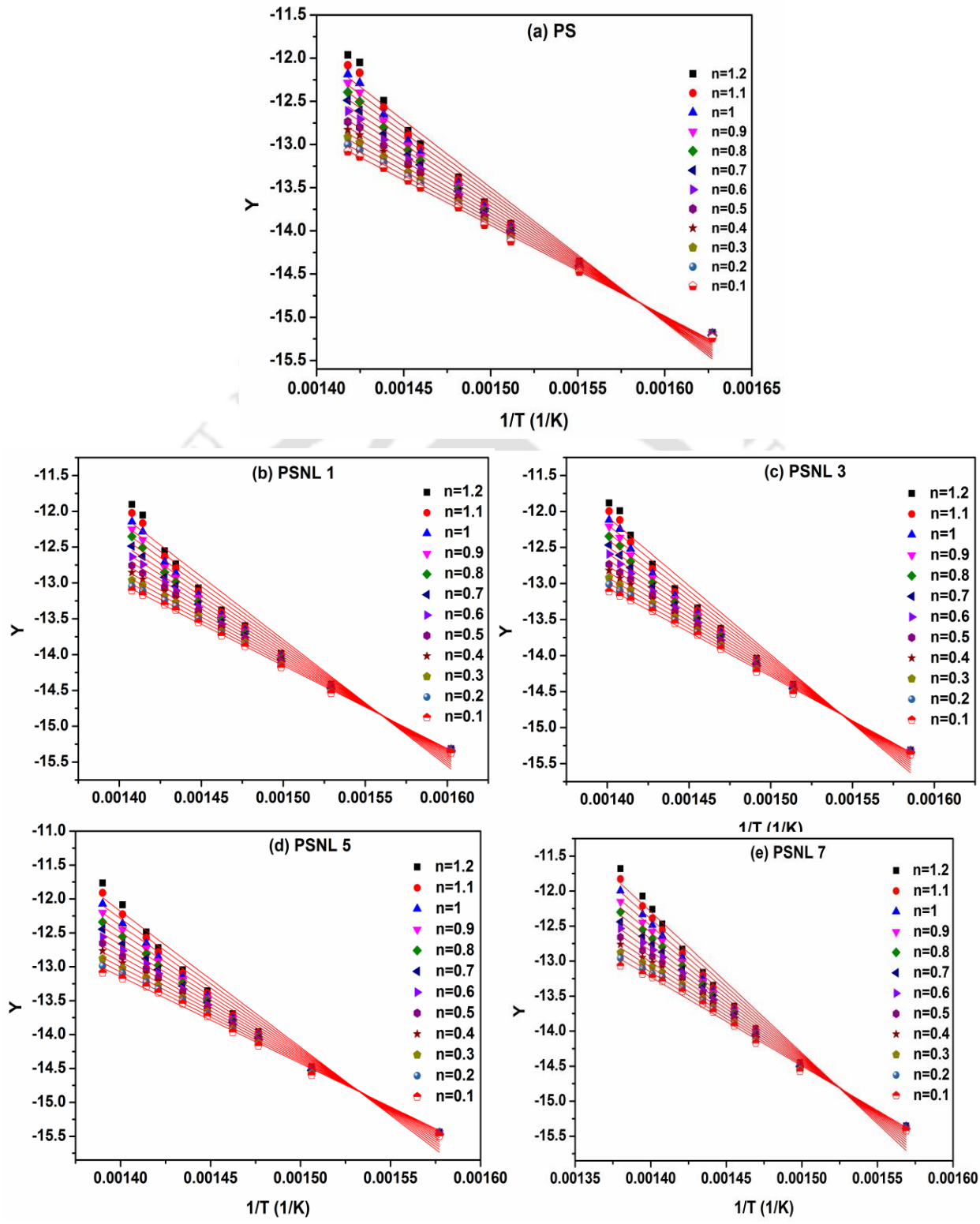

Figure 5.12: Coats-Redfern model fitness plots for (a) pristine PS (b) PSNL 1, (c) PSNL 3, (d) PSNL 5 and (e) PSNL 7 nanocomposites.

Table 5.2: Thermal degradation kinetic parameters obtained from Coats-Redfern method for pristine PS, PS/Co-Al LDH and PS/Ni-Al LDH nanocomposites.

Sample	E_a(kJ/mol)	A	n	R^2
PS	88.1	7.95×10^5	0.2	0.996
PSCL 1	106.2	2.51×10^7	0.4	0.996
PSCL 3	122.3	3.46×10^8	0.4	0.997
PSCL 5	130.3	9.41×10^8	0.4	0.996
PSCL 7	133.4	2.18×10^9	0.4	0.996
PSNL 1	108.5	4.70×10^7	0.4	0.997
PSNL 3	125.4	5.99×10^8	0.4	0.997
PSNL 5	132.2	2.01×10^9	0.4	0.998
PSNL 7	134.8	3.15×10^9	0.4	0.998

Similarly, Figure 5.12 illustrates the linear fitness plots of the model for pristine PS and PS/Ni-Al LDH nanocomposites. The evaluated E_a values for PS, PSNL 1, PSNL 3, PSNL 5 and PSNL 7 samples are 88.1, 108.5, 125.4, 132.2, and 134.8 kJ/mol. Thus, the activation energy for nanocomposite degradation enhanced by 20.4 – 46.7 kJ/mol in comparison with the value obtained for pristine PS. This is due to the enhanced thermal stability of the nanocomposite samples. The obtained data are in good agreement with TGA results.

5.3.9.2 Criado method for the reaction mechanism analysis

Criado method (Criado et al., 1989) involves reaction mechanism determination using E_a, A and n evaluated from Coats-Redfern method. Relevant expressions for the solid-phase reactions have been presented in section 4.2.5.2 of the Ph.D. thesis. In the mentioned section, while equation (4.15 a) is used to obtain master $Z(\alpha)$ versus α curves (Urbanovici et al.

(1999)), equation (4.15 b) is used to represent experimental Z(α) versus α curve. Thereby, comparative assessment of master Z(α) versus α curve with experimental Z(α) versus α curve enabled prediction of pertinent reaction mechanism of thermal degradation process. This analysis was conducted for pristine PS and all nanocomposite samples.

Figure 5.13 and 5.14 illustrate master and experimental Z(α) versus α curves for pristine PS, PS nanocomposites having Co-Al LDH and Ni-Al LDH, respectively. For pristine PS (Figure 5.13 and 5.14 (a)), the experimental curve is in good agreement with the master curve of Z(F1), thus indicating that the pristine PS thermal degradation process follows F1 reaction mechanism (random nucleation of one nucleus on individual particle). For the nanocomposite samples, (Figure 5.13 and 5.14 (b-e)), the initial phase involved thermal decomposition as per F1 reaction mechanism ($\alpha < 0.4$) followed with gradual transition to A4 mechanism (nucleation and growth for $\alpha = (0.7 – 0.9)$. Thus, it is apparent that the thermal degradation mechanism involved a shift at higher temperature.

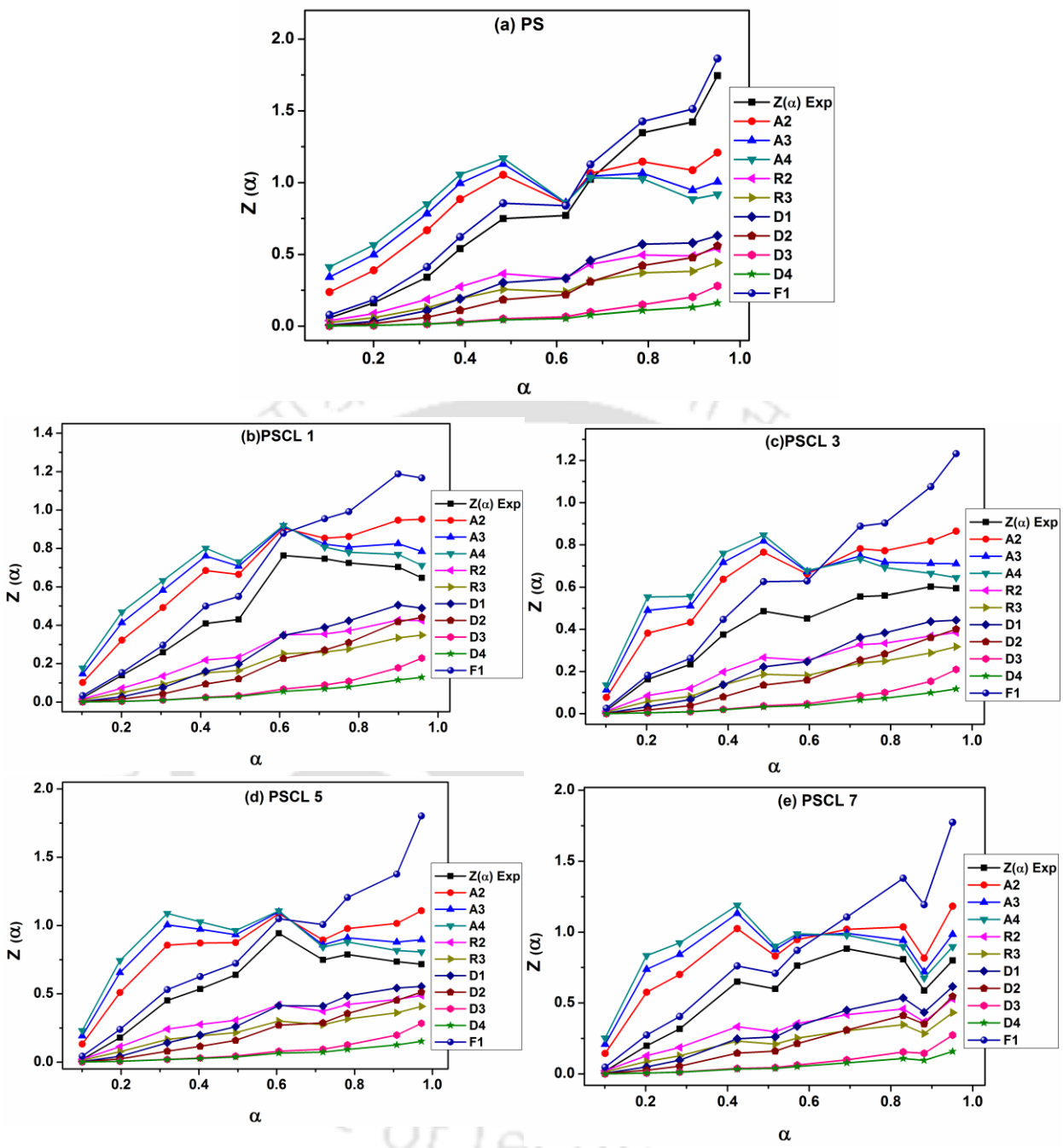

Figure 5.13: Z(α) versus α plots for various cases (a) pristine PS, (b) PSCL 1, (c) PSCL 3, (d) PSCL 5 and (e) PSCL 7 nanocomposites.

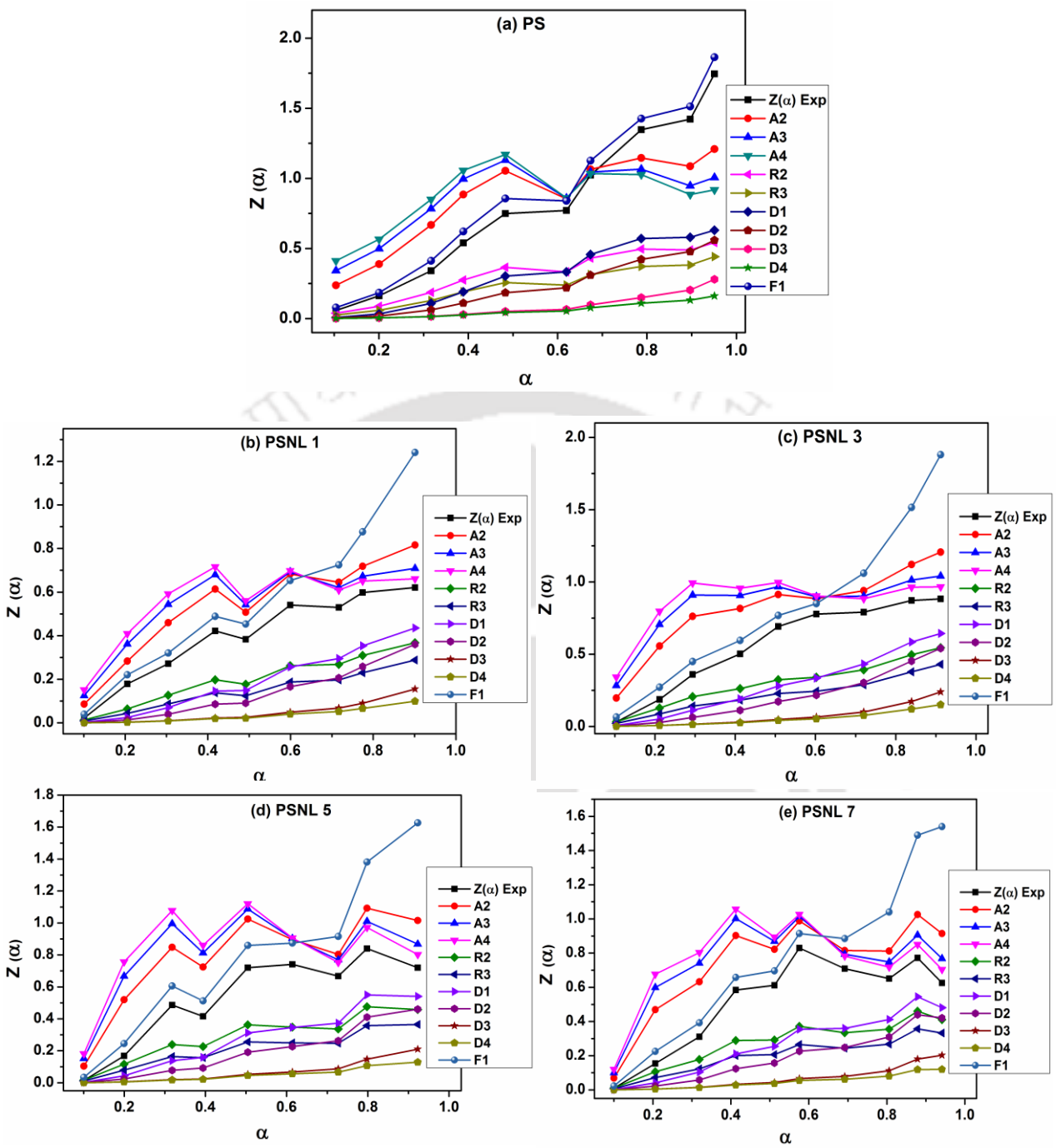

Figure 5.14: Z(α) versus α plots for various cases (a) pristine PS, (b) PSNL 1, (c) PSNL 3, (d) PSNL 5 and (e) PSNL 7 nanocomposites.

5.3.10 Integral procedure decomposition temperature

Integral procedure decomposition temperature method (Doyle 1961) was used for thermal stability evaluation of prepared pristine PS, PS/Co-Al LDH and PS/Ni-Al LDH nanocomposite samples. As compared with pristine PS, all nanocomposites exhibit higher IPDT, which indicate improved thermal stability of the nanocomposites. The IPDT values of pristine PS, PSCL 1, PSCL 3, PSCL 5 and PSCL 7 nanocomposites are 379.1, 386, 399.7, 407.6 and 412.1 °C, respectively. Similarly, these values for PS/Ni-Al LDH nanocomposites with 1, 3, 5 and 7 wt.% Ni-Al LDH loading are 387.1, 401.1, 408.9 and 413.2 ^{o}C, respectively. Thus, PS nanocomposites possess higher IPDT values in comparison with pristine PS and hence comparatively improved thermal stability (Table 5.3).

Table 5.3: IPDT results of pristine PS, PS/Co-Al LDH and PS/Ni-Al LDH nanocomposites samples.

Sample	Initial Temperature (T_i) °C	Final Temperature (T_f) °C	IPDT (°C)
PS	50	700	379.1
PSCL 1	50	700	386
PSCL 3	50	700	399.7
PSCL 5	50	700	407.6
PSCL 7	50	700	412.1
PSNL 1	50	700	387.1
PSNL 3	50	700	401.1
PSNL 5	50	700	408.9
PSNL 7	50	700	413.2

5.3.11 Rheological properties

It is believed that rheology offers an effective way to assess upon the state of nanofiller dispersion and to detect the state of interconnecting microstructure of the nanocomposites in molten state (Kashiwagi et al., 2008). The nanofiller loading of the particles as well as other factors, such as the shape and size of the particles and state of dispersion of particles are known to influence the rheology of polymer melts. The rheological properties of PS/Co-Al LDH and PS/Ni-Al LDH nanocomposites are discussed here in.

Rheological studies are very proficient in order to study the processing behaviour, content of clay, microstructure dispersion and adhesion between the nanofiller layers as well as polymer matrix chains and in between nanofillers and matrix. Usually, polymer nanocomposites demonstrate alteration in rheological characteristics (from liquid-like to solid-like) with an increase in the nanofiller content. This transition concentration is called the percolation threshold. In the frequency range of 0.01 – 100 sec^{-1}, Figure 5.15 and 5.16 depict the storage modulus and loss modulus *versus* angular frequency plot for PS/Co-Al LDH and PS/Ni-Al LDH nanocomposites, respectively at 190 °C. As expected, the addition of LDH influences the storage and loss modulus and this influence is more pronounced in the lower frequency region. Also both moduli increase with increasing nanoparticle content in the both nanocomposite systems. Thus both types of nanocomposites hold higher storage moduli and loss moduli values than the pristine PS. The storage and loss moduli also increase with respect to increment in angular frequency due to the result of nanofiller-polymer matrix and filler-filler interactions. Same observations were reported by Zidelkheir et al. (2006) for MMT based PS nanocomposites prepared by melt intercalative compounding.

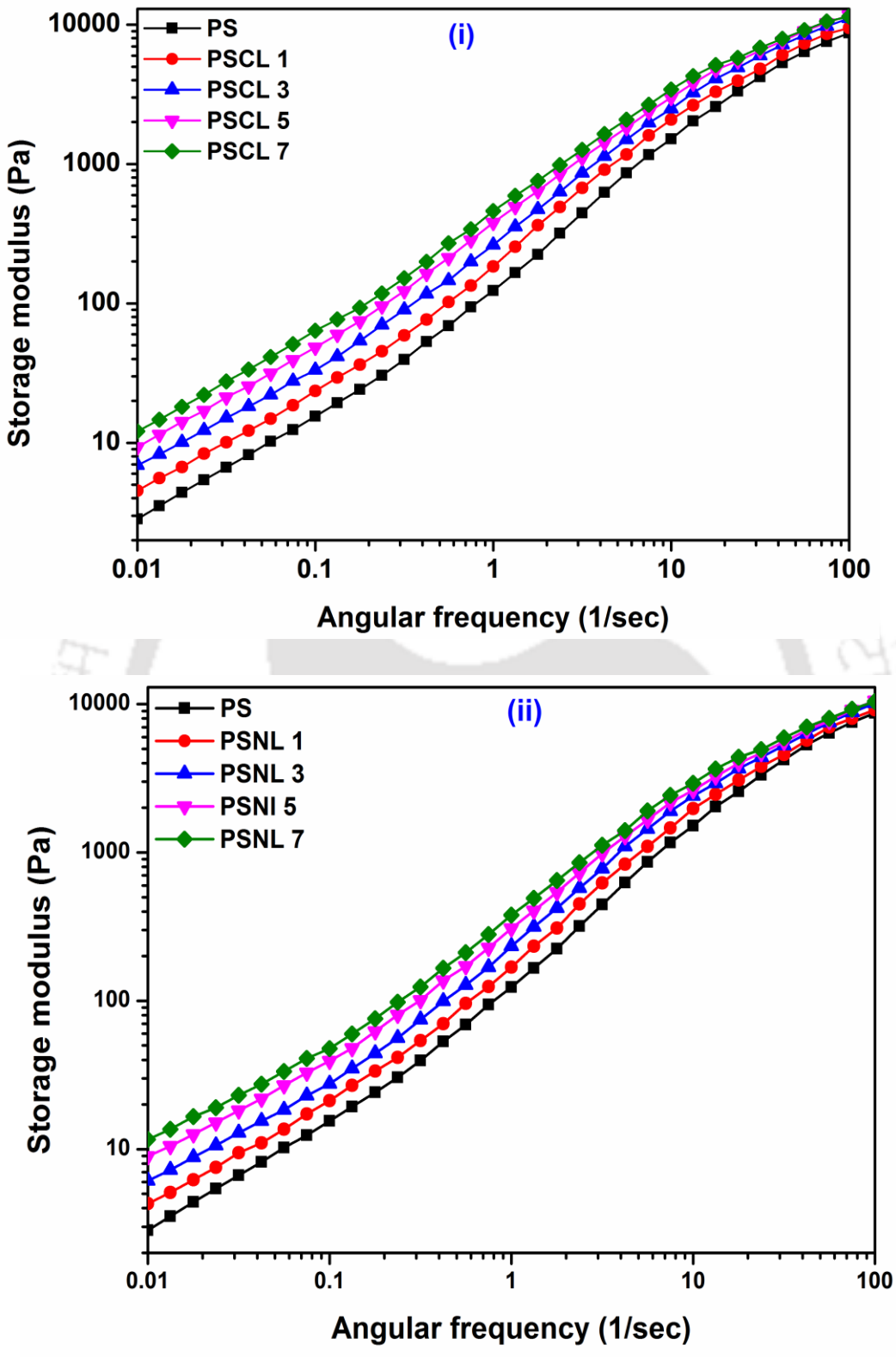

Figure 5.15: Storage modulus of (i) PS/Co-Al LDH and (ii) PS/Ni-Al LDH nanocomposites at 190 °C.

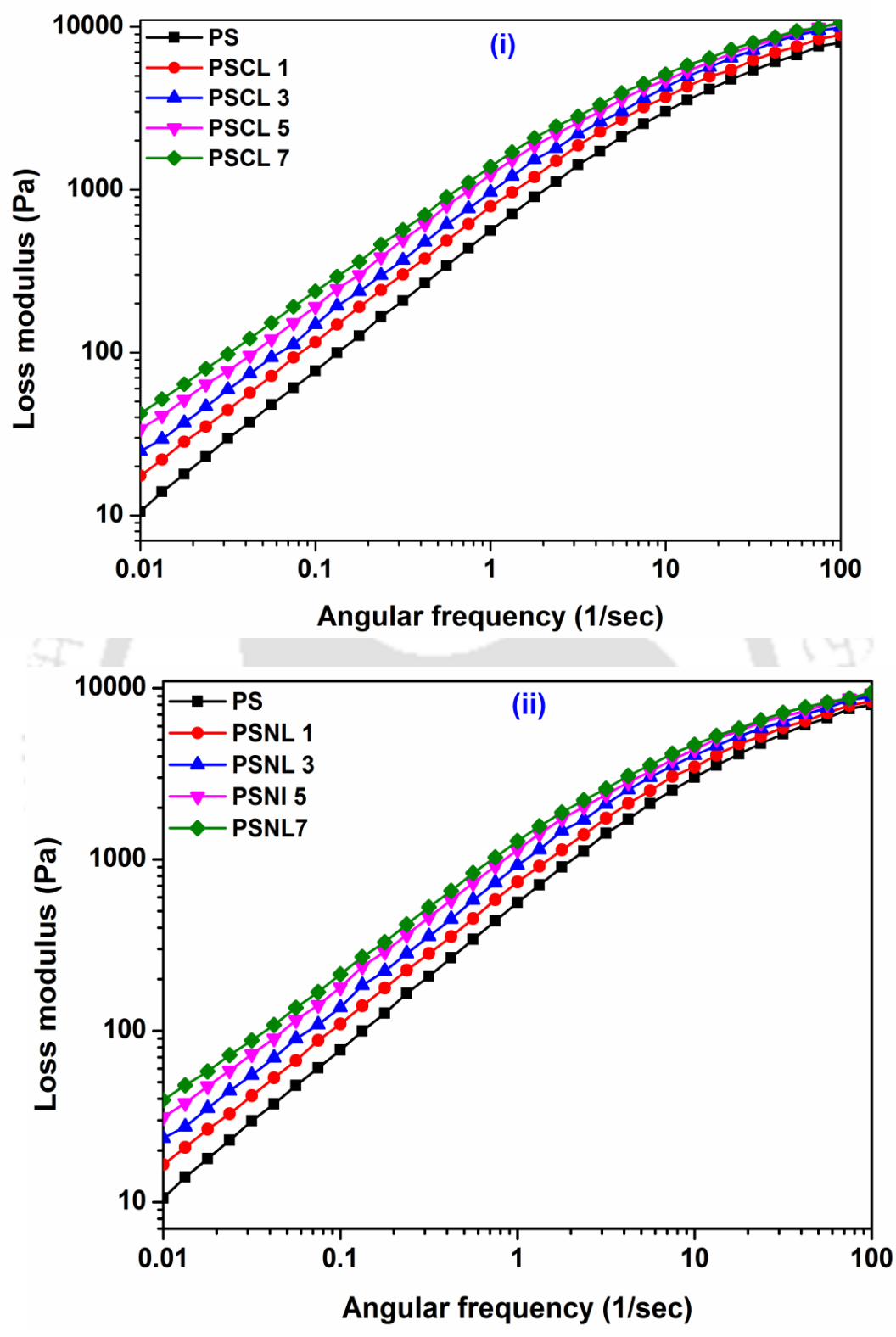

Figure 5.16: Loss modulus of (i) PS/Co-Al LDH and (ii) PS/Ni-Al LDH nanocomposites at 190 °C.

Figure 5.17 explicates the behaviour of complex viscosity with variation in angular frequency (0.01 – 100 sec^{-1}) at 190 °C for pristine PS, PS/Co-Al LDH and PS/Ni-Al LDH nanocomposites samples. The plot shows that the complex viscosity gets gently reduced with increasing angular frequency. There is an increment in the complex viscosity data with increasing filler concentration in the nanocomposites samples. This effect is more noticeable at lower frequency region than at higher frequency. This is due to formation of network like structures in the PS composites that arise from LDH-LDH and PS-LDH interactions. The complex viscosity gets slowly reduced for angular frequency variation from lower to higher regime. The plot shows a shift from Newtonian to shear thinning nature (viscosity reduces with increasing frequency) which in turn represents either stronger interaction between the PS and LDH or enhanced distribution of the LDH in polymer matrix. A similar behaviour was reported by Wang and Huang (2013) for polypropylene nanocomposites containing 2 to 8 wt.% loading of halloysite nanotubes (HNTs). In another study, Kim et al. (2003) also reported increment in complex viscosity due to increased clay content in the PS matrix.

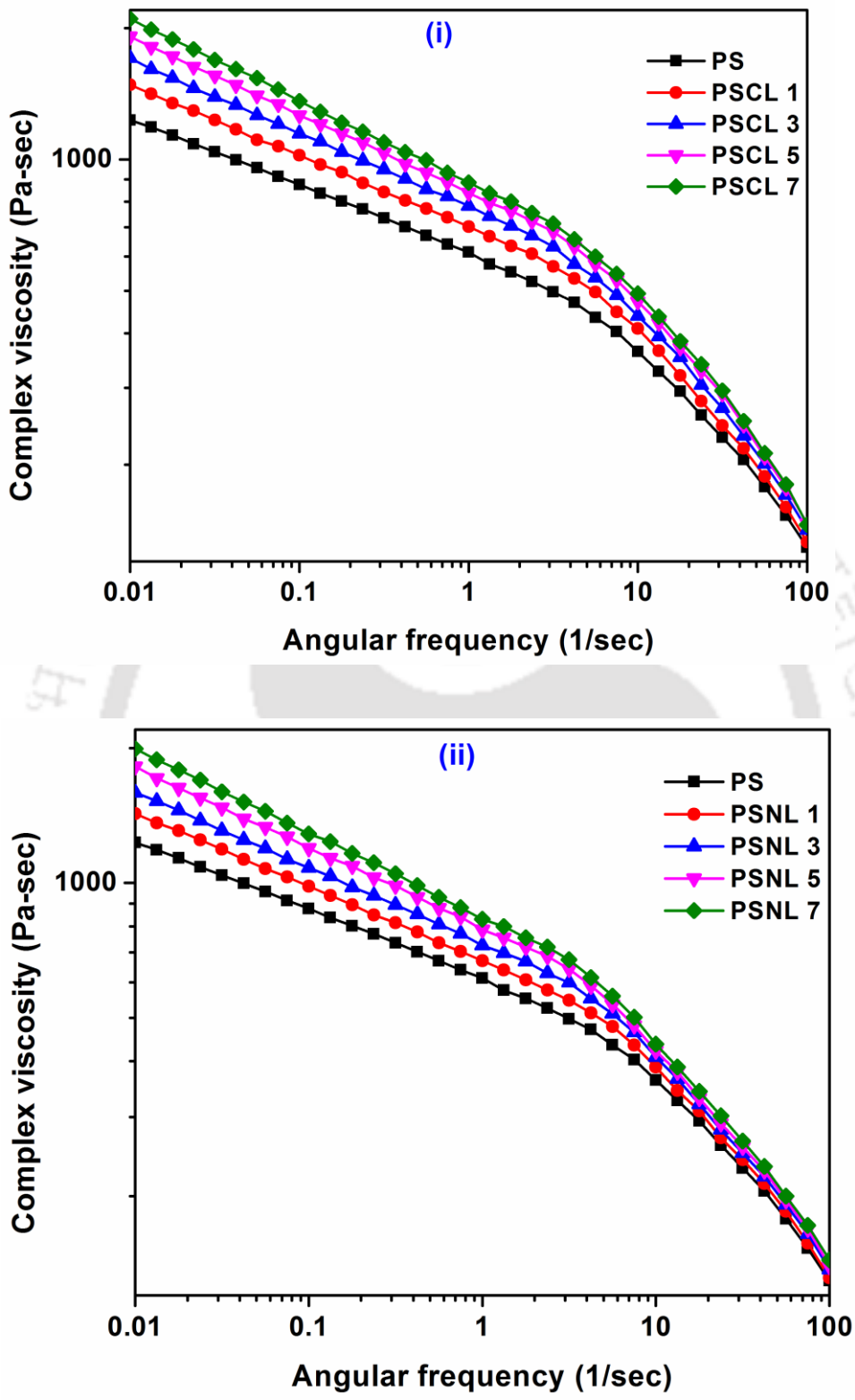

Figure 5.17: Complex viscosity of (i) PS/Co-Al LDH and (ii) PS/Ni-Al LDH nanocomposites at 190 °C.

5.3.12 Comparison analysis of preparation method

Morphological investigations explored nanofiller dispersion in the PS nanocomposite using TEM analysis. Figure 4.3 depicts the TEM micrographs of solvent based PS/LDH nanocomposites. As suggested by TEM analysis solvent blending based (PSCL 1 and PSNL 1), (PSCL 3 and PSNL 3), (PSCL 5 and PSNL 5) and (PSCL 7 and PSNL 7) nanocomposites exhibited exfoliated, exfoliated, partially exfoliated and intercalated structures, respectively. Considering 15% weight loss as a reference point in the TGA profile, compared to pristine PS, the Co-Al LDH and Ni-Al LDH based PS nanocomposites demonstrated 10.5 – 28.5 °C and 12.3 – 29.1 °C improvement in thermal stability, respectively. The PS/Ni-Al LDH nanocomposites prepared by solvent blending method demonstrate higher thermal stability than Co-Al LDH based nanocomposites due to better thermal stability of modified Ni-Al LDH than Co-Al LDH. Optimal nanofiller loading for solvent blending based PS/LDH nanocomposites is 7 wt.% for both types of nanocomposites from thermal property enhancement perspective.

In the melt blending method, the TEM images (see Figure 5.3) signify that (PSCL 1 and PSNL 1), (PSCL 3 and PSNL 3), (PSCL 5 and PSNL 5) and (PSCL 7 and PSNL 7) nanocomposites possess exfoliated, partially exfoliated, intercalated and intercalated structure, respectively. At 15% weight loss reference point, compared to pristine PS, the decomposition temperature of PS/Co-Al LDH and PS/Ni-Al LDH nanocomposites are enhanced by 9.4 – 26.1, and 11 – 27.4 °C, respectively. The tensile strength, flexural strength and impact strength of PS/Ni-Al LDH nanocomposite containing 1 wt.% filler content is maximum in comparison with pristine PS and all other nanocomposites.

Table 5.4: (i) Summary of structural, mechanical properties of PS, PS/Co-Al LDH and PS/Ni-Al LDH nanocomposites.

Sample	Solvent Blending	Melt blending method			
	Structural Properties (TEM)	Structural Properties (TEM)	Mechanical properties		
			Tensile strength (MPa)	Flexural strength (MPa)	Impact strength (kJ/m^2)
PS			29.01	54.08	6.68
PSCL 1	Exfoliated	Exfoliated	38.5	65.57	7.95
PSCL 3	Exfoliated	Partially exfoliated	35.62	63.81	7.31
PSCL 5	Partially exfoliated	Intercalated	31.91	58.40	6.96
PSCL 7	Intercalated	Intercalated	30.02	55.16	6.77
PSNL1	Exfoliated	Exfoliated	39.01	68.95	8.15
PSNL 3	Exfoliated	Partially exfoliated	36.29	64.46	7.43
PSNL 5	Partially exfoliated	Intercalated	32.30	59.00	7.03
PSNL 7	Intercalated	Intercalated	30.22	55.59	6.82

Table 5.4: (ii) Summary of thermal properties of PS, PS/Co-Al LDH and PS/Ni-Al LDH nanocomposites.

Sample	Solvent blending method			Melt blending method		
	Temperature at 15% weight loss (T_{15}) °C	T_{max} (°C)	T_g (°C)	Temperature at 15% weight loss (T_{15}) °C	T_{max} (°C)	T_g (°C)
PS	360.0	417.0	69.3	358.0	415.7	68.1
PSCL 1	370.5	419.9	71.8	367.4	417.7	69.9
PSCL 3	378.2	422.4	73.3	375.3	420.0	71.0
PSCL 5	384.6	423.9	74.4	380.8	421.3	71.9
PSCL 7	388.5	424.5	74.8	384.1	421.8	72.2
PSNL1	372.3	420.2	72.2	369.0	418.1	70.5
PSNL 3	381.5	422.7	73.5	378.1	420.5	71.2
PSNL 5	387.7	424.3	74.8	383.3	421.7	72.1
PSNL 7	389.1	424.6	75	385.4	422.5	72.4

Overall, PS/Ni-Al LDH nanocomposites exhibit better properties than PS/Co-Al LDH nanocomposites (see Table 5.4 (i)).

It can be concluded that in the case of PS/Ni-Al LDH nanocomposites, higher levels of adhesion and dispersion of modified Ni-Al LDH platelets are responsible for enhancement in the mechanical properties. For 1 wt.% Ni-Al LDH containing melt blending based nanocomposites, exfoliated structure contributes towards improved mechanical properties.

The nanocomposites prepared by solvent blending method indicate higher thermal stability of PS/Ni-Al LDH nanocomposites in comparison with melt blending based PS/Co-Al LDH and PS/Ni-Al LDH nancomposites.

The TEM analysis of both solvent blending and melt intercalation based PS/LDH nanocomposites indicates enhanced LDH dispersion in the materials fabricated with solvent blending technique. For the technique, delaminated PS/LDH nanocomposites have been achieved at lower loading of nanofiller (< 3 wt.%). The melt intercalation technique confirmed dominance of intercalation and agglomeration in structural morphology of samples prepared with more than 1 wt.% loading of LDH nanofiller. The same samples after undergoing extrusion process conveyed deteriorated thermal stability (Table 5.4 (ii)). This could be due to thermal degradation of PS polymer at the high working temperature of the extruder. Overall, the analysed decay in the thermal stability of melt blending based PS/LDH nanocomposites could be due to PS chain scission that was driven by mixing processes and nanofiller-PS interactions at higher temperatures maintained in the extrusion process. Also, the solvent blending process enabled greater interactions between PS and nanofiller in the presence of solvent which is not the case during melt intercalation. It might be the case that melt intercalation may have allowed melting and effective diffusion of nanofiller into the PS

matrix during fabrication process. However, it is well known that mixing always gives best results in terms of dispersion in comparison with melting process. Therefore, this might also be a reason for the better thermal properties of solvent blending based Ni-Al LDH nanocomposites in comparison with those prepared with melt intercalation method.

While the melt-intercalation process is widely accepted for industrial production of PS nanocomposites, for mechanical property enhancement, 1 wt.% Ni-Al LDH loading has been evaluated to be the optimal nanofiller loading in the melt blend based nanocomposites due to strong interaction between nanofiller and matrix.

5.4 Summary

Several PS nanocomposites were prepared by inclusion of variant quantities of Co-Al LDH and Ni-Al LDH (1, 3, 5 and 7 wt.% with respect to PS) in a PS matrix via melt intercalation using a twin screw extruder. The XRD results confirmed formation of exfoliated PS nanocomposites. The TEM micrographs reveal that LDH layers are well dispersed in the PS polymer. FTIR analysis indicates presence of LDH layers in the PS matrix.

The mechanical properties (Tensile strength, Flexural strength and Impact strength) of the nanocomposites have been found to be optimal at 1 wt.% loading of LDH nanofiller. Compared with the pristine PS, the improvement of tensile strength, flexural strength and impact strength for the PSNL 1 nanocomposite is found to be 34.5, 27.5 and 22%, respectively. It is also found that PSNL 1 nanocomposite exhibits improved mechanical properties in comparison with PS/Co-Al LDH nanocomposites. The TGA result demonstrates improved thermal stability of PS nanocomposites. Choosing 15% mass loss as a reference, thermal degradation temperature of PS nanocomposites with 1, 3, 5 and 7 wt.% Co-Al LDH

loading is 9.4, 17.3, 22.8 and 26.1 °C higher in comparison with pristine PS, respectively. Similarly, these values for PS nanocomposites with 1, 3, 5 and 7 wt.% Ni-Al LDH loading correspond to 11, 20.1, 25.3 and 27.4 °C increment over pristine PS. The glass transition temperature of PS/Co-Al LDH nanocomposites exhibit 1.8 – 4.1 °C higher enhancement than the corresponding value for pristine PS. On the other hand, PS/Ni-Al LDH nanocomposites demonstrate 2.4 – 4.3 °C increment in the glass transition temperature in comparison with pristine PS.

The Coats-Redfern method based analysis confirmed enhanced thermal stability of PS nanocomposites with higher thermal stability for PS/Ni-Al LDH nanocomposites in comparison with PS/Co-Al LDH nanocomposite samples.

The IPDT values of PS nanocomposites enhance with increasing LDH concentration and this is as well confirmed by the TGA data. The thermal degradation mechanism of pristine PS and all nanocomposite samples were determined by Criado method. For pristine PS, $Z(\alpha)$-α experimental curve followed F1 reaction mechanism in the entire range of α. However, the PS nanocomposites initially followed F1 mechanism which later shifted to A4 mechanism at higher temperature. The LDH inclusion in the PS matrix also influenced storage modulus, loss modulus and complex viscosity of the system. Compared to pristine PS, the storage modulus and loss modulus increased for nanocomposites. However, the complex viscosity values for the nanocomposites have been analysed to reduce with increasing frequency.

Chapter 6:

Injection-moulded PS/LDHs Nanocomposites Spur Gears Performance

Chapter 6

Injection-moulded PS/LDHs Nanocomposites Spur Gears Performance

This work addresses the development and performance analysis of PS/Co-Al and Ni-Al LDH nanocomposite gears. The LDHs were prepared using co-precipitation route and were subsequently used to prepare PS nanocomposite gears containing 1 wt.% of LDHs using melt intercalation in a twin screw extruder followed with injection moulding. Characterizations including XRD, TEM and FTIR were evaluated to understand the dispersion and morphology. Thereafter, pristine PS, PSCL 1 and PSNL 1 nanocomposite gears were evaluated for its performance using in-house developed power absorption gear test. Test was carried on the test gear at 1.5 Nm constant torque and 800 rpm for 1h duration. The measured net surface temperatures of PS nanocomposite gears were compared with the pristine PS gear. The transmission efficiency of test-steel gear pair was evaluated using measured in-line torque values. Compared to the pristine PS, the transmission efficiency of PSCL 1 and PSNL 1 nanocomposite gears was higher by 1.4 and 2.6%, respectively. The tooth surfaces of worn-out gears were observed using digital and scanning electron microscope to understand wear mechanism.

6.1 Introduction

Gears are used to transmit motion and power in machinery. Gear materials are being considered based on cost, efficiency, weight, strength, corrosion wear, noise and simplicity in production (Tsukamoto, 1995). Despite being made from wider choices of materials to

achieve desired properties for various applications, the mechanical engineering perspective in gear design analysis indicates the relevance of strength and wear resistance (Bloom et al., 2000). Poor material selection on gear wear, teeth fracture and teeth fatigue failure (Kleiss and Kleiss, 2000; Kansal et al., 2001).

Gears prepared with polymer materials are not suitable for elevated temperature applications due to its poor properties. Compared to conventional gears, polymer nanocomposites gears offer promising features such as being lighter, lower inertia, enhanced combinations of durability, chemical and corrosive resistances, low sliding friction, ability to function under dry conditions (Flodin, 2000). Due to these features, polymer nanocomposite gears have been successful in replacing metallic as well as fine critical gears in wide variety of applications. The increasing demand for polymer nanocomposite gear products is expected in near future (Shigley and Mischke, 2001). The past decade received significant attention from the research community to develop and design nanocomposite polymeric gears. For such applications, nanofillers could be reinforced into polymer matrix to enhance the thermal stability and power transmission efficiency (Senthilvelan and Gnanamoorthy, 2007).

The performance of polymer and nanocomposite gears have been studied extensively till date (Kurokawa et al., 2000b; Kurokawa et al., 2003; Li et al., 2001; Pogacnik and Tavcar, 2015; Hakimian and Sulong, 2012; Senthilvelan and Gnanamoorthy, 2006b; Weale et al., 1999; Goel et al., 2009; Furrow and Mabie, 1970; Yousef et al., 1973; Marshek and Chan, 1977; Marshek and Chan, 1981). Kurokawa et al. (2000b and 2003) conducted performance studies of various polymeric composite gears. The friction and wear behaviour of dissimilar gears were addressed by Li et al. (2011). An accelerated multi-level test procedure that involved the application of step level loads was proposed by Pognacnik and Tavcar for

polymer gears (Pogacnik and Tavcar, 2015). Shrinkage and warpage behaviour of fiber reinforced micro gears were investigated by Hakimian and Sulong (2012) to evaluate the role of fibre orientation. Shrinkage characteristics of injection-moulded short glass fibre reinforced polyamide gears were considered by Senthilvelan and Gnanamoorthy (2006b). Imaging techniques were adopted by Weale et al. (1999) to understand upon the role of fibre orientation in injection-moulded polymer composite gears. The fatigue behaviour of glass fibre reinforced PP was investigated by Goel et al. (2009) at various frequencies. Furrow and Mabie (1970) measured the static deflection of machined acrylic spur gear teeth using a specially designed jig and universal testing machine. Yousef et al. (1973) developed a test rig to hold the gear so that gear tooth is subjected to cyclic bending and the temperature at root circle diameter was measured. Marshek and Chan (1977 and 1981) evaluated performance of polymer worm gears using a special four square machine. A coil spring was used to load the test gear. The lubricant temperature, gear speed and input and output torques were measured.

Among various possible alternatives, polymer reinforcements to achieve nanocomposite gears could adopt LDHs (Leroux and Besse, 2001). LDHs are highly relevant to fabricate polymer nanocomposite gears with non-polar polymers and hence the fabricated gears could provide better combinations of design parameter characteristics from materials perspective. An elaborate review of the carried out work till date indicates that the development of PS/Co-Al LDH, PS/Ni-Al LDH nanocomposites gear and their performance has not been targeted till date. Hence, this work targets the evaluation of comprehensive durability characteristics of injection-moulded PS/Co-Al LDH and PS/Ni-Al LDH spur gears.

6.2 Materials and methods

6.2.1 Material

Section 4.2.1 summarizes various chemicals used for PS/Co-Al LDH and PS/Ni-Al LDH nanocomposite gear synthesis.

6.2.2 Preparation of modified Co-Al LDH and Ni-Al LDH

The procedure for the synthesis of modified Co-Al LDH and Ni-Al LDH has been presented respectively in sections 2.2.2 and 2.2.4 in the PhD thesis.

6.2.3 Development of gears using PS/Co-Al LDH and PS/Ni-Al LDH nanocomposites

Co-rotating twin-screw extruder was used to prepare 1 wt.% PS/Co-Al LDH and PS/Ni-Al LDH nanocomposites using melt compounding method. The moisture from PS, Co-Al LDH and Ni-Al LDH was removed by drying samples as 60, 70 and 70 °C respectively, for 12 h in a hot air oven.

Thereafter, Co-Al LDH (equivalent to 1 wt.% of pristine PS) was dispersed in 100 mL methanol and was sprayed onto the pristine PS pellets so as to achieve uniform distribution of Co-Al LDH on the pristine PS matrix. Eventually, methanol was removed from the coated PS pellets by drying them in a hot air oven for 24 h. The coated PS pellets were fed to the extruder (Make: Specifiq Engineering and Automats; Model-ZV-20 HI TORQUE) that was operated with temperatures of 185, 195, 210 and 200 °C for feed zone, metering zone, compression zone and adaptor zone, respectively. Thereafter, extruded product was quenched in cold water and then pelletised into granules. The dried compounded materials were then

transferred to injection-moulding equipment (Make: Texair; Model: JTS-40) to fabricate the gear. The equipment was maintained at 195, 200 and 210 °C in the three zones of the barrel. Gears were also prepared using pristine PS and without Co-Al LDH and Ni-Al LDH. Table 6.1 and Figure 6.1 summarize the test gear details. Henceforth, gears prepared with various compositions have been designated as PS, and PSCL 1 for polystyrene and PS/Co-Al LDH 1 (wt.%) nanocomposite material, respectively. Similarly, PS/Ni-Al LDH (1 wt.%) nanocomposite (PSNL 1) has also been prepared using the above described procedure and compared with the performance of gears using PSCL 1 nanocomposites. Prior to characterization, the gear samples with pristine PS and PS nanocomposite materials were stored in a desiccator. Figure 6.2 depicts an Injection-moulded based PSCL 1 and PSNL 1 gears.

Figure 6.3 depicts indigenous power absorption gear test rig that was used to evaluate the performance of pristine PS and PS nanocomposites gears. Test gears have been characterized with standard involute tooth profile with 18 teeth, 20° pressure angle and 4 mm module. Stainless steel gear with similar design parameter was prepared using hobbing process and used as the driver gear, which was attached to a speed controllable PMDC motor during the test. During the test, test gear mates with stainless steel standard gear were connected to PMDC generator. A rheostat was used to facilitate loading the generator with the test gear. Drive and driven shaft torques were measured with in-line torque sensors (HBM, T20WN) with 0.2% accuracy. Non-contact infrared temperature sensor (Raytech) was used to measure tooth temperature of pristine PS and PS nanocomposites gear. Data acquisition system (HBM, Spider 8) along with a personal computer were used for continuous measurement and storage of gear tooth temperature and torque. The PS, PSCL 1 and PSNL 1

nanocomposite gear tests were performed for 1 h at 1.5 Nm constant torque and 800 rpm speed. At three locations that are spaced equally along the circumference, base tangent length across three teeth was measured after 1 h to monitor tooth wear. The gear tooth profile after worn-out condition (after the test) was examined using vertical profile projector (PP400TE Optomech with 0.001 mm linear encoder resolution) at 20 times magnification. All tests were repeated for atleast three gear samples that exhibited same life span within 5% deviation. For each gear sample, the average life span obtained with three trails has been reported in the results and discussion section.

Table 6.1: Test gear parameter.

Parameters	**Test and Mating gear**
Pressure angle (o)	20
Module (mm)	3
Number of teeth	18
Pitch circle diameter (mm)	54
Face width (mm)	4
Root filler radius (mm)	1.14

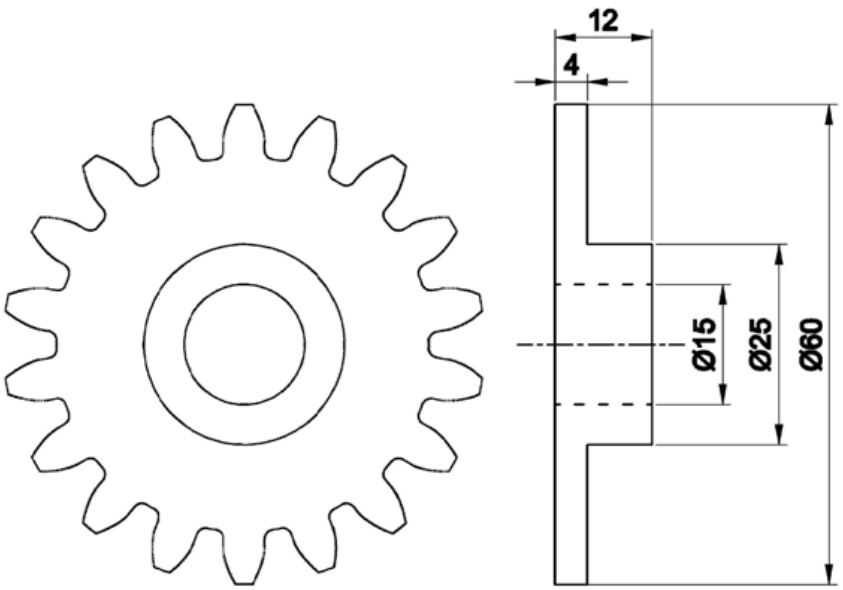

Figure 6.1: Test gear geometry and dimension.

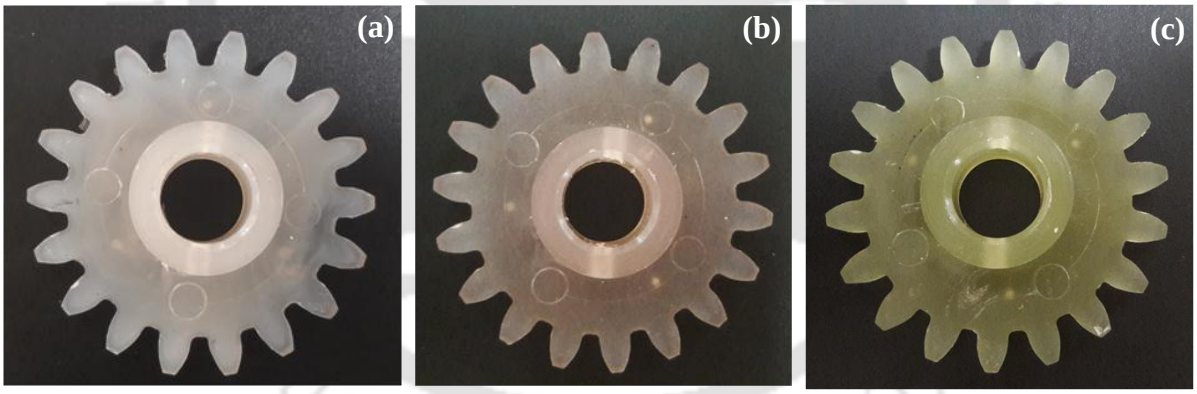

Figure 6.2: Injection-moulded pristine PS, PSCL 1 and PSNL 1 nanocomposite gears.

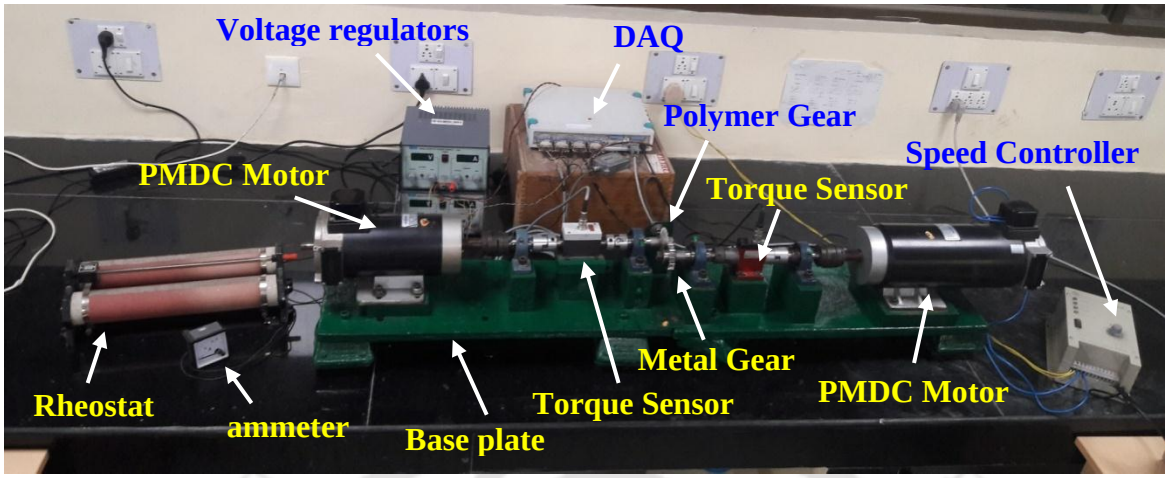

Figure 6.3: Photograph of in-house developed power absorption gear test rig.

6.2.4 Characterization

X-ray diffraction (XRD) equipment (Make: Bruker, Model: D8 ADVANCE) with Cu-Kα radiation and Ni filter was used to measure XRD patterns of organomodified Co-Al LDH and Ni-Al LDH samples in the 2θ range of 2 – 50°. Transmission electron microscopy images were measured using TEM instrument (Make: JEOL, Model: JEM 2100) operated at 200 kV accelerating voltage. Fourier transform infrared spectra were recorded using FTIR instrument (Make: Shimadzu, Model: IRAffinity-1) in 4000 – 400 cm^{-1} wavelength range for the sample. DSC analysis was conducted (heating rate and temperature range of 5 °C/min and 25 – 200 °**C**) in nitrogen gas atmosphere using DSC instrument (Make: Mettle Toledo, Model: 1). Polymeric gear patterns were recorded using indigenously developed gear test rig and computer based data acquisition system (HBM, Spider 8).

6.3 Results and discussion

6.3.1 XRD analysis

Figure 6.4 (i) illustrates XRD patterns of organomodified Co-Al LDH and Ni-Al LDH samples. Using these patterns, the d-spacing of the LDH samples were determined using Bragg's law [$d = \lambda/2\sin\theta$, where (λ=1.5406 Å)]. It can be observed that for modified Co-Al LDH, characteristic peak corresponding to (003) plane exists at 2θ value of 3.14° and basal spacing (d-spacing) of 2.8 nm (Figure 4a). Further, Figure 4 (b) depicts that for modified Ni-Al LDH basal spacing (d_{003}) value is 1.35 nm, which was based on the (003) peak affirmed at 2θ value of 6.54°.

Figure 6.4 (ii) (a-c) illustrate the XRD patterns of pristine PS, PSCL 1 and PSNL 1 nanocomposite based gears, respectively. For the pristine PS, it can be seen that two small halos exist cantered at approximate 2θ values of 10 and 20°. This is due to amorphous characteristic of pristine PS (Botan et al., 2012). The diffraction peaks corresponding to (003) plane disappeared completely for both PSCL 1 (Figure 6.4 ii (b)) and PSNL 1(Figure 6.4 ii (c)) nanocomposites gears. This confirms that LDH layers have been completely exfoliated in the PS polymer.

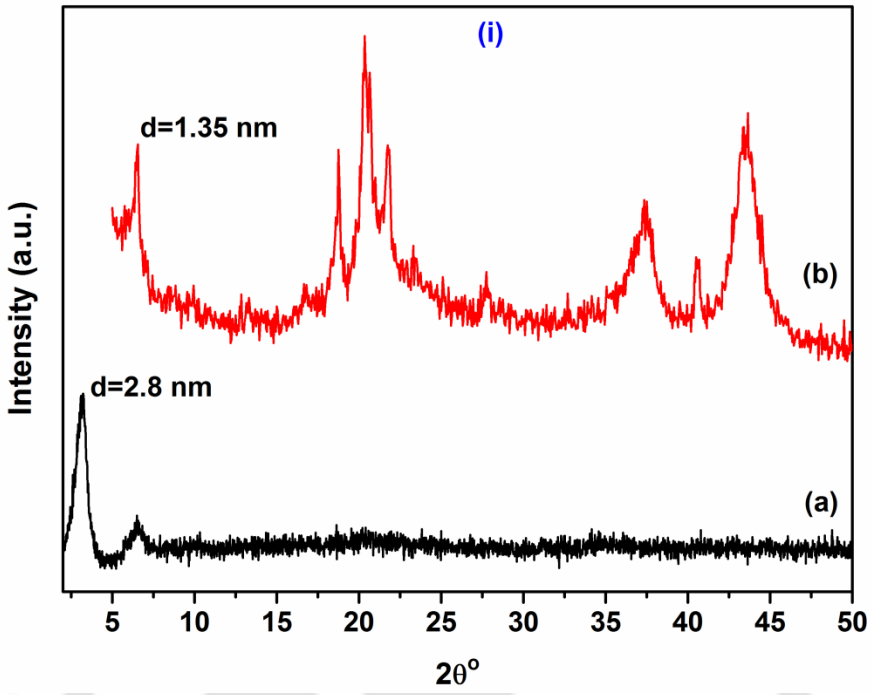

Figure 6.4 (i): XRD patterns of modified (a) Co-Al LDH and (b) Ni-Al LDH.

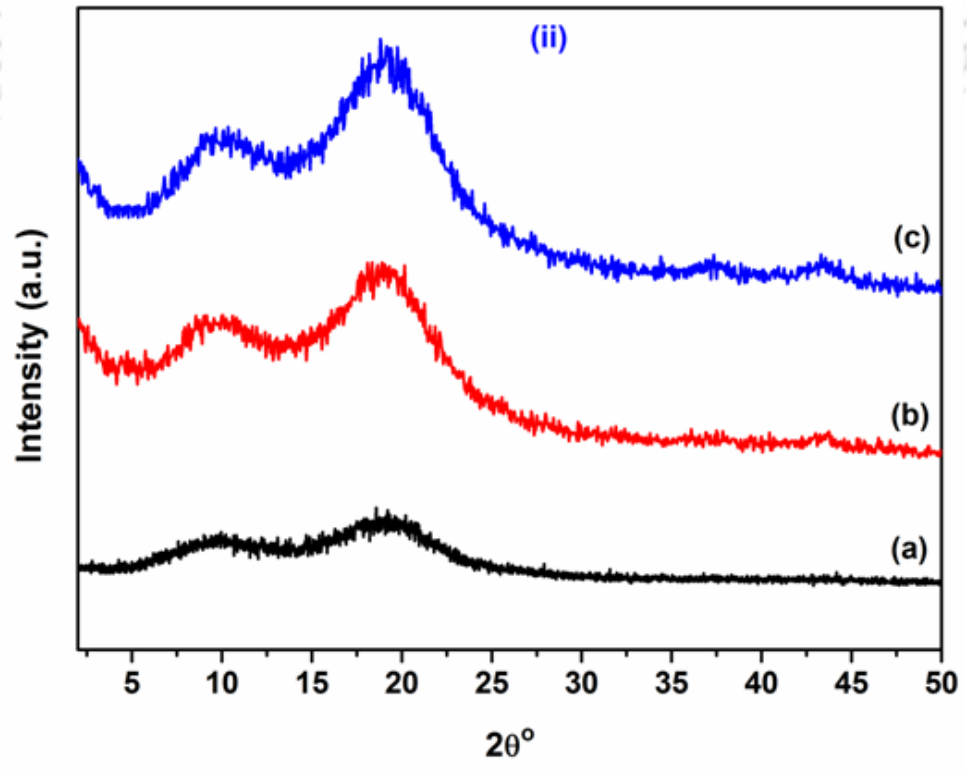

Fig. 6.4 (ii): XRD patterns of (a) PS, (b) PSCL 1 and (c) PSNL 1 nanocomposites.

6.3.2 TEM analysis

For further confirmation of nanocomposites in the gear structure, an extensive characterization of morphology of nanocomposites gear was required in the format of microscopic images. Figure 6.5 (a) and Figure 6.5 (b) show the TEM image of PSCL 1 and PSNL 1 nanocomposite, respectively. These images indicate that the LDH layers (black line) are subjected to good dispersion in the PS polymer (bright part). Shown with arrow marks, the lines of the layers indicate the exhibition of exfoliated structure in PSCL 1 and PSNL 1 nanocomposite gears. The observed exfoliated structure in PSCL 1 and PSNL 1 nanocomposite is in good agreement with the XRD patterns illustrated in Figure 6.4 ii (b) and Figure 6.4 ii (c), respectively.

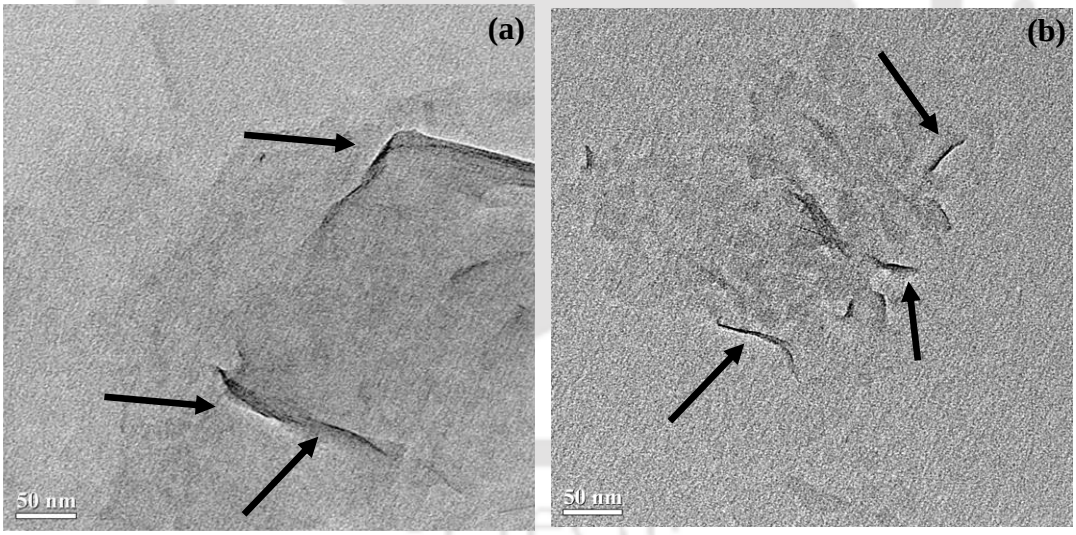

Figure 6.5: TEM images of (a) PSCL 1 and (b) PSNL 1 nanocomposites.

6.3.3 FTIR analysis

Figure 6.6 (i) illustrates the FTIR results of modified Co-Al LDH and Ni-Al LDH. Figure 6.6 i (a) affirmed the existence of several absorption bands in modified Co-Al LDH. These refer to the wavelengths of 3500 cm^{-1} (stretching of O-H in the metal hydroxide layer and interlayer water molecules in the Co-Al LDH), 2957 cm^{-1}, 1630 cm^{-1} (bending mode of water molecule), 2848 cm^{-1}, 2920 cm^{-1} (C-H stretching vibration), 1218 cm^{-1} (symmetric vibration of sulfate from dodecyl sulfate anion) and 1063 cm^{-1} (asymmetric vibration of sulfate from dodecyl sulfate anion). Similarly, the FTIR of modified Ni-Al LDH (Figure 6.6 i (b)) has characteristic peak at 3528 cm^{-1} (O-H stretching vibration of hydrogen-bonded metal hydroxide layer and lattice water), 2850 cm^{-1} (stretching vibration of CH_3 found in SDS), 2920 cm^{-1} (stretching vibration of CH_2 found in SDS), 1218 cm^{-1} (symmetric vibration ($\nu_{S=O}$) of sulfate from dodecyl sulfate anion) and 1063 cm^{-1} (asymmetric vibration ($\nu_{o\ S=O}$) of sulfate from dodecyl sulfate anion).

Figure 6.6 (ii) shows the FTIR spectra of the pristine PS, PSCL 1 and PSNL 1 nanocomposites. As shown, for the pristine PS sample (Figure 6.6 ii (a)), the characteristic peak at 698 cm^{-1} corresponds to mono-substituted benzene. Vibrational mode of CH_2 bending is located at 1453 cm^{-1} and 1368 cm^{-1}. The prominent peaks observed at 1504 cm^{-1} and 1496 cm^{-1} account for C=C bending vibration. The characteristic absorption bands due to aliphatic C-H and aromatic C-H stretching vibration are located at 2930 cm^{-1} and 3070 cm^{-1}, respectively.

The FTIR spectra of 1 wt.% LDH loaded PSCL 1 and PSNL 1 samples have been presented in Figure 6.6 ii (b) and (c), respectively. These are combination of the characteristic absorption bands of both Figure 6.6 i (a) and Figure 6.6 ii (a) for PSCL 1, and Figure 6.6 i (b)

and Figure 6.6 ii (a) for PSNL 1, respectively. Hence, it is apparent that LDH layers are appropriately doped into PS polymer matrix.

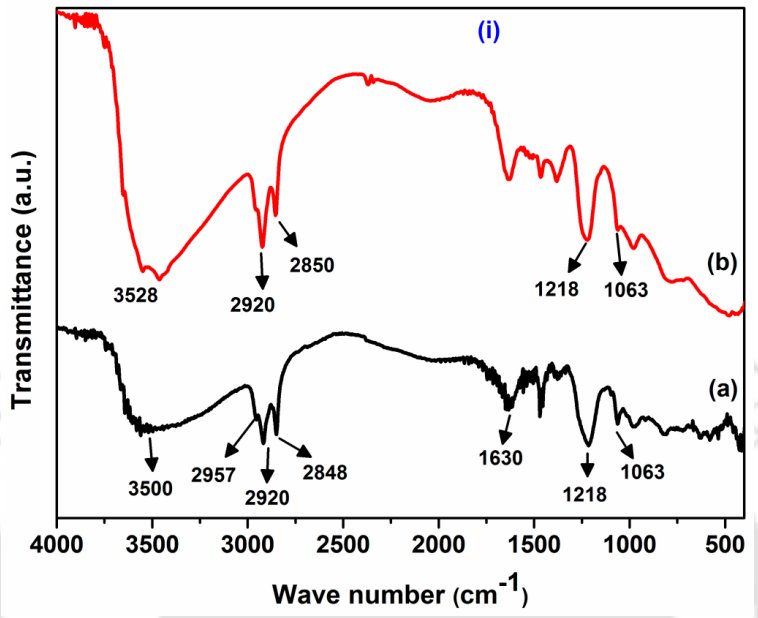

Figure 6.6 (i): FTIR spectra of modified (a) Co-Al LDH and (b) Ni-Al LDH.

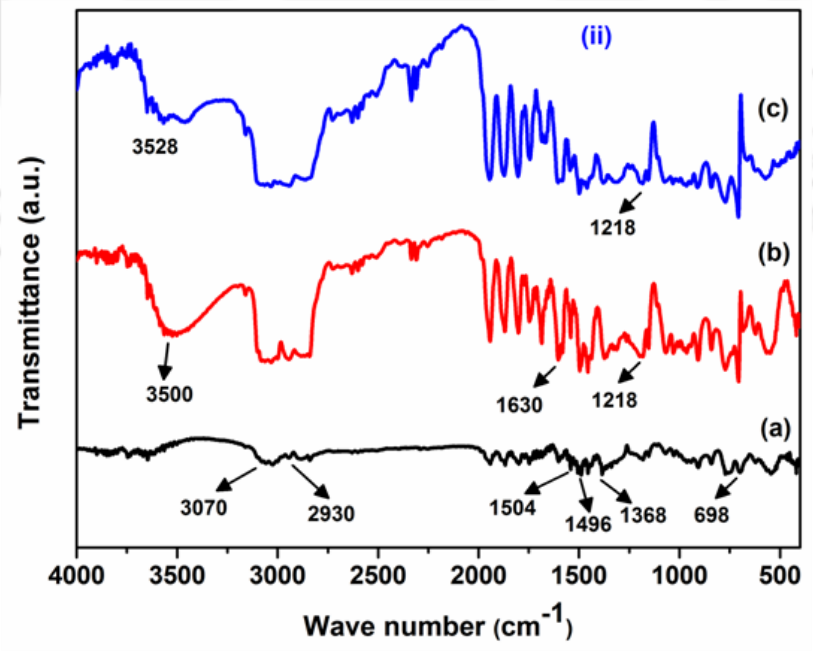

Figure 6.6 (ii): FTIR spectra of (a) pristine PS, (b) PSCL 1 and (c) PSNL 1 nanocomposites.

6.3.4 DSC analysis

The influence of incorporation of the modified LDHs inside the PS polymer on the molecular mobility of the PS chains can be assessed using DSC analysis. The inflection point between the onset and end-set values in the DSC curves has been evaluated T_g. For pristine PS, PSCL 1 and PSNL 1 nanocomposites, DSC curves are shown in Figure 6.7. T_g of pristine PS is revealed to be 68.1 °C. PSCL 1 and PSNL 1 nanocomposite show an enhanced T_g of 69.9 and 70.5 °C, respectively. The restricted movement of PS chains between LDH interlayer is responsible for improvement in T_g value of the nanocomposites. Among the investigated samples, T_g of PSNL 1 nanocomposite is found to be higher over pristine PS and other nanocomposite sample.

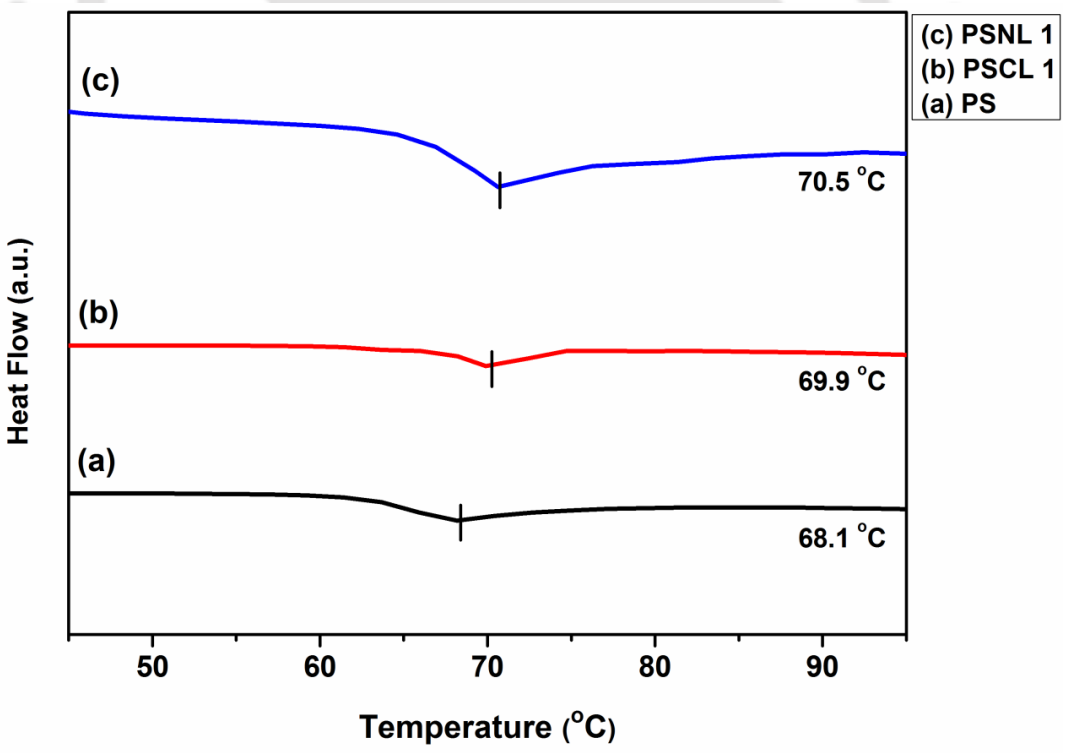

Figure 6.7: DSC analysis of (a) pristine PS, (b) PSCL 1 and (c) PSNL 1 nanocomposites.

6.3.5 Gear surface temperature

During gear testing, the measured temperature corresponds to the net surface temperature of test gears. Figure 6.8 depicts the net surface temperature of pristine PS, PSCL 1 and PSNL 1 nanocomposite test gears at 1.5 Nm load condition. As shown, the surface temperature of the gear gradually enhanced and stabilized at 750 sec. Initially, surface interaction and material hysteresis generate more heat than the heat dissipated to the surroundings. However, as gear rotates, convection facilitates increased heat dissipation and thereby enables saturation of temperature. Also, air pockets trapped between gear teeth are heated and move around the gear to get expelled during meshing operation. For the hot air, temperature within each pocket is close to gear surface temperature and turbulence ensures non-contact gear surface to get heated upto contact surface temperature. For pristine PS, PSCL 1 and PSNL 1 nanocomposite gears, the temperatures have been evaluated to be 36, 33.5 and 32.3 °C, respectively. The gear temperature for pristine PS is 2.5 and 3.7 °C higher in comparison with PSCL 1 and PSNL 1 nanocomposites gear, respectively. Thus, in comparison with pristine PS gear, PS nanocomposites gears exhibit lower surface temperature and improved performance. This is due to enhanced thermal stability of synthesized PSCL 1 and PSNL 1 nanocomposite gears in comparison with the pristine PS. The enhanced thermal stability of nanocomposites is possibly due to reduced frictional losses and hindered effect of LDH layers for temperature in PS nanocomposites gear during meshing. Among investigated gear samples, the nanocomposite with 1 wt.% Ni-Al LDH content has lower surface temperature for the test gear. Similar durability improvement has been reported by Pogacnik and Tavcar (2015) for PA and POM gears subjected to reinforcement with nanofillers.

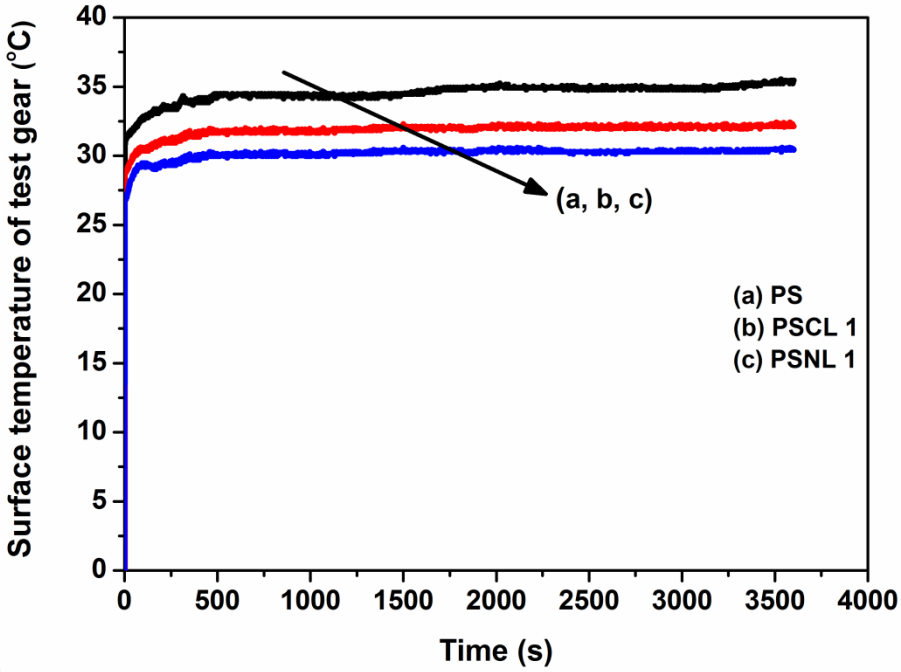

Figure 6.8: Measured surface temperature of (a) pristine PS, (b) PSCL 1 and (c) PSNL 1 nanocomposites test gear.

6.3.6 Transmission efficiency

The evaluation of gear transmission efficiency enables to provide insights with respect to gear tooth wear. Sliding and rolling motion of gear teeth affects the gear accuracy and frictional losses which eventually contribute to power losses and transmission efficiency. This work considers only frictional and wear losses to evaluate transmission efficiency. The transmitted torque between driven and driver shaft were measured using two in-line torque sensors. For the evaluation of transmission efficiency, bearing losses and gear inaccuracies were neglected and hence gear pair transmission efficiency was evaluated using the expression:

$$Transmission\ efficiency\ (\eta) = \frac{Driven\ \text{gear torque}}{\text{Driver gear torque}} \qquad (6.1)$$

Figure 6.9 shows the transmission efficiency of pristine PS and PS nanocomposite gears. Compared to pristine PS gears, the PS nanocomposite gears exhibit enhanced transmission efficiency with an improvement in transmission efficiency of 1.4% and 2.6% for PSCL 1 and PSNL 1 nanocomposite gears, respectively. Increased transmission efficiency of PS polymer at less content of the LDHs nanofiller could be a combined result of uniform dispersion of LDHs in the PS matrix, strong interfacial interaction between phases and increase in the T_g of the nanocomposites. Among investigated gears, the PSNL 1 nanocomposite gear exhibited improved transmission efficiency. The T_g of PSNL 1 nanocomposite is 2.4 °C higher than that of pristine PS. Similar trends have been reported for polyamide nanocomposites gear by Kirupasankar et al. (2012).

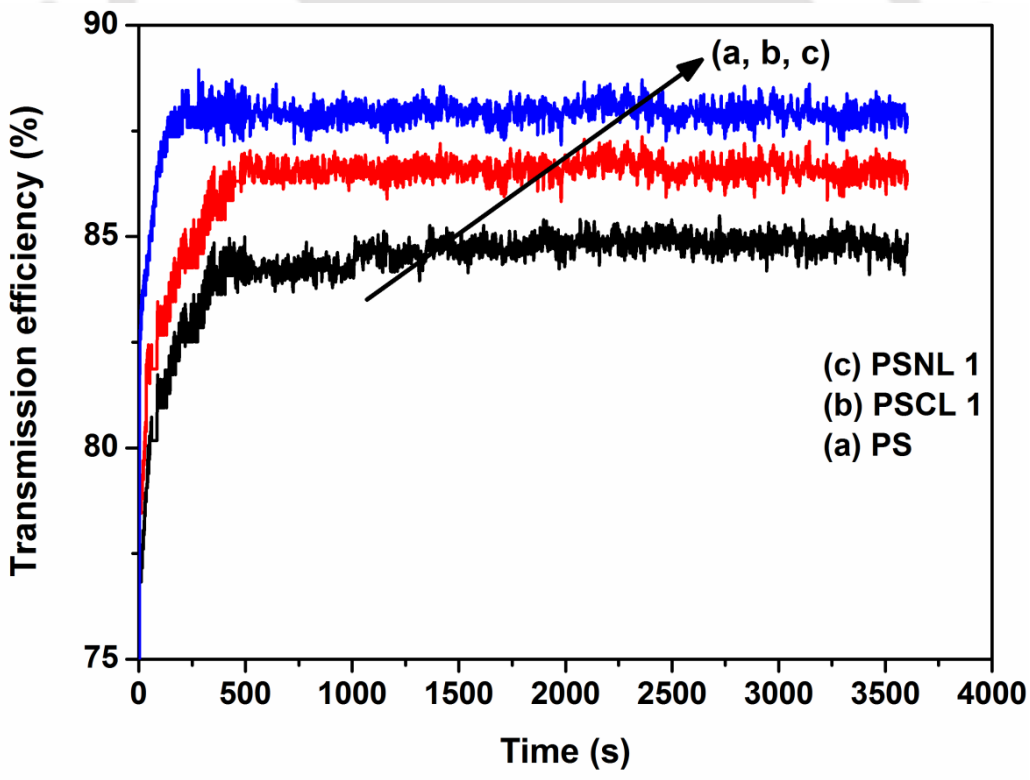

Figure 6.9: Transmission efficiency of (a) pristine PS, (b) PSCL 1 and (c) PSNL 1 nanocomposites test gear.

6.3.7 Gear tooth thickness reduction

At constant load (1.5 Nm) and speed (800 rpm), the pristine PS, PSCL 1 and PSNL 1 nanocomposite gears did not exhibit tooth deformation but tooth wear. Wear tracks in sliding direction confirmed that the teat gear wear was predominantly abrasive.

Figure 6.10 depicts gear tooth thickness measured before and after gear test (1 h). The gear tooth thickness of pristine PS, PSCL 1 and PSNL 1 nanocomposite gears has been determined initially to be 23.1 mm. After completion of test gear at load (1.5 Nm) and speed (800 rpm) for 1 h, the gear tooth thickness was 22.93, 23.01 and 23.04 for pristine PS, PSCL 1 and PSNL 1 nanocomposite gear, respectively. Once again, compared to pristine PS gear, the wear rate was lower for PS nanocomposite gears. Among investigated gear samples, nanocomposite with 1 wt.% Ni-Al LDH content has lowest wear index.

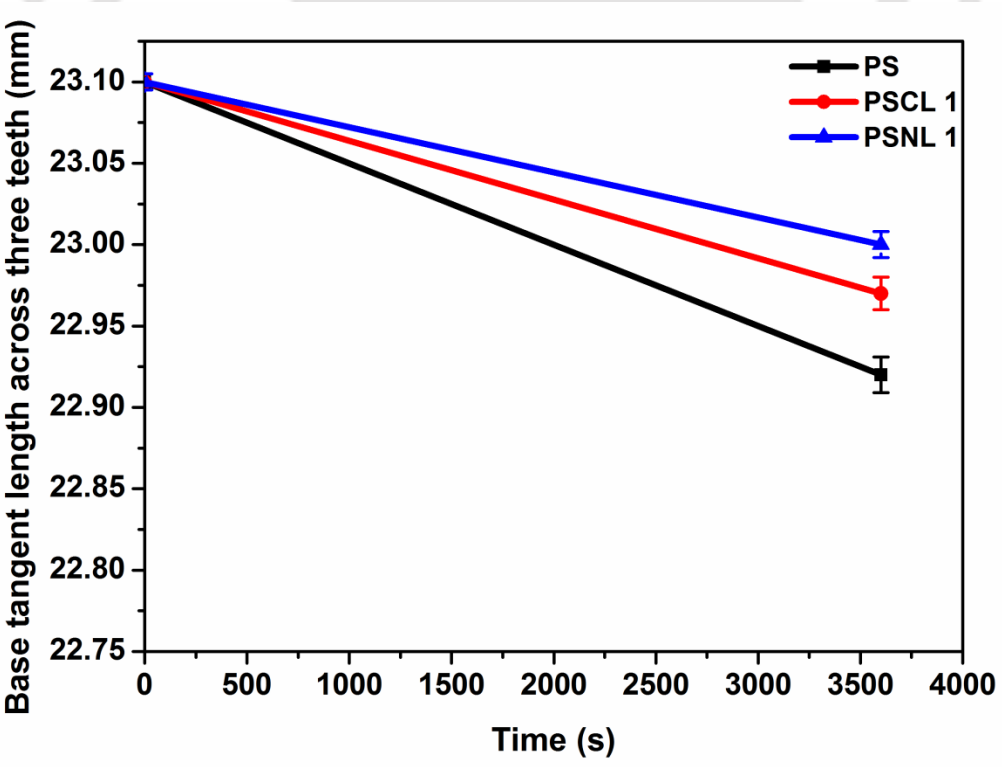

Figure 6.10: Measured gear tooth thickness across three teeth of the test gears.

The decrease in the tooth thickness of the PSNL 1 gear could also be due to the limit of moving scale of layers segments of the PS polymer with addition of modified Ni-Al LDH. Similar behaviour was reported by CNT-PP composite gears fabricated by Mertens and Senthilvelan (2016).

6.3.8 Gear tooth profile wear

Figure 6.11 depicts the gear tooth profile wear that was measured using optical profile projector after testing at 1.5 Nm load for 1h. For the measurements, coast-side gear tip was chosen as origin and 70 points were taken based on the tip to root of the involute profile.

As reference set, injected moulded gear profile was measured before testing. The maximum sliding velocity was determined using the expression:

$$Maximum\ sliding\ velocity = (\omega_1 + \omega_2) \times \left(\frac{path\ of\ approach}{recess} \right) \tag{6.2}$$

were ω_1, ω_2 are angular velocity of the driver and driven gear (rad/s), respectively.

$$\text{Path of a approach/recess} = \frac{\text{Path of contact}}{2} \tag{6.3}$$

$$Path\ of\ contact = \left[\sqrt{R_a^2 - R^2\ \cos^2\phi} - R\ \sin\phi \right] + \left[\sqrt{r_a^2 - r^2\ \cos^2\phi} - r\ \sin\phi \right] \tag{6.4}$$

where addendum circle radius of the driver and driven gears have been designated as R_a and r_a; R and r designate driver pitch circle radius and driven gears and ϕ refers to standard pressure angle of the driver and driven gear.

The figure 6.11 depicts that the tip and root regions correspond to maximum relative sliding velocity of 1.135 m/s and hence the wear at these regions is also maximum. Minimal wear exists near to the pitch region and this is due to lower relative sliding velocity at the pitch region. Among evaluated test gears, PS nanocomposite gears exhibit less wear than

pristine PS gears. This is due to higher sliding velocity at the root and tip of the standard unmodified gear tooth.

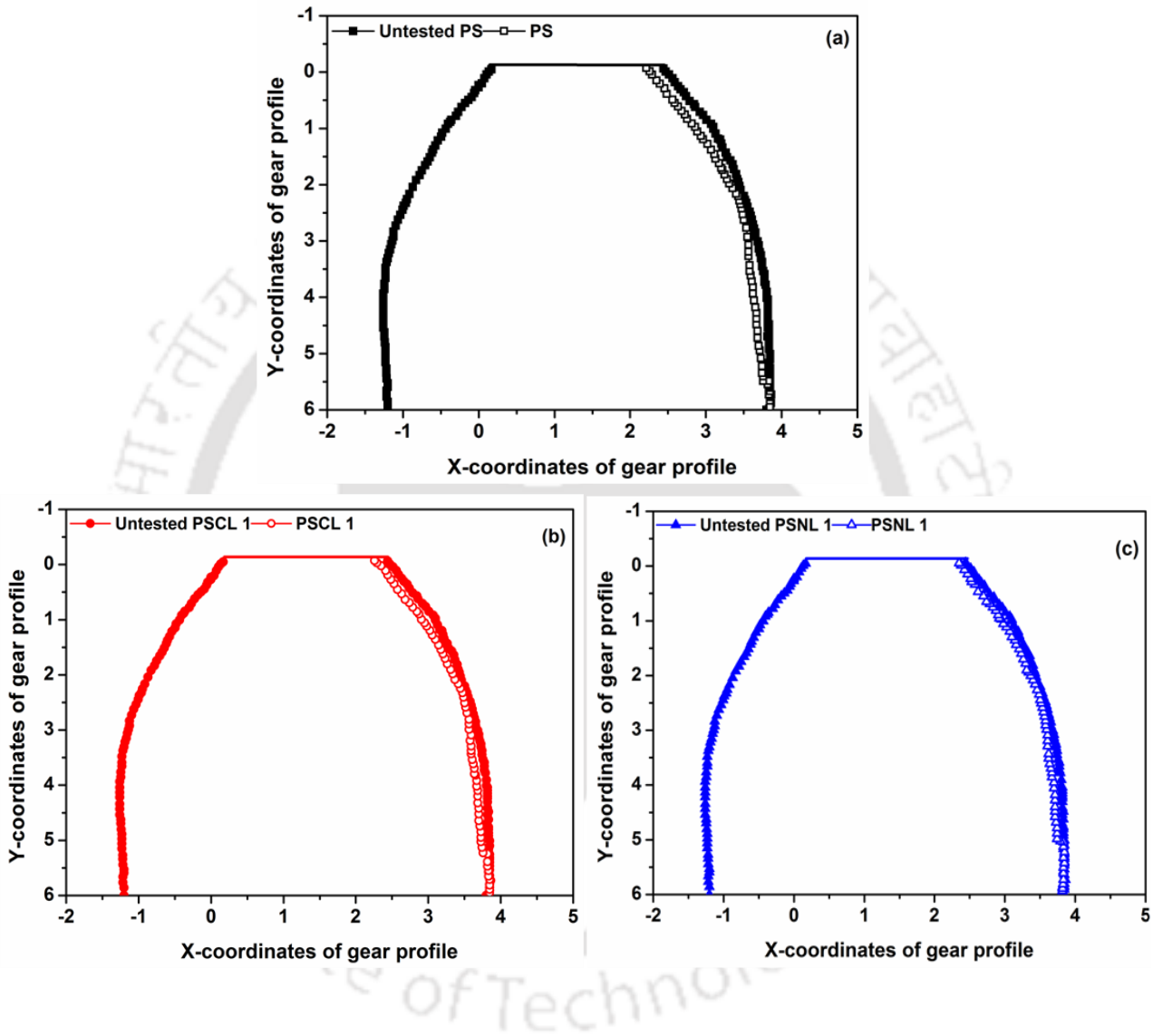

Figure 6.11: Worn-out gear tooth profile of test gear at 1.5 Nm for 1 h duration of (a) PS, (b) PSCL 1 and PSNL 1 nanocomposites.

6.3.9 Gear damage morphology

The view of the tooth surface of prepared gears is depicted in Figure 6.12 Common failure modes for polymer gears are due to wear. An excessive wear and formation of ridges were confirmed for test gears after 1 h in these figures. Compared to pristine PS gear, the PSCL 1 and PSNL 1 nanocomposites gear exhibited less wear. For the pristine PS and its nanocomposites, Figure 6.13 and 6.14 depicted the tooth surface after testing gears at 1.5 Nm load and 800 rpm speed for 1h. The marks affirm that the PS nanocomposite gears have enhanced thermal properties. From the DSC analysis, it can be noticed that T_g of PSCL 1 and PSNL 1 nanocomposites are 1.8 and 2.4 °C more than the T_g of pristine PS, respectively. Hence, it can be inferred that LDH significantly contributed towards wear resistance and plastic deformation resistance. Similar trends reported by Wright and Kukureka (2001) confirmed that excessive wear exists near to the root region of polyamide gears.

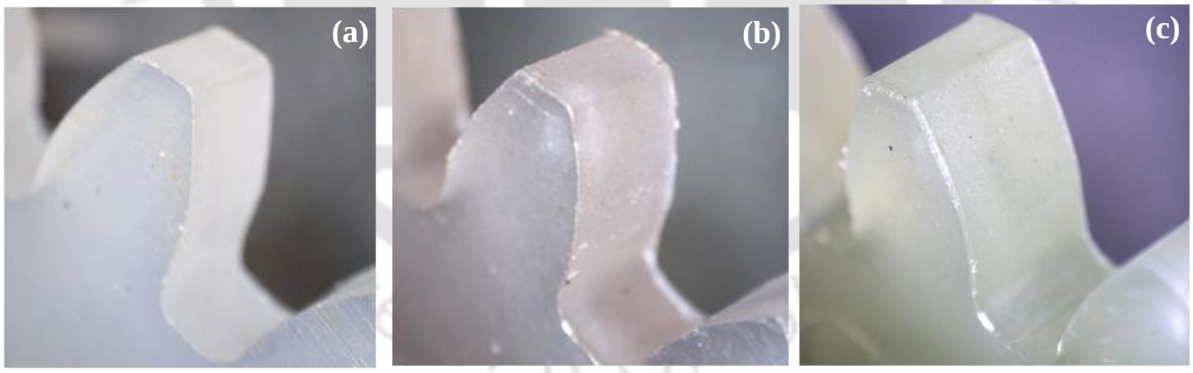

Figure 6.12: Tooth surface of prepared gear (a) pristine PS, (b) PSCL 1 and (c) PSNL 1 nanocomposites.

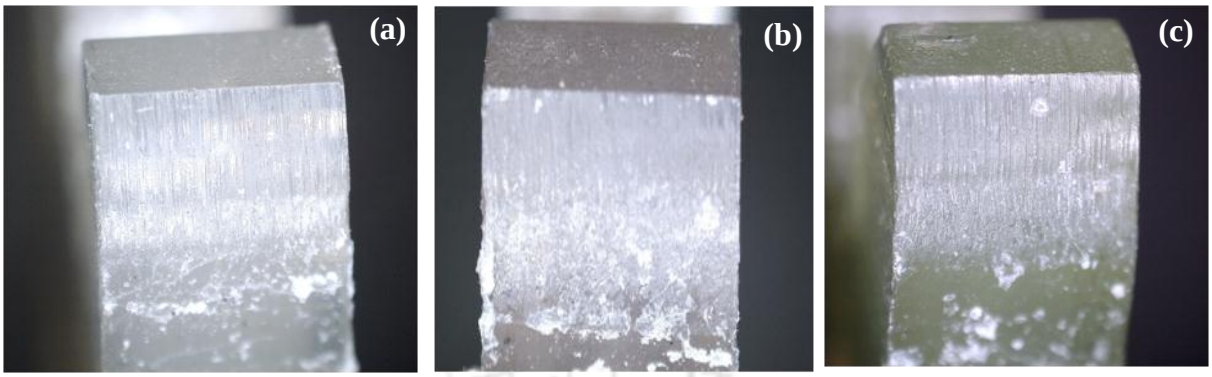

Figure 6.13: Tooth surface of test gear (a) pristine PS, (b) PSCL 1 and (c) PSNL 1 (Front view).

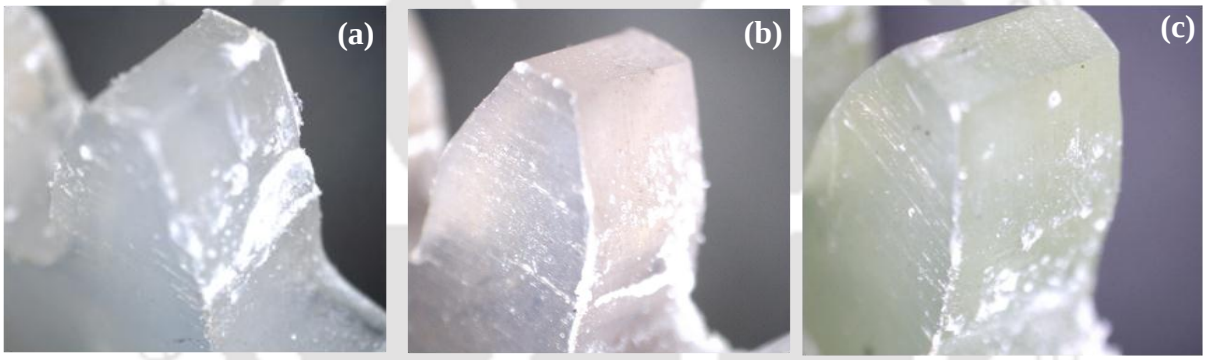

Figure 6.14: Tooth surface of test gear (a) pristine PS, (b) PSCL 1 and (c) PSNL 1 (Side view).

6.4 Summary

Pristine PS, PSCL 1 and PSNL 1 nanocomposite gears were fabricated using co-rotating twin-screw extruder and injection-moulding machine. The XRD and TEM micrographs affirm that the LDHs layers are well dispersed in the PS polymer matrix. FTIR analysis confirms upon the existence of LDHs layers in the PS polymer. Gear tests conducted at 1.5 Nm load and 800 rpm speed reveals that the PS nanocomposites generate lower surface temperature, improved transmission efficiency in comparison with pristine PS gears. Compared to the pristine PS, the transmission efficiency of PSCL 1 and PSNL 1 nanocomposite gears is improved about 1.4 and 2.6%, respectively. Compared to pristine PS and PSCL 1 nanocomposite gear, the PSNL 1 nanocomposite gear exhibit lower surface temperature and higher transmission efficiency.

Chapter 7:

Conclusions and Scope of Future Work

Conclusions and Scope of Future Work

This chapter summarizes the inferences drawn from the various research work presented in this thesis. Also, some suggestions towards the scope for future research are outlined.

7.1 Conclusions

The following sub-sections summarize important conclusions that can be drawn from the work carried out in the Ph.D. thesis:

Synthesis and characterization of organomodified Co-Al LDH and Ni-Al LDH

- The XRD studies inferred that the co-precipitation method based Co-Al LDH and Ni-Al LDH materials possessed a d-spacing value of 2.8 and 1.35 nm, respectively.
- For 10% mass loss reference point, the degradation temperature of Co-Al LDH is lower (266.4 °C) than that obtained for Ni-Al LDH (430.1 °C).

Rheological behaviour of PS/Co-Al LDH blend solution obtained through solvent blending route

- The PS/Co-Al LDH blends with maximum nanofiller loading of 7 wt.% possessed highest viscosity and shear stress among all samples investigated.
- Among various alternate rheological models, based on regression coefficient and bias factor analysis, Herschel-Bulkley model and Cross model are best fit models to

represent low temperature (20 °C) and high temperature (30 and 40 °C) rheological data of PS and PS/Co-Al LDH blend solutions.

Preparation and characterization of PS/Co-Al LDH and PS/Ni-Al LDH nanocomposites by solvent blending method

- ❖ XRD studies concluded that LDH exfoliated structure exists in both PS/Co-Al LDH and PS/Ni-Al LDH nanocomposites.
- ❖ FTIR analyses confirmed existence of LDH nanoparticles in the matrix of the fabricated nanocomposites.
- ❖ TEM analysis conveyed strong role of LDH nanofiller loading on the PS/LDH nanocomposite structure with existence of exfoliated, partial exfoliated and intercalated structure for loadings of 1 – 3, 5 and 7 wt.% LDH, respectively in both types of nanocomposites.
- ❖ Among all samples, the lowest WVTR has been obtained for 7 wt.% Ni-Al LDH nanofiller containing PS nanocomposite (11.9 g/m^2.day, given the corresponding value for pristine PS to be 18 g/m^2.day).
- ❖ Among all samples, highest thermal stability and T_{max} (TGA data), highest T_g value (DSC data), and highest activation energy (Coats-Redfern method) of thermal degradation process have been obtained for PSNL 7 nanocomposites. Thermal degradation mechanism involved F1 reaction mechanism at low temperature followed with A4 mechanism at higher temperature.

- Among all samples, 7 wt.% LDH loaded PS/Co-Al LDH and PS/Ni-Al LDH nanocomposites possessed highest patterns of storage modulus, loss modulus and complex viscosity.

- All PS/Ni-Al LDH nanocomposites exhibited higher thermal stability than PS/Co-Al LDH nanocomposites (TGA data, DSC data, Coats-Redfern method and IPDT method).

Fabrication and characterization of PS/Co-Al LDH and PS/Ni-Al LDH nanocomposites via melt blending method

- Inferences from XRD studies are similar to those provided for solvent blending based PS nanocomposites.
- TEM analysis conveyed existence of exfoliated, partial exfoliated and intercalated nanocomposite structure for loadings of 1, 3, 5 – 7 wt.% LDH respectively in both types of nanocomposites. These trends are distinct from those obtained from solvent blending method and hence fabrication method has a strong role in influencing nanocomposite structure.
- Among all nanocomposites, PSNL 1 nanocomposite possessed maximum improvement in tensile, flexural and impact strength values which are 34.5, 27.5 and 22% respectively higher than those obtained for pristine PS.
- All PS/Ni-Al LDH nanocomposites possessed better mechanical properties than PS/Co-Al LDH nanocomposite samples possessing similar nanofiller loading content.

Injection-moulded PS/LDHs nanocomposites spur gears performance

- Among injection moulding based spur gears fabricated with PSCL 1, PSNL 1 and PS, transmission efficiency of PSNL 1 is highest and improved by 2.6% with respect to corresponding value obtained for PS.
- All PSCL 1, PSNL 1 and PS based spur gears, PSNL 1 based spur gears exhibit lowest surface temperature (32.3 °C), which is 3.7 °C higher than the value obtained for pristine PS.

7.2 Scope for future work

Based on the outcome of this work, some recommendations for future research have been presented as follows:

- In order to examine the use of these materials in packaging application, oxygen permeability test can be performed for all the nanocomposites samples.
- Soil burial degradation study can be performed for PS nanocomposites.
- In the present investigation, surface durability of injection-moulded PS gear was evaluated under dry condition using power absorption gear test rig. In future, this test rig can be modified to run under liquid lubricant condition, so that effect of lubrication can be evaluated.
- In the present investigation, constant load was applied on test gear. In the future, this test rig can be modified to apply fatigue load so that the bending fatigue performance can be evaluated.

References

References

Acharya, H., Srivastava, S.K. and Bhowmick, A.K., Synthesis of partially exfoliated EPDM/LDH nanocomposites by solution intercalation: Structural characterization and properties, *Compos. Sci. Technol*. **67** (2007) 2807–2811.

Ahmadi, S.J., Huang, Y.D. and Li, W., Synthetic routes, properties and future applications of polymer-layered silicate nanocomposites, *J. Mater. Sci*. **39** (2004) 1919–1925.

Alansi, A.M., Alkayali, W.Z., Al-Qunaibit, M.H., Qahtan, T.F. and Saleh, T.A., Synthesis of exfoliated polystyrene/anionic clay MgAl-layered double hydroxide: Structural and thermal properties, *RSC Adv*. **5** (2015) 71441–71448.

Alcantara, A.C.S., Aranda, P., Darder, M. and Hitzky, E.R., Bionanocomposites based on alginate-zein/layered double hydroxide materials as drug delivery systems, *J. Mater. Chem.* **20** (2010) 9495–9504.

Al-Fariss, T.F. and Al-Zahrani, S.M., Rheology behavior of some dilute polymer solutions, *JKAU: Eng. Sci*. **5** (1993) 95–109.

Al-Fariss, T.F., Rheological behavior of Saudi medium crude oil, Proc. Second meet. Chems, (1987) 207–223.

Al-Fariss, T.F., Viscosity-temperature-shear rate correlation of crude oil and polymers, *J. Eng Sci.* **14** (1988) 231–245.

Al-Shammari, B., Al-Fariss, T., Al-Sewailm, F. and Ellithy, R., The effect of polymer concentration and temperature on the rheological behavior of metallocene linear low density polyethylene (mLLDPE) solutions, *J. King Saud. Univ. Engg. Sci*. **23** (2011) 9–14.

Alvarez, E., Correa, J.M., Riverol, C. and Navaza, J.M., Model based in neural networks for the prediction of the mass transfer coefficients in bubble columns. Study in newtonian and non-newtonianian fluids, *Int. Comm. Heat Mass Transfer*. **27** (2000) 93–98.

Al-Zahrani, S.M., Rheology of polymer solutions and their flow behaviour through porous media, M.Sc. thesis. Chemical Engineering Department, King Saud University, Riyadh, June (1990)

Ashby, M.F., Bush, S.F., Swindells, N., Bullough, R., Ellison, G., Lindblom, Y., Cahn, R.W. and Barnes, J. F., Technology of 1990s: Advanced materials and predictive design, *Phil. Trans. R. Soc. Lond. A*. **322** (1987) 393–407.

Barrett, T.S., Stachowiak, G.W. and Batchelor, A.W., Effect of roughness and sliding speed on the wear and friction of ultra-high molecular weight polyethylene, *Wear*. **153** (1992) 331–350.

Betts, G.D. and Walker, S.J., Verification and validation of food spoilage models, in: R. Steele (Ed.), Understanding and measuring shelf life of food, CRC Press, (2004) 184–217.

Bhanvase, B.A., Pinjari, D.V., Gogate, P.R., Sonawane, S.H. and Pandit, A.B., Synthesis of exfoliated poly(styrene-co-methyl methacrylate)/montmorillonite nanocomposite using ultrasound assisted in situ emulsion copolymerization, *Chem. Eng. J.* **181-182** (2012) 770–778.

Bingham, E.C., Fluidity and Plasticity, McGraw-Hill, New York, 1922.

Bloom, P.D., Baikerikar, K.G., Otaigbe, J.U. and Sheares, V.V., Development of novel polymer/quasicrystal composite materials, *Mater. Sci. Eng., A.* **294–296** (2000) 156–159.

Botan, R., Nogueira, T.R., Wypych, F. and Lona, L.M.F., In situ synthesis, morphology, and thermal properties of polystyrene-MgAl layered double hydroxide nanocomposites, *Polym. Eng. Sci.* **52** (2012) 1754–1760.

Bourbigot, S., Gilman, J.W. and Wilkie, C.A., Kinetic analysis of the thermal degradation of polystyrene montmorillonite nanocomposite, *Polym. Degrad. Stab.* **84** (2004) 483–492.

Briscoe, B., Luckham, P. and Zhu, S., The effects of hydrogen bonding upon the viscosity of aqueous poly (vinyl alcohol) solutions, *Polymer*. **41** (2000) 3851–3860.

Bueno, S.M. and Cruz, C.H.G., The influence of fermentation time and the presence of salts in the rheology of the fermentation broth of a polysaccharide-producing bacteria free of soil, *J. Food Eng.* **50** (2001) 41–46.

Carreau, P.J., MacDonald, I.F. and Bird, R.B., A nonlinear viscoelastic model for polymer solutions and melts: Part II, *Chem. Eng. Sci.* **23** (1968) 901–911.

Casson, N., Rheology of disperse systems, Pergamon Press, London 1989.

Chaiko D.J., Organoclay/polymer nanocomposites: Recent discoveries of new enabling technologies, GSA Resources, Inc., (2006).

Chakraborty, S., Kumar, M., Suresh, K. and Pugazhenthi, G., Influence of organically modified Ni-Al layered double hydroxide (LDH) loading on the rheological properties of poly (methyl methacrylate) (PMMA)/LDH blend solution, *Powder Technol*. **256** (2014) 196–203.

Chang, J.H., An, Y.U., Cho, D. and Giannelis, E.P., Poly(lactic acid) nanocomposites: comparison of their properties with montmorillonite and synthetic mica (II), *Polymer*. 44 (2003) 3715–3720.

Chen, W. and Qu, B., Enhanced thermal and mechanical properties of poly(methyl acrylate)/ZnAl layered double hydroxide nanocomposites formed by in situ polymerization, *Polym. Degrad. Stab.* **90** (2005) 162–166.

Chen, Y. and Wang, Q., Thermal oxidative degradation kinetics of flame-retarded polypropylene with intumescent flame-retardant master batches in situ prepared in twin-screw extruder, *Polym. Degrad. Stab.* **92** (2007) 280–291.

Choi, H.J. and Ray, S.S., A review on melt-state viscoelastic properties of polymer nanocomposites, *J. Nanosci. Nanotechnol.* **11** (2011) 8421–8449.

Choudary, B.M., Kantam, M.L., Neeraja, V., Rao, K.K., Figueras, F. and Delmotte, L., Layered double hydroxide fluoride: a novel solid base catalyst for C–C bond formation, *Green Chem.* **3** (2001) 257–260.

Choudary, B.M., Madhi, S., Chowdari, N.S., Kantam, M.L. and Sreedhar, B., Layered double hydroxide supported nanopalladium catalyst for Heck-, Suzuki-, Sonogashira-, and stille-type coupling reactions of chloroarenes, *J. Am. Chem. Soc.* **124** (2002) 14127–14136.

Chow, W.S., Khim, L.Y. and Kang, A.T., Flexural properties of polystyrene/organo-montmorillonite masterbatch composites, *J. Reinf. Plast. Compos.* **27** (2008) 255–261.

Choy, J.H., Kwak, S.Y., Jeong, Y.J. and Park, J.S., Inorganic layered double hydroxides as nonviral vectors, *Angew. Chem. Int. Ed.* **39** (2000) 4042–4045.

Chrissafis, K. and Bikiaris, D., Can nanoparticles really enhance thermal stability of polymers ? Part I: An overview on thermal decomposition of addition polymers, *Thermo. Acta.* **523** (2011) 1–24.

Coats, A.W. and Redfern, J.P., Kinetic Parameters from Thermogravimetric Data, *Nature*, **201**(1964) 68–69.

Constantino, V.R.L. and Pinnavaia, T.J., Structure-reactivity relationships for basic catalysts derived from a $Mg^{2+}/A1^{3+}$ $/CO_3^-$ layered double hydroxide, *Catal. Lett*. **23** (1994) 361–367.

Costa, F.R., Leuteritz, A., Wagenknecht, U., Jehnichen, D., Haubler, L. and Heinrich, G., Intercalation of Mg-Al layered double hydroxide by anionic surfactants: Preparation and characterization, *Appl. Clay Sci.* **38** (2008) 153–164.

Costa, F.R., Wagenknecht, U., Jehnichen, D. and Heinrich, G., Nanocomposites based on polyethylene and Mg-Al layered double hydroxide: characterization of modified clay, morphological and rheological analysis of nanocomposites, *Plast. Rubber Compos.* **35** (2006b) 139–148.

Costa, F.R., Wagenknecht, U., Jehnichen, D., Goad, M.A. and Heinrich, G., Nanocomposites based on polyethylene and Mg-Al layered double hydroxide. Part II. Rheological characterization, *Polymer.* **47** (2006a) 1649–1660.

Criado, J.M., Malek, J. and Ortega, A., Applicability of the master plots in kinetic analysis of non-isothermal data, *Thermochim Acta.* **147** (1989) 377–385.

Cross, M.M., Rheology of Non-Newtoinan Fluids: A new flow equation for pseudoplastic Systems, *J. Colloid. Sci.* **20** (1965) 417–437.

Diaz, D.G. and Navaja, J.M., Rheology of food stabilizers blends, *J. Food Eng.* **64** (2004) 143–149.

Diaz, D.G. and Navaza, J.M., Rheology of aqueous solutions of food additives: Effect of concentration, temperature and blending, *J. Food Eng.* **56** (2003) 387–392.

Ding, P. and Qu, B., Synthesis and characterization of exfoliated polystyrene/ZnAl layered double hydroxide nanocomposite via emulsion polymerization, *J. Colloid Interface Sci.* **291** (2005) 13–18.

Ding, P. and Qu, B., Synthesis of exfoliated PP/LDH nanocomposites via melt-intercalation: Structure, thermal properties, and photo-oxidative behaviour in comparison with PP/MMT nanocomposites, *Polym. Eng. Sci.* **46** (2006b) 1153–1159.

Ding, P. and Qu. B., Synthesis and characterization of polystyrene/layered double-hydroxide nanocomposites via in situ emulsion and suspension polymerization, *J. Appl. Polym. Sci.* **101** (2006a) 3758–3766.

Doyle, C.D., Estimating thermal stability of experimental polymers by empirical thermogravimetric analysis, *Anal. Chem.* **33** (1961) 77–79.

Drzal, L.T., Rich, M.J. and Lioyd, P.F., Adhesion of graphite fibers to epoxy matrices: I. The role of fiber surface treatment, *J. Adhes.* **16** (1983) 1–30.

Du, B., Guo, Z. and Fang, Z., Effects of organo-clay and sodium dodecyl sulfonate intercalated layered double hydroxide on thermal and flame behaviour of intumescent flame retarded polypropylene, *Polym. Degrad. Stab.* **94** (2009) 1979–1985.

Du, L., Qu, B. and Zhang, M., Thermal properties and combustion characterization of nylon 6/MgAl-LDH nanocomposites via organic modification and melt intercalation, *Polym. Degrad. Stab.* **92** (2007) 497–502.

Feitkneeht, W. and Gerber, M., Zur kenntnis der doppelhydroxyde und basischen doppelsalze III. Uber magnesium-aluminiumdoppelhydroxyd, *Helv. Chim. Acta*. **25** (1942) 131–137.

Flodin, A., Wear investigation of spur gear teeth, *Tribotest J.* **7** (2000) 45–60.

Flynn, J.H., The ‘temperature integral’–its use and abuse, *Thermochim. Acta*, **300** (1997) 83–92.

Fu, J. and Naguib, H.E., Effect of nanoclay on the mechanical properties of PMMA/clay nanocomposites foam, *J. Cell. Plas*. **42** (2006) 325–342.

Furrow, R.W. and Mabie, H.H., The measurement of static deflection in spur gear teeth, *Jnl. Mechanism.* **5** (1970) 147–168.

Garakani, A.K., Mehrnia, M.R., Mostoufi, N. and Sarrafzadeh, M.H., Analyze and control fouling in an airlift membrane bioreactor: CFD simulation and experimental studies, *Process Biochem*. **46** (2011) 1138–1145.

Garces, J.M., Moll, D.J., Bicerano, J., Fibiger, R. and Mcleod, D.G., Polymeric nanocomposites for automotive applications, *Adv. Mater*. **12** (2000) 1835–1839.

Garcia, M., Vliet, G.V., Jain, S.H., Chrauwen, B.A.G., Sarkissov, A.U., Vanzyl, W.E. and Boukamp, B.A., Polypropylene/SiO_2 nanocomposites with improved mechanical properties, *Rev. Adv. Mater. Sci.* **6** (2004) 169–175.

Genity, P.M.M., Hooper, J.J., Paynter, C.D., Riley, A.M., Nutbeem, C., Elton, N.J. and Adams, J.M., Nucleation and crystallization of polypropylene by mineral fillers: relationship to impact strength, J. *M. Polym.* **33** (1992) 5215–5224.

Goad, M.A., Rheological characterization of melt compounded polypropylene/clay nanocomposites, *Composites: Part B.* **42** (2011) 1044–1047.

Goel, A., Chawla, K.K., Vaidya, U.k., Chawla, N. and Koopman, M., Characterization of fatigue behaviour of long fibre reinforced thermoplastic (LFT) composites, *Mater. Charact.* **60** (2009) 537–544.

Gopakumar, T.G., Lee, J.A., Kontopoulou, M. and Parent, J.S., Influence of clay exfoliation on the physical properties of montmorillonite/polyethylene composites, *Polymer*. **43** (2002) 5483–5491.

Graessley, W.W., Polymer chain dimensions and the dependence of viscoelastic properties on concentration, molecular weight and solvent power, *Polymer*, **21** (1980) 258–262.

Graziano, F.R., Cohen, R.E. and Medalia, A.I., Rheology of concentrated suspensions of carbon black in low molecular weight vehicles, *Rheol. Acta.* **18** (1979) 640–656.

Guner, F.S., Baranak, M., Soytas, S. and Erciyes, A.T., Flow behavior of oil-modified polymer solution, *Prog. Org. Coat*. **50** (2004) 172–178.

Guo, S., Zhang, C., Peng, H., Wang, W. and Liu, T., Structural characterization, thermal and mechanical properties of polyurethane/CoAl layered double hydroxide nanocomposites prepared via in situ polymerization, *Compos. Sci. Technol.* **71** (2011) 791–796.

Guth, E., Theory of filler reinforcement, *J. Appl. Phy.***16** (1945) 20–25.

Gutierrez, C., Garcia, M.T., Curia, S., Howdle, S.M. and Rodriguez, J.F., The effect of CO_2 on the viscosity of polystyrene/limonene solutions, *J. Supercrit.* **88** (2014) 26–37.

Hajibeygi, M., Shabanian, M. and Ghallemohamadi, M.O., Development of new acid-imide modified Mg-Al/LDH reinforced semi-crystalline poly(amide-imide) containing naphthalene ring; study on thermal stability and optical properties, *Appl. Clay Sci*. **139** (2017) 9–19.

Hakimian, E. and Sulong, A.B., Analysis of warpage and shrinkage properties of injection-molded micro gears polymer composites using numerical simulations assisted by the Taguchi method, *Mater. Des.* **42** (2012) 62–71.

Hamed, S.B. and Belhadri, M., Rheological properties of biopolymers drilling fluids., *J. Petrol. Sci. Eng.* **67** (2009) 84–90.

He, F.A., Zhang, L.M., Yang, F., Chen, L.S. and Wu, Q., New nanocomposites based on syndiotactic polystyrene and organo-modified ZnAl layered double hydroxide, *J. Polym. Res.* **13** (2006) 483–493.

Herschel, W.H. and Bulkley, R., Konsistenzmessungen von Gummi-Benzollösungen, *Kolloid Z.* **39** (1926) 291–300.

Hoffmann, B., Kressler, J., Stoppelmann, G., Friedrich, C. and Kim G.M., Rheology of nanocomposites based on layered silicates and polyamide-12, *Colloid. Polym. Sci.* **278** (2000) 629–636.

Hohn, B.R., Michaelis, K. and Kreil, O., Influence of surface roughness on pressure distribution and flim thickness in EHl-contacts, *Tribol. Int.* **39** (2006) 1719–1725.

Hossan, M.R. and Hu Z., Strength evalution of polymer composite spur gear by finite element analysis, *Appl. Compos. Mater*. (2012). DOI: 10.1007/s10443–012–9274–7.

Hwu, J.M., Ko, T.H., Yang, W.T., Lin, J.C., Jiang, G.J., Xie, W. and Pan, W.P., Synthesis and properties of polystyrene-montmorillonite nanocomposites by suspension polymerization, *J. Appl. Polym. Sci.* **91** (2004) 101–109.

Jamshidian, M., Tehrany, E.A., Imran, M., Akhtar, M.J., Cleymand, F. and Desobry, S., Structural, mechanical and barrier properties of active PLA-antioxidant films, *J. Food Eng*. **110** (2012) 380–389.

Jang, B.N. and Wilkie, C.A., The thermal degradation of polystyrene nanocomposite, *Polymer*. **46** (2005) 2933–2942.

Johnson, T., (2013) http://composites.about.com./od/aboutcompositesplastics/a/History of Composites. 10/08/2013.

Kakati, K., Pugazhenthi, G. and Iyer, P.K., Effect of Organomodified Ni-Al layered double hydroxide (OLDH) on the properties of polypropylene (PP)/LDH nanocomposites, *J. Polym. Mater.* **61** (2012) 931–948.

Kanan, S. and Swamy, C.S., Synthesis and physicochemical characterization of cobalt aluminium hydrotalcite, *J. Mater. Sci. Lett.* **11** (1992) 1585-1587.

Kansal, G., Rao, P.N. and Atreya, S.K., Study: temperature and residual stress in an injection moulded gear, *J. Mater. Process. Technol.* **108** (2001)328–337.

Karamipour, S., Dehaghani, H.E., Ashouri, D. and Mousavian, S., Effect of nano $CaCO_3$ on rheological and dynamic mechanical properties of polypropylene: Experiments and models, *Polym. Test.* 30 (2011) 110–117.

Karimpour, M., Dearn, K.D. and Walton, D., A kinematic analysis of meshing polymer gear teeth, *Proc. IMechE Part L: J. Materials: Design and Applications.* **224** (2010) 101–115.

Kashiwagi, T., Mu, M., Winey, K. and Douglas, J., Relation between the viscoelastic and flammability of polymer nanocomposites, *Polymer*. **49** (2008) 4358–4368.

Kim, C.H., Durability improvement method for plastic spur gears, *Tribol. Int.* **39** (2006) 1454–1461.

Kim, J.Y., Choi, H.J., Kang, C.S. and Kim, S.H., Influence of modified carbon nanotube on physical properties and crystallization behavior of poly(ethylene terephthalate) nanocomposite, *Polym. Compos.* **31** (2010) 858–869.

Kim, S.H., Shin, M.C., Byun, J.W., Hwan, O.K. and Chu, C.N., Efficiency prediction of worn gear with plastic worm wheel, *Int. J. Precis. Eng. Man*. **13** (2012) 167–174.

Kim, T.H., Lim, S.T., Lee, C.H., Choi, H.J. and Jhon, M.S., Preparation and rheological characterization of intercalated polystyrene/organophilic montmorillonite nanocomposite, *J. Appl. Polym. Sci*. **87** (2003) 2106–2112.

Kirupasankar, S., Gurunathan, C. and Gnanamoorthy, R., Transmission efficiency of polyamide nanocomposites spur gears, *Mater. Des.* **39** (2012) 338–343.

Kleiss, R. and Kleiss, J., A Practical guide for molding better plastic geared transmissions, *Gear Technol.* **17** (2000) 27–31.

Kozai, N., Ohnuki, T. and Komarneni, S., Selenium oxyanions: highly selective up-take by a novel anion exchanger, *J. Mater. Res.* **17** (2002) 2993–2996.

Krevelen, D.W.V., Properties of Polymers, Elsevier Sciences Publishers. (1990).

Krikorian, V. and Pochan, D.J. Poly (L-Lactic Acid)/layered silicate nanocomposite: fabrication, characterization, and properties, *Chem. Mater.* **15** (2003) 4317–4324.

Kuila, T., Bose, S., Khanra, P., Kim, N.H., Rhee, K.Y. and Lee, J.H., Characterization and properties of in situ emulsion polymerized poly(methyl methacrylate)/graphene nanocomposites, *Composites Part A.* **42** (2011) 1856–1861.

Kuila, T., Acharya, H., Srivastava, S.K. and Bhowmick, A.K., Synthesis and characterization of ethyl vinyl acetate/Mg-Al layered double hydroxide nanocomposites, *J. Appl. Polym. Sci.* **104** (2007) 1845–1851.

Kumar, M., Chaudhary, V., Suresh, K. and Pugazhenthi, G., Synthesis and characterization of exfoliated PMMA/Co-Al LDH nanocomposites via solvent blending technique, *RSC Adv.* **5** (2015) 39810–39820.

Kumar, M., Kumar, V., Upadhyaya, P. and Pugazhenthi, G., Fabrication of poly(methyl methacrylate) (PMMA) nanocomposites with modified nanoclay by melt intercalation, *Compos. Interfaces.* **21** (2014) 819–832.

Kumar, T.P.S., Kumar, S.S. and Naveen, J., Glass fiber-reinforced polymer composites-a review, *J. Reinf. Plast.* **33** (2014) 1258–1275.

Kumar, V., Kumar, M. and Pugazhenthi, G., Effect of nanoclay content on the structural, thermal properties and thermal degradation kinetics of PMMA/organoclay nanocomposites, *Int. J. Nano Biomater*. **5** (2014) 27–44.

Kundu, P.P. and Kundu, M., Effect of salts and surfactant and their doses on the gelation of extremely dilute solutions of methyl cellulose, *Polymer*. **42** (2001) 2015–2020.

Kurahatti, R.V., Surendranathan, A.O., Kori, S.A., Singh, N., Kumar, A.V.R. and Srivastava, S., Defence applications of polymer nanocomposites, *Def. Sci. J*. **60** (2010) 551–563.

Kurokawa, M., Uchiyama, Y. and Nagai, S., Performance of plastic gear made of carbon fibre reinforced poly-ether-ether-ketone, *Tribol. Int.* **32** (2003) 491–497.

Kurokawa, M., Uchiyama, Y. and Nagai, S., Performance of plastic gear made of carbon fibre reinforced poly-ether-ether-ketone: Part 2, *Tribol. Int.* **33** (2000) 715–721

Kurokawa, M., Uchiyama, Y. and Nagai, S., Tribological properties and gear performance of polyoxymethylene composites, *J. Tribol.* **122** (2000) 809–814.

Kurokawa, M., Uchiyama, Y., Iwai, T. and Nagai, S., Performance of plastic gear made of carbon fiber reinforced polyamide 12, *Wear*. **254** (2003) 468–473.

Leroux, F. and Besse, J.P., Polymer interleaved layered double hydroxide: a new emerging class of nanocomposites, *Chem. Mater*. **13** (2001) 3507–3515.

Leroux, F., Pagano, M.A., Intissar, M., Chauviere, S., Rorano, C. and Besse, J.P., Delamination and restacking of layered double hydroxides, *J. Mater. Chem.* **11** (2001) 105–112.

Li, B., Hu, Y., Liu, J., Chen, Z. and Fan, W., Preparation of poly (methyl methacrylate)/LDH nanocomposite by exfoliation-adsorption process, *Colloid Polym. Sci.* **281** (2003) 998–1001.

Li, J.H., Hong, R.Y., Li, M.Y., Li, H.Z., Zheng, Y. and Ding, J., Effects of ZnO nanoparticles on the mechanical and antibacterial properties of polyurethane coatings, *Prog.Org. Coat.* **64** (2009) 504–509.

Li, W., Wood, A., Weidig, R. and Mao, K., An investigation on the wear behaviour of dissimilar polymer gear engagements, *Wear*. **271** (2011) 2176–2183.

Lim, Y.T. and Park, O.O., Phase morphology and rheological behavior of polymer/layered silicate nanocomposites, *Rheol. Acta.* **40** (2001) 220–229.

Limpanart, S., Khunthon, S., Taepaiboon, P., Supaphol, P., Srikhirin, T., Udomkichdecha, W. and Boontongkong, Y., Effect of the surfactant coverage on the preparation of polystyrene-clay nanocomposites prepared by melt intercalation, *Mater. Lett*. **59** (2005) 2292–2295.

Lin, A.D. and Kuang, J.H., Dyanamic interaction between contact loads and tooth wear of engaged plastic gear pairs, *Int. J. Mech.* **50** (2008) 205–213.

Liu, Z., Ma, R., Osada, M., Iyi, N., Ebina, Y., Takada, K. and Sasaki, T., Synthesis, Anion exchange, and delamination of Co-Al layered double hydroxide: Assembly of the exfoliated nanosheet/polyanion composite films and magneto-optical studies, *J. Am. Chem. Soc.* **128** (2006) 4872–4880.

Lv, S., Zhou, W., Miao, H. and Shi, W., Preparation and properties of polymer/LDH nanocomposites used for UV curing coatings, *Prog. Org. Coat.* **65** (2009) 450–456.

Ma, S., Hill, J.O. and Heng, S., A kinetic analysis of the pyrolysis of some australian coals by non-isothermal thermogravimetry, *J. Therm. Anal. Calorim.* **37** (1991) 1161–1177.

Majid, M., Hassan, E.D., Davoud, A. and Saman, M., A study on the effect of nano-ZnO on rheological and dynamic mechanical properties of polypropylene: Experiments and models, *Composites Part B.* **42** (2011) 2038–2046.

Majoni, S.J., Thermal and flammability study of polystyrene composites containing magnesium-aluminum layered double hydroxide (MgAl-C_{16} LDH), and an organophosphate, *J. Therm. Anal. Calorim.* **120** (2015) 1435–1443.

Mallakpour, S. and Dinari, M., Intercalation of amino acid containing chiral dicarboxylic acid between Mg–Al layered double hydroxide, *J. Therm. Anal. Calorim.* **119** (2015)1123–1130.

Mallakpour, S. and Dinari, M., Structural characterization and thermal properties of chiral poly(amide-imide)/modified MgAl layered double hydroxide nanocomposites prepared via solution intercalation, *Polym. Plast. Technol. Eng.* **53** (2014)) 1047–1055.

Manzi-Nshuti, C., Wang, D., Hossenlopp, J.M. and Wilkie, C.A., The role of the trivalent metal in an LDH: Synthesis, characterization and fire properties of thermally stable PMMA/LDH systems, *Polym. Degrad. Stab.* **94** (2009) 705–711.

Marcotte, M., Taherian, A.R., Trigui, M. and Ramaswamy, H.S., Evaluation of rheological properties of selected salt enriched food hydrocolloids, *J. Food Eng*. **48** (2001) 157–167.

Marshek, K.M. and Chan, P.K.C., Qualitative analysis of plastic worm and worm gear failures, *Wear*. **66** (1981) 261–271.

Marshek, K.M. and Chan, P.K.C., Wear damage to plastic worms and gears, *Wear*. **44** (1977) 405–409.

Matsumoto, T., Hitomi, C. and Onogi, S., Rheological properties of disperse systems of spherical particles in polystyrene solution at long time-scales, *T. Soc. Rheol.* **19** (l975) 541–555.

Matusinovic, Z., Lu , H. and Wilkie, C.A., The role of dispersion of LDH in fire retardancy: The effect of dispersion on fire retardant properties of polystyrene/Ca-Al layered double hydroxide nanocomposites, *Polym. Degrad. Stab.* **97** (2012) 1563–1568.

Matusinovic, Z., Rogosic, M. and Sipusic, J., Synthesis and characterization of poly(styrene-co-methyl methacrylate)/layered double hydroxide nanocomposites via in situ polymerization, *Polym. Degrad. Stab.* **94** (2009) 95–101.

Mertens, A.J. and Senthilvelan, S., Surface durability of injection-moulded carbon nanotube–polypropylene spur gears, *Proc IMechE Part L: J Materials: Design and Applications.* (2016) 1-13. DOI: 10.1177/1464420716654308.

Mitchell, C.A. and Krishnamoorti, R., Rheological properties of diblock copolymer/layered-silicate nanocomposites, *J. Polym. Sci. Part B: Polym. Phys*. **40** (2002) 1434–1443.

Mittal, V., Mechanical and gas permeation properties of compatibilized propylene-layered silicate nanocomposites, *J. Appl. Polym. Sci.* **107** (2008) 1350–1361.

Mittal, V., Polymer layered silicate nanocomposites: A review, *Materials*. **2** (2009) 992–1057.

Miyata, S. and Okada, A., Synthesis of hydrotalcite-like compounds and their physico-chemical properties The systems Mg^{2+} -Al^{3+}-SO_4^{2-} and Mg^{2+}-Al^{3+}-CrO_4^{2-}, *Clays Clay Miner*. **23** (1977) 14–18.

Moet, A.S. and Akelah, A., Polymer-clay nanocomposites: polystyrene grafted onto montmorillonite interlayers, *Mater. Lett.* **18** (1993) 97–102.

Mohanty, S. and Nayak, S.K., Effect of organo-modified silicates on the properties of poly(methyl methyacryalte) nanocomposites, *J. Thermoplast. Compos. Mater*. **23** (2010) 623–645.

Morgan, A.B. and Gilman, J.W., Characterization of polymer-layered silicate (clay) nanocomposites by transmission electron microscopy and X-ray diffraction: A comparative study, *J. Appl. Polym. Sci.* **87** (2003) 1329–1338.

Motahari, S., Kafashi, B., Taranehjoo, S. and Sarrafi, M., PMMA/polyamide 6/silica ternary nanocomposites; Investigation of dynamic rheology, crystallization and blend phase morphology, *Can. J. Envr. Cons. Civ. Engg.* **3** (2012) 80–93.

Najafi, N., Heuzey, M.C. and Carreau, P.J., Poly(lactic acid)-clay nanocomposites prepared by melt compounding in the presence of chain extender, *Compos. Sci. Technol*. **72** (2012) 608–615.

Nindo, C.I., Tang, J., Powers, J.R. and Takhar, P.S., Rheological properties of blueberry puree for processing application, *LWT-Food Sci. Tech*. **40** (2007) 292–299.

Noh, M.W. and Lee, D.C., Synthesis and characterization of PS-clay nanocomposite by emulsion polymerization, *Polym. Bull*. **42** (1999) 619–626.

Nyambo, C., Chen, D., Su, S. and Wilkie, C.A., Variation of benzyl anions in MgAl-layered double hydroxides: Fire and thermal properties in PMMA, *Polym. Degrad. Stab*. **94** (2009) 496–505.

Nyambo, C., Songtipya, P., Manias, E., Gasco, M.M.J. and Wilkie, C.A., Effect of MgAl-layered double hydroxide exchanged with linear alkyl carboxylates on fire-retardancy of PMMA and PS, *J. Mater. Chem*. **18** (2008) 4827–4838.

Ohta, Y., Suciyama, H. and Yasuda, H., Short branch effects on the creep properties of the ultra-high strength polyethylene fibers, *J. Polym. Sci., Part B: Polym. Phys*. **32** (1994) 261–269.

Okada, A. and Usuki, A., Twenty years of polymer-clay nanocomposites, *Macro. Mater. Eng*. **291** (2006) 1449–1476.

Okamoto, M., Morita, S., Taguchi, H., Kim, Y.H., Kotaka, T. and Tateyama, H., Synthesis and structure of smectic clay/poly(methyl-methacrylate) and clay polystyrene nanocomposites via in situ intercalative polymerization, *Polymer*. **41** (2000) 3887–3890.

Palmer, S.J., Frost, R.L. and Nguyen, T., Hydrotalcites and their role in coordination of anions in Bayer liquors: Anion binding in layered double hydroxides, *Coord. Chem. Rev*. **253** (2009) 250–267.

Park, S.J., Li, K. and Hong, S.K., Preparation and characterization of layered silicate-modified ultrahigh-molecular-weight polyethylene nanocomposites, *J. Ind. Eng. Chem*. **11** (2005) 561–566.

Paul, P.K., Hussain, S.A., Bhattacharjee, D. and Pal, M., Preparation of polystyrene-clay nanocomposite by solution intercalation technique, *Bull. Mater. Sci.* **36** (2013) 361–366.

Penga, H., Han, Y., Liu, T., Tjiu, W.C. and He, C., Morphology and thermal degradation behavior of highly exfoliated CoAl-layered double hydroxide/poly-caprolactone nanocomposites prepared by simple solution intercalation, *Thermochim. Acta.* **502** (2010) 1–7.

Pereira, C.M.C., Herrero, M., Labajos, F.M., Marques, A.T. and Rives, V., Preparation and properties of new flame retardant unsaturated polyester nanocomposites based on layered double hydroxides, *Polym. Degrad. Stab.* **94** (2009) 939–946.

Perez, R., Rojo, E., Fernandez, M., Leal, V., Lafuente, P. and Santamaria, A., Basic and applied rheology of m-LLDPE/LDPE blends: Miscibility and processing features, *Polymer*. **46** (2005) 8045–8053.

Plank, J., Zhimin, D., Keller, H., Hossle, F. and Seidl, W., Fundamental mechanisms for polycarboxylate intercalation into C_3A hydrate phases and the role of sulfate present in cement, *Cem. Concr. Res*. **40** (2010) 45–57.

Pogacnik, A. and Tavcar, J., An accelerated multilevel test and design procedure for polymer gears, *Mater. Des.* **65** (2015) 961–973.

Potschke, P., Fornes, T.D. and Paul, D.R., Rheological behavior of multiwalled carbon nanotube/polycarbonate composites, *Polymer*. 43 (2002) 3247–3255.

Pradhan, S., Costa, F.R., Wagenknecht, U., Jehnichen, D., Bhowmick, A.K. and Heinrich, G., Elastomer/LDH nanocomposites: Synthesis and studies on nanoparticle dispersion, mechanical properties and interfacial adhesion, *Eur. Polym. J.* **44** (2008) 3122–3132.

Qiu, J. and Villemure, G., Anionic clay modified electrodes: electron transfer mediated by electroactive nickel, cobalt or manganese sites in layered double hydroxide films, *J. Electroanal. Chem*. **428** (1997) 165–172.

Qiu, L. and Qu, B., Preparation and characterization of surfactant-free polystyrene/layered double hydroxide exfoliated nanocomposite via soap-free emulsion polymerization, *J. Colloid Interface Sci.* **301** (2006) 347–351.

Qiu, L. Chen, W. and Qu, B., Structural characterisation and thermal properties of exfoliated polystyrene/ZnAl layered double hydroxide nanocomposites prepared via solution intercalation, *Polym. Degrad. Stab.* **87** (2005) 433–440.

Rahim, J.W., Hong, S.L. and Ha, C.S., Tensile, water vapor barrier and antimicrobial properties of PLA/clay composites films, *Food Sci. Technol.* **42** (2009) 612–617.

Rao, M.A. and Steffe, J.F., Viscoelastic properties of foods, Elsevier Applied Science, London 1992.

Raquez, J.M., Habibi, Y., Murariu, M. and Dubois, P., Polylactide (PLA)-based nanocomposites, *Prog. Polym. Sci.* 38 (2013) 1504–1542.

Rawase, Y., Araki, T., Shimizu, K. and Miura, H., Liquid mass transfer in three-phase stirred tank reactors: Newtonian and non-newtonian fluids, *Can. J. Chem. Eng.* **75** (1997) 1159–1164.

Ray S.S. and Okamoto M., Polymer/layered silicate nanocomposites: A review from preparation to processing, *Prog. Polym. Sci*. **28** (2003) 1539–1641.

Ray, S.S., Maiti, P., Okamoto, M., Yamada, K. and Ueda, K., New polylactide/layered silicate nanocomposites. 1. Preparation, characterization, and properties, *Macromolecules.* **35** (2002) 3104–3110.

Realinho, V., Antunes, M., Arencon, D., Fernandez, A.I. and Velasco, J.I., Effect of a dodecylsulfate-modified magnesium-aluminum layered double hydroxide on the morphology and fracture of polystyrene and poly(styrene-co-acrylonitrile) composites, *J. Appl. Polym. Sci.* **111** (2009) 2574–2583.

Reiner, V.M., Ueber die Strömung einer elastischen Flüssigkeit durch eine Kapillare, *Kolloid Z.* **39** (1926) 80–87.

Rosenberger, S., Kubin, K. and Kraume, M., Rheology of activated sludge in membrane bioreactors, *Eng Life Sci*. **2** (2002) 269–275.

Sahu, B. and Pugazhenthi, G., Properties of polystyrene/organically modified layered double hydroxide nanocomposites synthesized by solvent blending method, *J. Appl. Polym. Sci*. **120** (2011) 2485–2495.

Sandford, P. and Baird, J., The polysaccharides (Vol.2), Academic Press, New York 1983.

Senthilvelan, S. and Gnanamoorthy, R., Damage mechanisms in injection molded unreinforced, glass and carbon reinforced nylon 66 spur gears, *Appl. Compos. Mater*. **11** (2004a) 377–397.

Senthilvelan, S. and Gnanamoorthy, R., Damping characteristics of unreinforced, glass and carbon fibre reinforced nylon 6/6 spur gears, *Polym. Test.* **25** (2006a) 56–62.

Senthilvelan, S. and Gnanamoorthy, R., Effect of rotational speed on the performance of unreinforced and glass fiber reinforced Nylon 6 spur gears, *Mater. Des.* **28** (2007) 765–772.

Senthilvelan, S. and Gnanamoorthy, R., Efficiency of injection-moulded polymer composite spur gears. *Proc inst mech Eng. Part J: J. Eng. Tribol.* **223** (2009) 925–928.

Senthilvelan, S. and Gnanamoorthy, R., Fiber reinforcement in injection molded nylon 6/6 spur gears, *Appl. Compos. Mater.* **13** (2006b) 237–248.

Senthilvelan, S. and Gnanamoorthy, R., Wear characteristics of injection-moulded in filled and glass-filled nlon 6 spur gears, *Proc. Inst. Mech. Eng. Part J: J. Eng Tribol.* **218** (2004b) 495–502.

Senum, G.I. and Yang, R.T., Rational approximations of the integral of Arrhenius function, *J. Therm. Analy*. **11** (1977) 445–447.

Sharma, S.K. and Nayak, S.K., Surface modified clay/polypropylene (PP) nanocomposites: Effect on physico-mechanical, thermal and morphological properties, *Polym. Degrad. Stab.* **94** (2009) 132–138.

Shigley, E.J. and Mischke, C.R., Mechanical engineering design, Sixth ed., McGraw-Hill, New York, 2001.

Silva, A.L.N., Rocha M.C.G., Coutinho F.M.B., Bretas, R. and Carlos, S., Rheological and morphological properties of blends based on ethylene-octene copolymer and polypropylene, *Polym. Test*. **19** (2000) 363–371.

Sisko, A.W., The flow of lubricating greases, *Ind. Eng. Chem*. 50 (1958) 1789-1792.

Solomon, M.J., Almusallam, A.S., Seefeldt, K.F., Omwangthanaroj, S.A. and Varadan, P., Rheology of polypropylene/clay hybrid materials, *Macromolecules*, **34** (2001) 1864–1872.

Song, W., Zheng, Z., Tang, W. and Wang, X., A facile approach to covalently functionalized carbon nanotubes with biocompatible polymer, *Polymer*. **48** (2007) 3658–3663.

Suin, S., Maiti, S., Shrivastava, N.K. and Khatua, B.B., Mechanically improved and optically transparent polycarbonate/clay nanocomposites using phosphonium modified organoclay, *Mater. Des.* **54** (2014) 553–563.

Taburdagitan, M. and Akkok, M., Determination of surface temperature rise with thermo-elastic analysis of spur gears, *Wear*. **216** (2006) 656–665.

Tai, Q. Chen, L., Song, L., Hu, Y. and Yuen, R.K.K., Effects of a phosphorus compound on the morphology, thermal properties, and flammability of polystyrene/MgAl-layered double hydroxide nanocomposites, *Polym. Compos.* **32** (2011) 168–176.

Takagi, K., Shichi, T., Usami, H. and Sawaki, Y., Controlled photocycloaddition of unsaturated carboxylates intercalated in hydrotalcite clay interlayers, *J. Am. Chem. Soc*. **115** (1993) 4339–4344.

Tanniru, M., Yuan, Q. and Misra, R.D.K., On significant retention of impact strength in clay-reinforced high-density polyethylene (HDPE) nanocomposites, *Polymer*. **47** (2006) 2133–2146.

Teisuke, B., Hiroshi, S. and Taku, A., Wear of plastic spur gear made by injection molding, *J. Jpn. Soc. Tribologis.* **46** (2001) 889–896.

Trujillano, R., Holgado, M.J., Pigazo, F. and Rives, V., Preparation, physicochemical characterization and magnetic properties of Cu-Al layered double hydroxides with CO_3^{2-} and anionic surfactants with different alkyl chains in the interlayer, *Physica B*, **373** (2006) 267–273.

Tsukamoto, N., Argument on plastic gears for power transmission, *JSME Int J., Ser. C.* **38** (1995) 1–8.

Tung, C.M. and Dynes, P.J., Morphological characterization of polyetheretherketone-carbon fiber composites, *J. Appl. Polym. Sci.* **33** (1987) 505–520.

Tzanakis, I., Conte, M., Hadfield, M. and Stolarski, T.A., Experimental and analytical thermal study of PTFE composite sliding against high carbon steel as a function of the surface roughness, sliding velocity and applied load, *Wear.* **303** (2013) 154–168.

Unnikrishnan, L., Mohanty, S., Nayak, S.K. and Ali, A., Preparation and characterization of poly(methyl methacrylate)-clay nanocomposites via melt intercalation: Effect of organoclay on thermal, mechanical and flammability properties, *Mat. Sci. Eng., A.* **528** (2011) 3943–3951.

Urbanovici, E., Popescu, C. and Segal, E., Improved iterative version of the Coats-Redfern method to evaluate non-isothermal kinetic parameters, *J. Therm. Anal. Calorim.* **58** (1999) 683–700.

Uthirakumar, P., Hahn, Y.B., Nahm, K.S. and Lee, Y., Exfoliated high-impact polystyrene/MMT nanocomposites prepared using anchored cationic radical initiator-MMT hybrid, *Eur. Polym. J.* **41** (2005a) 1582–1588.

Uthirakumar, P., Song, M.K., Nah, C. and Lee, Y.S., Preparation and characterization of exfoliated polystyrene/clay nanocomposites using a cationic radical initiator-MMT hybrid, *Eur. Polym. J.* **41** (2005b) 211–217.

Valandro, S.A., Poli, A.L., Neumann, M.G. and Schimtt, C.C., Organomontmorillonite/ poly(methyl methacrylate) nanocomposites prepared by in-situ photopolymerization. Effect of the organoclay on the photooxidative degradation, *Appl. Clay Sci.* **85** (2013) 19–24.

Voilley, A., Encapsulation and controlled release of food ingredients, American Chemical Society, Washington 1995.

Wanchoo, R.K., Sharma, S.K. and Bansal, R., Rheological parameters of some water soluble polymers, *J. Polym. Mater.* **13** (1996) 49–55.

Wang, B. and Huang, H.X., Effects of halloysite nanotube orientation on crystallization and thermal stability of polypropylene nanocomposites, *Polym. Degrad. Stab.* **98** (2013) 1601–1608 .

Wang, D.Y., Das, A., Leuteritz, A., Boldt, R., Haußler, L., Wagenknecht, U. and Heinrich, G., Thermal degradation behaviors of a novel nanocomposite based on polypropylene and Co-Al layered double hydroxide, *Polym. Degrad. Stab.* **96** (2011b) 285–290.

Wang, G., Wang, C.C. and Chen, C.Y., The disorderly exfoliated LDHs/PMMA nanocomposites synthesized by in-situ bulk polymerization: The effects of LDH-U on thermal and mechanical properties, *Polym. Degrad. Stab.* **91** (2006) 2443–2450.

Wang, G.H. and Zhang, L.M., Reinforcement in thermal and viscoelastic properties of polystyrene by in-situ incorporation of organophilic montmorillonite, *Appl. Clay Sci.* **38** (2007) 17–22.

Wang, H.W., Chang, K.C., Yeh, J.M. and Liou, S.J., Synthesis and dielectric properties of polystyrene-clay nanocomposite materials, *J. Appl. Polym. Sci.* **91** (2004) 1368–1373.

Wang, L., Su, S., Chen, D. and Wilkie, C.A., Variation of anions in layered double hydroxides: Effects on dispersion and fire properties, *Polym. Degrad. Stabil.* **94** (2009) 770–781.

Wang, Q., Wu, Z., Tay, H.H., Chen, L., Liu, Y., Chang, J., Zhong, Z., Luo, J. and Borgna, A., High temperature adsorption of CO_2 on Mg-Al hydrotalcite: effect of the charge compensating anions and the synthesis pH, *Catal. Today*. **164** (2011a) 198–203.

Wang, Q., Zhang, X., Wang, C.J., Zhu, J., Guo, Z. and O'Hare, D., Polypropylene/layered double hydroxide nanocomposites, *J. Mater. Chem*. **22** (2012) 19113–19121.

Wang, Z., Du, X., Yu, H., Jiang, Z., Liu, J. and Tang, T., Mechanism on flame retardancy of polystyrene/clay composites-The effect of surfactants and aggregate state of organoclay, *Polymer*. **50** (2009) 5794–5802.

Weale, D.J., White, J. and Walton, D., The effect of fiber orientation and distribution on the tooth stiffness of a polymer composite gear, *J. Reinf. Plast. Compos.* **18** (1999) 454–463.

Wei, S., Sampathi, J., Guo, Z., Anumandla, N., Rutman, D., Kucknoor, A., James, L. and Wang, A., Nanoporous poly(methyl methacrylate)-quantum dots nanocomposite fibers toward biomedical applications, *Polymer*, **52** (2011) 5817–5829.

Wieleba, W., The statistical correlation of friction and wear rate of PTFE composites with steel counterface roughness and hardness, *Wear*. **252** (2002) 719–729.

Wright, N.A. and Kukureka, S., Wear testing and measurement techniques for polymer composite gears, *Wear*. **251** (2001) 1567–1578.

Wu, B., Wang, Y.Z., Wang, X.L., Yang, K.K., Jin, Y.D. and Zhao, H., Kinetics of thermal oxidative degradation of phosphorus-containing flame retardant copolyesters, *Polym. Degrad. Stab.* **76** (2002) 401–409.

Xie, W., Gao, Z., Liu, K., Pan, W.P., Vaia, R., Hunter, D. and Singh, A., Thermal characterization of organically modified montmorillonite, *Thermochim. Acta*. **367-368** (2001) 339–350.

Yamagata, S., Hamba, Y., Akasaka, T., Ushijima, N., Uo, M., Lida, J. and Watari, F., The effect of enhancing the hydrophobicity of OMMT on the characteristics of PMMA/OMMT nanocomposites, *Appl. Surf. Sci.* **262** (2012) 56–59.

Yano, K., Usuki, A. and Okada, A., Synthesis and properties of polyimide-clay hybrid films, *J. Polym. Sci. Part A Polym. Chem.* **35** (1997) 2289–2294.

Yeh, J.M., Liou, S.J., Lin, C.G., Chang, Y.P., Yu, Y.H. and Cheng, C.F., Effective enhancement of anticorrosive properties of polystyrene by polystyrene-clay nanocomposite materials, *J. Appl. Polym. Sci.* **92** (2004) 1970–1976.

Yilmazer, U. and Ozden, G., Polystyrene-organoclay nanocomposites prepared by melt intercalation, in Situ, and masterbatch methods, *Polym. Compos*. **27** (2006) 249–255.

You, Y.W., Zhao, H.T. and Vance, G.F., Adsorption of dicamba (3,6-dichloro-2-methoxy benzoic acid) in aqueous solution by calcined-layered double hydroxide, *Appl. Clay Sci*. **21** (2002) 217–226.

Yousef, S.S., Burns, D.J. and Mckinlay, W., Techniques for assessing the running temperature and fatigue strength of thermoplastic gears, *Mechanisms and Machine Theory*. **8** (1973) 175–185.

Yuan, J.M., Fan, Z.F., Chen, X.H., Chen, X.H., Wu, Z.J. and He, L.P., Preparation of polystyrene–multiwalled carbon nanotube composites with individual-dispersed nanotubes and strong interfacial adhesion, *Polymer*. **50** (2009) 3285–3291.

Zakaria, M.B. and Rahman, Z.Ab., Rheological properties of cashew gum, *Carbohydr. Polym.* **29** (1996) 25–27.

Zare, Y., Effects of imperfect interfacial adhesion between polymer and nanoparticles on the tensile modulus of clay/polymer nanocomposites, *Appl Clay Sci*. **129** (2016) 65–70.

Zhang, M., Ding, P., Du, L. and Qu, B., Structural characterization and related properties of EVA/ZnAl-LDH nanocomposites prepared by melt and solution intercalation, *Mater. Chem. Phys.* **109** (2008) 206–211.

Zhang, W.A., Chen, D.Z., Xu, H.Y., Shen, X.F. and Fang, Y.E., Influence of four different types of organophilic clay on the morphology and thermal properties of polystyrene/clay nanocomposites prepared by using the γ-ray irradiation technique, *Eur. Polym. J.* **39** (2003) 2323–2328.

Zhao, C., Qin, H., Gong, F., Feng, M., Zhang, S. and Yang, M., Mechanical, thermal and flammability properties of polyethylene/clay nanocomposites, *Polym. Degrad. Stab.* **87** (2005) 183–189.

Zhao, H., Wang, Y.Z., Wang, D.Y., Wu, B., Chen, D.Q., Wang, X.L. and Yang, K.K., Kinetics of thermal degradation of flame retardant copolyesters containing phosphorus linked pendent groups, *Polym. Degrad. Stab.* **80** (2003) 135–140.

Zhu, J., Morgan, A.B., Lamelas, F.J. and Wilkie, C.A., Fire Properties of polystyrene-clay nanocomposites, *Chem. Mater*. **13** (2001) 3774–3780.

Zidelkheir, B., Boudjemaa, S., Goad, M.A. and Djellouli, B., Preparation and characterization of polystyrene/montmorillonite nanocomposite by melt intercalative compounding, *Iran. Polym. J.* **15** (2006) 645–653.

List of Publications

In Journals:

1. **Kelothu Suresh**, Manish Kumar, G. Pugazhenthi and R. Uppaluri, Enhanced mechanical and thermal properties of polystyrene (PS) nanocomposites prepared using modified Ni-Al layered double hydroxide (LDH) via melt intercalation technique, *Journal of Science: Advanced Materials and Devices*, 2 (2017) 245–254.
2. **Kelothu Suresh**, G. Pugazhenthi and R. Uppaluri, Properties of polystyrene (PS)/Co-Al LDH nanocomposites prepared by melt intercalation, *Materials Today: Proceedings* (Accepted).
3. **Kelothu Suresh**, R. Vinoth Kumar, Manish Kumar, M. Jeyapriya, R. Anbarasan and G. Pugazhenthi, Sonication-assisted synthesis of polystyrene (PS)/organoclay nanocomposites: influence of clay content, *Applied Nanoscience*, 7 (2017) 215–223.
4. **Kelothu Suresh**, Rijumoni Boro, R. Vinoth Kumar and G. Pugazhenthi, Effect of concentration and temperature on rheological behaviour of polystyrene solution, *Macromolecular Symposia*, 362 (2016) 87–100.
5. **Kelothu Suresh**, R. Vinoth Kumar and G. Pugazhenthi, Processing and characterization of polystyrene nanocomposites based on Co-Al layered double hydroxide, *Journal of Science: Advanced Materials and Devices*, 1 (2016) 351–361.
6. Payel Sen, **Kelothu Suresh**, R. Vinoth Kumar, Manish Kumar and G. Pugazhenthi, A simple solvent blending coupled sonication technique for synthesis of polystyrene (PS)/multi-walled carbon nanotube (MWCNT) nanocomposites: Effect of modified

MWCNT content, *Journal of Science: Advanced Materials and Devices*, 1 (2016) 311–323.

7. Samarshi Chakraborty, Manish Kumar, **Kelothu Suresh** and G. Pugazhenthi, Investigation of structural, rheological and thermal properties of PMMA/ONi-Al LDH nanocomposites synthesized via solvent blending method: Effect of LDH loading, *Chinese Journal of Polymer Science*, 34 (2016) 739–754.
8. Manish Kumar, Vivek Chaudhary, **Kelothu Suresh** and G. Pugazhenthi, Synthesis and characterization of exfoliated PMMA/Co-Al LDH nanocomposites via solvent blending technique, *RSC Advances*, 5 (2015) 39810–39820.
9. Samarshi Chakraborty, Manish Kumar, **Kelothu Suresh** and G. Pugazhenthi, Influence of organicallymodified Ni-Al layered double hydroxide (LDH) loading on the rheological properties of poly (methyl methacrylate) (PMMA)/LDH blend solution, *Powder Technology*, 256 (2014) 196–203.
10. **Kelothu Suresh**, R. Vinoth Kumar, Rijumoni Boro, Manish Kumar and G. Pugazhenthi, Rheological behavior of polystyrene (PS)/Co-Al layered double hydroxide (LDH) blend solution obtained through solvent blending route: Influence of LDH loading and temperature, *Materials Today: Proceedings* (Revised manuscript submitted).
11. **Kelothu Suresh**, R. Vinoth Kumar, Manish Kumar, Ritu Rajkumar Surin and G. Pugazhenthi, A Simple Sonication Assisted Solvent Blending Route for Fabrication of Exfoliated Polystyrene (PS)/Clay Nanocomposites: Role of Various Clay Modifiers, *Materials Today: Proceedings* (Revised manuscript submitted).

12. **Kelothu Suresh**, R. Vinoth Kumar, G. Pugazhenthi and R. Uppaluri, Effect of nanofiller loading on the structural, thermal and rheological characteristics of PS/S-LDH nanocomposites, *Applied Nanoscience* (Under Review).
13. **Kelothu Suresh**, R. Vinoth Kumar and G. Pugazhenthi, Effect of organically modified Co-Al and Ni-Al layered double hydroxides on the melt rheological properties of polystyrene nanocomposites, *Materials Today: Proceedings* (Under Review).
14. **Kelothu Suresh**, Alexis Johnney Mertens, Selvaraj Senthilvelan, R. Uppaluri, G. Pugazhenthi, Injection-moulded polystyrene/Layered double hydroxides nanocomposites spur gears performance, *Nano-Structure & Nano-Objects* (Under Review).

In Conferences:

1. **Kelothu Suresh,** R. Vinoth Kumar, Manish Kumar, Ritu Rajkumar Surin and G. Pugazhenthi, A Simple Sonication Assisted Solvent Blending Route for Fabrication of Exfoliated Polystyrene (PS)/Clay Nanocomposites: Role of Various Clay Modifiers, International Conference of Materials, Manufacturing and Modelling (**ICMMM-2017**), 9-11 March 2017, Vellore, Tamilnadu, India.
2. **Kelothu Suresh**, Alexis Johnney Mertens, Selvaraj Senthilvelan, R. Uppaluri and G. Pugazhenthi, Injection-moulded Polystyrene/Layered Double Hydroxides Nanocomposites Spur Gear Performace, International Conference on Nanostructured Materials and Nanocomposites **(ICNM-2017)**, 10-12 February 2017, Kottayam, Kerala, India.

3. **Kelothu Suresh**, R. Vinoth Kumar and G. Pugazhenthi, Effect of organically modified Co-Al and Ni-Al layered double hydroxides on the melt rheological properties of polystyrene nanocomposites, Hybrid and Composite Materials, Chemical Processing **(HCMCP-2016)**, 25-27 October 2016, Hyderabad, Telangana, India.
4. **Kelothu Suresh**, R. Vinoth Kumar, Rijumoni Boro, Manish Kumar and G. Pugazhenthi, Rheological Behavior of Polystyrene (PS)/Co-Al Layered Double Hydroxide (LDH) Blend Solution obtained Through Solvent Blending Route: Influence of LDH Loading and Temperature, International Conference on processing of materials, Minerals and Energy **(PMME-2016)**, 29-30 July 2016, Ongole, Andhrapradesh, India.
5. **Kelothu Suresh**, G. Saranya, M. Kaviya , S. Sowmiya , P. Abinaya sri , Manish Kumar, Payel Sen, R. Anbarasan and G. Pugazhenthi, Effect of Co-Al LDH Loading on Rheological Behaviour of Polyvinyl Alcohol (PVA)/LDH Solutions, **CHEMCON-2015**, 27-30 December 2015, Guwahati, Asaam, India.
6. Payel Sen, **Kelothu Suresh** and G. Pugazhenthi, Effect of modified Muti-walled Carbon Nanotubes (MWCNT) on the properties of Polystyrene/MWCNT nanocomposites, **CHEMCON-2015**, 27-30 December 2015, Guwahati, Assam, India.
7. **Kelothu Suresh**, Manish Kumar, R. Vinoth Kumar, M. Jeyapriya, R. Anbarasan and G. Pugazhenthi, Sonication Assisted Synthesis of Polystyrene/Organoclay Nanocomposites: Influence of Clay Content, International Conference On Nanomaterials And Nanotechnology **(NANO-2015)**, 7-10 December 2015, Tamil Nadu, India.

8. Manish Kumar, Samarshi Chakraborty, **Kelothu Suresh** and G. Pugazhenthi, Influence of Cu-Cr layered double hydroxide (LDH) on the rheological properties and thermal degradation kinetics of PMMA nanocomposites, American Institute of Chemical Engineers **(AIChE-2015),** 8-13 November 2015, Salt Lake City, USA.
9. **Kelothu Suresh**, R. Vinoth Kumar, M. Jeyapriya, R. Anbarasan and G. Pugazhenthi, Study on the Effect of Organically Modified Montmorillonite (OMMT) Content on Rheological Properties of Polystyrene Nanocomposites, Recent Trends in Fundamental and Applied Chemical Sciences **(RTFACS-2014)**, 19-21 November 2014, Dibrugarh, Assam, India.
10. **Kelothu Suresh**, Rijumoni Boro, R. Vinoth Kumar and G. Pugazhenthi, Effect of Temperature on Rheological Behaviour of Polystyrene Solution, International Conference on Polymer Processing and Characterization **(ICPPC 2014)**, 11-13 October 2014**,** Kottayam, Kerala, India.